UNIVERSITY OF EAST ANGLIA

JOHN INNES CENTRE

Encoding of calcium signals in innate immunity and development

JOSÉ NUNO DE ARAÚJO LEITÃO

Thesis submitted to the University of East Anglia

for the degree of Doctor of Philosophy

2017

This copy of the thesis has been supplied on condition that anyone who consults it is understood to recognise that its copyright rests with the author and that use of any information derived there-from must be in accordance with current UK Copyright Law. In addition, any quotation or extract must include full attribution. Copyright © J. N. A. Leitão, 2017.

Ao avô,

«Ja Kalzium, das ist alles!»

Otto Loewi

Nobel Prize in Physiology or Medicine in 1936,

for discoveries relating to chemical transmission of nerve impulses

Abstract

Calcium (Ca^{2+}) is a widely used second messenger in eukaryotes. Spatially-restricted and temporary variations in the concentration of Ca^{2+} in the cytosol or the nucleus mediate various physiological responses. This is the case of the pathways that control innate immunity or symbiosis in plants. In the first case, a cytosolic Ca^{2+} burst occurs upon pathogen perception and is required for the production of reactive oxygen species (ROS). A plasma membrane-localised channel is predicted to mediate this signal, but so far has not been identified. In the second, the Ca^{2+} oscillations required for establishment of rhizobial and arbuscular mycorrhizal symbioses occur in the nucleus. In *Medicago truncatula*, these are mediated by the potassium-permeable channel DOES NOT MAKE INFECTIONS 1 (DMI1) and the cyclic nucleotide-gated channels (CNGC) 15a/b/c. These genes are conserved in non-symbiotic species, which suggests additional roles for nuclear Ca^{2+} signalling.

In this work, I screened a collection of Ca^{2+} channel mutants for ROS production upon perception of flg22, the immunogenic peptide of bacterial flagellin and an activator of innate immunity. This led to the identification of a triple mutant in the glutamate receptor-like family, *glr3.1glr3.3aglr3.6a*, which had a decreased ROS production and reduced induction of the defence gene *NHL10*, upon treatment with flg22.

Furthermore, using a Ca^{2+} sensor that allows distinction between nuclear and cytosolic Ca^{2+}, I showed that nuclear Ca^{2+} oscillations, dependent on *AtDMI1* and *AtCNGC15*, occur during normal root growth in Arabidopsis. *dmi1* and *cngc15* mutants had defects in root development, due to perturbations in endogenous auxin levels. For the first time, nuclear Ca^{2+} oscillations were linked to auxin-mediated signalling and a key developmental process in a non-symbiotic species.

This thesis highlights the dynamic complexity of Ca^{2+} signalling and the impact that understanding the mechanisms of Ca^{2+} influx can have in defence and development.

Keywords: Calcium, influx, CNGC, GLR, DMI1, defence, root development, auxin.

Resumo

Cálcio (Ca^{2+}) é um mensageiro secundário comum em eucariotas. Variações na concentração de Ca^{2+}, temporárias e espacialmente restritas ao citosol ou ao núcleo, regulam várias respostas fisiológicas em plantas, tal como imunidade inata e simbiose. No primeiro caso, a perceção de um organismo patogénico promove um aumento da concentração de Ca^{2+} no citosol, necessária para a produção de espécies reativas de oxigénio (ROS). Este sinal é hipoteticamente mediado por um canal localizado na membrana plasmática, que até hoje ainda não foi identificado. No segundo caso, os sinais de Ca^{2+} necessários para as interações simbióticas com rizóbia e com micorriza arbuscular ocorrem no núcleo. Em *Medicago truncatula*, estes sinais são mediados pelo canal permeável a potássio DOES NOT MAKE INFECTIONS 1 (DMI1) e pelos canais de Ca^{2+} dependentes de nucleótidos cíclicos (CNGC) 15a/b/c. Estes genes estão conservados em espécies não-simbióticas, o que sugere papéis adicionais para sinalização por Ca^{2+} no núcleo.

Neste trabalho, testei a produção de ROS numa coleção de mutantes de canais de Ca^{2+}, após tratamento com flg22, o péptido imunogénico da flagelina bacteriana e um promotor de imunidade inata. Isto permitiu a identificação de um mutante triplo na família dos recetores de glutamato, *glr3.1glr3.3aglr3.6a*, que evidencia uma menor produção de ROS e reduzida indução do gene de defesa *NHL10*, após tratamento com flg22.

Fazendo uso de um sensor de Ca^{2+} que permite distinguir Ca^{2+} nuclear e citosólico, demonstrei que oscilações de Ca^{2+} nuclear, dependentes de *AtDMI1* e *AtCNGC15*, ocorrem durante o crescimento da raiz em Arabidopsis. Mutantes nestes genes mostraram problemas no desenvolvimento da raiz, devido a perturbações nos níveis endógenos de auxina. Pela primeira vez, oscilações em Ca^{2+} nuclear foram ligadas a sinalização mediada por auxina, e a uma via de desenvolvimento fulcral numa espécie não-simbiótica.

Esta tese sublinha a complexidade e dinâmica de sinalização por Ca^{2+} e o impacto que os mecanismos de influxo de Ca^{2+} têm nas vias de sinalização de defesa e desenvolvimento.

Palavras-chave: Cálcio, influxo, CNGC, GLR, DMI1 defesa, desenvolvimento, raiz, auxina.

Acknowledgements

To Myriam, for everything you taught me, your direction and support, and for inviting me to these projects. I promise never to drag you down a favela in Rio again.

To Giles, who first welcomed me in his lab and lured me into the world of calcium imaging. Thank you for the guidance, discussion, and the opportunity to be part of this field.

To my supervisory committee, Cyril Zipfel and Richard Morris, for discussion and direction. To Allan Downie and Jeremy Murray, for their ideas and contributions during lab meetings.

To José Feijó and Michael Wudick, for providing me with *glr* mutant alleles. To Tom Vincent, for the YC3.6 expressing plants, and useful discussion on all things calcium.

To the John Innes Foundation, for funding the JIC/TSL/EI Rotation PhD Programme, which gave me the opportunity to embark on this journey. To Steph Bornemann and Nick Brewin, who make this PhD programme run and are so dedicated to their students.

To Alison Smith and Alistair McCormick, for the opportunity to do an excellent rotation, from which I took way many useful lessons. To Nicola Patron and Mark Youles, with whom I learnt golden gate cloning and CRISPR.

To the current and former members of the Oldroyd and Murray groups, namely: Aaron Thomas, Akira Akamatsu, Andy Breakspear, Ben Miller, Chengwu Liu, Donna Cousins, Doreen Feike, Eleni Soumpourou, Feng Feng, Fran Robson, Guru Radhakrishnan, Ioannis Tamvakis, Jian Feng, Jo Harrison, Jodi Lilley, Jongho Sun, Katharina Schiessl, Leonie Luginbühl, Matt Heaton, Ram Karunakaran, and Sylvia Singh, for experimental suggestions and help, discussion, comradery, and companionship. In particular, thanks to Feng for help with ROS assays, Jongho with calcium imaging, and Katharina with confocal staining protocols. Also a huge thanks to Julie Ellwood, not just for all the organising work that keeps the department running, but also for her incisive and hilarious takes on pretty much everything.

To the up and coming Charpentier lab, Aisling Cooke, Pierre Dangeville, and Pablo del Cerro, for a truly great work environment, interesting discussion, friendship, and so much cake. Remember to #HopeForTheBest, but #PrepareForTheWorst.

To Tjelvar Olsson and Matthew Hartley, for developing the image analysis script to quantify yeast complementation assays. To Ross Carter for the algorithm to quantify spike periods.

To Grant Calder for being a microscopy wizard. To Andrew Davies for helping me photograph thousands of plants for growth assays. To the media kitchen and horticultural services, who

are a fundamental part of the John Innes and make the life of the researchers so much easier. In particular, thanks to Tim Wells, for taking especially good care of my plants and teaching me about horticulture.

To Aisling, Guru and Leonie, for accompanying me on the adventure of doing a PhD in this lab. It wouldn't have been half ~~as fun/as bizarre/as silly/as (sometimes) ridiculous~~ as enjoyable without you, even with the occasional emergency landing somewhere in Africa. Thank you for all your help, support, motivation, reality-checks, and most of all, your friendship.

To my fellow students and friends, Andrew, Daisy, Dash, Emily, Guru, Jemima, Jenny, Jie, Mabon, Marc, Marie, Rachel, Sibyl, Sebastian, and Tom, who were not only of valuable help throughout this PhD, but whose friendship also made moving to Britain a lot easier.

To Andrew, Marc, Bethan, and Hélène, for being the best housemates I could have asked for, with whom I will treasure many memories of *The Marble Factory*, which, ideally, we'll keep between ourselves, ok guys?

To my lindy family, Lara, Kez, Hannah and Hannah, John, Phil, Robert, Bernie, and everyone with whom I've shared many dances, laughs, or unreasonable amounts of food. You helped me in more ways than you imagine.

To the floorball gang, Peter, Daisy, Tjelvar, Freddie, Donovan, Štefan, Jakub, Jeremy, Ervijs, Jake, and Simon, for always guaranteeing a healthy way to vent.

To Word's «Replace All» function, which made a whole lot easier guaranteeing that in all 748 times that the word «Ca^{2+}» appears, the charge number is superscripted.

Aos Biotecos, Andreia, Zé, Sofia, Joana, Catarina, Diogo, André, Mariana, Paulina, e Bruno, que mesmo à distância nunca deixam de motivar, ajudar, e me fazer rir às gargalhadas.

À Ana e ao Luís, à Kika, Ana Luisa, Pipas, Carol e Pepa, à Moniquita e ao João, à Daniela e à Ana Maria, que sempre me recebem no Marco ou onde seja de braços abertos. Obrigado por todos estes anos de amizade.

To all my past teachers, lecturers, and supervisors, in Marco, Porto, Stockholm, and Norwich, who always motivated me towards a career in Science and made me the researcher I am today.

Aos meus pais e ao Luís, que me disseram para vir, mesmo querendo-me lá, que apoiaram minhas decisões, e que sempre me dão bons conselhos. Obrigado.

Table of Contents

List of Figures

List of Tables

Chapter I

Introduction

Plants, while mostly sessile, are extraordinarily aware of their surroundings. They effectively measure the concentration of a variety of different chemicals in their environment and evaluate the quality, intensity, and period of the light to which they are exposed. Plants also recognise symbionts in their vicinity and distinguish them from pathogenic organisms. And importantly, they actively mount appropriate adaptive and developmental responses to all the cues they are constantly receiving from the environment. From a molecular point of view, this process of sensing followed by an adaptive response implies the transport of information from the sensing point, often a receptor at the cell surface, to the cell nucleus, where changes in gene expression effectively orchestrate the adaptation that ensues. This process is carried out by complex signalling pathways, often with controls – positive and negative regulators, as well as amplifiers – that occur at the cellular and tissue levels and may lead to organismal-wide responses. This thesis is dedicated to the study of one such mechanism of signal transduction in plants and how it is encoded at the molecular level – calcium signalling.

1.1. Calcium signalling in plants

Calcium (Ca^{2+}) is an important second messenger in eukaryotic organisms and is involved in immunity, fertilisation, symbioses, and stress-tolerance, in plants, and in neurotransmission, muscle contraction, and cell proliferation, in animals. The Ca^{2+} ion can coordinate six to eight uncharged oxygen atoms, which means that Ca^{2+} can form complexes with proteins, membranes, and organic acids (Mcphalen *et al*., 1991). As such, and because Ca^{2+} and phosphate complexes have very low solubility (Sanders *et al*., 1999), Ca^{2+} is a toxic compound when present at high concentrations, for it jeopardizes ATP homeostasis, causes protein and nucleic acid aggregation, and affects the integrity of lipid membranes (Case *et al*., 2007). For this reason, the cytosolic concentration of free Ca^{2+} is kept low and under a tight

spatial and temporal control, establishing great concentration differences across the cell membrane. As a result, a large electrochemical gradient becomes established, which can drive very fast increases in the concentration of cytosolic Ca^{2+} ($[Ca^{2+}]_{cyt}$). This may have allowed the evolutionary emergence of Ca^{2+} signalling (Sanders *et al*., 1999; Dodd *et al*., 2010). Highly localised and temporally defined increases in the $[Ca^{2+}]$ are tolerated and serve as an effector. Briefly, when a stimulus causes a change in cytosolic or nuclear-free Ca^{2+}, these changes are perceived by Ca^{2+}-binding proteins. These sensors decode the Ca^{2+} signal and relay information onto downstream targets, such as channels, transporters, enzymes, or transcription factors, eliciting protein-protein interactions, phosphorylation cascades or transcriptional changes (Luan *et al*., 2002; Finkler *et al*., 2007; Edel *et al*., 2017). It is therefore not surprising that Ca^{2+} signalling plays a key role in many cellular processes in plants, such as development (Hepler *et al*., 2001; Himschoot *et al*.; Vanneste and Friml, 2013), defence (Seybold *et al*., 2014; Zhang *et al*., 2014; Yuan *et al*., 2017), symbioses (Charpentier and Oldroyd, 2013), fertilisation (Wudick and Feijó, 2014), stomatal aperture (Roelfsema and Hedrich, 2010; Murata *et al*., 2015), circadian signalling (Johnson *et al*., 1995; Spalding, 2000), and abiotic stress responses (Ranty *et al*., 2016; Wilkins *et al*., 2016).

The control over the $[Ca^{2+}]$ within the cell leads to drastic concentration differences across different cell compartments, such as between the cytosol and the apoplast, where it can be up to 100.000 times higher (Figure 1.1) (Bose *et al*., 2011; Edel *et al*., 2017). Thus, for an increase in $[Ca^{2+}]_{cyt}$ or $[Ca^{2+}]_{nucleus,\ nu}$ to occur, Ca^{2+} moves in favour of its concentration gradient in a controlled manner. This function is carried out by ion channels and the main gene families responsible for this function in plants will be discussed in more depth in the next section and are indicated in Figure 1.1.

Efflux systems, conversely, re-establish the $[Ca^{2+}]$ to pre-stimulus levels, by transporting Ca^{2+} against its concentration gradient, requiring energised transport systems (Berridge *et al*., 2003). These include antiporters, which power Ca^{2+} transport by moving a counter-ion in favour of its concentration gradient, and Ca^{2+}-adenosine triphosphatases (Ca^{2+}-ATPases), which use ATP hydrolysis to fuel Ca^{2+} transport. In Arabidopsis, the major groups of efflux machinery include the Ca^{2+} exchangers (CAX) (Manohar *et al*., 2011; Pittman and Hirschi, 2016), the auto-inhibited Ca^{2+}-ATPases (ACAs), and the endoplasmic reticulum (ER)-type Ca^{2+}-ATPases (ECAs) (Baxter *et al*., 2003). Both Ca^{2+}-ATPases and Ca^{2+}-exchangers

contribute differently to shape the Ca^{2+} signal, as the first are high-affinity, but low capacity transporters, while the latter have low-affinity yet high capacity (Sze *et al*., 2000). Non-canonical efflux systems may also contribute to the regulation of the $[Ca^{2+}]$, as exemplified by the chloroplast-associated Zinc (Zn^{2+})-transporting heavy metal pump HMA1, which also transports Ca^{2+} (Kim *et al*., 2009; Moreno *et al*., 2008) (Figure 1.1).

Both influx and efflux mechanisms contribute to defining the variation in the $[Ca^{2+}]$ over time. It has been hypothesised that stimulus-specific information can be encoded in the amplitude, frequency, duration, and spatial location of the Ca^{2+} release, a concept that was named "Ca^{2+} signature" (Webb *et al*., 1996). Evidence to support this hypothesis was provided when Allen *et al*. showed that artificially imposing variations in $[Ca^{2+}]_{cyt}$ with parameters that elicited stomatal closure in wild-type plants restored stomatal closure in *growth control exerted by ABA 2* (*gca2*) guard cells, which would otherwise display a decreased stomatal closure phenotype and abnormal Ca^{2+} kinetics in response to abscisic acid (ABA) (Allen *et al*., 2001).

The signature is interpreted by Ca^{2+} binding proteins, also known as decoders, which relay the information and confer an additional level of specificity and regulation. Ca^{2+} binding, through EF-hand domains, for example, typically causes a conformational change that modulates the activity (if the decoder is an enzyme), or promotes interaction with targets. In plants, the major decoders are the calcineurin B-like (CBL) interacting protein kinases (CIPKs) (Luan, 2009), the Ca^{2+}-dependent protein kinases (CDPKs, known as CPKs in Arabidopsis) (Schulz *et al*., 2013; Valmonte *et al*., 2013), and the calmodulins (CaM)/CaM-like (Poovaiah *et al*., 2013; Zhu *et al*., 2015). EF-hand domains have been identified in other proteins, notably the RESPIRATORY BURST OXIDASE HOMOLOGUES (RBOHs) (Keller *et al*., 1998; Torres and Dangl, 2005), or the Ca^{2+}-permeable TWO-PORE CHANNEL 1 (TPC1) (Peiter *et al*., 2005).

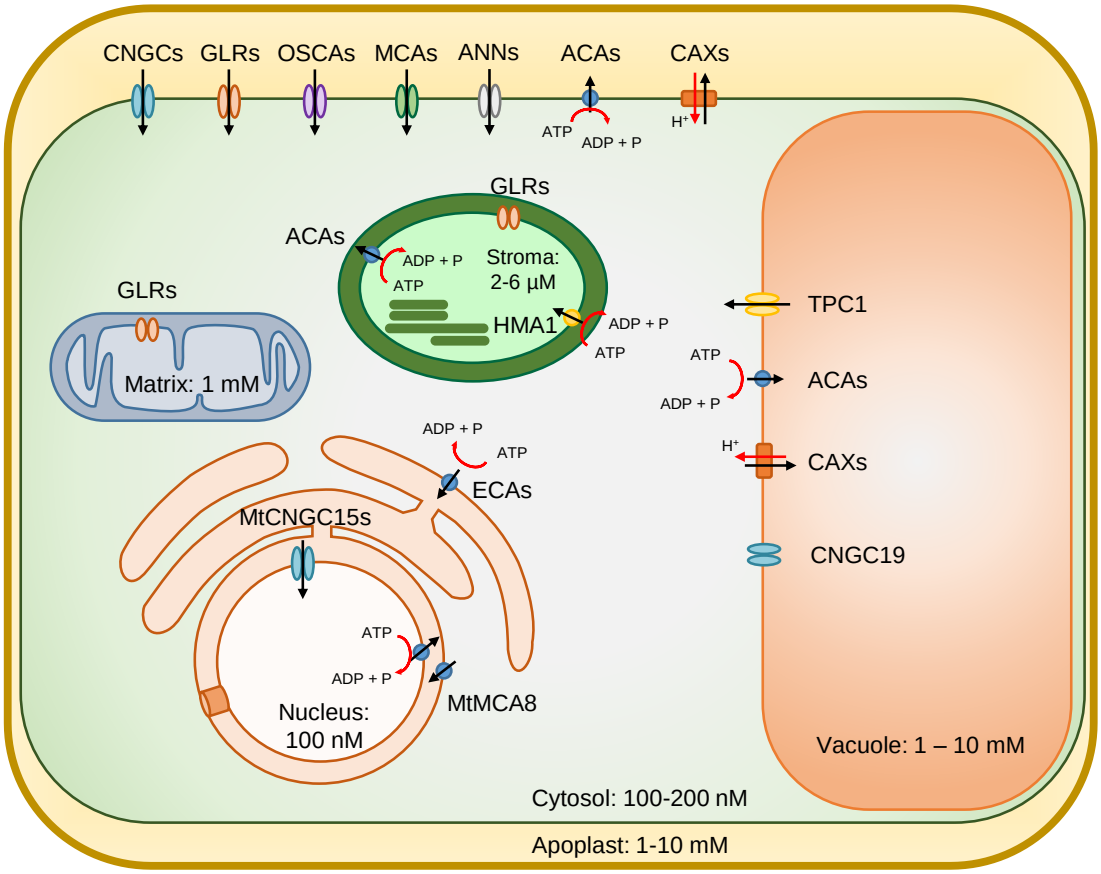

Figure 1.1 | Summary of the molecular components of Ca^{2+} signalling in plants.

Overview of the major elements involved in the generation of Ca^{2+} signals (influx and efflux mechanisms) and the Ca^{2+} concentrations in different organelles (Bose *et al*., 2011; Edel *et al*., 2017). Influx mechanisms: cyclic nucleotide-gated channels (CNGCs), glutamate receptor-like channels (GLRs), hyperosmolality-gated Ca^{2+}-permeable channels (OSCAs), annexins (ANN), *mid1*-complementing activity (MCAs), and two-pore channel (TPC1). Efflux mechanisms: Ca^{2+}-ATPases (ACAs), ER-type Ca^{2+}-ATPases (ECAs), Ca^{2+}-exchangers (CAX), and MtMCA8, a *Medicago truncatula* sarco/endoplasmic reticulum Ca^{2+}-ATPase (SERCA). The direction of Ca^{2+} transport is represented by black arrows, ATP hydrolysis by curved red arrows, and counter-ion transport by red straight arrows. Ca^{2+} transport was not indicated when transport activity in a specific organelle has not been demonstrated.

1.2. Mechanisms of calcium influx

In land plants, members belonging to six protein families have been shown to transport Ca^{2+}, namely the cyclic nucleotide-gated channels (CNGCs) (Zelman *et al*., 2012; DeFalco *et al*., 2016a), the glutamate receptor-like channels (GLRs) (Price *et al*., 2012), the hyperosmolality-gated Ca^{2+}-permeable channels (OSCAs) (Yuan *et al*., 2014), the annexins (Davies, 2014), the *mid1*-complementing activity (MCAs) (Kurusu *et al*., 2013), and the TPCs (Peiter *et al*., 2005). It is also worth mentioning the mechanosensitive channel of small conductance (MscS)-like (MSL) family, considering that there is evidence for Ca^{2+}-permeable mechanosensitive channels in plants (Cosgrove and Hedrich, 1991; Dutta and Robinson, 2004), but thus far no MSL has been unequivocally characterised as a Ca^{2+}channel (Edel and Kudla, 2015). Animals, on the other hand, appear to have a higher diversity of mechanisms available for Ca^{2+} influx (Verret *et al*., 2010; Edel and Kudla, 2015; Marchadier *et al*., 2016). Notably, genes homologous to animal Ca^{2+} channels such as the cysteine-loop superfamily of ligand-gated ion channels (Cys-loop), inositol (1, 4, 5)-trisphosphate receptors (IP_3Rs), voltage-dependent cation channels (VDCCs), ATP-gated purinergic channels (P2XRs), or transient receptor potential channels (TRPs) have not been identified in higher plants, albeit some are present in algae (Wheeler and Brownlee, 2008; Verret *et al*., 2010). This suggests that these channels were lost during plant evolution. The loss of diversity is apparently concomitant with an amplification within the gene families that are present, as given, e.g., by the number of *CNGC* and *OSCA* genes, which is 20 for both families in Arabidopsis and six and three in *Homo sapiens*, respectively. It is worth noting, nonetheless, that non-canonical or novel types of Ca^{2+} channels are perhaps yet to be identified. In the following sections, I will expand on the CNGCs, GLRs, and annexins, as these were the Ca^{2+} influx mechanisms studied in this thesis.

1.2.1. Cyclic nucleotide-gated channels

CNGCs are ligand-gated non-selective cation channels (Dietrich *et al*., 2010; Jammes *et al*., 2011; Zelman *et al*., 2012). Ca^{2+} permeability has been demonstrated for several CNGC proteins, including *Medicago truncatula* MtCNGC15a, through heterologous expression in *Xenopus laevis* oocytes (Charpentier *et al*., 2016), AtCNGC2/8/9/10/16 and AtCNGC18, in human embryonic kidney (HEK) cells (Leng *et al*., 1999; Gao *et al*., 2014, 2016), and

AtCNGC2/5 and AtCNGC6 using patch-clamp in guard cell protoplasts (Ali *et al*., 2007; Wang *et al*., 2013).

In Arabidopsis, there are 20 CNGC genes (Mäser *et al*., 2001), thought to form homo- and heterotetramers (Chin *et al*., 2013). They are composed of six transmembrane domains with a pore domain between helices 5 and 6, and a cytosolic C-terminal domain that contains both a cyclic nucleotide- and a CaM-binding domain, which partially overlap (Arazi *et al*., 2000; Köhler and Neuhaus, 2000; Spalding and Harper, 2011). This is in contrast to animal CNGCs, where the CaM-binding domain is present in the N-terminal (Ungerer *et al*., 2011). This suggests that in plants, Ca^{2+} can modulate its own CNGC-mediated flux through binding of CaM to the C-terminal, which blocks the binding site for cyclic nucleotides, believed to activate the channel (Hua *et al*., 2003; Kaplan *et al*., 2007). Nevertheless, it was recently shown that CNGCs can have multiple CaM-binding domains, which, in the case of CNGC12, can both positively and negatively regulate channel activity (DeFalco *et al*., 2016b). CNGCs have been associated with abiotic stress, defence, fertility, flowering time, gravistimulation, senescence, and symbiosis (reviewed in DeFalco *et al*, 2016a, and Jha *et al*., 2016). The role of *M. truncatula* CNGC15 proteins is discussed in section 1.3.1.2.

1.2.2. Glutamate receptor-like channels

GLRs are homologues of the mammalian ionotropic glutamate receptors (iGluRs), glutamate-activated ion channels involved in neurotransmission in the central nervous system, and were identified in plants in 1998 (Lam *et al*., 1998). Despite their name, GLRs seem to display a much broader ligand specificity, as so far 12 amino acids and glutathione have been shown to be agonists (Qi *et al*., 2006; Stephens *et al*., 2008; Michard *et al*., 2011; Tapken *et al*., 2013). This family is composed of 20 members in Arabidopsis (Davenport, 2002), generally considered to be non-selective cation channels. While Ca^{2+} currents have been quantified for GLR1.4, GLR3.4, and GLR3.7 in *X. laevis* oocytes (Roy *et al*., 2008; Tapken *et al*., 2013) and GLR3.2 and GLR3.4 in HEK cells (Vincill *et al*., 2012, 2013), there are documented differences in the ion selectivity across different members. While GLR1.4 is a non-selective cation channel (Tapken *et al*., 2013), GLR3.4 is highly selective for Ca^{2+} over Na^{+} (Vincill *et al*., 2012).

GLRs, thought to form heterotetramers (Stephens *et al*., 2008; Price *et al*., 2013; Vincill *et al*., 2013), are composed of two extracellular ligand-binding domains, three transmembrane

domains with a fourth half membrane-spanning motif, which together form the pore domain, and a cytosolic C-terminal domain (Lam *et al*., 1998). Despite the inherent difficulty of studying multi-gene families, GLRs have been linked to ABA signalling, Ca^{2+} homeostasis, carbon metabolism, defence, fertility, gravitropism, photosynthesis, root development, and senescence (extensively reviewed in Weiland *et al*., 2016).

1.2.3. Annexins

Annexins are phospholipid-binding proteins that can associate with or insert into membranes. There are eight members in Arabidopsis, and the basis for their channel-like activity is the presence of a hydrophilic pore at the centre of the molecule (reviewed in Davies, 2014). Electrophysiology studies showed Ca^{2+} conductance capacity for maize ZmANN33 and ZmANN35 (Laohavisit *et al*., 2009). Similar Ca^{2+} permeability was later shown for AtANN1 using protoplasts isolated from the root epidermis (Laohavisit *et al*., 2012, 2013), and it has been proposed that they form ROS-responsive channels (Laohavisit *et al*., 2010). Plant annexins have been implicated in drought and salt stress responses, pollen development, and H_2O_2-induced Ca^{2+} influx in root cells (Huh *et al*., 2010; Richards *et al*., 2014; Zhu *et al*., 2014).

1.3. Calcium signalling in the nucleus

It is well established that Ca^{2+}-dependent processes occur in mitochondria (Logan and Knight, 2003), chloroplasts (Johnson *et al*., 1995), and nuclei, but for a long time it was unclear whether the nucleus had the capacity to generate Ca^{2+} signals independently of the cytosol.

It has since been demonstrated that isolated nuclei are able to perceive stimuli and elicit a Ca^{2+} signal. First, Pauly *et al*. (2000) showed that the nucleus is not passively permeable to Ca^{2+}. Addition of 1 mM or 10 mM $CaCl_2$ to isolated nuclei obtained from tobacco protoplasts expressing the bioluminescent Ca^{2+} sensor apoaequorin had no effect in the resting $[Ca^{2+}]$. These authors further showed that these isolated nuclei were still able to mount a Ca^{2+} response to mastoparan (Pauly *et al*., 2000), establishing that nuclei are able to generate Ca^{2+} signals independently.

Furthermore, a variety of studies has shown that variations in the $[Ca^{2+}]$ upon a given stimulus can differ in the cytosol and the nucleus. Pauly *et al*. (2000) demonstrated that

different Ca^{2+} signals are elicited in the nucleus and the cytosol upon application of mastoparan to tobacco protoplasts. In a similar experiment, it was shown that the nuclear and cytosolic Ca^{2+} signals elicited by hyper- and hypo-osmotic shocks were different in each compartment, in tobacco cell cultures expressing apoaequorin (Pauly *et al*., 2001). The same discrepancies between nuclear and cytosolic Ca^{2+} signals have been observed in response to wind and cold water in *Nicotiana plumbaginifolia* seedlings (Luit *et al*., 1999). More recently, similar observations were made in Arabidopsis plants expressing the Yellow CaMeleon 3.6 (YC3.6) Ca^{2+} sensor either in the nucleus, or excluded from the nucleus, in response to adenosine triphosphate (ATP) (Krebs *et al*., 2012; Krebs and Schumacher, 2013). These studies demonstrate that the nucleus and the cytosol generate Ca^{2+} signals with different kinetics.

Moreover, it has been shown that an increase in $[Ca^{2+}]_{cyt}$ does not automatically elicit an increase in $[Ca^{2+}]_{nu}$, and vice-versa, i.e., changes in $[Ca^{2+}]_{nu}$ may occur without changes in $[Ca^{2+}]_{cyt}$. Treatment with the oligosaccharide laminarin triggered a marked increase in $[Ca^{2+}]_{cyt}$, with no observable changes in $[Ca^{2+}]_{nu}$, as measured in apoaequorin expressing tobacco cell lines (Lecourieux *et al*., 2005). Conversely, while jasmonate (JA) induces Ca^{2+} signals with different profiles in both the cytosol and the nucleus, conjugation of JA with isoleucine only induces nuclear Ca^{2+} signals, which differ from those induced by JA (Walter *et al*., 2007; Mazars *et al*., 2009). These studies indicate that Ca^{2+} signals in the cytosol and the nucleus can be disconnected.

Finally, nuclear Ca^{2+} signals have also been shown to be translated into physiological responses, as evidenced by induction of CaM expression by wind-elicited nuclear Ca^{2+} (Luit *et al*., 1999), and nuclear Ca^{2+}-dependent sphingolipid-induced programmed cell death (Lachaud *et al*., 2010).

The most extensively characterised example of nuclear Ca^{2+} signalling in plants, and the only one for which the nuclear Ca^{2+} influx mechanism has been identified, is the case of the nuclear Ca^{2+} spiking that occurs during arbuscular mycorrhizal and rhizobial symbioses, which will be described more thoroughly in the next section.

1.3.1. The case of the arbuscular mycorrhizal and rhizobial symbioses

Nuclear Ca^{2+} spiking is a hallmark of the symbiotic interactions that occur between plants and arbuscular mycorrhizal fungi (AMF), and between legumes and rhizobial bacteria.

The use of Ca^{2+} sensors that allow imaging and quantification of these Ca^{2+} signals *in vivo* was paramount over the last two decades to characterise the signalling pathways that establish the colonisation of plant roots by beneficial fungal and bacterial symbionts. In these symbioses, a dynamic chemical communication is established between both partners, which involves the activation of receptors in the plasma membrane, Ca^{2+} spiking in the nucleus, and transcriptional reprogramming. In the case of the rhizobial-symbiosis this results in de novo organ formation, the nodule, which provides the conditions for the bacteria to fix atmospheric nitrogen, and in the case of the AMF symbiosis, this leads to colonisation of the root cortex, where branched fungal hyphal networks, the arbuscules, develop. As a result, a nutrient exchange between plant and fungi or rhizobia is established, benefiting both organisms (reviewed in Oldroyd, 2013).

1.3.1.1. Symbiotic calcium spiking

Nodulation (Nod) factors are rhizobial-produced lipochitooligosaccharides (Dénarié *et al*., 1996). Within two to twenty minutes of Nod factor perception, Ca^{2+} oscillations are detected in the nucleus of root hair cells, in the form of successive spikes that reach a stable frequency with a period ranging between 30 s and 150 s (the average value reported in literature is 100 s) (Oldroyd and Downie, 2004, 2008). These oscillations are cell autonomous, with the initial lag time and frequency varying across different cells, and have been reported to last up to three hours. An initial short period of fast-spiking has also been reported but is not always observed (Ehrhardt *et al*., 1996; Miwa *et al*., 2006; Sieberer *et al*., 2009). Spike shape is asymmetric, pointing to different kinetics of the influx and reuptake systems, as the time to reach maximum amplitude is shorter than the time required to return to baseline levels (Oldroyd and Downie, 2004; Sieberer *et al*., 2009).

Nuclear Ca^{2+} oscillations in response to AMF are similar in spike shape and frequency upon direct contact of the hyphopodia to rhizobial-induced Ca^{2+} spiking, which suggests that specificity between symbionts is not encoded by the Ca^{2+} signature (Chabaud *et al*., 2011; Sieberer *et al*., 2009). Additionally, a switch from low-frequency to high-frequency spiking predicts the path of colonisation by both fungus and bacteria, which ends by the time infection is complete (Sieberer *et al*., 2012). It has been proposed that robust Ca^{2+} spiking triggers the cells to adapt to colonisation (Charpentier and Oldroyd, 2013).

1.3.1.2. The encoding mechanism of nuclear calcium spiking in symbioses

Twenty years passed since the first description of nuclear Ca^{2+} spiking in response to Nod factors in alfalfa (Ehrhardt *et al*., 1996), to the identification of the Ca^{2+} channels responsible for this process in *M. truncatula* (Charpentier *et al*., 2016). Genes with predicted transmembrane domains, motifs present in Ca^{2+} channels in particular and ion channels in general, and encompassing nuclear localisation signals, were chosen as targets, silenced, and their symbiotic phenotype quantified (nodule number and AMF colonisation). This allowed the identification of three members of the CNGC family, namely MtCNGC15a, MtCNGC15b, and MtCNGC15c, which when silenced have fewer nodules and reduced AMF colonisation. Loss of function mutants further confirmed the symbiotic phenotype. Ca^{2+} permeability was demonstrated through the complementation of the yeast mutant *cch1mid1* and with expression in *X. laevis* oocytes, where an inward Ca^{2+} current was measured. Importantly, Nod factor- and Myc-factor-induced nuclear Ca^{2+} spiking is impaired in these mutants. A higher percentage of abnormal Ca^{2+} spiking is detected, including irregular frequency and maintenance of the oscillations, and fewer cells are responsive, a phenotype that worsens in *Mtcngc15* double mutants. Furthermore, these proteins localise to the nuclear envelope (Figure 1.1), where they interact with the potassium (K^+)-permeable channel DOES NOT MAKE INFECTIONS 1 (MtDMI1) (Charpentier *et al*., 2016). MtDMI1 also localises to nuclear membranes and is required for Ca^{2+} spiking and symbioses (Wais *et al*., 2000; Ané *et al*., 2004; Peiter *et al*., 2007; Riely *et al*., 2007; Capoen *et al*., 2011). In *L. japonicus*, the function of MtDMI1 is carried out by its orthologue LjPOLLUX and the K^+-permeable channel LjCASTOR, both of which localise to the nuclear membrane and are required for Ca^{2+} spiking and symbioses (Miwa *et al*., 2006; Charpentier *et al*., 2008). Mathematical modelling indicates that MtDMI1 not only functions to counter-balance the flux of positive charges generated by the MtCNGC15s, but also modulates the Ca^{2+} signal, and that activation of the MtCNGC15s and MtDMI1 must be simultaneous for oscillations to occur (Granqvist *et al*., 2012; Charpentier *et al*., 2013, 2016). The third element required in this model of symbiotic Ca^{2+} spiking is a Ca^{2+} pump, which transports Ca^{2+} out of the nucleoplasm and replenishes the Ca^{2+} store. This function is carried out by the sarco/ER Ca^{2+}-ATPase MtMCA8, which also localises to the nuclear envelope (Figure 1.1) (Capoen *et al*., 2011). Silencing *MtMCA8* severely reduces

Nod factor-induced Ca^{2+} spiking and impacts AMF colonisation (Capoen *et al*., 2011). Considering that MtCNGC15a/b/c, MtDMI1, and MtMCA8 all localise to the nuclear envelope, and that Ca^{2+} signals seem to emerge from the nuclear membranes (Sieberer *et al*., 2009; Capoen *et al*., 2011), the lumen of the nuclear envelope continuous with the ER is the predicted Ca^{2+} store (Charpentier and Oldroyd, 2013).

1.4. The role of calcium in plant immunity

Ca^{2+} is one of the earliest detectable signals upon recognition of pathogens by a plant, occurring from approximately 30 seconds to 2 minutes of pathogen perception (Ranf *et al*., 2008; Jeworutzki *et al*., 2010), and it is a prerequisite for pathogen resistance (Dubiella *et al*., 2013). The plant response to pathogen infection is based on a two-branched innate immune system (Jones and Dangl, 2006). The first branch of the response starts with the recognition of conserved microbial- or pathogen-associated molecular patterns (MAMPs or PAMPs) by pattern recognition receptors (PRRs) (Böhm *et al*., 2014; Zipfel, 2014). Perception of PAMPs, such as flagellin or bacterial elongation factor, by PRRs activates downstream responses, including Ca^{2+} signals, production of reactive oxygen species (ROS) by the nicotinamide adenine dinucleotide phosphate (NADPH) oxidase RESPIRATORY BURST OXIDASE HOMOLOGUE D (RBOHD), phosphorylation cascades, and transcriptional reprogramming (reviewed in Bigeard *et al*., 2015). This response can prevent further colonisation of the plant by the pathogen, a process known as pattern-triggered immunity (PTI, also known as PRR-triggered immunity), which is sufficient to deter most non-adapt pathogens. Adapted pathogens can deploy a range of effectors into plant cells that overcome PTI and allow the pathogen to propagate further in the plant tissue and elicit disease. These effectors can be recognised by intracellular nucleotide-binding domain leucine-rich repeat (NLR or NBS-LRR) proteins, prompting the second layer of the immune response, known as effector-triggered immunity (ETI) (Dangl *et al*., 2013; Cui *et al*., 2015). ETI re-establishes and magnifies PTI and often leads to the hypersensitive response (HR), i.e., localised plant cell death, surrounding the site of infection, preventing further spread of the pathogen (Coll *et al*., 2011).

1.4.1. The signalling pathway of plant innate immunity

In Arabidopsis, upon binding of flagellin or bacterial elongation factor (or their immunogenic peptides flg22 and elf18, respectively), to their corresponding PRRs, FLAGELLIN SENSING 2 (FLS2) and EF-Tu RECEPTOR (EFR) (Gómez-Gómez and Boller, 2000; Zipfel *et al*., 2004, 2006), these proteins associate with the co-receptor BRASSINOSTEROID INSENSITIVE 1-ASSOCIATED KINASE 1 (BAK1, also known as SERK3) (Chinchilla *et al*., 2007; Heese *et al*., 2007; Sun *et al*., 2013). Both proteins become phosphorylated in their cytosolic domains and the PRR complex phosphorylates and activates the associated receptor-like cytoplasmic kinase (RLCK) BOTRYTIS-INDUCED KINASE 1 (BIK1) (Lu *et al*., 2010; Zhang *et al*., 2010a). Kadota *et al*. (2014) demonstrated that RBOHD exists in a complex with FLS2 and EFR and that BIK1 directly interacts with and phosphorylates this enzyme in a Ca^{2+}-independent manner upon PAMP perception. This phosphorylation is essential for RBOHD activation and occurs in parallel to its Ca^{2+}-dependent regulation, namely binding of Ca^{2+} to its EF-hand motifs and phosphorylation by CPKs (Drerup *et al*., 2013; Dubiella *et al*., 2013; Ogasawara *et al*., 2008). Full RBOHD activation results in the production of ROS in the apoplast, which acts both as an antimicrobial agent and a signalling molecule (Figure 1.2).

The recognition of PAMPs and MAMPs lead to convergent signalling pathways involving CDPK and mitogen-activated protein kinase (MAPK) cascades, which cause global transcriptional reprogramming that boosts immunity (Boudsocq *et al*., 2010). In multiple CPK4, CPK5, CPK6, and CPK11 knockout mutants, several immune phenotypes were observed, including failure to induce the transcription of a subset of flg22-inducible genes, decreased flg22- and oligogalacturonide-induced ethylene production, and increased susceptibility to the necrotrophic fungus *Botrytis cinerea* (Boudsocq *et al*., 2010; Dubiella *et al*., 2013; Gravino *et al*., 2015). Four different PTI-induced MAPKs have been identified, which are activated within minutes of PAMP perception: MPK4 and MPK11 are activated by the MAPK kinases MKK1 and MKK2, which in turn are activated by the MAPK kinase kinase MEKK1; and MPK3 and MPK6, which are activated by MKK4 and MKK5 (Asai *et al*., 2002; Mészáros *et al*., 2006; Suarez-Rodriguez *et al*., 2007; Gao *et al*., 2008; Bethke *et al*., 2012). Target genes of kinases belonging to these two groups are involved in the synthesis of antimicrobial

compounds or enzymes, cell wall modifications, such as callose deposition, and synthesis of hormones that may cause secondary transcriptional changes (Meng and Zhang, 2013; Lee *et al.*, 2015).

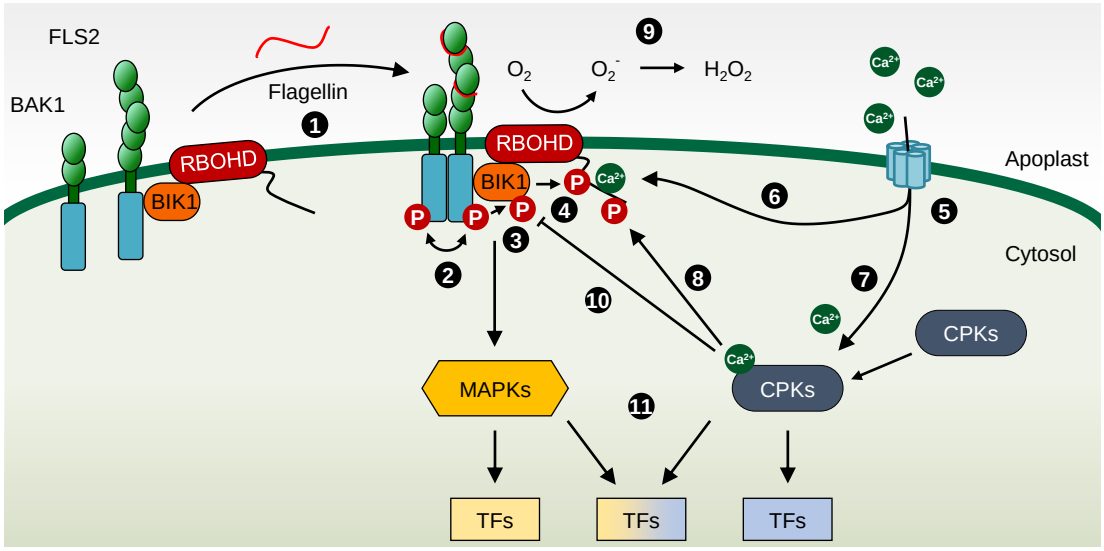

Figure 1.2 | Early molecular events triggered by flagellin in Arabidopsis.

Binding of flagellin to the receptor kinase FLS2 induces its instant association with the co-receptor BAK1 (1), phosphorylation of both proteins (2), and initiation of downstream responses. FLS2 also constitutively associates with BIK1 and RBOHD. BIK1 is phosphorylated by the FLS2/BAK1 complex (3) and directly interacts with and phosphorylates RBOHD in a Ca^{2+}-independent manner upon PAMP perception (4). Ca^{2+} influx occurs from the apoplast via a currently unidentified Ca^{2+} channel (5). Ca^{2+} can directly bind RBOHD (6) and is necessary for the activation of Ca^{2+}-dependent protein kinases (CPKs) (7), which also phosphorylate RBOHD (8). The residues in RBOHD targeted by BIK1 and CPKs are distinct. Once both Ca^{2+}-independent phosphorylation and Ca^{2+}-dependent regulation of RBOHD occurs, RBOHD becomes fully activated and produces reactive oxygen species (ROS) in the apoplast (9). BIK1 turnover is regulated by the activity of CPK28, which acts as a negative regulator of plant immunity (10). Finally, the elicitation of plant immunity leads to transcription reprogramming due to the activation of specific transcription factors by MAPK, CPKs or both (11). These transcription factors can be directly regulated by MAPKs or CPKs alone (yellow or blue, respectively), or through the synergistic action of both pathways (yellow and blue).

Given that the activation of PRR complexes diverts resources to innate immunity that would otherwise be directed towards growth and development (Gómez-Gómez *et al*., 1999; Zipfel *et al*., 2006; Krol *et al*., 2010), it is essential to exert a tight control over this system. These complexes should activate promptly in case of pathogen attack, but also swiftly be switched off once the threat disappears. Negative control mechanisms exist at multiple levels and include regulation of PRR activation and signalling amplitude, control over cytoplasmic targets of the pathway, regulation of transcriptional reprogramming, and integration of hormonal signalling (extensively reviewed by Macho and Zipfel, 2014, and Couto and Zipfel, 2016). Ca^{2+} also exerts a negative role in the regulation of PTI. Work by Monaghan *et al*. (2014) showed that CPK28 attenuates PAMP-triggered immune responses. CPK28 interacts with and phosphorylates BIK1, contributing to its turnover (Figure 1.2). BIK1 was shown to be the rate-limiting step in this signalling pathway and controlling its turnover is required to maintain cellular homeostasis. Accordingly, *cpk28* mutants have increased ROS and Ca^{2+} bursts, while in overexpression lines both these bursts are reduced. CPK28 is thus a negative regulator of plant innate immunity (Monaghan *et al*., 2014, 2015).

1.4.2. Calcium signalling in innate immunity

As mentioned above, Ca^{2+} signalling is central in plant innate immunity, extending from the control of RBOHD to the modulation of negative regulators. However, the intricate relation between Ca^{2+} and ROS signalling is yet to be fully described and, importantly, the identity of the Ca^{2+} channels involved in the influx of Ca^{2+} into the cytoplasm upon PAMP-, MAMP- or damage-associated molecular patterns (DAMP)- sensing remains unknown.

1.4.2.1. The calcium signature induced by PAMPs, MAMPs and DAMPS

In lines expressing apoaequorin, it was shown that different PAMPs, MAMPs and DAMPs, namely flg22, elf18, chitin oligomers (CO8), and Pep1, induce distinct cytosolic Ca^{2+} signatures in Arabidopsis seedling shoots and roots (Ranf *et al*., 2011). At 1 µM concentrations, after a lag phase of about 40 s (flg22/CO8) to one min (elf18/Pep1), there is a sharp increase in $[Ca^{2+}]_{cyt}$, followed by a short plateau phase and a slow decline over 30 to 40 min to baseline levels. Flg22 has the maximum peak amplitude, which differs across the tested PAMPs, MAMPs and DAMPs. Two distinct peaks are detectable for flg22, whereas for elf18 and Pep1

there is a prolonged plateau phase. In this study, the response in roots response was only visible for the Pep1 and CO8 treatments, as roots seemed to be insensitive to elf18 and showed only a minor response to flg22. The authors attribute this null or minor response to the low levels of EFR and FLS2 expression, respectively, in the root, suggesting that the weak to inexistent Ca^{2+} signal is due to reduced sensing of these PAMPs in the root tissue (Ranf *et al*., 2011).

While much paramount work has been carried using aequorin, the low spatiotemporal resolution offered by this Ca^{2+} sensor renders this system unfeasible to study the dynamics of Ca^{2+} signalling at the tissue and cellular level (Plieth, 2001; Alonso *et al*., 2009). Aequorin-based Ca^{2+} imaging describes a mean response of whole seedlings or tissues, averaging out differences that may exist between distinct cell types. In the particular case of plant immunity, where many of the responses are perceived as cell autonomous (Dodds and Rathjen, 2010; Lipka *et al*., 2010), cell resolution of the Ca^{2+} signal is essential.

Using the Ca^{2+} sensor YC3.6, Thor and Peiter (2014) describe oscillations in the cytosolic [Ca^{2+}] in response to 100 nM of flg22, in guard cells of Arabidopsis epidermal strips. These oscillations were variable in peak amplitude and frequency, and cell asynchronous. Pre-treatment with the Ca^{2+} chelator EGTA, or lanthanum ions (La^{3+}), seen as a non-specific blocker of plasma membrane Ca^{2+} channels, abolished these signals, suggesting that the Ca^{2+} that moved into the cytosol was extracellular in origin and that transport was mediated by Ca^{2+}-permeable channels (Thor and Peiter, 2014).

Subsequently, using the R-GECO Ca^{2+} sensor, Keinath *et al*. (2015) describe flg22- (100 nM) and chitin- (100 $\mu g \cdot mL^{-1}$) induced Ca^{2+} oscillations in pavement cells of detached Arabidopsis leaves, which last up to 30 min for flg22 and 20 min for chitin. These signals were abolished when plants were pre-treated with La^{3+}. Ca^{2+} responses were also observed in guard cells, and the authors suggest that guard cell perception of flg22 is cell autonomous. Guard cells are symplastically isolated, and neighbouring epidermal cells showing Ca^{2+} signals were not sufficient to trigger Ca^{2+} in adjacent guard cells. In roots, a response was also observed, and initiated from the elongation zone, propagating towards the root tip, as well as shootwards (Keinath *et al*., 2015).

1.4.2.2. The interplay between calcium and ROS signalling

Kadota *et al*. (2014) and Li *et al*. (2014) showed that RBOHD is phosphorylated in Ca^{2+} dependent and independent manners, and that both events are required for full RBOHD activation. It is not clear, though, which step of this dual regulation occurs first, i.e., if phosphorylation of RBOHD by BIK1 primes RBOHD for CPK-mediated phosphorylation. Interestingly, it has been suggested that RBOHD impacts on the Ca^{2+} signal as well. In *rbohd* knockout lines, the second peak in the flg22-induced rise in $[Ca^{2+}]_{cyt}$ disappears, suggesting a role of RBOHD in amplifying the influx of Ca^{2+} to the cytosol (Ranf *et al*., 2011). Hydrogen peroxide (H_2O_2), the most stable of ROS, can activate Ca^{2+} channels in guard cells (Pei *et al*., 2000), and root protoplasts (Demidchik *et al*., 2003), further supporting this hypothesis. However this question has not been re-evaluated with the recently available Ca^{2+} sensors, which report the Ca^{2+} signal with higher resolution. Work by Dubiella and colleagues (2013) identified a Ca^{2+}-dependent, ROS-mediated cell-to-cell mechanism of signal transduction required for defence induction in distal sites of the plant. RBOHD was identified as a phosphorylation target of CPK5, but CPK5 activity was induced both by PAMPs and ROS. And importantly, CPK5-dependent induction of defence responses in distal sites, namely upregulation of the defence marker gene *NHL10*, was abolished in *rbohd* mutant plants (Dubiella *et al*., 2013). These studies support the idea of a Ca^{2+}-ROS feedback loop in PTI.

1.4.2.3. The possible encoders

Despite a rather thorough understanding of the main molecular players involved in plant immunity in general and PTI in particular, the identity of the Ca^{2+} channel or channels responsible for the PAMP-, MAMP- and DAMP-induced Ca^{2+} influx, as well as its mechanism of activation and regulation, have remained unknown. Nonetheless, several members of putative Ca^{2+} channel families have been associated with immunity, and are more comprehensively discussed in Chapter IV. CNGC2, CNGC4, CNGC11, and CNGC12, have been linked with a role in ETI, such as the hypersensitive response (Yu *et al*., 1998; Clough *et al*., 2000; Yu *et al*., 2000; Yoshioka *et al*., 2001, 2006; Balagué *et al*., 2003; Jurkowski *et al*., 2004; Ali *et al*., 2007; Urquhart *et al*., 2007, 2011; Baxter *et al*., 2008; Abdel-Hamid *et al*., 2013; Chin *et al*., 2013), but quantification of flg22-induced $[Ca^{2+}]_{cyt}$ and callose deposition seem to reject a role for these proteins in PTI (Moeder *et al*., 2011; Ma *et al*., 2012). A pharmacological

approach suggested that GLRs may be involved in MAMP-triggered Ca^{2+} influx (Kwaaitaal *et al*., 2011), but no *glr* mutants have thus far yielded a clear PTI phenotype. ANN1 might contribute to the chitin-induced Ca^{2+} signal, but how that affects chitin-triggered immunity is unclear (Espinoza *et al*., 2017).

1.5. The role of calcium in root development

Root growth and development is achieved through a balance between cell division in the meristem, and cell expansion-differentiation in the elongation and differentiation zones. This balance is mostly driven by the apical-basal gradient of auxin across the root meristem, along with the antagonistic activity of cytokinin (Aida *et al*., 2004; Grieneisen *et al*., 2007; Sabatini *et al*., 1999). The ratio between these two hormones is critical to define the division/differentiation boundary (transition zone) and thus maintain meristem size (Dello Ioio *et al*., 2007; Ioio *et al*., 2008; Moubayidin *et al*., 2010). The effect of cytokinin on polar auxin transport and auxin degradation shapes the auxin profile along the root, creating an auxin minimum that positions the transition zone and triggers the developmental transition (Mambro *et al*., 2017). Active cell-to-cell transport of auxin across root tissues is essential to establish normal auxin levels, and this is mediated by cell-polarised PIN-FORMED (PIN) efflux carriers (Petrášek *et al*., 2006; Wiśniewska *et al*., 2006). PIN-driven changes in auxin distribution in the root regulate cell division and expansion (Blilou *et al*., 2005). PIN efflux activity and polarity are controlled via phosphorylation by members of the AGCVIII kinase family - D6 protein kinase (D6PK), and PINOID (PID) (Zourelidou *et al*., 2014). While D6PK has been shown to modulate efflux activity, PID can regulate both efflux and polar localisation (Weller *et al*., 2017).

1.5.1. Calcium signalling in root development

In roots, an increase in $[Ca^{2+}]_{cyt}$ is the earliest known physiological response to elevated auxin levels (Monshausen *et al*., 2011). Seconds after auxin treatment, there is influx of Ca^{2+} from the apoplast, which results in apoplastic alkalinisation. In epidermal cells in the elongation zone, this effect was shown to be completely dependent on CNGC14 (Shih *et al*., 2015). The authors further explored a role of CNGC14 in gravitropism, as an example of

endogenous auxin signalling. Root reorientation in response to a change in the gravity vector occurs through the displacement of amyloplasts in the columella, redirecting auxin flow to the lower side of the gravistimulated root (Sato *et al*., 2015). This increase in auxin results in increased $[Ca^{2+}]_{cyt}$ and extracellular alkalinisation (Mulkey and Evans, 1981; Zieschang *et al*., 1993; Monshausen and Sievers, 2002; Monshausen *et al*., 2011). In *cngc14* alleles however, extracellular alkalinisation was delayed, the Ca^{2+} signal impaired, and the gravitropic response, i.e., root bending, compromised. CNGC14 was also required for rapid indole-3-acetic acid (IAA)-induced growth inhibition in the elongation zone (Shih *et al*., 2015). Interestingly, the second messenger cyclic guanosine 3', 5'-monophosphate (cGMP), a possible CNGC-activating ligand (Gao *et al*., 2014, 2016), is produced in response to auxin and promotes auxin-dependent developmental processes, such as primary root growth (Nan *et al*., 2014).

Another putative Ca^{2+} channel has been linked to auxin signalling and primary root growth (Singh *et al*., 2016). Loss of function of *GLR3.6* results in reduced primary root length and lateral root density, a defect due to a smaller meristem size caused by a reduction in mitotic activity in the meristem. Expression of a cell cycle inhibitor, the cyclin-dependent kinase inhibitor KIP-RELATED PROTEIN 4 (KRP4) was upregulated in *glr3.6* and downregulated in *GLR3.6* overexpression lines. The authors found that silencing or overexpressing *KRP4* in *glr3.6* or *GLR3.6* overexpression lines, respectively, rescued the root phenotypes, suggesting that the reduced mitotic activity and premature endocycling in *glr3.6* could be mediated by KRP4. KRP4 expression was repressed when plants were grown in the presence of the auxin analogue 1-naphthaleneacetic acid (NAA) or $CaCl_2$, induced by EGTA, but repressed when EGTA and NAA were present simultaneously. This suggests that Ca^{2+} is upstream of auxin in this signalling pathway. Accordingly, the *glr3.6* phenotypes were rescued when plants were grown in the presence of 25 or 50 nM NAA (Singh *et al*., 2016). Other members of the GLR family have been associated with root development, namely GLR3.2 and GLR3.4, which were shown to interact in the phloem and be negative regulators of lateral root development, limiting primordia numbers (Vincill *et al*., 2013).

Polar auxin transport has also been connected to Ca^{2+} signalling. PID activity can be enhanced or repressed by interaction with the Ca^{2+}-binding proteins PID-BINDING PROTEIN 1 (PBP1) and TOUCH 3 (TCH3), respectively (Benjamins *et al*., 2003). PBP1 contains EF-hand domains and its interaction with PID is enhanced by Ca^{2+}. PBP1 also

promotes PID autophosphorylation in vitro, though the *in vivo* implications of this are unknown. The interaction of the CaM-like protein TCH3 with PID was shown to be Ca^{2+}-dependent (Benjamins *et al*., 2003). Previous work demonstrated that *PID* overexpression led to primary root collapse (Benjamins *et al*., 2001). The growth of *PID* overexpression lines in the presence of a CaM inhibitor, $LaCl_3$, or $GdCl_3$, aggravated the root collapse phenotype, suggesting that Ca^{2+} negatively regulates PID *in vivo* (Benjamins *et al*., 2003). Because TCH3 is a CaM-like protein, the authors propose that TCH3 is a negative regulator of PID. Both *PBL1* and *TCH3* are induced by IAA (Antosiewicz *et al*., 1995; Benjamins *et al*., 2003).

While Benjamins *et al*. (2003) provide mostly in vitro biochemical evidence of a role of Ca^{2+} in controlling PID activity, Zhang *et al*. (2011) use genetic and pharmacological tools to establish a link between inositol (1, 4, 5)-trisphosphate ($InsP_3$)-induced Ca^{2+} signalling, PIN polarity, auxin transport, and PID activity. Despite the fact that animal $InsP_3$ receptors, a family of Ca^{2+} channels that generally release Ca^{2+} to the cytosol in response to the second messenger $InsP_3$ (reviewed in Foskett *et al*., 2007), are not conserved in land plants (Wheeler and Brownlee, 2008), multiple studies have demonstrated that, in plants, $InsP_3$ prompts Ca^{2+} release from intracellular stores to the cytosol (Blatt *et al*., 1990; Gilroy *et al*., 1990; Tang *et al*., 2007). Treatment of *PID* overexpression plants with compounds elevating $InsP_3$ or $[Ca^{2+}]_{cyt}$ delayed PID-mediated root collapse, and conversely, this phenotype was enhanced by treatment with the Ca^{2+} chelator EGTA (Zhang *et al*., 2011), agreeing with the biochemical work that proposed a negative role for Ca^{2+} in the regulation of PID activity (Benjamins *et al*., 2003). These authors further showed that genetically or pharmacologically manipulating the levels of $InsP_3$ or $[Ca^{2+}]_{cyt}$ affects PIN1 and PIN2 polarity. Raising $InsP_3$ levels or $[Ca^{2+}]_{cyt}$ in *PIN1* overexpression lines, which ectopically express *PIN1* in the basal side of the epidermis (Mravec *et al*., 2008), reduced targeting of PIN1 to the basal cell side in this tissue, resulting in loss of polarity. Similarly, basal targeting of PIN2 in the cortex was reduced and polarity lost. Conversely, inhibiting cytosolic Ca^{2+} signalling preferentially reduced apical PIN2 polarity in the epidermis, while it did not affect its basal localisation in the cortex (Zhang *et al*., 2011). These studies suggest that Ca^{2+} signalling may be determinant in the apical versus basal polar targeting of PIN proteins.

1.6. Thesis outline and objectives

The widespread resort to Ca^{2+} signalling mechanisms in processes that range from development to biotic interactions and abiotic stress responses suggests that a complex spatiotemporal regulation is in place to ensure stimulus-specific, timely, and adequate outcomes. This is reflected by the wealth of proteins involved in these processes, from Ca^{2+} channels to Ca^{2+} decoders, which are organised in complex signalling pathways that guarantee that the Ca^{2+} signal occurs in the precise subcellular location, with the right kinetics, in the appropriate tissue at the correct time. The main objective of this thesis is to understand the regulation and impact of two distinct Ca^{2+} encoding mechanisms that localise to different subcellular compartments: one that elicits cytosolic Ca^{2+} upon induction of innate immune responses, and one that occurs in the nucleus during root growth.

First, different genetically-encoded fluorescent reporters for *in vivo* imaging of Ca^{2+} signals will be described (Chapter III). Second, the results of a reverse genetics screen that identified a triple mutant involved in the ROS-Ca^{2+} feedback system in the innate immune response will be presented (Chapter IV). Finally, the role of a conserved mechanism required for encoding nuclear Ca^{2+} signals in symbiotic interactions will be discussed in the context of a non-symbiotic plant and linked to the mechanisms that control root development (Chapter V).

Chapter II

Materials and methods

2.1. Plant material and growth conditions

For plants grown on plates, seeds were surface-sterilized in 1.5% bleach for 15 min, followed by five washes in sterile water, and the seeds were then plated in Murashige and Skoog (MS) solid medium, or MS-MES solid medium, with or without plant selection, according to the experiment (Table 2.1). After 3-5 days at 4 ˚C, plates were moved to a growth cabinet (23 ˚C, 16-hour photoperiod, and 300 $\mu mol \cdot m^{-2} \cdot s^{-1}$ light intensity).

For soil-grown plants used in leaf-to-leaf signalling experiments (Chapter IV), seeds were sown directly in Arabidopsis mix soil (Table 2.1), incubated 3-5 days at 4 ˚C, and then grown in a growth cabinet that was only opened for watering and that contained no other plants to prevent disease (22 ˚C day, 18 ˚C night, 10-hour photoperiod, 70% relative humidity, 120 $\mu mol \cdot m^{-2} \cdot s^{-1}$ light intensity).

For all other plants grown in soil (namely ROS assays), seeds were sown directly in Arabidopsis mix soil (Table 2.1), incubated 3-5 days at 4 ˚C, and then grown in a controlled environment room (CER, 22 ˚C day, 20 ˚C night, 16-hour photoperiod, 80% relative humidity, SANYO). Plants used for floral dipping were grown as described before, but moved to glasshouses before dipping and resumed their life cycle under glasshouse conditions.

2.2. Genotyping of Arabidopsis lines

2.2.1. Genotyping of T-DNA lines

Homozygosity was assessed by polymerase chain reaction (PCR), using a pair of gene-specific primers that flank the T-DNA insertion (left border primer (LP) and right border primer (RP)), which yield a band in wild-type or heterozygote samples, and using a combination of the gene-specific LP primer and a T-DNA insertion primer, which yields a band in heterozygote or homozygote samples. Primers were designed using the SIGnAL T-

DNA Primer Design algorithm (http://signal.salk.edu/tdnaprimers.2.html), for SALK, SAIL and WiscDsLox lines, or manually for the remaining lines. All primers used are listed in Table 2.2.

PCR reactions were prepared using GoTaq® G2 Green Master Mix (Promega) in 25 μL final volume (20 ng of gDNA were used as template, 0.2 mM dNTPs, 0.4 μM primers, 1.5 mM $MgCl_2$). The conditions of the PCR were the following: initial denaturation (two min at 95 °C), followed by 30 or 35 cycles of amplification (10 s at 95 °C; 20 s at the primer's annealing temperature (56 °C to 58 °C), and 60 s at 72 °C), and a final extension of five min at 72 °C. The products of PCR reactions were resolved in 1% (w/v) agarose Tris-Acetate-EDTA (TAE) buffer gels (Melford), along with a 2-log DNA ladder (New England Biolabs®) and stained for 10-15 min in a 10 $mg \cdot mL^{-1}$ ethidium bromide solution.

2.2.2. Genotyping of *cngc15-1* line

cngc15-1 is the result of an ethyl methanesulfonate (EMS) induced mutation and, as such, homozygosity was determined through sequencing. A 743 bp fragment was amplified by PCR as described above, and the PCR product was sequenced using primer 1200 (Table 2.2). The electropherogram was analysed at position +1570, where the G to A point mutation lies.

2.3. Molecular cloning

2.3.1. Golden gate cloning

Golden gate cloning followed the principles outlined in Engler *et al*. (2008, 2009) and Weber *et al.* (2011). Level 0 modules were synthesised by Life Technologies™ (ThermoFisher Scientific). Level 1 vectors were generated in a 15 μL reaction mix containing 100 ng of each level 0 plasmid, 100 ng backbone plasmid, 1.5 μL 100x BSA, 1.5 μL 10x T4 buffer, 1 μL *Bsa*I (New England Biolabs), and 1 μL T4 DNA ligase (New England Biolabs). The reaction was incubated for 25 cycles of three min at 37 °C and four min at 16 °C, followed by five min at 50 °C and five min at 80 °C, to allow digestion and ligation of the different DNA modules. Level 2 vectors were generated in the same way, using 1 μL *Bpi*I (Thermo Fisher Scientific), as opposed to *Bsa*I. Level 2 vectors used in this study are listed in Table 2.3.

2.3.2. Gateway cloning

The *GLR* coding sequences were retrieved from The Arabidopsis Information Resource (TAIR), converted to yeast codon usage using Geneious® 8.1.8, and synthesised by Life Technologies™ (ThermoFisher Scientific) into the entry vector pENTR221. 150 ng of entry and destination (pYES-DEST52) vectors were used in a 10 µL reaction in TE buffer with Gateway™ LR Clonase™ II Enzyme Mix (Invitrogen™). The reaction was vortexed briefly twice, spun down, and incubated at 25 °C for 2 h. The reaction was terminated by adding 1 µL of Proteinase K solution at 2 $\mu g \cdot \mu L^{-1}$ and incubating at 37 °C for ten min. Gateway vectors used in this study are listed in Table 2.4.

2.3.3. Transformation of *Escherichia coli* and plasmid purification

Chemically competent *E. coli* (DH5α, Invitrogen™) were transformed by adding 10-100 ng of plasmid or 1 µL of the golden gate or gateway reaction to a 20 µL cell aliquot, incubating on ice for 30 min, followed by a 30 s heat shock at 42 °C and two min on ice. Cells were then incubated with 300 µL Super Optimal broth with Catabolite repression (SOC) medium at 37 °C and 220 rpm, after which they were plated in lysogeny broth (LB) medium supplemented with the appropriate antibiotic marker and incubated overnight at 37 °C. Colony PCR was used to evaluate individual colonies. PCR reactions were prepared using GoTaq® G2 Green Master Mix (Promega) in 25 µL final volume (0.2 mM dNTPs, 0.4 µM primers, 1.5 mM MgCl) and bacterial cells from a single colony were transferred to the PCR mix using a pipette tip, which was also used to inoculate a small 500 µL culture. The conditions of the PCR were the following: initial denaturation (10 min at 98 °C), followed by 30 cycles of amplification (10 s at 98 °C; 20 s at the primer's annealing temperature, and 1-2 min at 72 °C), and a final extension of five min at 72 °C. The products of the PCR reactions were resolved in 1% (w/v) agarose TAE buffer gels (Melford), along with a 2-log DNA ladder (New England Biolabs®) and stained for 10-15 min in a 10 $mg \cdot mL^{-1}$ ethidium bromide solution. Positive single colonies were grown overnight in 5 mL of liquid LB medium (Table 2.1) at 37 °C and 220 rpm. Plasmids were purified using the QIAprep® Spin Miniprep Kit (Qiagen) according to the instructions of the manufacturer. All plasmids were subsequently sequenced (Eurofins Genomics, Germany).

2.3.4. Transformation of *Agrobacterium tumefaciens*

A. tumefaciens (GV3101) electrocompetent cells were transformed by electroporation (200 Ω, 125 V, 25 μF; Gene Pulser (Bio-Rad)) with 1 μL of plasmid DNA in an electroporation cuvette (Geneflow). Cells were then incubated in 300 μL SOC medium at 28 °C and 220 rpm for 1 h, after which they were plated in LB medium supplemented with the appropriate selection markers and incubated overnight at 28 °C (McCormac *et al*., 1998).

2.4. Yeast transformation and complementation

2.4.1. Transformation of yeast strains

The yeast strain JK93da (*MATa, leu2-3, Il2, his4, trp1, ura3-52, rme1*) and the mutant and *cch1mid1* (Fischer *et al*., 1997) were transformed using the lithium acetate method (Gietz and Woods, 2001). Briefly, 50 mL yeast cultures were grown at 30 °C until an OD600 of 0.6-0.8, centrifuged for five min at 4000 rpm, resuspended in sterile dH_2O, centrifuged for five min at 1000 rpm, and the pellet was carefully resuspended in 1.5 mL of 100 mM LiOAc. For each transformation reaction, 100 μL of yeast cells were carefully added to 300 μL of transformation mix (40% polyethylene glycol, 0.12 M LiOAc, 0.83 $mg \cdot mL^{-1}$ salmon sperm DNA previously boiled at 99 °C for two min, and 2-5 μg of plasmid). The mixture was vortexed vigorously for one min, incubated at 30 °C for 30 min, and then at 42 °C for 30 min. The transformation reactions were then centrifuged for five min at 700 g and gently resuspended in 100 μL of 0.9% NaCl. Transformants were selected in Synthetic Defined (SD) medium lacking uracil (SD-ura) (Table 2.1).

2.4.2. Complementation of the *cch1mid1* α-factor-induced phenotype

Complementation of the *cch1mid1* was assessed as described by Ali *et al*. (2006). Yeast cultures grown overnight under selection were washed three times with sterile dH_2O and resuspended in YPDA medium to a final OD600 of 2. A mixture of 100 μL yeast culture and 4 mL YPDA (top agar, 0.7% agar) was poured over a YPDA plate. Sterile cellulose filter discs (6 mm diameter and 45 μm pore size), loaded with 10 or 20 μg of synthetic alpha factor (Sigma 6901) were placed over the nascent lawn, the plates were incubated at 30 °C for 24 or 48 h, at which time photographs were taken.

2.4.3. Image analysis

In collaboration with Matthew Hartley and Tjelvar Olsson (JIC Computational Bioimaging), an algorithm was designed to quantify the growth inhibition halo characteristic of this assay. Briefly, the algorithm extends a series of lines along the radii of the circle from its centre over a 90° angle, measures the intensity along each line and averages the result. The algorithm is described in Figure 4.7 (Chapter IV).

2.5. Arabidopsis transformation by floral dip

Plants were grown for 4-5 weeks under CER conditions (T0 generation). They were then moved to containment glasshouses and fertilised flowers and siliques were clipped before dipping.

A. tumefaciens transformed with the plasmid of interest, either from single colonies or glycerol stock, was used to inoculate 5 mL of LB liquid medium. After overnight growth at 28 °C/220 rpm, this culture was used to inoculate 2-3 petri dishes per construct (500 µL inoculum), and the plates were incubated for 2-3 days so that a bacterial lawn would form. On the day of the flower dipping, the bacterial lawn was gently scraped off the plates with a razor and dissolved in 30 mL of 5 % sucrose 0.03% Tween-20. Plants were dipped in this culture, while gently shaking, for up to 30 seconds. They were then covered in propagator lids and protected from sunlight for 24 hours, before being returned to standard conditions for the remaining of their life cycle. Seeds were collected and germinated under the appropriate selection in the T1 and T2 generations.

2.6. Quantification of gene expression

2.6.1. RNA isolation

Total RNA was extracted using the RNeasy® Plant Mini Kit (QIAGEN) according to the instructions of the manufacturer. A subsequent step of on-column DNase digestion was included. Concentration and purity were determined by spectrophotometry ($A_{260/280}$ and $A_{260/230}$ ratios) and integrity was confirmed by gel electrophoresis (1% (w/v) agarose).

2.6.2. cDNA synthesis

cDNA was obtained from 500-2000 ng of RNA using the SuperScript™ III Reverse Transcriptase (Invitrogen™) according to the instructions of the manufacturer.

2.6.3. Quantitative PCR

Quantitative PCR (qPCR) was performed using a CFX96 Touch™ Real-Time PCR Detection System (BIO-RAD) with SYBR® Green JumpStart™ Taq ReadyMix™ (Sigma-Aldrich). For each primer set, amplification efficiency (E) was first determined by calculating the slope of a cDNA dilution series standard curve (two technical replicates per data point and seven data points corresponding to 5x, 50x, 150x, 500x, 1500x, 5000x dilutions of cDNA, in 20 µL of reaction mix, including 500 nM of each primer).

The conditions of the qPCR were the following: initial denaturation (2 min at 95 °C), followed by 40 cycles of amplification and quantification (15 seconds at 95 °C; 15 seconds at 56 °C or 58 °C, and 30 seconds at 72 °C, with a single fluorescence measurement). A melt curve was also generated to verify the specificity of the amplification reaction (50 °C to 95 °C, with a fluorescence measurement every 0.5 °C). Calculation of the normalised expression and fold change ratio was performed using the mathematical model described by Pfaffl (2001). Primers used for qPCR are listed in Table 2.5.

2.7. Seedling growth inhibition assays

Seeds were surface-sterilized and sown on MS 0.8% agar 1% sucrose plates. After stratification for 3 days at 4 °C, the plates were transferred to light for 4 days. On the fifth day, seedlings were then transferred to single well in 24-well plates containing liquid MS 1% sucrose media, with or without 10^{-6} M flg22. After 11 days, individual seedlings were gently blotted dry and weighed using a precision scale (Sartorius).

2.8. Quantification of production of reactive oxygen species

Leaf discs (4 mm diameter) from 3-4 week old plants were collected in 96-well plates and allowed to recover overnight in sterile water. The water was then removed and replaced with a solution containing 20 µM luminol (Sigma-Aldrich), 10 µg·mL^{-1} horseradish peroxidase

(Sigma-Aldrich), and 100 nM flg22 (or water). Luminescence was recorded over a 30 min period using a Varioskan Flash (Thermo Scientific) multiplate reader.

2.9. Root phenotyping assays

2.9.1. Primary root length measurements

Seedlings were grown vertically on MS-MES plates (6 seedlings of control genotype, and six seedlings of test genotype, per plate) and photographed at days 4, 5, 6, 7, 8, 10, or 12. Root length was measured using ImageJ 1.48v (NeuronJ plugin, 1.4.3v).

2.9.2. Tissue characterisation of the root meristem and transition zone

Seedlings were grown vertically on MS-MES plates (6 seedlings of control genotype, and six seedlings of test genotype, per plate) and analysed at days 6 or 12. Plants were fixed in 50% methanol 10% acetic acid, for at least 24 h at 4 °C. Samples were then washed with dH_2O, incubated in 1% periodic acid at room temperature for 40 min, washed with dH_2O, incubated in freshly prepared Schiff's reagent (100 mM sodium metabisulfite; 0.15 N HCl; 20 $\mu g \cdot mL^{-1}$ propidium iodide) for 30 min or until roots had acquired a pink colour, washed with dH_2O, and incubated overnight at room temperature in chloral hydrate : glycerol : water (8 g : 1 mL : 2 mL). Samples were then mounted in chloral hydrate and imaged using a Zeiss LSM 780 confocal microscope (Carl Zeiss, Welwyn Garden City, UK).

Cell counting and cell length measuring was performed using ImageJ 1.48v (Cell-o-Tape plugin, 0.7.7v) (French *et al*., 2012).

2.10. Histochemical GUS staining of Arabidopsis plants

Seedlings were fixed in cold 90% acetone for at least 30 min at 4 °C in 6-well plates. Acetone was removed and the material was washed twice with rinse solution (0.5 M Na_2HPO_4, 0.5 M NaH_2PO_4, 0.1 M $K_3Fe(CN)_6$, 0.1 M $K_4Fe(CN)_6$). The rinse solution was removed and stain solution added (rinse solution complemented with 2 mM x-Gluc (5-bromo-4-chloro-3-indolyl-beta-D-glucuronide). This was gently vacuum-infiltrated for 30 min. The material was then incubated at 37 °C, in the dark, for 30 min or 24 hours. The material was then washed in water and cleared in chloral hydrate (8 g choral hydrate, 3 mL 100 % glycerol, 1 mL dH_2O) for

at least 45 min, before mounting in chloral hydrate. Images were obtained with a DM6000 microscope (Leica).

2.11. Calcium imaging

Ca^{2+} imaging was performed using a Nikon ECLIPSE FN1. For imaging with YC3.6, CFP was excited at a wavelength of 440 ± 20 nm and emitted fluorescence was separated by an image splitter with a dichroic mirror and then passed through an emission filter of 470 ± 24 nm for CFP fluorescence or 520 ± 21 nm for YFP fluorescence (Optosplit, Cairn Research, UK). For imaging with R-GECO1.2 and G-GECO1.2-NES/R-GECO1.2-NLS, the sensors were excited at a wavelength of 470 ± 24 nm. Emitted fluorescence was also separated by an image splitter and passed through an emission filter of 520 ± 40 nm for G-GECO fluorescence, 632 ± 60 nm for R-GECO1.2 fluorescence (dual sensor), or 605 ± 40 nm for R-GECO1.2 (single Ca^{2+} sensor) (Optosplit, Cairn Research, UK).

2.11.1. Growth imaging

Seedlings were collected five days after germination and carefully placed in a small chamber made on a coverslip using high-vacuum grease (Dow Corning GMBH, Wiesbaden, Germany). The chamber was filled with a small volume of MS (50 to 100 µl) and closed with a smaller coverslip, covering the entire root. The seedling was then incubated at room temperature for at least 45 min before imaging. Images were collected every 2 or 3 s.

2.11.2. Treatment application

For each experiment, the plant material was harvested at the time indicated in the respective figure and carefully placed in a perfusing or non-perfusing chamber (as described in Figure 3.1). The sample was then incubated at room temperature for at least 15 min before imaging. Images were collected every 2 or 3 s.

2.11.3. Image analysis

For image processing the following steps were conducted using ImageJ 1.48v: background subtraction, registration (for images obtained with YC3.6 or with the dual sensor) using MultiStackReg v1.45 (http://bradbusse.net/sciencedownloads.html), ratio calculation (for images obtained using YC3.6) using Ratio Plus (https://imagej.nih.gov/ij/plugins/ratio-plus.html), and application of a lookup table. Image data were obtained from processed images using Time Series Analyser V3_2 (https://imagej.nih.gov/ij/plugins/time-series.html). Normalised datasets ($\Delta F/F$ and $\Delta R/R$) were calculated as $(F - F_0)/F_0$ or $(R - R_0)/R_0$, where F_0 and R_0 represent the average of at least two min of baseline values.

For the experiments described in Chapter V, analysis of spike shape was performed in collaboration with Ross Carter (The Sainsbury Laboratory, University of Cambridge). An algorithm was designed to quantify the rise and fall times of the spikes observed during Ca^{2+} imaging. The algorithm is described in Figure 5.17.

2.12. Statistical analyses

Statistical analyses were performed using GraphPad Prism version 5.00 for Windows, (GraphPad Software, La Jolla California USA, www.graphpad.com).

Table 2.1 | List of media and soil used for culture of bacteria, yeast and plants.

Medium	Composition
Media for bacteria culture	
LB	10 $g \cdot L^{-1}$ tryptone, 5 $g \cdot L^{-1}$ yeast extract, 5 $g \cdot L^{-1}$ NaCl. pH adjusted to 7.0 with 1.0 NaOH. For solid medium, Lab M No.1 agar was added to a final concentration of 1.5%.
SOC	20 $g \cdot L^{-1}$ tryptone, 5 $g \cdot L^{-1}$ yeast extract, 0.58 $g \cdot L^{-1}$ NaCl, 0.19 $g \cdot L^{-1}$ KCl, 2.03 $g \cdot L^{-1}$ $MgCl_2$, 2.46 $g \cdot L^{-1}$ $MgSO_4.7H_2O$, 3.6 $g \cdot L^{-1}$ glucose.
Media for yeast culture	
SD-ura	1.9 $g \cdot L^{-1}$ yeast nitrogen base without $(NH_4)_2SO_4$ and amino acids (Formedium), 5 $g \cdot L^{-1}$ $(NH_4)_2SO_4$, 20 $g \cdot L^{-1}$ glucose, 0.03 $g \cdot L^{-1}$ L-isoleucine, 0.15 $g \cdot L^{-1}$ L-valine, 0.02 $g \cdot L^{-1}$ L-adenine hemisulphate, 0.02 $g \cdot L^{-1}$ L-arginine, 0.03 $g \cdot L^{-1}$ L-lysine, 0.02 $g \cdot L^{-1}$ L-methionine, 0.05 $g \cdot L^{-1}$ L-phenylalanine, 0.2 $g \cdot L^{-1}$ L-threonine, 0.03 $g \cdot L^{-1}$ L-tyrosine, 0.02 $g \cdot L^{-1}$ L-histidine, 0.1 $g \cdot L^{-1}$ L-leucine, 0.02 $g \cdot L^{-1}$ L-tryptophan, 0.02 $g \cdot L^{-1}$ L-uracil. For solid medium, Formedium agar was added to a final concentration of 2%.
YPDA	10 $g \cdot L^{-1}$ yeast extract, 20 $g \cdot L^{-1}$ peptone, 20 $g \cdot L^{-1}$ glucose, 0.020 $g \cdot L^{-1}$ adenine. For solid medium, Formedium agar was added to a final concentration of 2% or 0.7% (top agar).
Media for plant culture	
MS	5 $g \cdot L^{-1}$ Murashige and Skoog (micro and macro elements including vitamins: 0.025 $mg \cdot L^{-1}$ $CoCl_2.6H_2O$, 0.025 $mg \cdot L^{-1}$ $CuSO_4.5H_2O$, 36.7 $mg \cdot L^{-1}$ NaFe-EDTA, 6.2 $mg \cdot L^{-1}$ H_3BO_3, 0.83 $mg \cdot L^{-1}$ KI, 16.9 $mg \cdot L^{-1}$ $MnSO_4.H_2O$, 0.25 $mg \cdot L^{-1}$ $Na_2.MoO_4.2H_2O$, 8.6 $mg \cdot L^{-1}$ $ZnSO_4.7H_2O$, 332.02 $mg \cdot L^{-1}$ $CaCl_2.2H_2O$, 170 $mg \cdot L^{-1}$ KH_2PO_4, 1900 $mg \cdot L^{-1}$ KNO_3, 180.5 $mg \cdot L^{-1}$ $MgSO_4.7H_2O$, 1650 $mg \cdot L^{-1}$ NH_4NO_3, 2 $mg \cdot L^{-1}$ glycine, 100 $mg \cdot L^{-1}$ myo-inositol, 0.5 $mg \cdot L^{-1}$ nicotinic acid, 0.5 $mg \cdot L^{-1}$ pyridoxine HCl, 0.1 $mg \cdot L^{-1}$ thiamine HCl), 1% or 3% sucrose. pH adjusted to 5.8 with 1 M NaOH. For solid medium, bacto agar was added to a final concentration of 0.8%.
MS-MES	5 $g \cdot L^{-1}$ Murashige and Skoog (micro and macro elements including vitamins, as above), 0.5 $g \cdot L^{-1}$ 2-(N-morpholino)ethanesulfonic acid (MES), 1% sucrose. pH adjusted to 5.8 with 1 M NaOH. For solid medium, bacto agar was added to a final concentration of 0.8%.
Soil for plant growth	
Arabidopsis mix	Levington F2 peat and 4 mm grit (6:1 ratio), supplemented with 0.28 $g \cdot L^{-1}$ Exemptor®.

Table 2.2 | List of primers used for genotyping.

Name		Sequence (5' to 3')	Allele	Germplasm
PG001	-	ATTTTGCCGATTTCGGAAC	-	SALK lines
PG002	-	TAGCATCTGAATTTCATAACCAATCTCGATACAC	-	SAIL lines
PG003	-	TACGAATAAGAGCGTCCATTTTAGAGTGA	-	SM lines
PG005	-	AACGTCCGCAATGTGTTATTAAGTTGTC	-	WDL lines
PG152	-	AGATTTCCCGGACATGAAGCC	-	GK lines
PG153	-	TCAGATTGTCGTTTCCCGCC	-	GK lines
PG008	LP	GCCTGCTTCAGCTTTTGTATG	*ann1-1*	SALK_132169
PG009	RP	AACGCTACCGACACAACATTC	*ann1-1*	SALK_132169
PG006	LP	TGTTGTTGGTCTCCCTTTTTG	*ann1-2*	SALK_015426
PG007	RP	AATCTTGGCTCACAGAAGTGC	*ann1-2*	SALK_015426
PG038	LP	CTTCTGCAAGATCCTTATGCG	*ann1-3*	WiscDsLox477-480
PG039	RP	CCATGCTCGCTACAAGAAGTC	*ann1-3*	WiscDsLox477-480
PG014	LP	TGGGATCAATCTTTTGGTCTG	*ann2-1*	SALK_054223
PG015	RP	GATGCTTGCAAGATCTGAAGC	*ann2-1*	SALK_054223
PG022	LP	CCTTTTCCTCTTGCAAAGGTC	*ann3-1*	SALK_075525
PG023	RP	CAAAACAAGCTTGAGCCAGTC	*ann3-1*	SALK_075525
PG026	LP	TCCTCAAAACGAAAAATCTCG	*ann3-2*	SALK_082344
PG027	RP	CATAGCCGCCTCAATAGTAGC	*ann3-2*	SALK_082344
PG036	LP	ATAGGTCCATGTGTGTTTCGC	*ann4*	SALK_121732
PG037	RP	AGCTTGAGGTGTCTGACGAAG	*ann4*	SALK_121732
PG122	LP	CAAGCTCTGCAAGGATCAAAC	*cngc1*	SAIL_443_B11
PG123	RP	TAGAAATGAACACCGCGAAAC	*cngc1*	SAIL_443_B11
PG082	LP	AAATCAGAACCTTTAAGCGGC	*cngc3-1*	SALK_056832
PG083	RP	TACCAAAGTTGAAAACCGTCG	*cngc3-1*	SALK_056832
PG084	LP	CTGTTGTGCTCTCCAAATTCC	*cngc4-5*	SALK_081369
PG085	RP	TCACATGGACCTTTTCCATTG	*cngc4-5*	SALK_081369
PG086	LP	GAGCTTTCTGGTTAAGCCGTC	*cngc5-1*	SALK_149893
PG087	RP	CACGCTCCCTAAGATCTTGTG	*cngc5-1*	SALK_149893
PG088	LP	TCGATAAACACCGAAACCAAG	*cngc5-2*	SALK_053354
PG089	RP	GAGACTGGAGGTTGGAATTCC	*cngc5-2*	SALK_053354
PG124	LP	TAAGTGGGCCTTATTATGGCC	*cngc7*	SAIL_59_F03
PG125	RP	TTCACTCTGTTTTACCTGCGG	*cngc7*	SAIL_59_F03
PG094	LP	ACTTGACCCTAAAGCAGGCTC	*cngc8*	SALK_004230
PG095	RP	TCAACCAATCAAAAACCAAGC	*cngc8*	SALK_004230
PG096	LP	ATTTGCAGCAAACTTTGAAGC	*cngc9*	SALK_026086
PG097	RP	TGTTTATGGTGGGGACTTCAG	*cngc9*	SALK_026086
PG150	LP	TTCTCACTGCCAAAGCCATAC	*cngc11*	SM_3.15048
PG151	RP	GGAATCTAGAATTTCGGGCTG	*cngc11*	SM_3.15048
PG100	LP	ATTGATGCATTGAAGTCAGGG	*cngc12*	SALK_092622
PG101	RP	TACTTTGGTTTCGAAGCTTGC	*cngc12*	SALK_092622
PG102	LP	CCTTCTCGAATTGCATAGCTG	*cngc13*	SALK_013536
PG103	RP	TGGCATAGTTACTGAAACCGC	*cngc13*	SALK_013536
1200	-	CAATATGCAAACCAGCAAGCAAG	*cngc15-1*	-

Continued overleaf

Table 2.2 | Continued.

Name		Sequence (5' to 3')	Allele	Germplasm
1201	-	TTAACCGGGTCGCCTTCTCTTACAA	*cngc15-1*	-
PG280	LP	TTTGGTTTGCACAAAATCATG	*cngc16*	SALK_065792
PG281	RP	TTTAACCTGGGCTTTAGTGCC	*cngc16*	SALK_065792
PG114	LP	CGCGGATCTCTTTATTCACAC	*cngc19*	SALK_027306
PG115	RP	ATGAGGATTCATTATTCCGGG	*cngc19*	SALK_027306
PG120	LP	CAGAGTTTGCATGGAACAATG	*dmi1-1*	SALK_066135
PG121	RP	TGTGGTTGTGTTAGCAGAACG	*dmi1-1*	SALK_066135
PG130	LP	TCATATGCAATCTCGAGCATC	*dmi1-2*	SAIL_303_C02
PG131	RP	GAGTTATCCTCTGACTCGGGG	*dmi1-2*	SAIL_303_C02
PG270	LP	GGTTTTCAAGACTTGCATTGC	*glr1.1*	SALK_117347
PG271	RP	ATCGTCGTTGGTAGATGCAAC	*glr1.1*	SALK_117347
PG307	LP	CGGGAGCTTAAGGACTTGGG	*glr1.2*	SALK_114822
PG308	RP	AGGTGCAATGGATGCCTGAA	*glr1.2*	SALK_114822
PG284	LP	TATATTTGGCCAAGCTCAACG	*glr1.4-1*	SALK_129955
PG285	RP	CTTATAGTGCGGGCTTTGTTG	*glr1.4-1*	SALK_129955
PG282	LP	TGTGAGGATCCAAGCATATCC	*glr1.4-2*	SALK_124605
PG283	RP	TTGTATGATTCGCAACACTGG	*glr1.4-2*	SALK_124605
PG144	LP	AAATGATGTTGTTACCGCAGC	*glr2.1*	GK-897G01.05
PG145	RP	CTTGACCTGAGGAGCATTGAC	*glr2.1*	GK-897G01.05
PG286	LP	TCATCTTTCAATGGGACGATC	*glr2.2*	GABI_436H08
PG287	RP	AACATGCCCACAAGAGTGTTC	*glr2.2*	GABI_436H08
PG048	LP	AGGGAAAACATGTGATTGTGC	*glr2.4*	SALK_010571
PG049	RP	TCCAATAATGCCCTTGTCAAG	*glr2.4*	SALK_010571
PG078	LP	CTTCAGGTACTCGATCTTGCG	*glr2.5*	SAIL_1243_E09
PG079	RP	ATTTCCAAAATCCAACCGTTC	*glr2.5*	SAIL_1243_E09
PG050	LP	TCTACGGTGAACCAAAGTTGG	*glr2.6-1*	SALK_066558
PG051	RP	TTTTCACAAGGGTTCTTGTGG	*glr2.6-1*	SALK_066558
PG288	LP	TGAAATGAAATTCGAAACACG	*glr2.6-2*	SALK_115448
PG289	RP	TTTGAAGAGACCAATTCCGC	*glr2.6-2*	SALK_115448
PG052	LP	GGAAATCTTGCCGGTTAAAAG	*glr2.7*	SALK_121990
PG053	RP	ACAAATTTGGGGACATTAGGG	*glr2.7*	SALK_121990
PG146	LP	GAAAGACACTGTGCAGGCTTC	*glr2.8*	CS374123 (GK)
PG147	RP	TTACGCCATATCGAATCTTCG	*glr2.8*	CS374123 (GK)
PG138	LP	TGACAAGGTGCTCCCATTATC	*glr2.9*	SALK_125496
PG139	RP	AGAAATTCATGGTGACGGTTG	*glr2.9*	SALK_125496
PG300	LP	AGATGAACAAACGTGACCACC	*glr3.1*	SALK_063873
PG301	RP	TGGCTTTTTGTGGTTCTGATC	*glr3.1*	SALK_063873
PG054	LP	TTTTGGATCCAGCATTAGTCG	*glr3.2a*	SALK_150710
PG055	RP	TTTTGCGGTTTTGTTTGTAGG	*glr3.2a*	SALK_150710
PG302	LP	GATGCTGCATATGGTTGTGTG	*glr3.3a*	SALK_099757
PG303	RP	GTTGAACGATAAGCTTGCGAG	*glr3.3a*	SALK_099757
PG290	LP	TGCTGTTGATCTCTTGCAATG	*glr3.3b*	SALK_077608
PG291	RP	CACACAACCATATGCAGCATC	*glr3.3b*	SALK_077608

Continued overleaf

Table 2.2 | Continued.

Name		Sequence (5' to 3')	Allele	Germplasm
PG292	LP	CAGCTCTCTTCACCCATCAAG	*glr3.3c*	SALK_082194
PG293	RP	ACCAACCTTTATGGTCCCAAC	*glr3.3c*	SALK_082194
PG060	LP	TTCAGAGAGGAGCCAACAGAG	*glr3.4*	SALK_016904
PG061	RP	TGCAAATTCCGTACAGTAGGG	*glr3.4*	SALK_016904
PG064	LP	TGAAGTTGCTGCAAATGTGAG	*glr3.5-1*	SALK_035264
PG065	RP	TGTCGACATGTCCACAGCTAG	*glr3.5-1*	SALK_035264
PG304	LP	TTCGTTCAAAGGTGGCATAAC	*glr3.6a*	SALK_091801
PG305	RP	CGACTATGAGGAAAGACGCAG	*glr3.6a*	SALK_091801
PG070	LP	ATAGTCGGTGCTGTCATTTGG	*glr3.6b*	SALK_035353
PG071	RP	TCCCCAAAAGCTCTTAAGCTC	*glr3.6b*	SALK_035353
PG074	LP	TGTAAGAAAGAAAGGGAATGGC	*glr3.7*	SALK_101122
PG075	RP	AGCGAAGAGCAATCACAAGTC	*glr3.7*	SALK_101122

Table 2.3 | List of level 2 golden gate vectors generated and used in this work.

Identifier	R1 / Backbone	Position R2			Position R3			Position R4			End linker
		P[1]	CDS[2]	T[3]	P[1]	CDS[2]	T[3]	P[1]	CDS[2]	T[3]	
Ca^{2+} reporters											
R-GECO1.2-BAR	pNOS-BAR-tNOS	*LjUbi*	*R-GECO1.2*	*t35S*	-	-	-	-	-	-	EC41744
R-GECO1.2-HYG	p35S-HPTII-tNOS	*LjUbi*	*R-GECO1.2*	*t35S*	-	-	-	-	-	-	EC41744
Split-YFP vectors											
L2-102	pNOS-BAR-tNOS	*LjUbi*	*YNE-CNGC15*	*t35S*	*AtUbi10*	*DMI1-YCE*	*tOCs*	*p35S*	*DsRed*	*t35S*	EC41780
L2-103	pNOS-BAR-tNOS	*LjUbi*	*YNE-CNGC15*	*t35S*	*AtUbi10*	*dmi1-1-YCE*	*tOCs*	*p35S*	*DsRed*	*t35S*	EC41780
L2-105	pNOS-BAR-tNOS	*LjUbi*	*DMI1-YNE*	*t35S*	*AtUbi10*	*DMI1-YCE*	*tOCs*	*p35S*	*DsRed*	*t35S*	EC41780
L2-106	pNOS-BAR-tNOS	*LjUbi*	*CNGC15-YNE*	*t35S*	*AtUbi10*	*CNGC15-YCE*	*tOCs*	*p35S*	*DsRed*	*t35S*	EC41780
L2-107	pNOS-BAR-tNOS	*LjUbi*	*YNE-CNGC15*	*t35S*	*AtUbi10*	*CNGC15-YCE*	*tOCs*	*p35S*	*DsRed*	*t35S*	EC41780
L2-108	pNOS-BAR-tNOS	*LjUbi*	*dmi1-1-YNE*	*t35S*	*AtUbi10*	*dmi1-1-YCE*	*tOCs*	*p35S*	*DsRed*	*t35S*	EC41780
L2-110	pNOS-BAR-tNOS	*LjUbi*	*YNE-CNGC15-1*	*t35S*	*AtUbi10*	*DMI1-YCE*	*tOCs*	*p35S*	*DsRed*	*t35S*	EC41780
L2-111	pNOS-BAR-tNOS	*LjUbi*	*CNGC15-1-YNE*	*t35S*	*AtUbi10*	*CNGC15-1-YCE*	*tOCs*	*p35S*	*DsRed*	*t35S*	EC41780

[1]Promoter
[2]Coding sequence
[3]Terminator

Table 2.4 | List of Gateway vectors generated and used in this work.

Identifier	CDS	Codon usage	Vector backbone	Entry vector
Entry vectors				
GE017	*GLR3.1*	Yeast	pENTR221	-
GE018	*GLR3.2*	Yeast	pENTR221	-
GE019	*GLR3.3*	Yeast	pENTR221	-
GE020	*GLR3.4*	Yeast	pENTR221	-
GE021	*GLR3.5*	Yeast	pENTR221	-
GE022	*GLR3.6*	Yeast	pENTR221	-
GE023	*GLR3.7*	Yeast	pENTR221	-
Expression vectors				
GX046	*GLR3.1*	Yeast	pYES-DEST52	GE017
GX047	*GLR3.2*	Yeast	pYES-DEST52	GE018
GX048	*GLR3.3*	Yeast	pYES-DEST52	GE019
GX049	*GLR3.4*	Yeast	pYES-DEST52	GE020
GX050	*GLR3.5*	Yeast	pYES-DEST52	GE021
GX051	*GLR3.6*	Yeast	pYES-DEST52	GE022
GX052	*GLR3.7*	Yeast	pYES-DEST52	GE023

Table 2.5 | List of primers used for qPCR and RT-PCR.

Name	Direction	Sequence (5' to 3')	Gene	Efficiency
qPCR				
PG186	Forward	CAAGACTGAGCTGAGGGCAA	*CNGC15*	E = 100.1%; T_a = 58 ˚C
PG187	Reverse	CCACCATTCACTGCTAGCCT		
PG198	Forward	GTTATCGCCTTGCGGGAATG	*DMI1*	E = 111.1%; T_a = 58 ˚C
PG199	Reverse	ACTGACTTGAGGCGATGACA		
PG226	Forward	GCATGGGTCTCAGTCAGGTG	*GLR3.1*	E = 99.60%; T_a = 56 ˚C
PG227	Reverse	TCTTTGCAGAAGTCGCGGAT		
PG230	Forward	GCCAACCGATGATGCCATTG	*GLR3.3*	E = 88.70%; T_a = 56 ˚C
PG231	Reverse	TGCTTTCGTGCTTGGACTCT		
PG236	Forward	GCAGAAGGGTCGATCAGGAG	*GLR3.6*	E = 84.80%; T_a = 58 ˚C
PG237	Reverse	GACCTAGCCTTGGCGTCTTC		
PG311	Forward	TGCAGCGCAAGGACTAGAG	*FRK1*	E = 103.3%; T_a = 56 ˚C
PG312	Reverse	ATCTTCGCTTGGAGCTTCTC		
PG315	Forward	TACCTCTAATGGCTTCCCGC	*AT2G17740*	E = 90.40%; T_a = 56 ˚C
PG316	Reverse	CAACTTGGGCTTTGTGACCG		
PG319	Forward	TGCGCTGCCAGATAATACACTATT	*UBOX*	E = 100.8%; T_a = 56 ˚C
PG320	Reverse	TGCTGCCCAACATCAGGTT		E = 105.0%; T_a = 58 ˚C
PG321	Forward	TGTTTTCCCGATCAAGTGCG	*NHL10*	E = 102.9%; T_a = 56 ˚C
PG322	Reverse	AGAAGATAAGTCGTAGGGATGCAA		
PG329	Forward	TTGGTTTAGACGGGATGGTG	*PHI-I*	E = 98.30%; T_a = 56 ˚C
PG330	Reverse	ACTCCAGTACAAGCCGATCC		
PG496	Forward	TACTCCGAGACCTTCCAACTACG	*PIN1*	E = 100.2%; T_a = 58 ˚C
PG497	Reverse	TCCACCGCCACCACTTCC		
PG498	Forward	AAGGCGGAAGATCTGACCAAGG	*PIN3*	E = 97.00%; T_a = 58 ˚C
PG499	Reverse	TGCTGGATGAGCTACAGCTTTG		
PG502	Forward	CGGCTGATATTGATAATGGTGTGG	*PIN7*	E = 105.2%; T_a = 58 ˚C
PG503	Reverse	GCAATGCAGCTTGAACAATGG		
PG506	Forward	ATCATAGCCGGTGGTTCCAA	*IPT5*	E = 101.1%; T_a = 58 ˚C
PG507	Reverse	GCAATCGTTGACCAGAGCCT		
PG508	Forward	AAACCTAACGGCCACCCAGT	*IPT7*	E = 100.3%; T_a = 58 ˚C
PG509	Reverse	TCCACCGGCTACTATGGGAA		
PG510	Forward	GTGACCAGGCCAAGAACTTA	*AHK3*	E = 98.20%; T_a = 58 ˚C
PG511	Reverse	CTTCCCTGTCCAAAGCAA		
PG514	Forward	CGGTGCGGTTGATTACCTTA	*ARR1*	E = 97.60%; T_a = 58 ˚C
PG515	Reverse	CGGTACACTCCATTCACTTCTC		
PG516	Forward	GTTGCATGTTCTTGCCGTCGATGA	*ARR7*	E = 98.80%; T_a = 58 ˚C
PG517	Reverse	ACTGCAAAGCCCTAGTTCCACTCT		
PG518	Forward	AGAGGTGGTGAAGCTGAAGAAGGA	*ARR15*	E = 96.90%; T_a = 58 ˚C
PG519	Reverse	TCCTCTTGGAAGATGGAGTGTCGT		
PG528	Forward	GTTTGGACTGTTGAGCTGC	*ARR12*	E = 95.10%; T_a = 58 ˚C
PG529	Reverse	ATTAGCCACACCACTGATCC		
RT-PCR				
PG395	Forward	TGACTTGAGGCGATGACAACA	*DMI1*	-
PG421	Reverse	CGAGTCAATCCCCGAGTCAG	*DMI1*	-
PG422	Reverse	GGTGAAAAGAAAAACCACCCCA	*DMI1*	-
PG423	Reverse	CTCCCATATCTGCGCAAGACC	*DMI1*	-

Chapter III

Tools for imaging and quantifying calcium signals

3.1. Introduction

Calcium (Ca^{2+}) is an important second messenger in eukaryotes, linking extracellular stimuli to intracellular responses and participating in a multitude of signalling pathways. The versatility of the Ca^{2+} signals, varying in amplitude, speed, frequency, and spatial distribution, accounts for its ability to regulate a large variety of responses (Berridge *et al*., 2000). *In vivo* measurement of the [Ca^{2+}] with cellular and subcellular resolution is thus required to understand the complex roles that Ca^{2+} plays in signalling pathways, and constitutes a powerful phenotypic tool.

A variety of bioluminescent or fluorescent Ca^{2+} sensors has been developed, which can be grouped into either small-molecule injectable dyes, such as Fura-2 (Grynkiewicz *et al*., 1985), or genetically-encoded Ca^{2+} sensors. The latter are favoured over the former, since they are less technically challenging, and offer the advantages of tissue-specific expression and subcellular targeting (Kanchiswamy *et al*., 2014). The use of dyes, on the other hand, is desirable in systems in which transformation is not feasible, however only cell types accessible to a micropipette can be injected.

Aequorin was the first genetically-encoded bioluminescent Ca^{2+} sensor to be used in plants (Knight *et al*., 1991). It has since been employed to report a variety of Ca^{2+} responses, including salt and drought stress (Knight *et al*., 1997; Kiegle *et al*., 2000; Zhang *et al*., 2015), innate immune signalling (Kwaaitaal *et al*., 2011; Ranf *et al*., 2011; Maintz *et al*., 2014), temperature shock (Knight *et al*., 1991; Campbell *et al*., 1996; Gong *et al*., 1998), and wounding (Kiep *et al*., 2015). Aequorin is composed of an apoprotein (apoaequorin) and the luminophore coelenterazine. The protein possesses three Ca^{2+}-binding EF-hand domains and, when these are occupied by Ca^{2+}, it undergoes a conformational change that allows the oxidation of coelenterazine to coelenteramide, producing CO_2 (Shimomura *et al*., 1974). Blue

light is emitted when coelenteramide relaxes to its ground state (Shimomura and Johnson, 1970). The main advantages of aequorin, as opposed to other genetically-encoded sensors, are its high signal-to-noise ratio and the lack of need for an external light source, avoiding photobleaching and autofluorescence (Plieth, 2001). It is also very scalable, which allows for high-throughput screening (Tanaka *et al*., 2013). As a result, aequorin has successfully been used in many mutant screens that led to the identification of an extracellular ATP receptor (Choi *et al*., 2014a), a Ca^{2+} channel involved in osmotic stress (Yuan *et al*., 2014), a receptor for lipopolysaccharide (Ranf *et al*., 2015), and several genes central to innate immunity (Ranf *et al*., 2012). However, it is non-ratiometric and has a low spatiotemporal resolution, since the low light emission characteristic of this system forces signal detection to occur from whole seedlings or tissues (Alonso *et al*., 2009; Plieth, 2001). Mathematical modelling has additionally shown that aequorin cannot resolve single-cell oscillatory Ca^{2+} signals (Dodd *et al*., 2006).

Fluorescent Ca^{2+} sensors, on the other hand, offer higher spatial and temporal resolution, allowing imaging and quantification of Ca^{2+} in single cells. These Ca^{2+} sensors can be classified as ratiometric or intensiometric. Yellow cameleons (YC) are the most commonly used ratiometric sensors, and are composed of an enhanced cyan fluorescent protein (ECFP) and a yellow fluorescent protein (YFP), linked by calmodulin (CaM), a glycylglycine linker, and the myosin light-chain kinase peptide (M13), which binds CaM in a Ca^{2+}-dependent manner (Ikura *et al*., 1992; Porumb *et al*., 1994). Binding of Ca^{2+} to CaM results in a conformational change that brings both fluorophores closer together, allowing Förster resonance energy transfer (FRET) to occur (Miyawaki *et al*., 1997). As a result, some of the energy previously emitted by ECFP now excites YFP, leading to a concomitant increase in the YFP and decrease in ECFP fluorescence emission intensities. Measuring both the YFP and ECFP emissions and calculating their ratio prevents optical artefacts that can arise due to varying amounts of the fluorescent protein, caused by differences in expression or distribution, instrument noise, or sample motion (O'Connor and Silver, 2013; Pérez Koldenkova and Nagai, 2013). These advantages have resulted in the ratiometric sensor YC3.6 (Nagai *et al*., 2004) becoming the most frequently published Ca^{2+} reporter in plants (Choi *et al*., 2012). YC3.6 has been used to document Ca^{2+} responses to auxin (Monshausen *et al*., 2011; Shih *et al*., 2015), cold, and nodulation factor, (Krebs *et al*., 2012), growing pollen tubes (Michard *et al*., 2011), the immunogenic peptide of flagellin, flg22 (Thor and Peiter, 2014; Keinath *et al*., 2015),

stomatal responses to extracellular Ca^{2+} (Weinl *et al*., 2008), mechanical stimulation (Monshausen *et al*., 2009), growing root hairs (Monshausen *et al*., 2008), and nucleoside triphosphates, including ATP (Tanaka *et al*., 2010; Krebs *et al*., 2012).

Intensiometric, single-fluorophore, Ca^{2+} sensors typically relay a change in fluorescent intensity upon Ca^{2+} binding. These sensors are usually composed of a circularly-permuted fluorescent protein fused to CaM and M13. Similarly to YCs, the interaction of the M13 and the CaM domains upon Ca^{2+} binding induces conformational changes, which, in the case of intensiometric sensors, alter the protonation state of the fluorescent protein and increase its brightness (Wang *et al*., 2008; Akerboom *et al*., 2009). Unlike ratiometric sensors, these reporters allow a simpler imaging set-up, as they do not require an image splitter or fast switching between different excitation and emission settings, and often have a higher dynamic range and faster association/dissociation kinetics due to their smaller molecular size (Okumoto, 2012). This grants increased spatial and temporal resolution (Tian *et al*., 2009). Having single differently coloured sensors also offers the possibility of performing multiple parameter acquisition. This allows, for instance, the simultaneous imaging of Ca^{2+} in different subcellular locations, through subcellular targeting of differently coloured sensors, or the parallel quantification of Ca^{2+} and other molecules, such as recently demonstrated by Waadt *et al*. (2017) for abscisic acid (ABA). The main disadvantages of single-fluorophore sensors include pH sensitivity and changes in intensity due to variations in the concentration of the sensor itself. The GECO family of Ca^{2+} sensors is an example of this type of reporters (Zhao *et al*., 2011). In Arabidopsis, R-GECO1 has been shown to relay Ca^{2+} responses to ATP, flg22, and chitin. The same study demonstrated that R-GECO1 has a higher signal-to-noise ratio than YC3.6 (Keinath *et al*., 2015). It was also found that R-GECO1 reports Ca^{2+} peaks during pollen tube reception in living ovules (Ngo *et al*., 2014). Another example of an intensiometric sensor is GCaMP3 (Tian *et al*., 2009), recently used to characterise the Ca^{2+} response occurring during aphid feeding (Vincent *et al*., 2017).

In a recent study, R-GECO1 was fused to a reference, spectrally non-overlapping, fluorescent protein (mTurquoise (Goedhart *et al*., 2010)) to create a sensor that combines the high sensitivity of R-GECO1 with the advantages of ratiometric sensors. This reporter has a higher dynamic range than FRET-based indicators, such as YC3.6 or YC-Nano50 (Waadt *et al*., 2017).

In this chapter, I summarise the experiments performed using the Ca^{2+} sensors YC3.6, R-GECO1.2, as well as the testing of a dual sensor G-GECO1.2-NES/R-GECO1.2-NLS. I compare how different sensors relay the same stimulus and how the use of a dually targeted sensor can distinguish nuclear and cytosolic Ca^{2+} signals.

3.2. Results

3.2.1. Experimental set-up

Two main ways to mount samples for live Ca^{2+} imaging were used in this work: perfusing and non-perfusing (Figure 3.1). Non-perfusing chambers are simple to prepare and easier to set up (Figure 3.1 a, b), more appropriate if the volume of elicitor is limiting, and convenient if no elicitors are being applied, such as the experiment described in Chapter V. However, this system does not allow the accurate and reproducible quantification of the response time to the application of a specific elicitor, as the time between application and sample contact varies for each sample (mostly dependent on the diffusion time of the elicitor through the chamber volume). Additionally, sample movement upon treatment application can occur, meaning that the previously imaged baseline does not match the cells being quantified after treatment application. To circumvent this issue, I set up a live imaging perfusion system that allows continuous perfusion of the sample with medium and treatment application with minimum perturbation of the sample (Figure 3.1 c). It is also possible to stop perfusion after the whole chamber volume has been exchanged with medium containing the elicitor of interest, which is important if the elicitor is limiting.

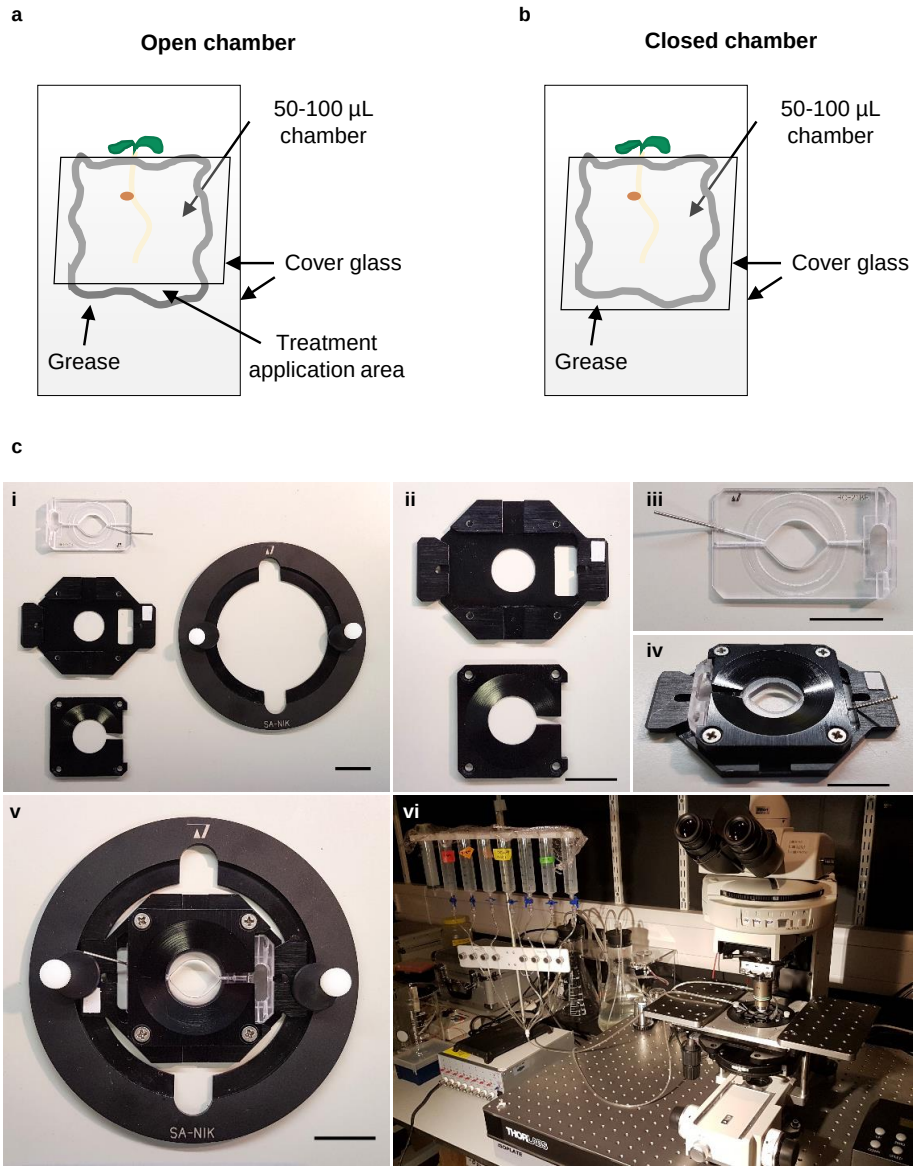

Figure 3.1 | Experimental set-up for Ca^{2+} imaging.

a, b, Schematic representation of an open (a) and closed (b) non-perfusing imaging chamber. For each plant being imaged, a small 50-100 µL chamber was built using coverslips and vacuum grease. The set-up varied slightly according to the tissue being imaged (roots or cotyledons/leaves). c, Perfusion system experimental set-up. i, RC-21BR chamber (top left), P-2 platform (middle and bottom left), and microscope stage adapter (right). ii, P-2 platform. iii, RC-21BR perfusion chamber. iv, Perfusion chamber assembled on the platform. v, Chamber assembled in the platform, secured in the microscope stage adapter. vi, Complete set-up, including the eight channel perfusion valve control system (bottom right), the vacuum pump, and the assembled perfusion chamber on the microscope stage (all equipment was acquired from Warner Instruments, Harvard Apparatus, https://www.warneronline.com). Scale bars represent 2 cm.

3.2.2. YC3.6 as a versatile tool to image Ca^{2+} signals

Col-0 plants expressing YC3.6 were generated by Marco Pitino in the groups of Anthony Miller and Dale Sanders and kindly provided by Thomas Vincent. The vector used is described in Krebs *et al*. (2012) (YC3.6-Kan, lacking localisation signals).

Previous work in Arabidopsis has demonstrated that ATP elicits a Ca^{2+} response that can be quantified using YC3.6 (Krebs *et al*., 2012). To validate the sensor, I used ATP to replicate the same study. Repeated applications of ATP to a final concentration of 100 µM resulted in an increase in the $[Ca^{2+}]$, a signal characterised by a sharp peak followed by a second and third smaller peaks, in epidermis cells in the root differentiation zone (Figure 3.2 a, b).

To test the versatility of the perfusion system, I used cold as a Ca^{2+}-inducing stimulus (Knight *et al*., 1996; Allen *et al*., 2000; Krebs *et al*., 2012). Both roots and leaves showed a single peak in $[Ca^{2+}]$, which starts approximately 15 seconds upon exchange of perfusion of room-temperature medium with ice-cold medium, and lasts for approximately 60 seconds (Figure 3.2 c-f). Importantly, perfusion alone did not induce any Ca^{2+} signal.

To further assay the capacity of YC3.6 to report Ca^{2+} changes induced by endogenous signalling molecules, auxin was used as a stimulus. In roots, an increase in $[Ca^{2+}]_{cyt}$ is the fastest known physiological response to higher levels of auxin (Monshausen *et al*., 2011), an effect which was shown to be dependent on CNGC14 (Shih *et al*., 2015). Upon treatment with 10 µM IAA, which was applied close to the root tip, all plants tested (4/4) showed a marked increase in $[Ca^{2+}]$ in the root tip, establishing a wave that moved shootwards (Figure 3.3). The Ca^{2+} signal appeared first in the columella and lateral root cap, and spread shootwards first through the epidermis and cortex files, and later through the stele. In the columella root cap, the signal was characterised by a sharp peak that equilibrated at levels below the baseline within one minute (ROI 1). In the lateral root cap and the cortex and epidermal cells closer to the quiescent centre (ROI 2), the peak was, to a three second resolution, simultaneous to the one in the root tip, but after a small decrease, there was a second, wider peak that decreased to levels below the baseline over a period of ten min. This was similar to the signal observed in the stele at the beginning of the elongation zone (ROI 3), which was characterised by a sharp rise followed by a small decrease, but afterwards the $[Ca^{2+}]$ was maintained higher than

baseline over a period of at least 15 min. Higher up in the elongation zone (ROI 4), the signal was characterised by a single, wide peak that slowly returned to baseline levels over 15 min.

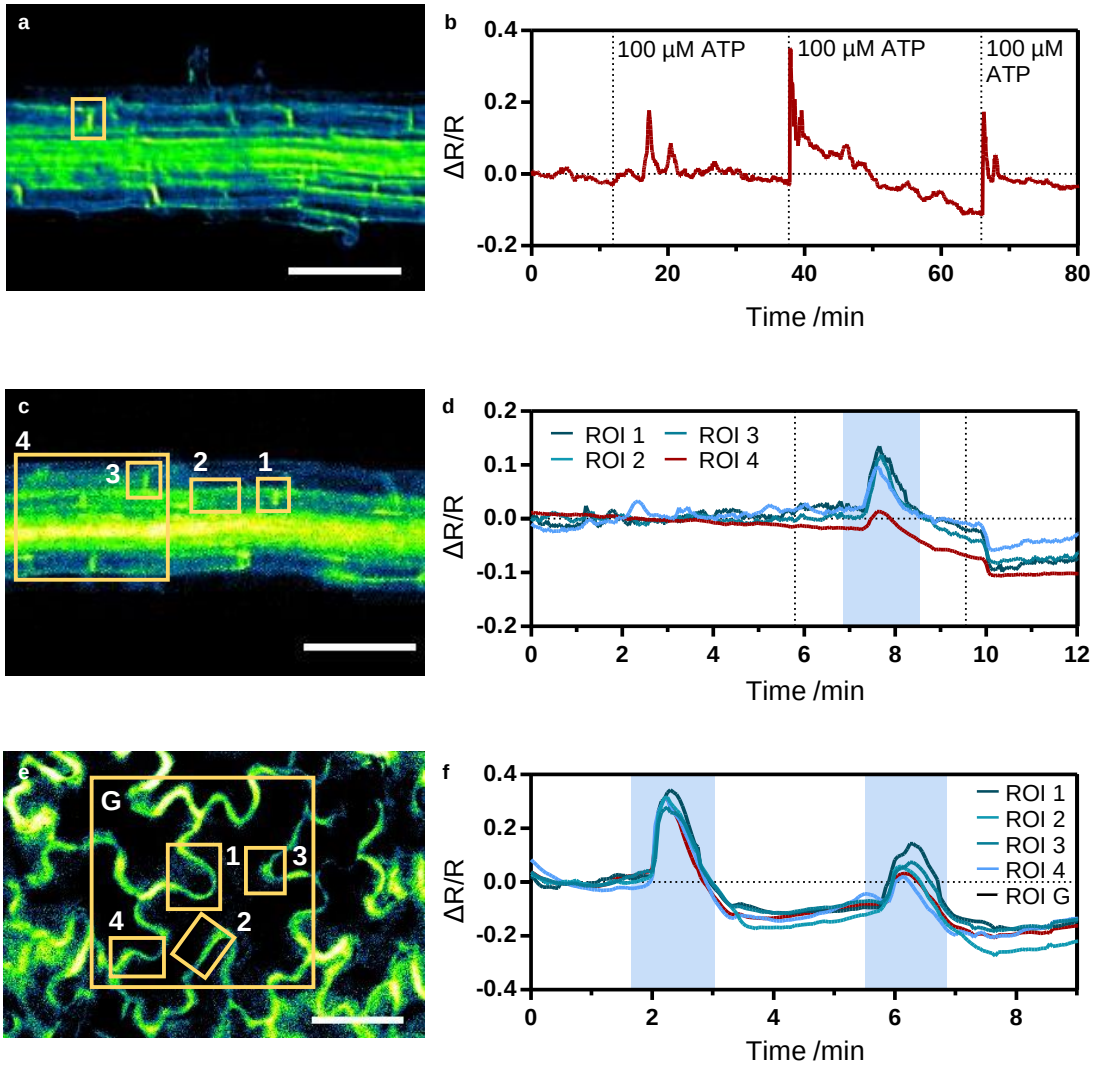

Figure 3.2 | YC3.6 reports Ca^{2+} dynamics to different stimuli in root and leaf tissues.

a, b, Ca^{2+} signals induced by successive application of 100 µM ATP in a lateral root of a 2-week-old plant expressing YC3.6. Dashed vertical lines in b mark the moment of treatment application. c-f, Cold-induced Ca^{2+} signals in a lateral root of a 3-week old plant (c, d) or a 2-week old leaf (e, f) expressing YC3.6. Ice-cold medium was perfused through the sample during the periods shaded blue in d and f. Dashed vertical lines in d mark the start and end perfusion with room-temperature medium. Scale bars represent 100 µm (a, c) and 20 µm (e).

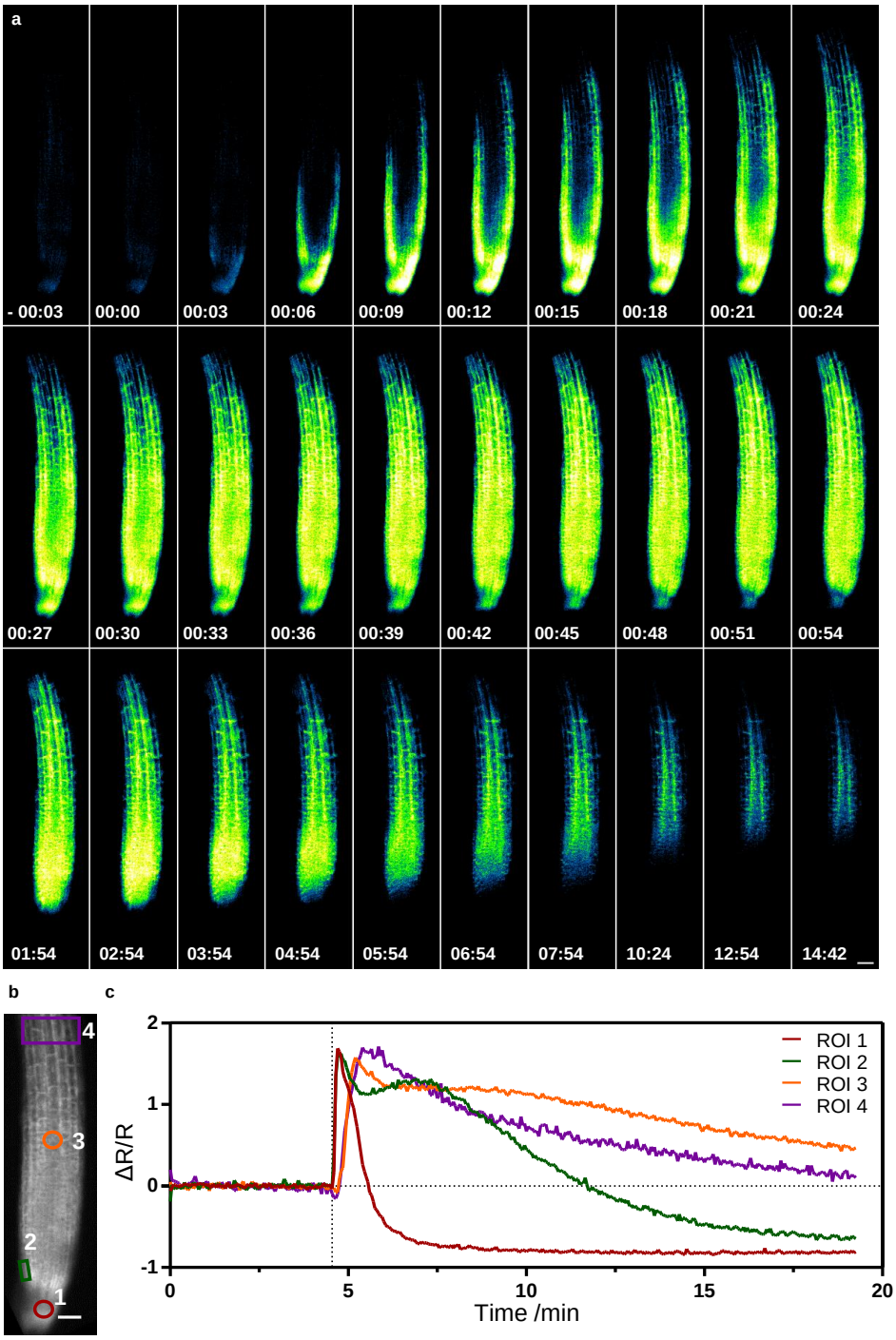

Figure 3.3 | YC3.6 reports Ca^{2+} dynamics to auxin treatment.

Representative live imaging of a root of a 7-day-old plant expressing YC3.6 upon application of 10 µM IAA. a, Time-lapse images showing the progression of the signal through time and along the tissue (timestamps are in minutes and seconds, and time zero corresponds to treatment application). c, Quantification of the IAA-induced Ca^{2+} signal in different regions of interest (ROI), marked in b. The dashed vertical line marks the moment of IAA application. Scale bars represent 50 µm.

3.2.3. Investigating the flg22-induced Ca^{2+} response using YC3.6

Having established that YC3.6 can quantify Ca^{2+} signals induced by a variety of stimuli, and with a perfusion system in place that allows the accurate quantification of treatment response times, I aimed to carefully characterise the flg22-induced Ca^{2+} response. Even though positive signals were detected in roots, leaves, and cotyledons (Table 3.1, Figure 3.4), on average only 16% of the plants tested showed Ca^{2+} responses to flg22 treatment. Nonetheless, it is possible that there is a correlation between a positive response and developmental age.

Table 3.1 | Summary of experimental conditions tested and percentage of wild-type plants showing a positive flg22-induced Ca^{2+} response, using YC3.6.

Tissue	Age	[flg22]	Positive signals
Cotyledon	4-6 d	10^{-6} M	12% (2/17 plants)
Cotyledon	8 d	10^{-5} M	33% (1/3 plants)
Leaf	11-19 d	10^{-5} M	20% (1/5 plants)
Leaf	9-14 d	10^{-6} M	0% (0/6 plants)
Leaf (soil-grown)	4-week	10^{-6} M	23% (3/13 plants)
Root	8-9 d	10^{-6} M	0% (0/8 plants)
Root	7-10 d	10^{-5} M	20% (1/5 plants)
Root	15-17 d	10^{-5} M	15% (2/13 plants)
Root	16 d	10^{-4} M	40% (2/5 plants)
		Total	16% (12/75 plants)

In root epidermal cells, 10^{-5} M flg22 induced a Ca^{2+} peak, followed by a second, longer peak that decreased more slowly to levels below baseline over a period of ten min (Figure 3.4 a, b). In 19-day-old abaxial leaf epidermis cells, the response started immediately upon application of 10^{-5} M of flg22 (Figure 3.4 c, d). The signal consisted of a single peak that reached the maximum amplitude in approximately 40 s. In 4-week-old leaf discs collected from soil-grown plants, 10^{-6} M flg22 induced a similar response in abaxial epidermis cells after 72 s, reaching the maximum amplitude in approximately 54 s. Cells were seemingly synchronous to a 3 s resolution (Figure 3.4 e, f).

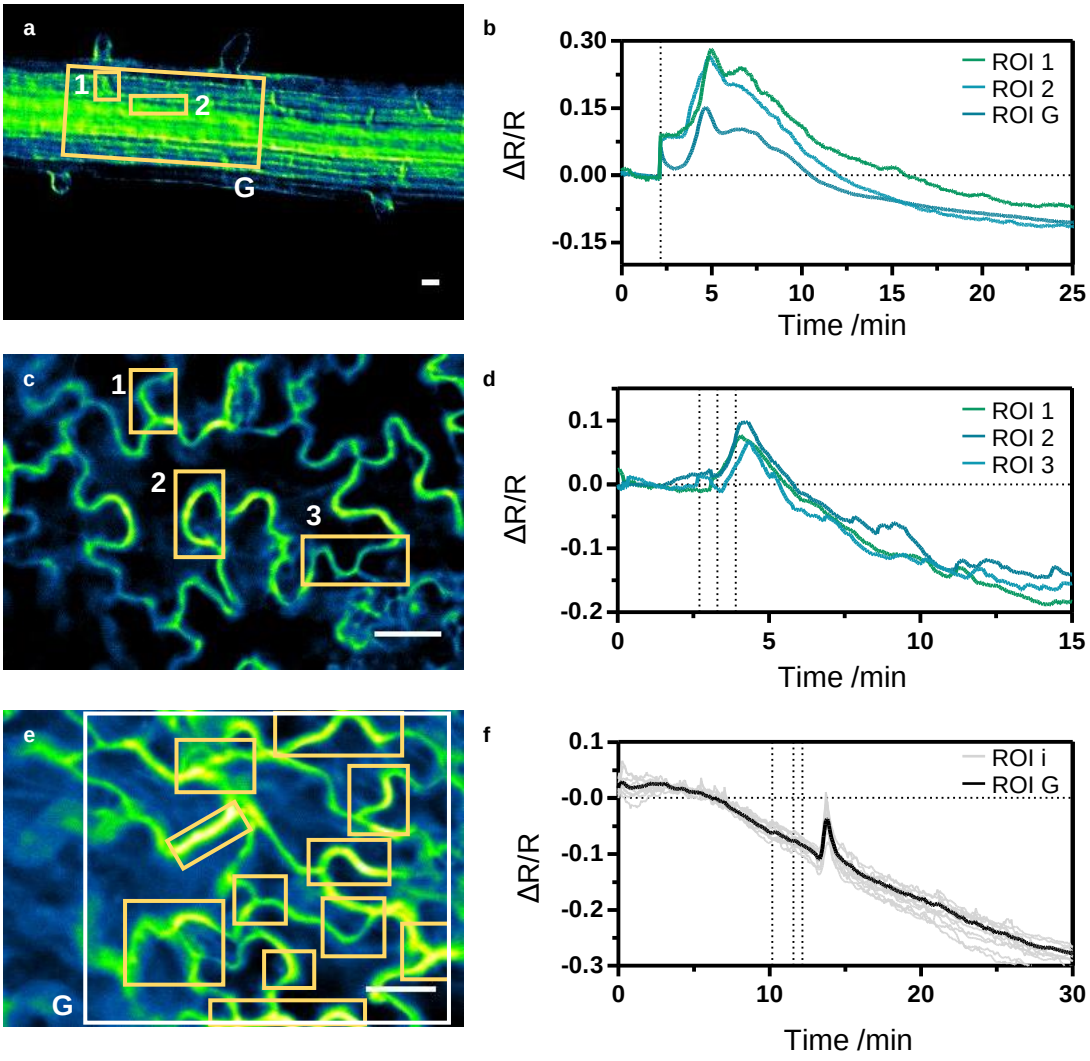

Figure 3.4 | YC3.6 reports Ca^{2+} dynamics to flg22 treatment.

a, b, Ca^{2+} signals induced by application of 10^{-5} M flg22 (open chamber) in a root of an 8-day-old plant expressing YC3.6. Dashed vertical lines in b mark the moment of treatment application. c, d, Ca^{2+} signals induced by application of 10^{-5} M flg22 (perfusion) in a leaf of a 19-day-old plant expressing YC3.6. e, f, Ca^{2+} signals induced by application of 10^{-6} M flg22 (perfusion) in a leaf disc of a 4-week old soil-grown plant expressing YC3.6. In d and f, the first dashed vertical line marks the start of perfusion, the second marks the moment flg22 started being perfused, and the third the moment perfusion was stopped (after the entire volume of the chamber had been replaced by medium containing flg22). Regions of interest are marked in a, c, e, and quantified in b, d, and f, respectively. Scale bars represent 20 µm.

3.2.4. R-GECO1.2 as a tool to image Ca^{2+} in plants

The R-GECO1.2 Ca^{2+} reporter was generated through directed evolution of R-GECO1, i.e., screening for a higher intensity change upon Ca^{2+} binding in *E. coli* expressing a library created through error-prone PCR (Wu *et al*., 2013). In comparison to R-GECO1 (Zhao *et al*., 2011), R-GECO1.2 has eight amino acid changes that account for a two-fold increased intensity change upon Ca^{2+} binding (33 x as opposed to 16 x for R-GECO1) and a dissociation constant (K_d) for Ca^{2+} of 1200 nM (482 nM for R-GECO1; in vitro calibration). Recently, the intensity change upon Ca^{2+} binding and K_d for Ca^{2+} of R-GECO1 were re-estimated *in vivo*, in roots of Arabidopsis plants expressing R-GECO1, and found to be 5.8 x and 158 nM, respectively (Waadt *et al*., 2017). In addition, the R-GECO1.2 construct also includes four synonymous point mutations that eliminate restriction sites used in the golden gate system. These sequences were cloned under the *Lotus japonicus UBIQUITIN10* promoter (Figure 3.5) and stably transformed into Arabidopsis (Col-0). T2 and T3 plants were screened for fluorescence and ability to relay Ca^{2+} signals using voltage stimulation. Previous reports using aequorin have shown that imposing voltage elicits increases in $[Ca^{2+}]_{cyt}$, that different voltage treatments induce different Ca^{2+} signals, and that each distinct type of signal translates different transcriptional responses (Whalley *et al*., 2011; Whalley and Knight, 2013). This is also a simple, reliable, and fast way to screen multiple independent lines. As shown in Figure 3.6, imposing 15 V for 5 s every 40 s repeatedly resulted in increases in R-GECO1.2 fluorescence, both in leaves and roots of R-GECO1.2 expressing plants.

To assay the potential of R-GECO1.2 to relay the Ca^{2+} response to an abiotic elicitor, I tested cold using the perfusion system. Three sequential cold pulses induced three sequential peaks in R-GECO1.2 fluorescence (Figure 3.7). Similarly to what was observed with YC3.6 (Figure 3.2), the response started approximately after 15 s of perfusion of cold medium, and the signal lasted for approximately 60 s. In accordance with previous reports (Knight *et al*., 1996; Krebs *et al*., 2012), the amplitude of the cold-induced Ca^{2+} signals was attenuated after successive cold-shock applications.

Flg22 was also used as an elicitor, but no signals were observed. Using 14-day-old leaf samples, taken from plants shown to be responsive to voltage stimulation, no flg22-induced Ca^{2+} signals were detected (0/4 plants, [flg22] = 10^{-7} M; 0/3 plants, [flg22] = 10^{-4} M).

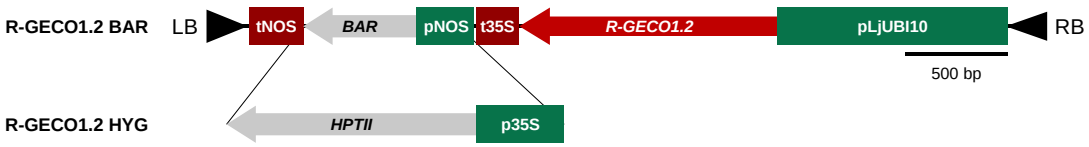

Figure 3.5 | R-GECO1.2 expression vectors.

Schematic representation of the golden gate pL2V-1-50505-based R-GECO1.2 expression vectors. The R-GECO1.2 expression cassette is flanked by the *L. japonicus UBIQUITIN10* (*UBI10*) promoter and the 35S terminator (t35S). The vectors are available with different plant selection genes, *BAR* and *HYGROMYCIN PHOSPHOTRANSFERASE II* (*HPTII*), conferring resistance to glufosinate and hygromycin B, respectively. Expression of the selection markers is controlled by the nopaline synthase (NOS) promoter or the 35S promoter, and the NOS terminator.

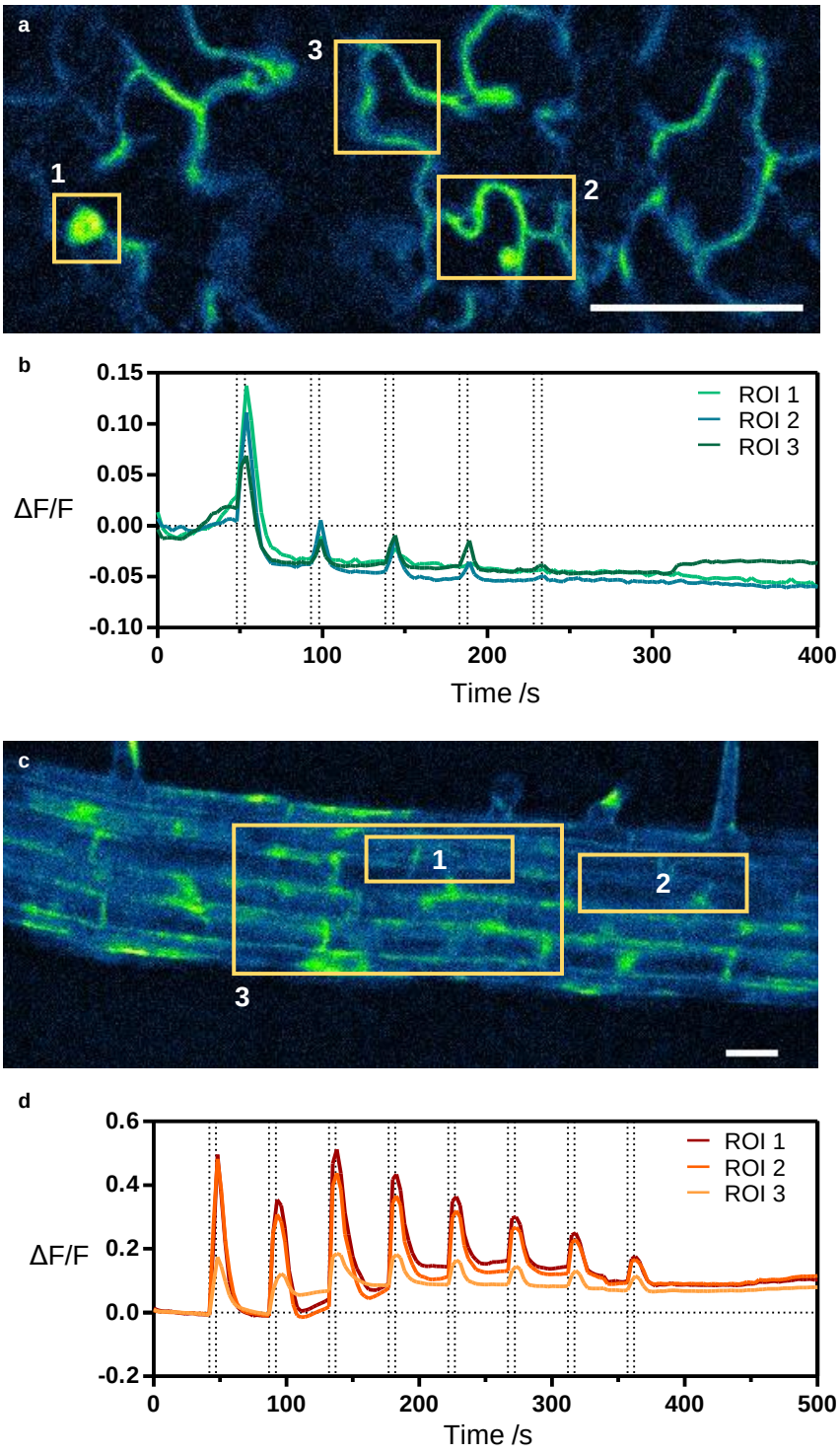

Figure 3.6 | R-GECO1.2 reports Ca^{2+} dynamics to voltage stimulation.

a, b, Ca^{2+} signals induced by voltage stimulation in a leaf of a 3-week-old plant expressing R-GECO1.2. Scale bar represents 50 µm. c, d, Ca^{2+} signals induced by voltage stimulation in a root of a 3-week-old plant expressing R-GECO1.2. Scale bar represents 30 µm. Regions of interest are marked in a and c, and are quantified in b and d, respectively. Dashed vertical lines mark the moment of voltage stimulation (15 V for 5 s).

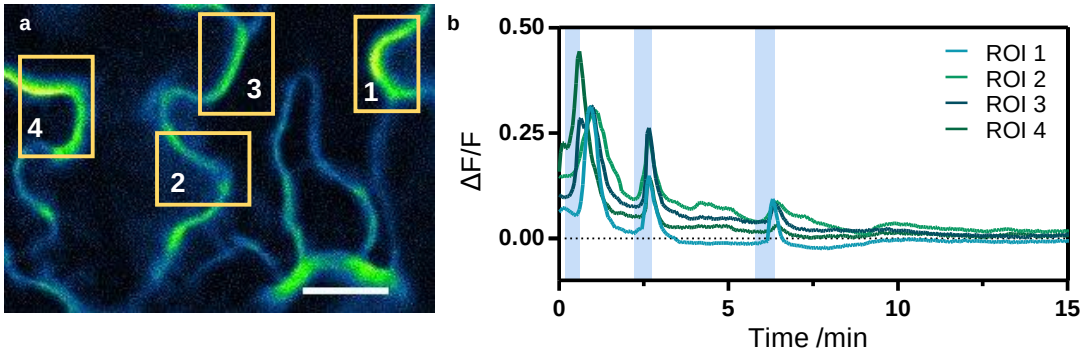

Figure 3.7 | R-GECO1.2 reports Ca^{2+} dynamics to cold treatment.

a, b, Cold-induced Ca^{2+} signals in a leaf of a 2-week-old plant expressing R-GECO1.2. Ice-cold medium was perfused through the sample during the periods shaded blue in b. Regions of interest are marked in a and quantified in b. Scale bar represents 20 µm.

3.2.5. Development of a dual nuclear and cytosolic Ca^{2+} sensor

Genetically-encoded Ca^{2+} reporters offer the possibility of subcellular resolution through targeting of the reporter to specific subcellular compartments. The GECO Ca^{2+} reporters have been generated in a variety of fluorescent proteins (Zhao *et al*., 2011; Wu *et al*., 2013), and so it is conceivable to design a dual reporter, in which two GECO fluorophores with non-overlapping emission wavelengths are targeted to different subcellular compartments. This should allow for a simultaneous quantification of Ca^{2+} signals in distinct cellular compartments within the same cell, and possibly the determination of intracellular movement of Ca^{2+}. To this effect, the vector depicted in Figure 3.8 was developed by Myriam Charpentier, featuring R-GECO1.2 upstream of a nuclear localisation signal (NLS) and Green (G)-GECO1.2 upstream of a nuclear exclusion signal (NES) (Figure 3.8). These sequences were cloned using the golden gate cloning system under the Arabidopsis and *L. japonicus UBIQUITIN10* promoters (Figure 3.8) and stably transformed into Arabidopsis (Col-0). T2 and T3 plants were screened for fluorescence under hygromycin B selection. G-GECO1.2 and R-GECO1.2 have similar K_d for Ca^{2+} (1150 nM and 1200 nM, respectively), yet G-GECO1.2 has a smaller intensity change upon Ca^{2+} binding (23 x as opposed to 33 x for R-GECO1.2) (Zhao *et al*., 2011; Wu *et al*., 2013). This means that both sensors should be able to report the same range of signals, but that weaker signals might be more readily observable by R-GECO1.2. This should guarantee that if different Ca^{2+} kinetics are seen in different cell compartments, this is due to a localisation effect rather than an affinity effect of the sensors to Ca^{2+}.

Similar to YC3.6, the dual sensor was able to detect an ATP-induced Ca^{2+} signal (Figure 3.9). The response was observed in the cytosol seven min after application of ATP to a final concentration of 100 µM, and the signal was similar in shape to the signals observed with YC3.6 (Figure 3.2), namely a sharp peak followed by a second and third smaller peaks. No nuclear signals were observed during the period imaged.

Flg22 was also used as an elicitor, but no signals were observed. Imaging 5-day-old roots, no flg22-induced Ca^{2+} signals were detected (0/4 plants, [flg22] = 10^{-6} M). In order to evaluate the dual sensor's ability to relay the Ca^{2+} signals induced by a biotic elicitor known to activate the defence response, I tested the short chain chitin oligomer chitooctaose (CO8, also

referred in literature as ch8 and CT8) (Boller and Felix, 2009; Ranf *et al*., 2011). Treating 5-day-old roots with CO8 to a final concentration of 10^{-7} M elicited an increase in $[Ca^{2+}]_{cyt}$ within approximately two min of application in 73% of the plants tested (8/11 plants) (Figure 3.10). The signal was characterised by a sharp increase followed by progressively smaller oscillations, resulting in the overall $[Ca^{2+}]_{cyt}$ steadily returning to baseline levels over a period of 15 min (Figure 3.10). No distinguishable variations in $[Ca^{2+}]_{nucleus,\ nu}$ were detected. Because CO8 was dissolved in 0.1% dimethyl sulfoxide (DMSO), this solvent was tested under the same conditions as a control. There was no evidence of DMSO-induced Ca^{2+} signals (0/4 plants, Figure 3.10 e-h).

In summary, the dual sensor G-GECO1.2-NES/R-GECO1.2-NLS reports variations in $[Ca^{2+}]$ in response to different elicitors and allows the distinction between cytosolic- and nuclear-localised Ca^{2+} signals.

Figure 3.8 | A GECO-based dual-localised Ca^{2+} sensor.

Schematic representation of the golden gate pL2V-1-50505-based dual sensor expression vector. The R-GECO1.2 expression cassette is flanked by the *L. japonicus* UBIQUITIN10 (LjUBI10) promoter and the 35S terminator (t35S) and features a nuclear localisation signal (NLS) at the 3' end. The G-GECO1.2 expression cassette is flanked by the Arabidopsis UBIQUITIN10 (AtUBI10) promoter and the NOS terminator and features a nuclear exclusion signal (NES) at the 3' end. The vector also features a plant selection cassette (*HPTII*, conferring resistance to hygromycin B, controlled by the AtUBI10 promoter, and the terminator for 1-*AMINOCYCLOPROPANE-1-CARBOXYLATE SYNTHASE 2* (*ACS2*)).

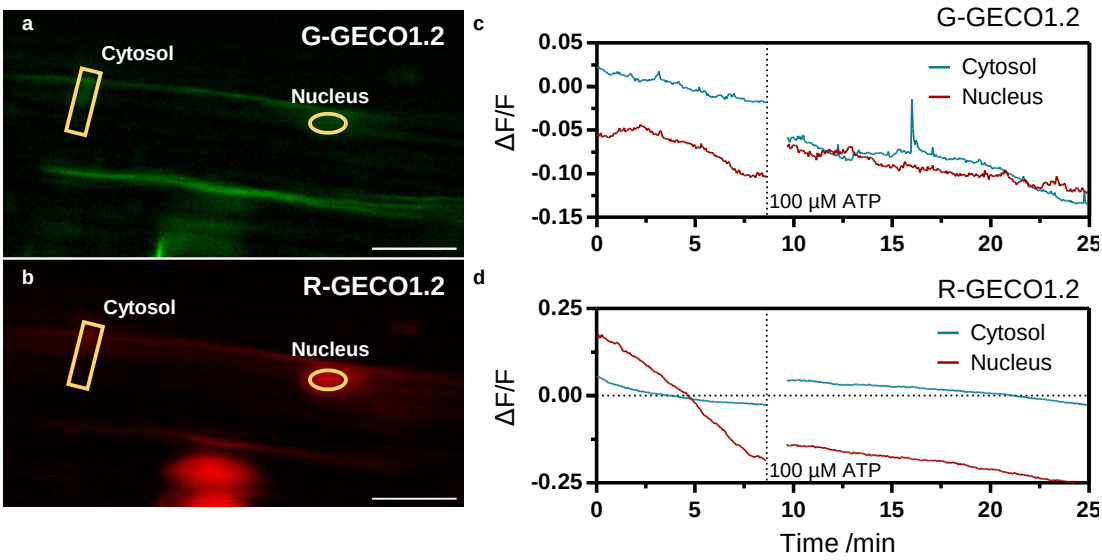

Figure 3.9 | The dual Ca^{2+} sensor reports Ca^{2+} dynamics to ATP application.

Ca^{2+} signals induced by 100 µM ATP in a 5-day-old root (elongation zone) expressing the dual Ca^{2+} reporter (a, G-GECO channel; b, R-GECO channel). c, d, Normalised fluorescence intensities in the G-GECO channel (c) and the R-GECO channel (d) of the ROIs marked in a and b. Dashed vertical lines mark the moment of ATP application. Scale bars represent 20 µm.

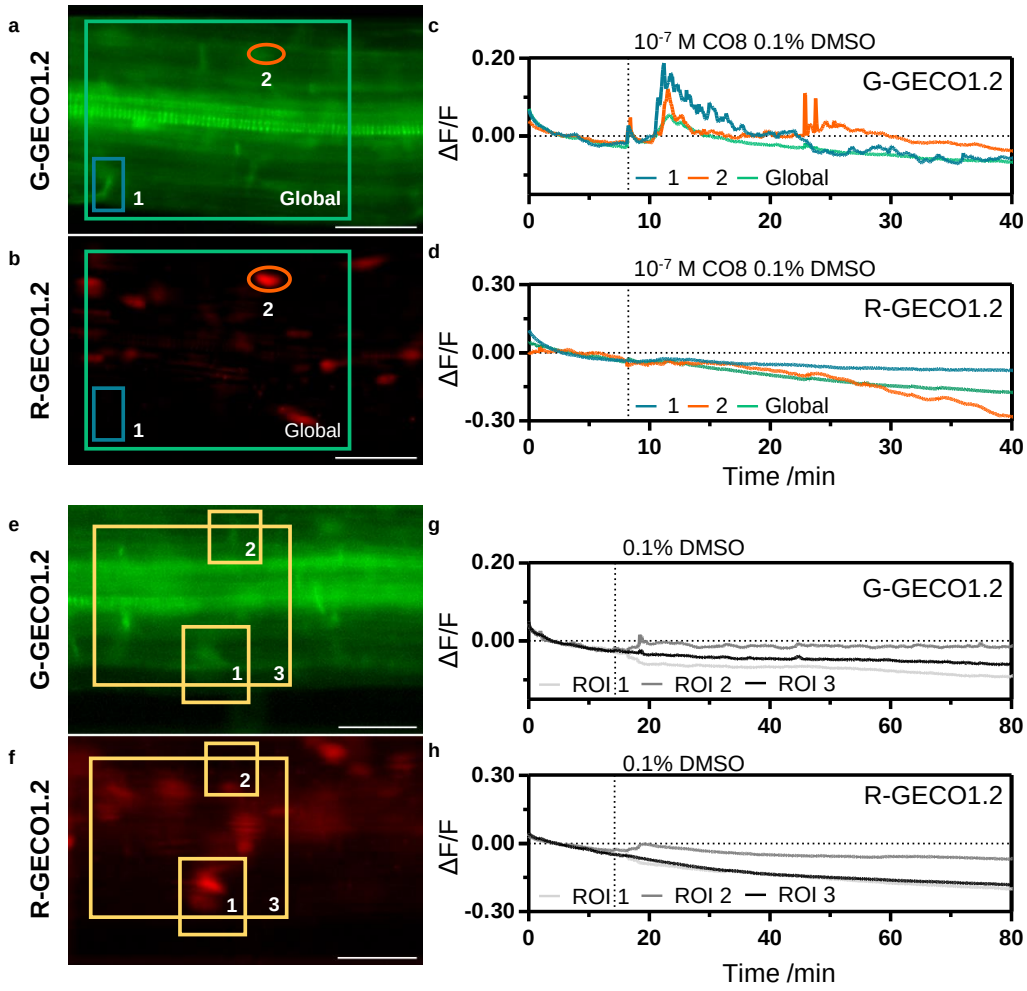

Figure 3.10 | The dual Ca^{2+} sensor reports Ca^{2+} dynamics to the application of CO8.

a-d, Representative Ca^{2+} signals induced by 10^{-7} M CO8 in a 5-day-old root (elongation zone) expressing the dual Ca^{2+} reporter (a, G-GECO channel; b, R-GECO channel). c, d, Normalised fluorescence intensities in the G-GECO channel (c) and the R-GECO channel (d) of the ROIs marked in a and b. e-h, 0.1% DMSO did not induce Ca^{2+} signals in a 5-day-old root (elongation zone) expressing the dual Ca^{2+} reporter (e, G-GECO channel; f, R-GECO channel). g, h, Normalised fluorescence intensities in the G-GECO channel (g) and the R-GECO channel (h) of the ROIs marked in e and f. Dashed vertical lines mark the moment of CO8 and DMSO application. Scale bars represent 50 µm.

3.3. Discussion

Imaging Ca^{2+} in living plant cells has improved greatly over the last twenty years and has had a significant impact on the study of a variety of signalling pathways and physiological processes. The availability and diversity of genetically-encoded Ca^{2+} reporters have allowed the execution of innovative genetic screens, the tackling of biological questions that could not, until then, be addressed experimentally, and offered a greater understanding of the complexities of Ca^{2+} signalling that underlie many developmental and physiological processes. The range of Ca^{2+} sensors available suits diverse experimental questions and settings differently, and so it is beneficial to recognise the shortcomings and advantages of each sensor in order to maximise the outcome of this experimental approach.

In this chapter, I established perfusing and non-perfusing experimental set-ups to image Ca^{2+} in Arabidopsis roots and leaves, using three different genetically-encoded Ca^{2+} sensors: the ratiometric reporter YC3.6, the intensiometric reporter R-GECO1.2, and a dual sensor G-GECO1.2-NES/R-GECO1.2-NLS.

YC3.6 has been extensively published in plants to report a variety of signals induced by different stimuli (Weinl *et al*., 2008; Monshausen *et al*., 2008, 2009, 2011; Tanaka *et al*., 2010; Michard *et al*., 2011; Krebs *et al*., 2012; Thor and Peiter, 2014; Shih *et al*., 2015). Under the experimental conditions tested here, the ATP- and cold-induced responses (Figure 3.2) were similar to what is reported in the literature (Tanaka *et al*., 2010; Krebs *et al*., 2012). I proceeded to characterise the Ca^{2+} response to auxin, a hormone central to root development, which has been linked to Ca^{2+} signalling. In roots, a rise in the cytosolic [Ca^{2+}] is the earliest known response to increased amounts of auxin (Monshausen *et al*., 2011). A Ca^{2+} wave similar to the one described here has been reported before, but the authors only quantified the Ca^{2+} signal in the root epidermis in the elongation zone (Monshausen *et al*., 2011; Shih *et al*., 2015). The results presented here indicate that the auxin-induced Ca^{2+} signatures were distinct in different parts of the root. This raises the possibility of having tissue-specific determinants encoding the Ca^{2+} signal, be it at the level of the Ca^{2+} channel responsible for the influx of Ca^{2+}, or at the level of the efflux machinery that restores the [Ca^{2+}] to basal levels. If that is the case, it would be interesting to investigate if and how these different signatures are decoded, into

different responses to the auxin stimulus, as this would suggest that Ca^{2+} is used as a versatile way to amplify the range of auxin responses in a tissue-specific manner.

In this work, it was also shown for the first time in plants that R-GECO1.2 is able to report *in vivo* fluctuations in [Ca^{2+}] in roots and leaves (Figures 3.5 and 3.6), thus expanding the range of Ca^{2+} reporters available.

One of the goals of this project was to characterise the flg22-induced Ca^{2+} signal. The immunogenic peptide of bacterial flagellin, a microbial-associated molecular pattern (MAMP) that activates innate immune responses, has been shown by multiple groups to induce a cytosolic Ca^{2+} burst (Kwaaitaal *et al*., 2011; Ranf *et al*., 2011, 2012; Maintz *et al*., 2014; Thor and Peiter, 2014; Monaghan *et al*., 2015). These studies used aequorin as a Ca^{2+} reporter, and as such a fine characterisation of this response at a cell resolution was lacking. During the course of this PhD work, two articles were published reporting flg22-induced Ca^{2+} signals using YC3.6 (Thor and Peiter, 2014) and R-GECO1 (Keinath *et al*., 2015). Thor and Peiter describe oscillations in $[Ca^{2+}]_{cyt}$ in response to 10^{-7} M of flg22 in guard cells of Arabidopsis epidermal strips. These oscillations were variable in peak amplitude and frequency, and cell asynchronous. Keinath *et al*. directly compare the efficacy of NES-YC3.6 and R-GECO1 by co-expressing both reporters. Importantly, they show that R-GECO1, when compared to NES-YC3.6, has a significantly increased Ca^{2+}-dependent signal change. It was additionally reported that 10^{-7} M of flg22 induced Ca^{2+} oscillations in detached Arabidopsis leaves, which lasted up to 30 min. Moreover, they show that application of 10^{-6} M flg22 in roots also elicited Ca^{2+} signals, which originated from the elongation zone. In this work, despite the fact that all the sensors used were able to resolve a variety of Ca^{2+} signals induced by different elicitors, only limited success was obtained in attempting to describe the flg22-induced Ca^{2+} response (Table 3.1 and Figure 3.4). While the signal observed in roots (Figure 3.4 a) was similar in shape to the one reported by Keinath *et al*. (2015), no oscillations were detected in leaf samples, but rather a single peak (Figure 3.4 b, c). The differences observed, especially in terms of plant responsiveness, can potentially be explained by differences in the developmental stage of the leaf imaged. The study by Keinath *et al*. used mostly leaves showing signs of senescence, in which damage to the cuticle can improve flg22 permeability (Melanie Krebs, personal communication). These differences can also be due to the different Ca^{2+} affinities of each sensor. The variation in the [Ca^{2+}] upon stimulation depends on the organism, cell type, and

elicitor, and thus low-affinity sensors might not be able to report low [Ca^{2+}] (Horikawa *et al*., 2010). The K_d for Ca^{2+} of R-GECO1.2 (1200 nM) is almost 2.5 times higher than that of R-GECO1, based on in vitro estimations, and 4.8 times higher than YC3.6, and as such, these two last reporters have higher affinities for Ca^{2+} and are better equipped to detect lower [Ca^{2+}]. In fact, a recent study estimated the K_d of R-GECO1 *in vivo* and indicates that R-GECO1 has a higher affinity for Ca^{2+} than previously thought (K_d = 158 ± 3 nM, mean ± s.e.m.) (Waadt *et al*., 2017). The range of $[Ca^{2+}]_{cyt}$ upon flg22 treatment extends from 50-100 nM (baseline) to 250-300 nM (peak maximum) as measured by aequorin (Ranf *et al*., 2011; Thor and Peiter, 2014). To successfully image these Ca^{2+} signals, the K_d of the reporter should ideally be 175 nM, i.e. the middle value of the range, as this would elicit maximum changes in signal strength (Horikawa *et al*., 2010). This can thus possibly explain why both YC3.6 and R-GECO1 are better at detecting flg22-induced Ca^{2+} signals. In agreement with this, the high-affinity YC-Nano65 reporter (K_d = 65 nM) (Horikawa *et al*., 2010) has also been used in Arabidopsis to resolve flg22-induced Ca^{2+} signals in roots (Simon Gilroy, personal communication). Finally, it is also important to consider the spatial expression pattern of *FLAGELLIN SENSING 2* (*FLS2*), the gene that encodes the flg22 receptor and is required to induce flg22-triggered immune responses (Gómez-Gómez and Boller, 2000; Zipfel *et al*., 2004). *FLS2* expression is regulated in cell type-specific and developmental manners (Beck *et al*., 2014). In roots, *FLS2* is almost exclusively expressed in the stele, and is absent from the primary root meristem. In leaves, the expression of *FLS2* is higher in stomata, hydathodes, and wound sites (Beck *et al*., 2014). This indicates that analysis of flg22-induced Ca^{2+} responses with cell resolution has to be correctly targeted to the sites of *FLS2* expression. Pre-treatment with 10 μM flg22, 50 μM salicylic acid, 1 mM H_2O_2, or 10 μM of the ethylene precursor 1-aminocyclopropane-1-carboxylic acid expanded *FLS2* expression to the root cap, meristem, and cortex cells (Beck *et al*., 2014), suggesting a possible way to facilitate flg22-induced Ca^{2+} analysis.

In this work, a nuclear and cytosolic localised, GECO-based, dual reporter was also tested. Such a reporter should allow a fine temporal and spatial distinction between nuclear and cytosolic Ca^{2+} signals. Importantly, this is the first time that such a reporter is developed and that nuclear and cytosolic signals can be compared in the same plant, as previous studies have used nuclear-localised or nuclear-excluded sensors in different plant lines (Krebs *et al*.,

2012; Krebs and Schumacher, 2013). The dual sensor was able to resolve ATP-induced Ca^{2+} signals, similar to those observed with YC3.6 here (Figure 3.2), and reported for YC3.6 and R-GECO1 previously (Krebs *et al*., 2012; Keinath *et al*., 2015). Although a nuclear ATP response has been shown before (Krebs *et al*., 2012; Krebs and Schumacher, 2013), only cytosolic signals were observed here using the dual sensor. In these published studies, the variation in the $[Ca^{2+}]_{nu}$ occurred only 15 to 20 min after treatment application, while the cytosolic signals occurred 3-7 min after ATP treatment. It is conceivable that similar signals would have been observed using the dual sensor had the imaging time been extended.

The MAMP CO8 was also used to test the dual sensor. CO8-induced Ca^{2+} signals measured using aequorin have been described in Arabidopsis (Ranf *et al*., 2011, 2014), but this is, to my knowledge, the first report of a CO8-induced Ca^{2+} response at cell resolution. No Ca^{2+} signals were detected in the nucleus. While CO8 is a strong inducer of the defence response in Arabidopsis and rice (Boller and Felix, 2009; Shimizu *et al*., 2010), short chain chitin oligomers induce nuclear Ca^{2+} spiking and transcriptional changes in *Medicago truncatula* and rice, hallmarks of the establishment of the arbuscular mycorrhizal symbiosis (Genre *et al*., 2013; Sun *et al*., 2015). Given that, unlike flg22, the response to CO8 is frequently observed, this reporter can potentially be used to further characterise the CO8-induced Ca^{2+} response, identify key players in the perception and transduction of the CO8 signal, and clarify, in the context of the arbuscular mycorrhizal symbiosis, how the distinction between activation of immunity and symbiosis establishment is achieved.

In conclusion, I have shown that both biotic and abiotic elicitors can induce Ca^{2+} signals in Arabidopsis, which can be characterised with high spatial and temporal resolution using the reporters YC3.6, R-GECO1.2, and the dual reporter G-GECO1.2-NES/R-GECO1.2-NLS. While there is now a range of genetically-encoded Ca^{2+} reporters available, it is important to recognise that different sensors are better suited to resolve different Ca^{2+} signals. The range of fluorescent proteins available and the practicality of modular cloning also makes the design of new types of Ca^{2+} reporters more straightforward. Importantly, new protocols for the absolute quantification of the $[Ca^{2+}]$ in plant cells using these reporters have now been developed (Waadt *et al*., 2017), which will allow a more thorough characterisation of Ca^{2+} signals and aid the study of both the encoders and decoders of these stimuli.

Chapter IV

A reverse genetics screen on putative calcium channels for altered innate immune responses

4.1. Introduction

The two-tier plant immune system is generally successful is fighting the myriad of challenges elicited by plant pathogens (Jones and Dangl, 2006). The first layer of defence, pattern-triggered immunity (PTI), is a large-spectrum surveillance system that recognises conserved microbial-associated molecular patterns (MAMPs) by pattern recognition receptors (PRRs) at the plasma membrane (Böhm *et al*., 2014; Zipfel, 2014). The second branch of this system, effector-triggered immunity (ETI), is based on specific recognition of a pathogen effector, which often results in the hypersensitive response (HR), consisting of the programmed cell death of plant cells surrounding the site of infection, thus preventing further spread of the pathogen (Coll *et al*., 2011).

A rapid influx of calcium (Ca^{2+}) to the cytosol is one of the earliest detectable signals upon activation of PTI (Ranf *et al*., 2008; Jeworutzki *et al*., 2010). Apart from Ca^{2+} influx, perception of MAMPs by PRRs elicits a phosphorelay signalling pathway that results in the production of reactive oxygen species (ROS) in the apoplast, the induction of mitogen-activated protein kinases (MAPKs), and transcriptional reprogramming that coordinates local and systemic defence responses (Chinchilla *et al*., 2007; Boudsocq *et al*., 2010; Lu *et al*., 2010; Zhang *et al*., 2010a; Sun *et al*., 2013). ROS production by RESPIRATORY BURST OXIDASE HOMOLOGUE D (RBOHD) upon MAMP perception is regulated in both a Ca^{2+}-independent and a Ca^{2+}-dependent manners. The Ca^{2+}-independent regulation is effected by BOTRYTIS-INDUCED KINASE 1 (BIK1) phosphorylation, while the Ca^{2+}-dependent regulation occurs in two ways: Ca^{2+} binding to EF-hand motifs in RBOHD, and phosphorylation by Ca^{2+}-dependent protein kinases (CPKs) (Ogasawara *et al*., 2008; Dubiella *et al*., 2013; Kadota *et al*., 2014; Li *et al*., 2014). This places Ca^{2+} upstream of ROS production, however, in *rbohd* null

alleles expressing the Ca^{2+} sensitive luminescent protein aequorin, the profile of the MAMP-induced Ca^{2+} signal is different from wild type. While usually characterised by a double peak, the second peak is abolished in *rbohd* plants. This suggests that RBOHD affects Ca^{2+} influx to the cytosol, and highlights the dynamic crosstalk occurring between ROS and Ca^{2+} signalling in innate immunity (Ranf *et al*., 2011).

For over 20 years, the existence of a plasma membrane-localised, elicitor-responsive, Ca^{2+}-permeable channel involved in plant immunity has been hypothesised (Gelli *et al*., 1997; Zimmermann *et al*., 1997). The immunity-induced Ca^{2+} signal was first observed in aequorin-expressing parsley in response to the *Phytophthora sojae*-derived pep13 elicitor (Blume *et al*., 2000). Work by Ranf *et al*. (2008) subsequently showed for the first time that the immunogenic peptides of the bacterial MAMPs flagellin and elongation factor, flg22 and elf18 respectively, induce Ca^{2+} signals in apoaequorin expressing Arabidopsis lines. More recently, this was observed with cell resolution, using the Ca^{2+} sensors YC3.6 and R-GECO1 (Thor and Peiter, 2014; Keinath *et al*., 2015). Thus far, however, the identity of the hypothesised channels has remained elusive.

Different putative Ca^{2+} channels have been linked to plant defence, namely members of the cyclic nucleotide-gated channel (CNGC) family, the glutamate receptor-like channel (GLR) family, and the annexins. *cngc2* (identified first as *defense no death1* or *dnd1*) and *cngc4* (*dnd2* or *HR-like lesion mimic* 1, *hml1*) show similar phenotypes, including constitutive expression of defence genes, elevated levels of salicylic acid (SA), impaired HR, and increased resistance against virulent strains of *Pseudomonas syringae* and *Hyaloperonospora arabidopsidis* (Yu *et al*., 1998; Clough *et al*., 2000; Yu *et al*., 2000; Balagué *et al*., 2003; Jurkowski *et al*., 2004; Ali *et al*., 2007; Genger *et al*., 2008; Chin *et al*., 2013). Bimolecular fluorescence complementation analyses showed that these two channels likely form homo- and heteromeric complexes, which suggests that they might be part of the same heterotetrameric channel (Chin *et al*., 2013). It was shown nevertheless that the flg22-induced Ca^{2+} signals were not changed in *cngc2/dnd1* (Ma *et al*., 2012), but no similar reports have been published for *cngc4*. Studies on *CNGC11*, *CNGC12*, and the chimeric allele *CNGC11/12* (*constitutive expresser of PR genes 22, cpr22*) have suggested that these genes are positive mediators of resistance to an avirulent biotype of *H. parasitica* (Yoshioka *et al*., 2001, 2006; Urquhart *et al*., 2007; Baxter *et al*., 2008;

Urquhart *et al*., 2011; Abdel-Hamid *et al*., 2013). After infection with the avirulent *Pseudomonas syringae avrRpt2* strain, *cngc11* and *cngc12* null mutants had a significantly higher bacterial titre than wild type, but no differences were observed when these plants were infected with a virulent strain of *P. syringae*. Additionally, treatment with flg22 induced callose deposition, an output of PTI, to levels similar to wild type (Moeder *et al*., 2011). This evidence suggests that CNGC11 and CNGC12 are involved in ETI, but not in PTI.

Another study has shown that a subset of inhibitors of mammalian glutamate receptors blocks cytosol Ca^{2+} transients after flg22 and elf18 treatment (Kwaaitaal *et al*., 2011), which places GLRs downstream of MAMP perception by PRRs, though the precise targets and specificity of these inhibitors in plants is unclear. Overexpressing a radish GLR in Arabidopsis resulted in increased expression of defence genes and enhanced resistance to necrotic fungal pathogens (Kang *et al*., 2006). Moreover, *GLR3.3* has been genetically linked to a role in defence, as *glr3.3* mutants are more susceptible to *P. syringae* (Li *et al*., 2013) and *H. arabidopsidis* (Manzoor *et al*., 2013). However, these mutants are not more susceptible to *Botrytis cinerea*, suggesting a role in resistance against biotrophic, but not necrotrophic pathogens, and linking *GLR3.3* to the SA-dependent defence response. Recently, Vincent *et al*. (2017) showed that GLR3.3 and GLR3.6 are required for an increase in the $[Ca^{2+}]_{cytosolic,\ cyt}$ around the feeding site of the aphid *Myzus persicae*, establishing a direct link between the GLRs and changes in $[Ca^{2+}]_{cyt}$ during biotic interactions for the first time. Finally, GLR3.3 and GLR3.6 have been shown to be required for wound and herbivory-induced transmission of systemic electric signals (Mousavi *et al*., 2013; Salvador-Recatalà *et al*., 2014).

Lastly, it was recently shown through bimolecular fluorescence complementation and co-immunoprecipitation assays that ANNEXIN 1 (ANN1) interacts with the chitin receptor CHITIN ELICITOR RECEPTOR KINASE 1 (CERK1). The chitin-induced increase in $[Ca^{2+}]_{cyt}$ is slightly reduced in *ann1* mutants, and ANN1 is not phosphorylated by CERK1. Moreover, the flg22-induced ROS production is not altered in *ann1* (Espinoza *et al*., 2017).

The aim of the research presented in this chapter was to conduct a reverse genetic screen on genes encoding putative Ca^{2+} channels to investigate their role in PTI signalling. A triple mutant belonging to the GLR family was identified with impaired ROS production and induction of downstream defence genes. Further research is required to fully understand the role of GLRs in generating the MAMP-induced Ca^{2+} signal.

4.2. Results

4.2.1. A collection of putative Ca^{2+} channel mutants

A number of T-DNA insertion alleles of members of the *CNGC*, *ANNEXIN*, and *GLR* families was retrieved from the Nottingham Arabidopsis Stock Centre (NASC, UK), or kindly provided by José Feijó (University of Maryland). All lines were genotyped and the following table summarises the homozygous mutant alleles used in this study (Table 4.1). The alleles used are all in a Col-0 background and were named following the standard Arabidopsis nomenclature guidelines or the name under which they were previously published.

4.2.2. Screening of the allele collection for defects in PTI signalling

ROS production is one of the earliest detectable signals upon flagellin sensing, and evidence shows that Ca^{2+} is required for a full ROS response (Kadota *et al*., 2014). For this reason, the ROS phenotype upon flg22 treatment of the homozygous Ca^{2+} mutants was evaluated (Figure 4.1).

Single *cngc* and *ann* mutants did not show a significant ROS phenotype upon treatment with 100 nM flg22 (Figure 4.1 a, b). In the group of mutants of the *GLR* family, a reduction in ROS production was seen for two independent *glr3.1glr3.3aglr3.6a* triple mutant lines (Figure 4.1 c).

Prolonged exposure to MAMPs correlates with growth inhibition in wild-type plants (Gómez-Gómez *et al*., 1999; Zipfel *et al*., 2006; Krol *et al*., 2010). This is likely due to a mechanism in which resources otherwise allocated to growth are directed towards defence, including diversion of mechanisms used in transcription, translation, and protein secretion, and redirecting of carbon and nitrogen to the production of defence compounds (Jung *et al*., 2007; Bilgin *et al*., 2010; Sugano *et al*., 2010; Göhre *et al*., 2012; Borges *et al*., 2013). Seedling growth inhibition assays are thus a simple way to test candidate genes for their involvement in the PTI pathway, yet it measures a long-term adaptation to MAMP stimulation. As such, this assay is not necessarily eliminatory for the assessment of candidate Ca^{2+} channel genes, considering that these are responsible for an early-response to MAMPs. As in wild-type plants, seedling growth was inhibited across all the genotypes tested after prolonged exposure to 1 µM flg22 (Figure 4.2).

Table 4.1 | List of T-DNA insertion mutants of putative Ca^{2+} channels used in this work.

Gene	Accession	Allele	Polymorphism	Origin	Reference
CNGCs					
CNGC1	*AT5G53130*	*cngc1*	SAIL_443_B11	NASC	-
CNGC3	*AT2G46430*	*cngc3-1*	SALK_056832	NASC	Gobert *et al.* (2006)
CNGC4	*AT5G54250*	*cngc4-5*	SALK_081369	NASC	Wang *et al.* (2016)
CNGC5	*AT5G57940*	*cngc5-1*	SALK_149893	NASC	Wang *et al.* (2013)
CNGC5	*AT5G57940*	*cngc5-2*	SALK_053354	NASC	-
CNGC7	*AT1G15990*	*cngc7*	SAIL_59_F03	NASC	-
CNGC8	*AT1G19780*	*cngc8*	SALK_004230	NASC	-
CNGC9	*AT4G30560*	*cngc9*	SALK_026086	NASC	Gao *et al.* (2016)
CNGC11	*AT2G46440*	*cngc11*	SM_3.15048	NASC	-
CNGC12	*AT2G46450*	*cngc12*	SALK_092622	NASC	Mousavi *et al.* (2013)
CNGC13	*AT4G01010*	*cngc13*	SALK_013536	NASC	-
CNGC16	*AT3G48010*	*cngc16*	SALK_065792	NASC	-
CNGC19	*AT3G17690*	*cngc19*	SALK_027306	NASC	-
Annexins					
ANN1	*AT1G35720*	*ann1-1*	SALK_132169	NASC	Wang *et al.* (2015)
ANN1	*AT1G35720*	*ann1-2*	SALK_015426	NASC	Wang *et al.* (2015) (*ann1* in Lee *et al.* (2004) and Espinoza *et al.* (2017))
ANN1	*AT1G35720*	*ann1-3*	WiscDsLox477	NASC	Wang *et al.* (2015)
ANN2	*AT5G65020*	*ann2-1*	SALK_054223	NASC	Lee *et al.* (2004), Wang *et al.* (2015)
ANN3	*AT2G38760*	*ann3-1*	SALK_075525	NASC	-
ANN3	*AT2G38760*	*ann3-2*	SALK_082344	NASC	-
ANN4	*AT2G38750*	*ann4*	SALK_121732	NASC	-

Continued overleaf

Table 4.1 | Continued.

Gene	Accession	Allele	Polymorphism	Origin	Reference
GLRs					
GLR1.1	AT3G04110	*glr1.1*	SALK_117347	José Feijó	-
GLR1.2	AT5G48400	*glr1.2*	SALK_114822	José Feijó	-
GLR1.4	AT3G07520	*glr1.4-1*	SALK_129955	José Feijó	*glr1.4* in Mousavi *et al.* (2013)
GLR1.4	AT3G07520	*glr1.4-2*	SALK_124605	José Feijó	-
GLR2.1	AT5G27100	*glr2.1*	GK-897G01.05	NASC	-
GLR2.2	AT2G24720	*glr2.2*	GABI_436H08	José Feijó	-
GLR2.4	AT4G31710	*glr2.4*	SALK_010571	NASC	-
GLR2.5	AT5G11210	*glr2.5*	SAIL_1243_E09	NASC	-
GLR2.6	AT5G11180	*glr2.6-1*	SALK_066558	NASC	-
GLR2.6	AT5G11180	*glr2.6-2*	SALK_115448	José Feijó	-
GLR2.7	AT2G29120	*glr2.7*	SALK_121990	NASC	-
GLR2.8	AT2G29110	*glr2.8*	CS374123	NASC	-
GLR2.9	AT2G29100	*glr2.9*	SALK_125496	NASC	Mousavi *et al.* (2013)
GLR3.1	AT2G17260	*glr3.1*	SALK_063873	NASC	Kong *et al.* (2016), Mousavi *et al.* (2013)
GLR3.2	AT4G35290	*glr3.2a*	SALK_150710	NASC	Mousavi *et al.* (2013)
GLR3.3	AT1G42540	*glr3.3a*	SALK_099757	NASC	Mousavi *et al.* (2013)
GLR3.3	AT1G42540	*glr3.3b*	SALK_077608	José Feijó	Mousavi *et al.* (2013)
GLR3.3	AT1G42540	*glr3.3c*	SALK_082194	José Feijó	-
GLR3.4	AT1G05200	*glr3.4*	SALK_016904	NASC	-
GLR3.5	AT2G32390	*glr3.5-1*	SALK_035264	NASC	Teardo *et al.* (2015)
GLR3.6	AT3G51480	*glr3.6a*	SALK_091801	NASC	Mousavi *et al.* (2013)

Continued overleaf

Table 4.1 | Continued

Gene	Accession	Allele	Polymorphism	Origin	Reference
GLRs					
GLR3.6	AT3G51480	*glr3.6b*	SALK_035353	NASC	Mousavi *et al.* (2013)
GLR3.7	AT2G32400	*glr3.7*	SALK_101122	NASC	-
GLR1.1; GLR1.2	-	*glr1.1glr1.2*	SALK_117347 x SALK_114822	José Feijó	-
GLR1.1; GLR1.4	-	*glr1.1glr1.4-1*	SALK_117347 x SALK_129955	José Feijó	-
GLR1.2; GLR1.4	-	*glr1.2glr1.4-2*	SALK_114822 x SALK_124605	José Feijó	-
GLR1.2; GLR3.3	-	*glr1.2glr3.3b*	SALK_114822 x SALK_077608	José Feijó	-
GLR1.2; GLR1.4; GLR3.3	-	*glr1.2glr1.4-2glr3.3b*	SALK_114822 x SALK_124605 x SALK_077608	José Feijó	-
GLR1.2; GLR2.2; GLR3.3	-	*glr1.2glr2.2glr3.3b*	SALK_114822 x GABI_43H08 x SALK_077608	José Feijó	-
GLR1.2; GLR1.4; GLR2.2; GLR3.3	-	*glr1.2glr1.4-2 glr2.2glr3.3b*	SALK_114822 x SALK_124605 x GABI_436H08 x SALK_077608	José Feijó	-
GLR1.4; GLR2.2; GLR3.3	-	*glr1.4-2glr2.2glr3.3b*	SALK_124605 x GABI_436H08 x SALK_077608	José Feijó	-
GLR1.4; GLR3.3	-	*glr1.4-2glr3.3c*	SALK_124605 x SALK_082194	José Feijó	-
GLR2.2; GLR3.3	-	*glr2.2glr3.3b*	GABI_436H08 x SALK_077608	José Feijó	-
GLR3.3; GLR3.6 #1	-	*glr3.3aglr3.6a #1*	SALK_099757 x SALK_091801	José Feijó	Mousavi *et al.* (2013)
GLR3.3; GLR3.6 #2	-	*glr3.3aglr3.6a #2*	SALK_099757 x SALK_091801	José Feijó	-
GLR3.1; GLR3.3; GLR3.6	-	*glr3.1glr3.3aglr3.6a #1*	SALK_063873 x SALK_099757 x SALK_091801	José Feijó	-
GLR3.1; GLR3.3; GLR3.6	-	*glr3.1glr3.3aglr3.6a #2*	SALK_063873 x SALK_099757 x SALK_091801	José Feijó	-

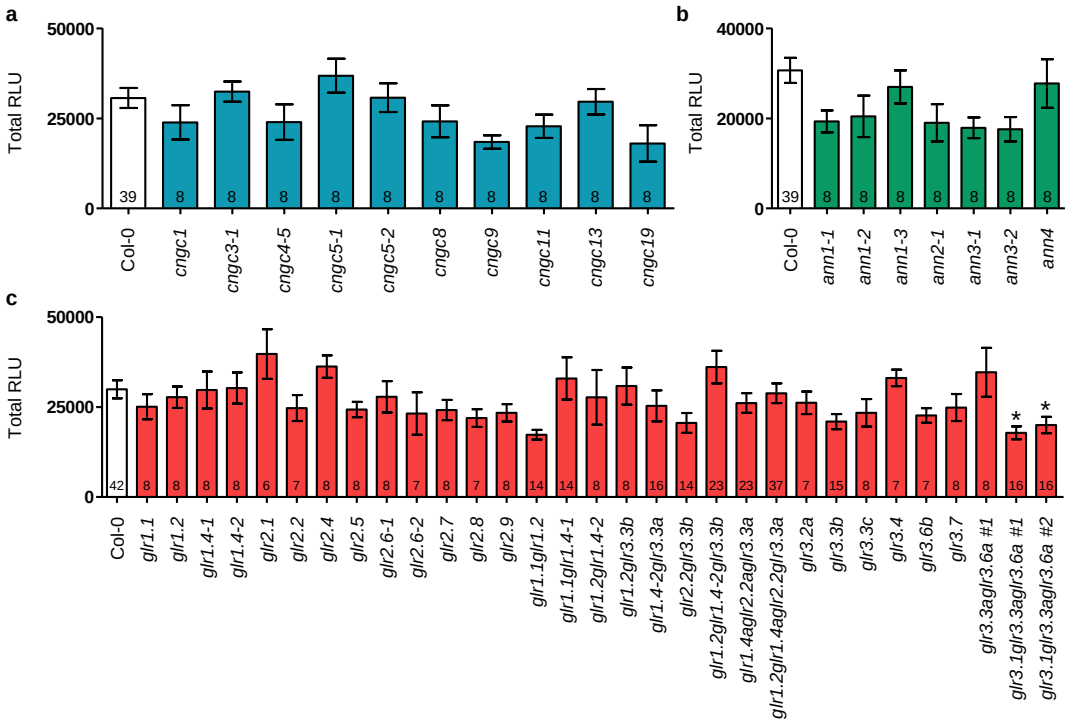

Figure 4.1 | flg22-induced ROS production screen in *cngc*, *ann*, and *glr* alleles.

a-c, ROS assay following treatment with 100 nM flg22 in Col-0 and *cngc* (a), *ann* (b), and *glr* (c) mutant alleles. Values are means of total relative light units (RLUs) counts over 35 min ± s. e. m.. Numbers in bars denote sample size (n). * $p < 0.05$ (one-way ANOVA with a Dunnett post-test).

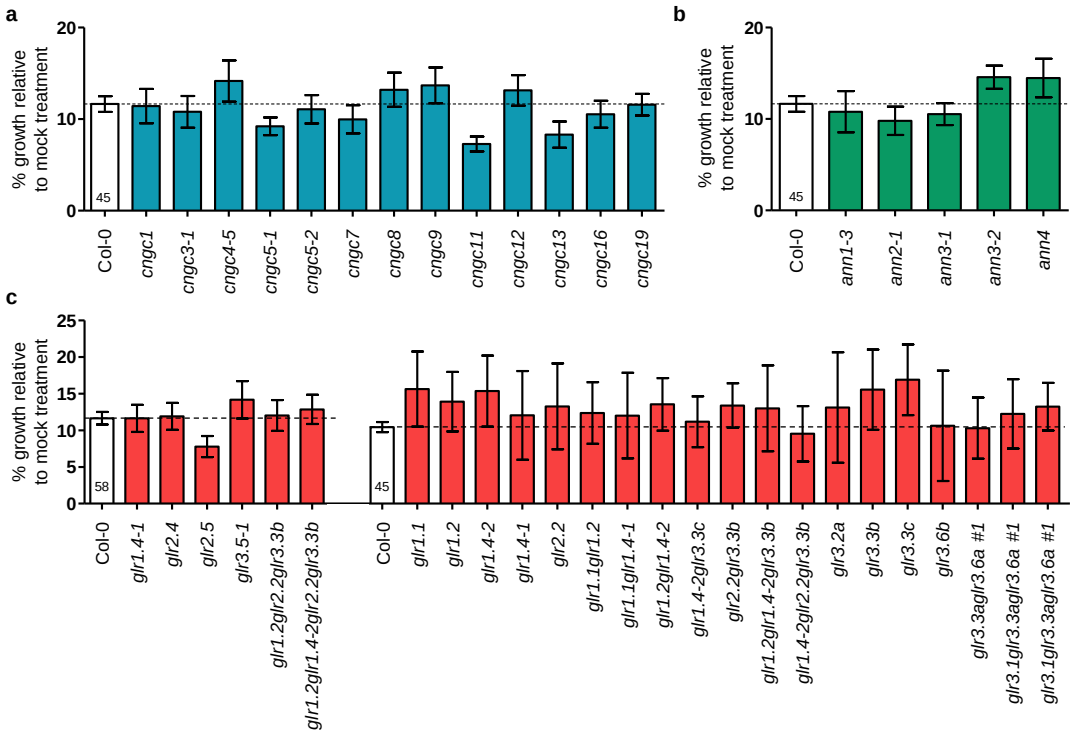

Figure 4.2 | flg22-induced growth inhibition screen in *cngc*, *ann*, and *glr* alleles.

a-c, Seedling growth inhibition assay on MS medium containing 1 µM flg22 normalised against growth without peptide. Values are means ± s. d. (n = 8 for each test genotype, unless otherwise inscribed on the graph).

4.2.3. Glutamate receptor-like genes are involved in early MAMP signalling

To confirm the decreased ROS phenotype, ROS assays were repeated three more times with higher sample number, including single alleles that were previously unavailable (a representative experiment is shown in Figure 4.3). Both independent *glr3.1glr3.3aglr3.6a* lines showed a significant decrease in the amount of ROS production upon treatment with 100 nM of flg22 (Figure 4.3 e, f), while the single mutant alleles and the *glr3.3aglr3.6a* did not (Figure 4.3 a-d). This indicates that at least one of these channels must be present for the full ROS production in MAMP signalling.

To rule out the possibility of loss of the T-DNA insertion and confirm its location, the T-DNA insertion borders were sequenced and *GLR* expression was quantified in 4-week-old leaves (same as plants used for ROS assays) (Figure 4.4). The expression level of *GLR3.1* was reduced by 35% to 50% when compared to Col-0, in *glr3.1* and *glr3.1glr3.3aglr3.6a* (Figure 4.4 c). Additionally, the insertion localised to the last exon of *GLR3.1* (Figure 4.4 a). In animals, the phosphorylation status of the C-terminus impacts on plasma membrane insertion, subcellular localisation, receptor trafficking and recycling (reviewed in Traynelis *et al.*, 2010). This domain also comprises motifs for binding of proteins involved in, e.g., targeting for protein degradation (reviewed in Traynelis *et al.*, 2010). Accordingly, it has been shown that deletion of this domain alters channel regulation, but does not necessarily abolish function (Köhr and Seeburg, 1996; Ehlers *et al.*, 1998; Vissel *et al.*, 2001). It is conceivable that, in plants, the C-terminus is also involved in channel regulation. This idea is supported by work in *Raphanus sativus* L., where RsGluR (highest sequence homology to AtGLR3.2) has an ER retention signal in the C-terminus (Kang *et al.*, 2006).

Expression levels of *GLR3.3* and *GLR3.6* were strongly reduced in the double and triple mutant lines. In *glr3.6a* expression of *GLR3.6* was upregulated, an effect that was seen repeatedly in independently generated cDNA samples, including different tissues (two-week-old seedlings, not shown). Using the same primers, this upregulation was not seen in the double and triple mutants that were generated through crossing using this allele (Figure 4.4 c). Considering that homozygosity was confirmed, this is likely explained by the presence of another insertion in the *GLR3.6* locus that impacts *GLR3.6* expression, one that was subsequently lost in further crossings. The T-DNA insertions in *GLR3.3* and *GLR3.6* both

localised to the third exon (Figure 4.4 a), before the transmembrane domains, and considering that expression is barely detectable, these are considered null alleles.

Given the decrease in ROS production in the *glr3.1glr3.3aglr3.6a* mutants (figure 4.1 and 4.3), I also evaluated other early PTI responses. MAMP perception is associated with rapid transcriptional reprogramming (Zipfel *et al*., 2004), and *FRK1 (FLG22-INDUCED RECEPTOR KINASE 1*), *At2G17740*, *NHL10* (*NDR1/HIN1-LIKE 10/YLS9*), and *PHI-1* (*PHOSPHATE-INDUCED 1*) are commonly used early-response PTI marker genes (He *et al*., 2006; Shan *et al*., 2008; Boudsocq *et al*., 2010). Induction of *FRK1* expression has been shown to be a result of MAPK activation, *NHL10* is induced both by MAPKs and CPKs, and *PHI-1* expression is specifically induced by CPKs (Boudsocq *et al*., 2010).

In two-week-old plants, incubation with 100 nM flg22 resulted in a time-dependent induction of all four marker genes tested, both in Col-0 and the different mutant lines (Figure 4.5). The only differences observed between genotypes were in the expression of *NHL10*, which was reduced in *glr3.1glr3.3aglr3.6a* lines at 60 min (Figure 4.5 b and c), but not in *glr3.3aglr3.6a* (Figure 4.5 a).

Ca^{2+} signalling has been shown to play a role in leaf-to-leaf signalling in PTI (Dubiella *et al*., 2013). Additionally, GLRs from clade III, in particular GLR3.3 and GLR3.6, are involved in the transmission of leaf-to-leaf electric signals in response to herbivory and wounding (Mousavi *et al*., 2013). Therefore, and considering that the experimental set-up had thus far not allowed for a distinction between local stimulation and distal induction (Figures 4.3 and 4.5), I tested whether GLR3.1, GLR3.3, and GLR3.6 are involved in leaf-to-leaf signalling in response to flg22. To decrease experimental variability, leaves of 5-week-old plants were numbered as described by Farmer *et al.* (2013), and leaf 8 was infiltrated with 200 nM flg22 (or a water control). Leaves 8 (local response) and 13 (distal response) were then harvested for quantification of *NHL10*, which has been previously used to report distal defence gene induction upon flg22 treatment (Dubiella *et al*., 2013). Leaf 13 was chosen as a distal leaf sample because in vegetative Arabidopsis rosettes vascular sympodia connect the leaves along the n + 5 parastichy (Kang *et al*., 2003; Dengler, 2006), and this developmental pattern fitted with the observed induction of *JAZ10* in leaves 5 and 13, but not others, after wounding of leaf 8 (Mousavi *et al*., 2013). It has also been reported that wounding of leaf 8 induces systemic

Ca^{2+} signals in leaf 13 (Kiep *et al*., 2015). Because MAMP and wounding signalling are associated, and to discriminate between infiltration (wounding)- and flg22-induced gene expression, a water infiltration control was used. Similarly to the results presented in Figure 4.5, induction of *NHL10* expression was lost in the *glr3.1glr3.3aglr3.6a*, at the local level (leaf 8), but not in Col-0 or *glr3.3aglr3.6a* (Figure 4.6 a). At the distal level, expression of *NHL10* was too low to quantify any significant induction between controls and flg22-treated plants, even in Col-0 (Figure 4.6 b). Considering that induction was already lost locally in *glr3.1glr3.3aglr3.6a*, it is not possible to conclude on whether the GLRs play a role in flg22-induced leaf-to-leaf signals. It is worth noticing that *NHL10* is an adequate marker gene to distinguish between wounding and MAMP signalling, as no induction was seen in the water controls. However, under these conditions, it may not be an appropriate marker for distal induction of defence genes.

In summary, the combination of *GLR3.1*, *GLR3.3*, and *GLR3.6* is required for a normal ROS burst upon flg22 sensing and induction of the defence gene *NHL10* in the local leaf.

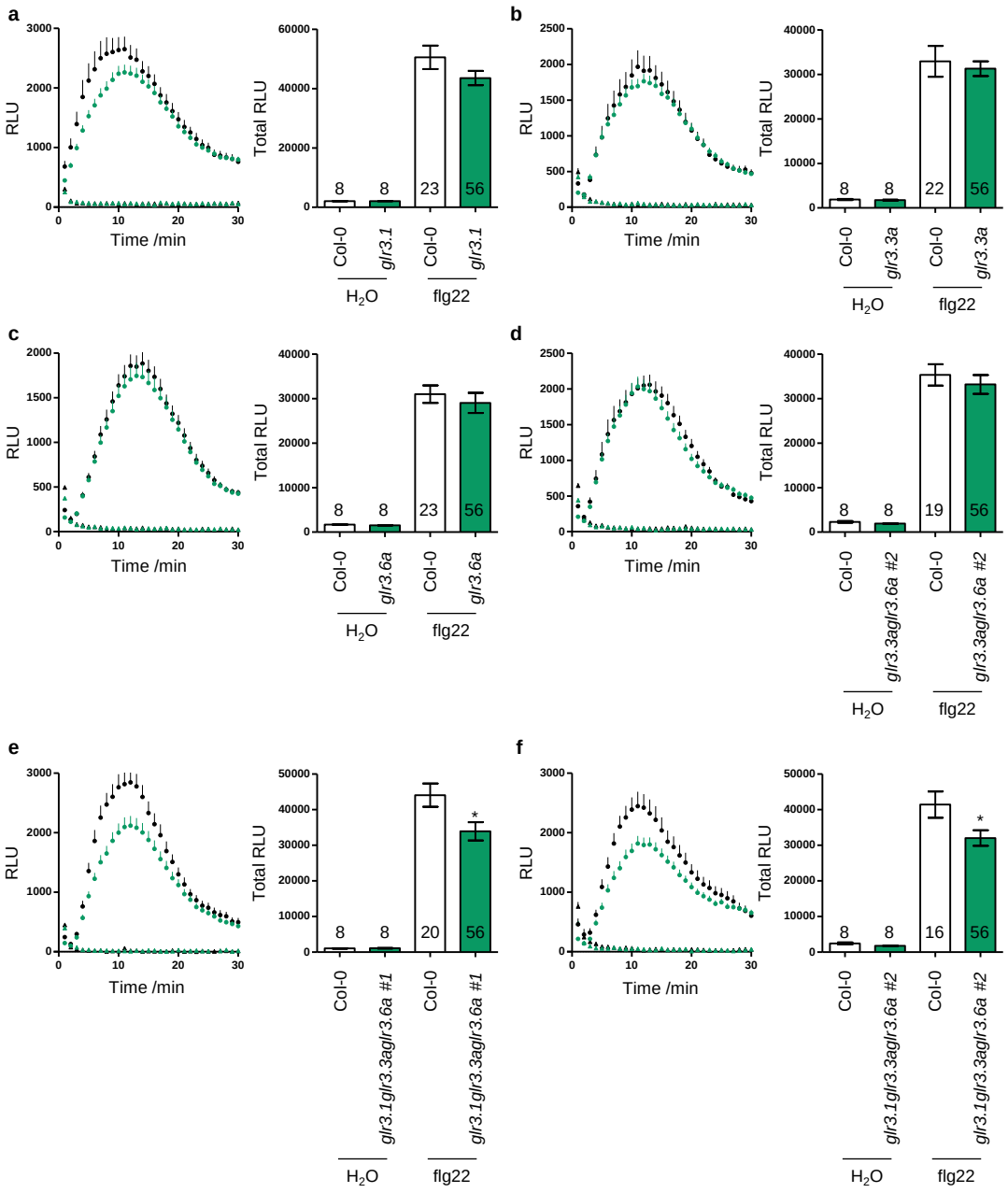

Figure 4.3 | flg22-induced ROS production in *glr* mutants.

a-f, ROS assay following treatment with 100 nM flg22 in Col-0 and *glr3.1* (a), *glr3.3a* (b), *glr3.6a* (c), *glr3.3aglr3.6a* (d), *glr3.1glr3.3aglr3.6a #1* (e), *glr3.1glr3.3aglr3.6a #2* (f). Relative light units (RLU) production over time (left) and total RLUs (right). Values are means ± s. e. m.. Numbers in bars denote sample size (n). * $p < 0.05$ (two-tailed t-test with a prior F-test for homoscedasticity).

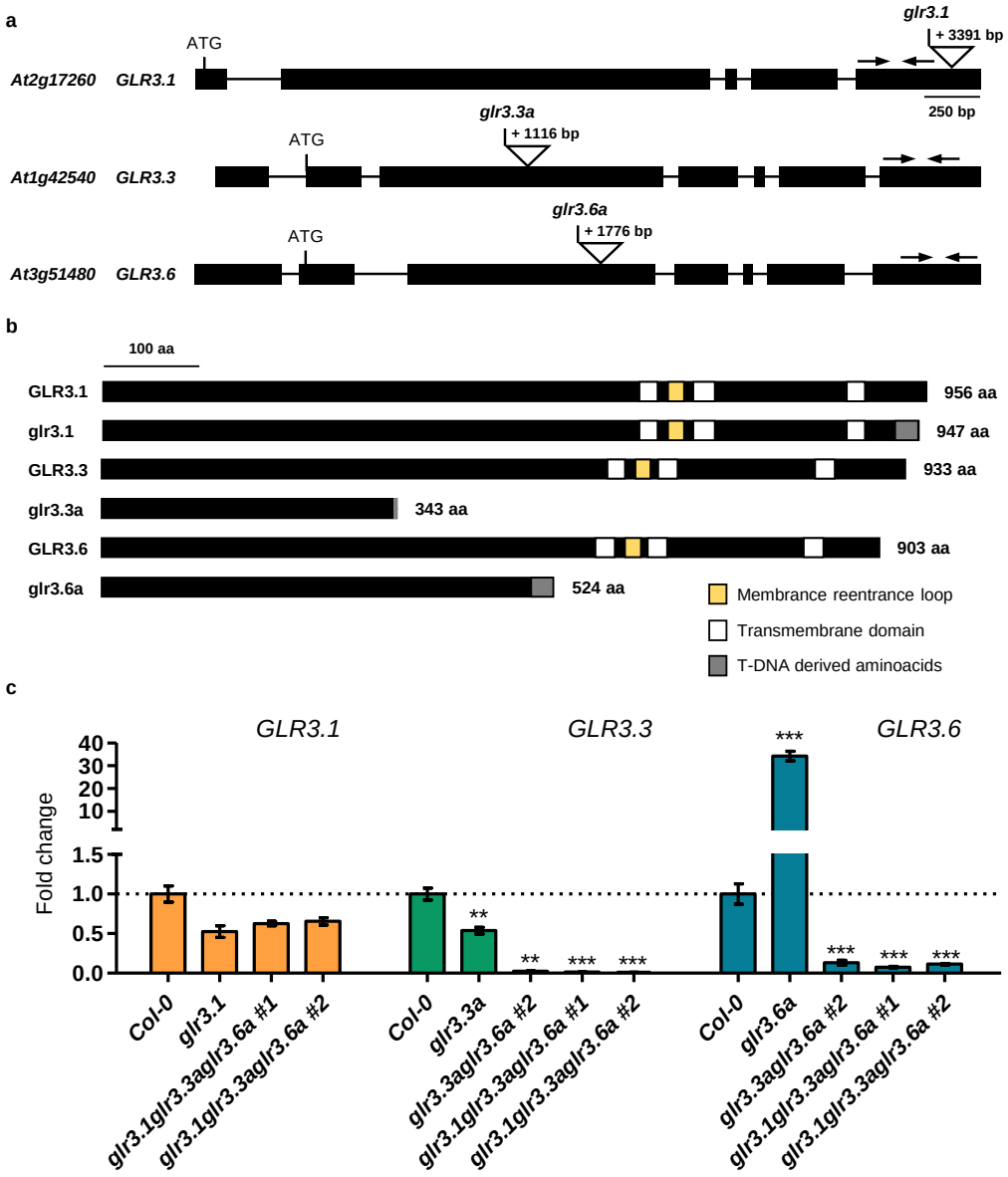

Figure 4.4 | Genetic characterization of *GLR* mutants in *A. thaliana*.

a, Positions of the T-DNA insertions in *GLR3.1*, *GLR3.3*, and *GLR3.6* confirmed by PCR and sequencing. Exons are represented by black boxes and introns by black lines. b, Predicted structure of the wild-type amino acid sequences, with transmembrane domains in white, membrane reentrance loops in yellow, and the modified C-terminus derived from the T-DNA in grey. c, Quantitative expression analyses of the transcript level of *GLR3.1*, *GLR3.3*, and *GLR3.6* by RT-qPCR in rosette leaf samples (n = 3 or 4) of Col-0, *glr3.1*, *glr3.3a, glr3.6a, glr3.3aglr3.6a #2,* and two independently generated *glr3.1glr3.3aglr3.6a* alleles (#1 and #2). Expression was normalised to *UBOX* (*At5g15400*) and presented as fold change over control (Col-0). The position of the primers on the gDNA is indicated by arrows in a. Values are means ± s. e. m.. ** $p < 0.01$, *** $p < 0.001$ (two-tailed t-test with a prior F-test for homoscedasticity).

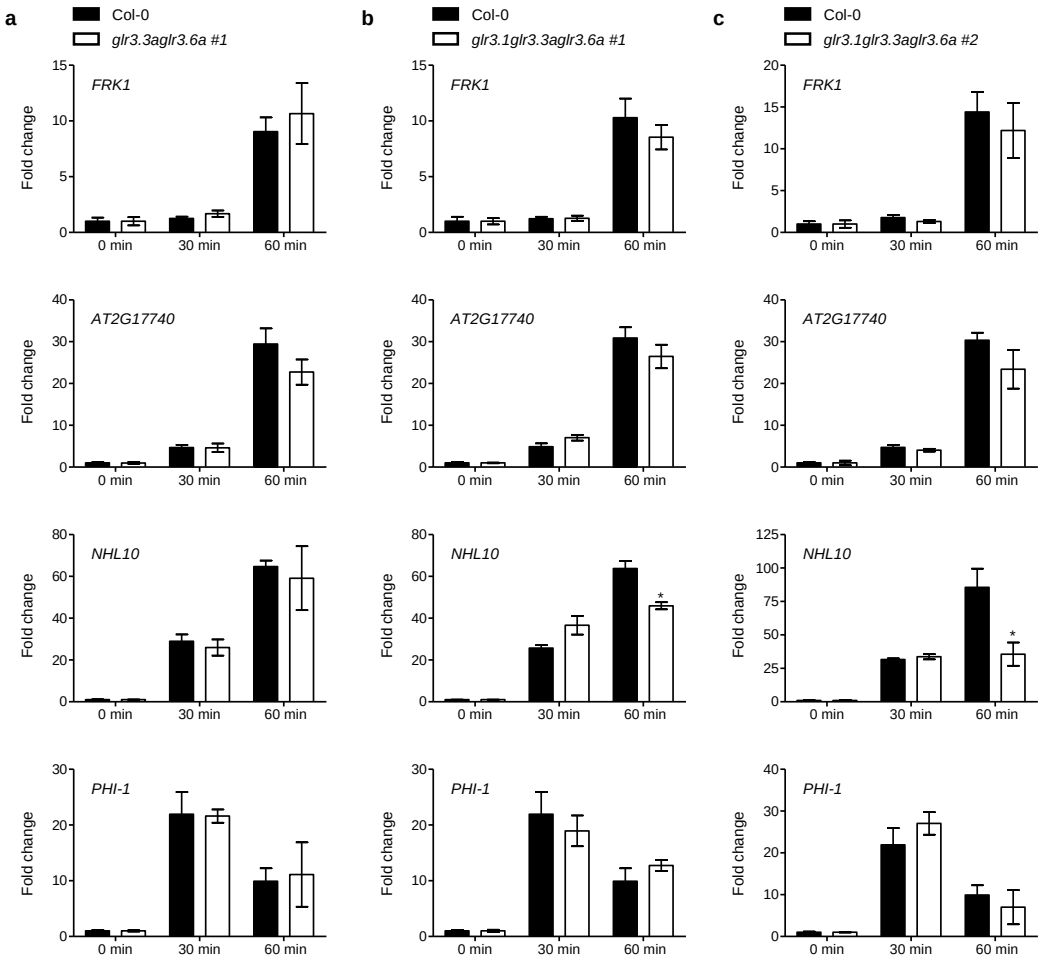

Figure 4.5 | Expression of MAMP-inducible genes in *glr* mutants after treatment with 100 nM flg22.

Quantitative expression analysis of the transcript level of *FRK1*, *AT2G17740*, *NHL10*, and *PHI-1* after 0, 30, and 60 min of incubation with 100 nM flg22, in *glr3.3aglr3.3a #1* (a), *glr3.1glr3.3aglr3.3a #1* (b), *glr3.1glr3.3aglr3.3a #2* (c). Expression was normalised to *UBOX* (*At5g15400*) and presented as fold change over the first time point (t = 0 min; n = 3 or 4, pools of two seedlings). Values are means ± s. e. m.. * $p < 0.05$ (two-tailed t-test with a prior F-test for homoscedasticity).

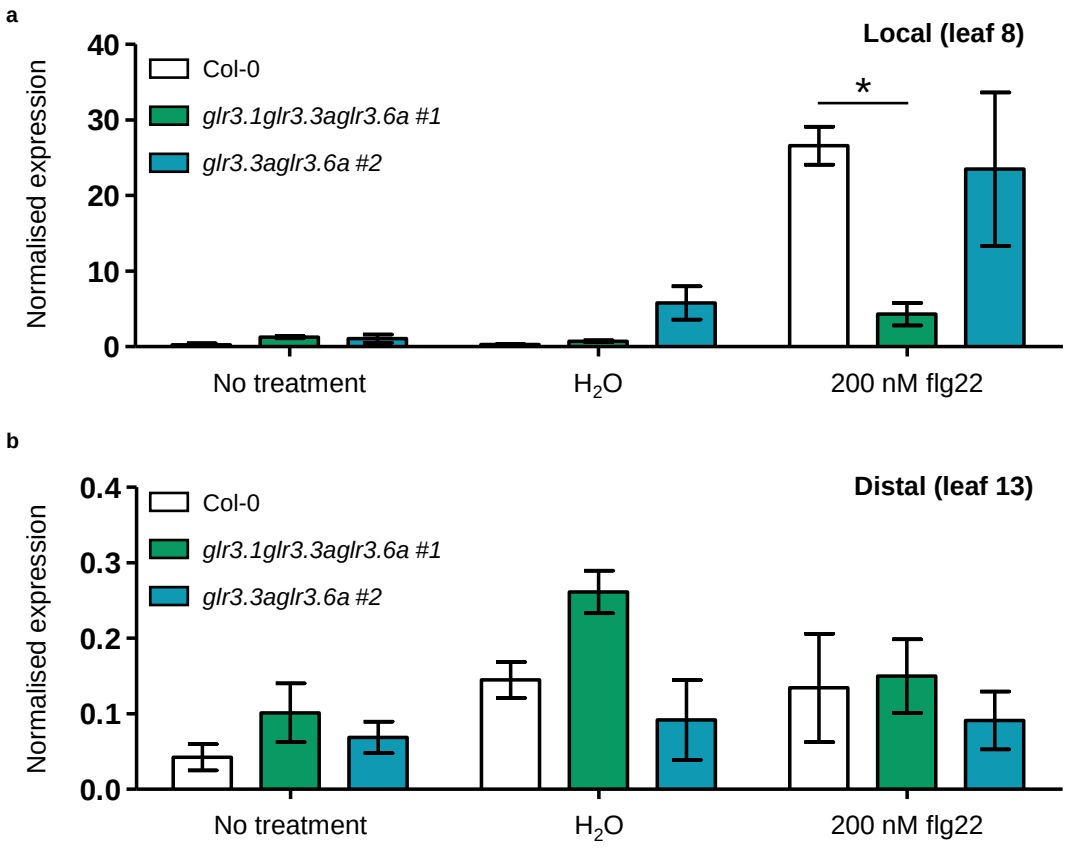

Figure 4.6 | Local and distal quantification of *NHL10* expression upon infiltration with 200 nM flg22.

Normalised expression of *NHL10* in leaf 8 (local) (a) and leaf 13 (distal) (b) after 45 minutes of infiltration with 200 nM flg22 in leaf 8. Expression was normalised to *UBOX* (*At5g15400*) (n = 4). Values are means ± s. e. m.. * $p < 0.05$ (two-tailed t-test with a prior F-test for homoscedasticity).

4.2.4. Yeast complementation studies to assay channel permeability to Ca^{2+}

To determine whether GLRs of clade III are permeable to Ca^{2+}, yeast codon-optimised coding sequences were expressed in the yeast mutant *cch1mid1*. CCH1 and MID1 have been identified as necessary factors for Ca^{2+} influx to the cytosol and survival in response to the mating pheromone α factor (Iida *et al*., 1994; Fischer *et al*., 1997; Paidhungat and Garrett, 1997). This phenotype can be complemented by Ca^{2+} release into the cytosol and evaluated by visual inspection of the α factor-induced growth inhibition zone (Figure 4.7 a). In order to quantify this phenotype, and in collaboration with JIC Computational Bioimaging (Matthew Hartley and Tjelvar Olsson), an algorithm was developed to measure the growth inhibition zone, as described in Figure 4.7. The algorithm readily distinguishes between growth inhibition zones of different sizes, as generated by applying increasing amounts of α factor (Figure 4.7 c).

Expressing the GLR proteins in *cch1mid1* did not complement the growth phenotype (Figure 4.8. Vectors described in Chapter II, Table 2.4). However, I cannot conclude on the permeability of the channels, as it is possible that the GLRs are not being correctly expressed in yeast, targeted to the plasma membrane, or inserted into the membrane in the correct orientation to allow the generation of the Ca^{2+} signal. It should be highlighted, nevertheless, that previous studies have attested the capacity of members of the GLR family to transport Ca^{2+} using patch-clamp analyses, both in Arabidopsis (Michard *et al*., 2011; Kong *et al*., 2016) and other species (Ortiz-Ramírez *et al*., 2017).

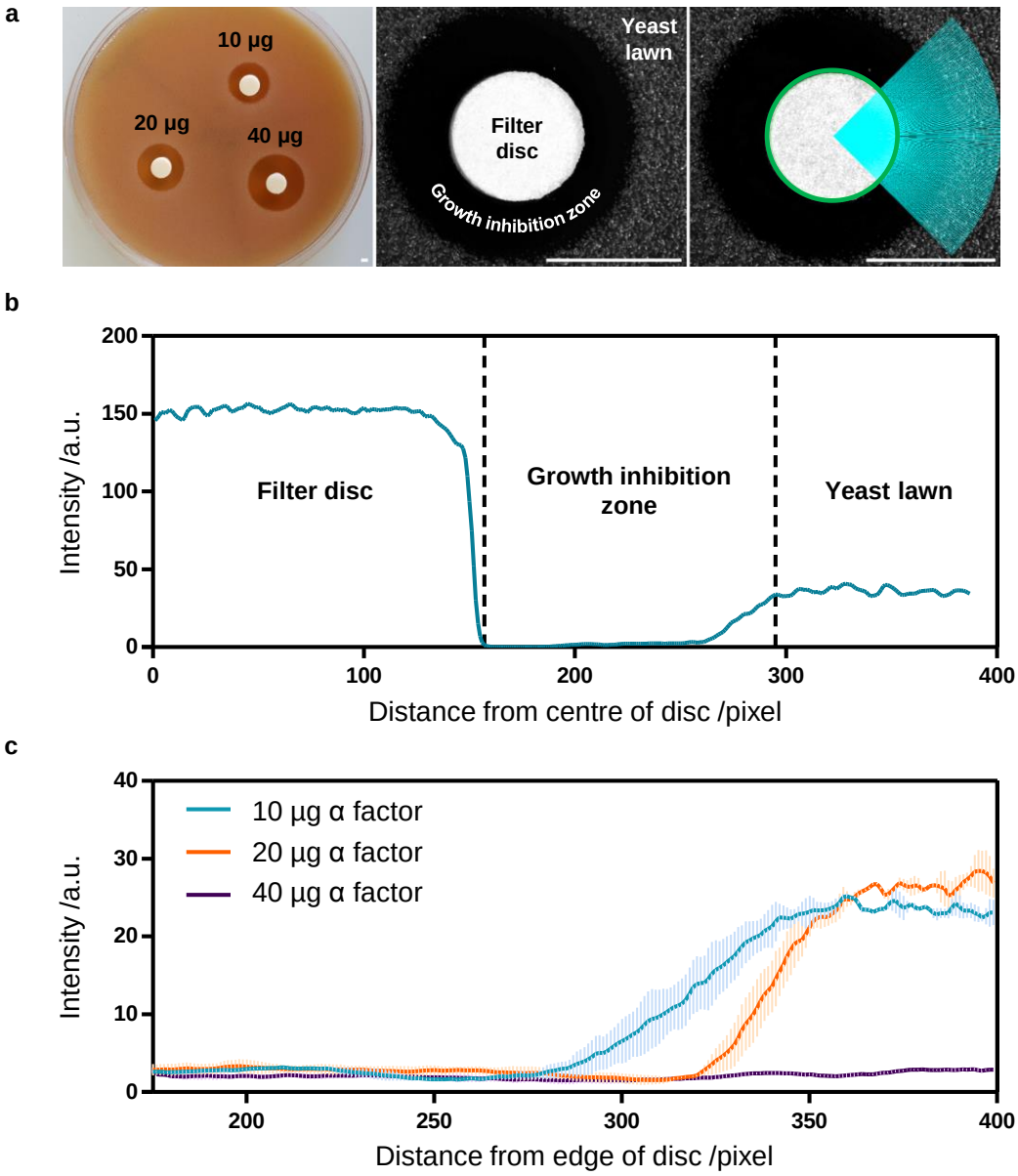

Figure 4.7 | An algorithm to quantify *cch1mid1* complementation assays.

a, Representative image of the *cch1mid1* strain exposed to α factor and indication of the main parameters of the algorithm. Petri dish with a yeast lawn and three disc assays with different amounts of α factor (left). Detail image of an α factor containing assay disc, growth inhibition zone and yeast lawn (middle). Output of the image processing algorithm (right). The algorithm extends a series of lines along the radii of the circle from its centre over a 90^0 angle, measures the intensity along each line and averages the result. Scale bars represent 2 mm. b, Mean intensity profile over the distance from disc centre. The intensity plot distinguishes three zones: the filter disc, the growth inhibition zone and the yeast lawn. c, Mean intensity profile over the distance from the edge of the disc for assays performed with 10 µg, 20 µg, and 40 µg of α factor in *cch1mid1*. Values are means ± s. e. m. (shaded, n = 2).

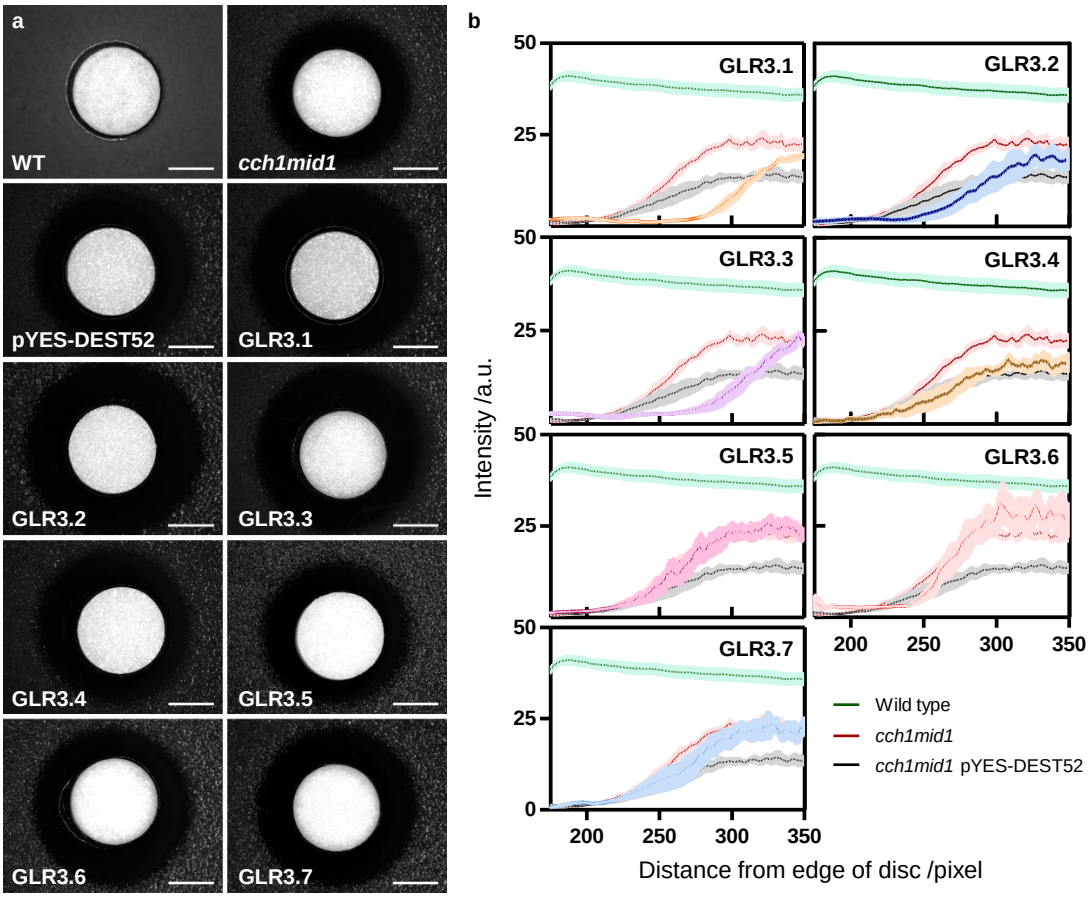

Figure 4.8 | *cch1mid1* complementation assay of GLRs.

a, Representative example of *cch1mid1* complementation assays of GLR3.1, GLR3.2, GLR3.3, GLR3.4, GLR3.5, GLR3.6, and GLR3.7. Scale bars represent 1 mm. b, Mean intensity profile over the distance from disc edge of assays performed using 10 µg α factor (the experiment was repeated using 20 µg α factor with similar results, not shown). Values are means ± s. e. m. (shaded). (GLR3.1, GLR3.2, GLR3.3, GLR3.4, GLR3.5, GLR3.7, pYES-DEST52, n = 4 each; GLR3.6, n = 3; wild type, n = 8; *cch1mid1*, n = 5).

4.3. Discussion

Over the last two decades, plenty of evidence has been brought forth highlighting the role of Ca^{2+} in plant immunity, but only recently have the Ca^{2+} signals associated with different MAMPs begun to be described (Ranf *et al*., 2011; Thor and Peiter, 2014; Keinath *et al*., 2015). The flg22-induced variation in the $[Ca^{2+}]_{cyt}$ has been the basis of genetic screens that identified several important mutants in the PTI pathway or provided novel alleles of known targets (Ranf *et al*., 2012), emphasising the importance of this second messenger in plant innate immunity.

From the decoding perspective, several important players have been identified. CPK4, 5, 6, and 11 are critical for MAMP-induced transcriptional reprogramming (Boudsocq *et al*., 2010), and CPK5 mediates Ca^{2+}-dependent RBOHD phosphorylation (Kadota *et al*., 2014). CPK5 has also been implicated in a rapid, MAMP-induced, RBOHD-dependent, long distance mechanism of signal transduction (Dubiella *et al*., 2013). Concurrently, CPK28 is a negative regulator of plant innate immunity and thus important in maintaining cellular homeostasis. This decoder promotes BIK1 degradation and thus attenuates MAMP-triggered immune responses, specifically the Ca^{2+} and ROS bursts (Monaghan *et al*., 2014, 2015). Other positive and negative Ca^{2+}-decoding modulators of the defence response have been identified, including the Ca^{2+}/calmodulin (CaM)-binding transcription factor (CAMTA) 3, which reduces SA accumulation by repressing expression of *EDS1* through binding to its promoter (Galon *et al*., 2008; Du *et al*., 2009); the CaM-binding protein 60a (CBP60a), a global transcriptional repressor of defence responses (Truman *et al*., 2013); CBP60g, which promotes SA production (Zhang *et al*., 2010b; Wang *et al*., 2011); and the tomato CALCINEURIN B-LIKE 10 (SlCBL10)/CBL-INTERACTING PROTEIN KINASE 6 (SlCIPK6) pair, which interact with SlRBOHB and are required for ROS production during PTI and ETI (Torre *et al*., 2013). These studies highlight the central position that Ca^{2+} occupies in this signalling pathway, mediating both positive and negative control mechanisms.

Despite the wealth of knowledge on the decoders of the Ca^{2+} signal, research into the encoders has not been quite as prolific. A few genes have been identified, namely *CNGC2*, *CNGC4*, *CNGC11*, *CNGC12*, and *GLR3.3*, mostly associated with the HR or SA-mediated immunity (Moeder *et al*., 2011; Ma *et al*., 2012; Li *et al*., 2013; Manzoor *et al*., 2013). However,

the identity of the channel(s) responsible for the MAMP-induced Ca^{2+} influx has thus far remained elusive.

In this chapter, I generated a collection of putative Ca^{2+} channel mutant alleles belonging to the *CNGC*, *ANNEXIN*, and *GLR* families and screened them for the production of ROS. Both the Ca^{2+} and the ROS bursts occur within minutes of MAMP sensing, but the Ca^{2+}-dependent regulation of RBOHD places Ca^{2+} upstream of ROS (Kadota *et al*., 2014). As such, a reduction in the $[Ca^{2+}]_{cyt}$ burst due to the lack of a functional MAMP-responsive Ca^{2+} channel should translate into a reduced ROS burst.

A *glr* triple mutant with a dampened ROS response was identified in the genetic screen (Figure 4.1). That no single mutants, or a mutant with a very strong reduction in ROS production, were identified is not surprising. In large gene families, expanded through gene duplication events, such as the *CNGC* and *GLR* families (Mäser *et al*., 2001; Davenport, 2002), cases of genetic redundancy and functional compensation among paralogues are common (Bouché and Bouchez, 2001; Hirschi, 2003). This is particularly relevant in the case of the gene families in question, known to act in multimeric complexes, often comprised of subunits encoded by different genes.

The careful investigation of the ROS phenotype in the *glr3.1glr3.3aglr3.6a* lines, and the single and double *glr3.3aglr3.6a* alleles (Figure 4.3), suggests that the combination of *GLR3.1*, *GLR3.3*, and *GLR3.6* is required for ROS production in flg22-induced PTI. The fact that only the triple mutant shows a reduced induction of the expression of the downstream gene *NHL10*, in seedlings and in adult leaves (Figures 4.5 and 4.6), further supports this hypothesis.

Quantification of gene expression after flg22 treatment did not show any differences in *FRK1*, *At2G17740*, or *PHI-1* expression (Figure 4.5). Boudsocq *et al.* (2010) showed that *FRK1* induction is specifically promoted by the MAPK pathway, in a mostly Ca^{2+}-independent manner. *NHL10,* on the other hand, is induced as the synergistic result of both the MAPK and CPK pathways, while *PHI-1* induction is CPK-specific. For this reason, the strongest effect when blocking the generation of the Ca^{2+} signal might be expected in the induction of *PHI-I*, which was not seen in the *glr* mutants. Despite the multitude of studies that use *NHL10* as a marker gene of activation of PTI, none have so far addressed NHL10 function. Members of the NHL family have been linked to ABA signalling and senescence, but these studies have

only measured transcriptional outputs (Bao *et al*., 2016a, 2016b). It is possible that the GLRs are not involved in the generation of the initial $[Ca^{2+}]_{cyt}$ elevation that activates the CPKs, but instead contribute to amplify this signal, an effect that was more readily seen for *NHL10* expression. It is also worth considering that the ROS phenotype observed is small, and the inherent homeostasis of the signalling network might buffer the initial effect and allow for downstream genes, such as *FRK1* and *PHI-I*, to ultimately be activated to a similar extent, a process that occurs at the level of a signal amplification step, such as the MAPK pathway (Asai *et al*., 2002; Cutler and McCourt, 2005).

The interplay between ROS and Ca^{2+} signalling in PTI has been well documented, and potentially forms the basis of a signal propagation mechanism across cells and tissues (Dubiella *et al*., 2013; Kadota *et al*., 2014). A ROS-assisted Ca^{2+}-induced Ca^{2+}-release mechanism has been modelled and, in part, experimentally validated, for systemic signalling in response to salt stress (Choi *et al*., 2014b; Evans *et al*., 2016). This model implies apoplastic ROS, produced by RBOHD, as a trigger to plasma membrane-localised Ca^{2+} channels. The influx of Ca^{2+} to the cytosol contributes to the activation of the vacuolar ion channel TWO-PORE CHANNEL 1 (TPC1), further increasing the $[Ca^{2+}]_{cyt}$. Diffusion of ROS and Ca^{2+} within the apoplast and the cytosol, respectively, would activate neighbouring channels and propagate the signal along a cell and across different cells and tissues (Evans *et al*., 2016). TPC1 has also been shown to promote systemic Ca^{2+} signals in the response to the aphid *M. persicae* and to contribute to the local Ca^{2+} response to aphid feeding (Vincent *et al*., 2017). TPC1, however, was shown not to be involved in the Ca^{2+} or ROS bursts in response to flg22 or elf18 (Ranf *et al*., 2008).

It is thus possible that the GLRs might be, not the presumed FLS2/BAK1 controlled channel that elicits the first Ca^{2+} signal, but rather a node of an amplification mechanism, which could be controlled by ROS or Ca^{2+}. It is relevant to note that the GLRs of clade III portray several CPK phosphorylation motifs (Table 4.2). CNGC18 has been shown to be activated by CPK32, reinforcing the Ca^{2+} oscillations during polar pollen tube growth in a feed-forward mechanism (Zhou *et al*., 2014). GLRs could be targets of CPK and establish a similar form of regulation.

Plant GLRs can also be gated by multiple amino acids (Qi *et al*., 2006; Stephens *et al*., 2008), including glutamate. Cryptogein, a MAMP produced by the oomycete *Phytophthora cryptogea*, can elicit glutamate exocytosis and induce an elevation in $[Ca^{2+}]_{cyt}$ (Vatsa *et al*.,

2011). It has been hypothesised that GLRs could sense a myriad of host-, notably damage-associated molecular patterns (DAMPs), and non-host-derived molecules, regulating alternative pathways of the defence response (Forde and Roberts, 2014).

Table 4.2 | Number of predicted CPK phosphorylation motifs in GLRs of clade III. The position of residues within brackets may not be critical (Key: S/T - phosphorylated residue; B - basic residue; φ - hydrophobic residue; X - any residue). The motifs have been described by Huang and Huber (2001), Huang *et al*. (2001), and Sebastià *et al*. (2004).

CDS	Motif 1 [B-B-X-B]-φ-X-X-X-X-S/T-X-B	Motif 2 φ-X-B-X-X-S-X-X-X-φ	Motif 3 φ-S/T-φ-X-B-B
GLR3.1	5	3	No hits
GLR3.2	7	1	No hits
GLR3.3	4	4	No hits
GLR3.4	5	2	No hits
GLR3.5	5	3	No hits
GLR3.6	11	2	No hits
GLR3.7	8	4	No hits

At this point, several hypothetical models can be drawn to describe the Ca^{2+} dynamics that take place during PTI, which are summarised in Figure 4.9. Activation of the PRRs FLAGELLIN SENSING 2 (FLS2)/BIK1-ASSOCIATED KINASE 1 (BAK1) by the bacterial MAMP flagellin (or flg22) activates a currently unidentified plasma membrane-localised Ca^{2+} channel. Ca^{2+} influx to the cytosol is required for activation of RBOHD and production of ROS in the apoplast. The cytosolic Ca^{2+} signal can be further reinforced by activation of Ca^{2+}-dependent Ca^{2+} channels (through CPK-mediated phosphorylation, for example), and/or via activation of ROS-dependent Ca^{2+}-channels. This ROS-Ca^{2+} feed-forward loop can also establish signal transduction across different cells and tissues, and activate defence responses in distal areas via CPK5 (Miller *et al*., 2009; Mittler *et al*., 2011; Dubiella *et al*., 2013; Evans *et al*., 2016).

To investigate these hypotheses, it is necessary to carefully characterise the $[Ca^{2+}]_{cyt}$ in response to a MAMP stimulus, with cell resolution and in an experimental set-up that would allow a clear distinction between local stimulation and distal induction. This is made difficult

by the inherent nature of the MAMP-induced Ca^{2+} signal, which has eluded a thorough and reproducible characterisation for a long time, as evidenced in Chapter III. It is also essential to accurately characterise the subcellular localisation of GLR proteins in the tissues under analysis. In Arabidopsis mesophyll protoplasts, GLR3.1 and GLR3.6 localise to the plasma membrane (Kong *et al*., 2016; Singh *et al*., 2016), and, to my knowledge, there have been no reports of the localisation of GLR3.3. Other GLRs of clade III have been localised to internal membranes, namely GLR3.4, which is not only detected in the plasma membrane but also in the chloroplast (Teardo *et al*., 2011), and GLR3.5, which, apart from localising to the plasma membrane in mesophyll protoplasts (Kong *et al*., 2016), is targeted to the chloroplast or the mitochondrion by different splice variants (Teardo *et al*., 2015). Evidence is emerging that GLR trafficking can be modulated by chaperone-like proteins (José Feijó, unpublished data, presented in the Plant Calcium Signalling Meeting 2017), suggesting that GLR subcellular localisation is more dynamic than initially anticipated.

This work indicates that the combination of GLR3.1, GLR3.3, and GLR3.6 is required for a reduction in MAMP responses and so it is possible that GLR3.1, GLR3.3, and GLR3.6 are part of the same complex. To validate this hypothesis, apart from investigating if these channels co-localise, it is necessary to evaluate if they physically interact *in vivo*, for example through split-YFP assays. Equally important is to validate the permeability of these proteins to Ca^{2+} using electrophysiology. This has been shown for GLR3.1 through patch-clamp analyses in guard cells (Kong *et al*., 2016), but not for GLR3.3 or GLR3.6. Additionally, to evaluate if the activity of these GLRs is CPK-dependent, in vitro phosphorylation assays can be developed to identify the most likely effector kinase(s), testing first CPK5, CPK6, and CPK11. This could be followed by *in vivo* quantification of the defence phenotypes in transgenic lines complemented with wild-type and phospho-ablated versions of the different GLRs. To fully implicate CPKs in the regulation of GLR function, one could perform voltage or patch-clamp in heterologous electrophysiology models, such as *Xenopus laevis* oocytes or human embryonic kidney (HEK) cells, expressing the GLRs in the presence or absence of the identified CPKs. Electrophysiology could also potentially establish a link between channel function and regulation by ROS, such as shown for ANN1 (Laohavisit *et al*., 2012). Finally, other PTI related phenotypes could be evaluated in the *glr* mutants, such as stomatal closure, callose deposition in plasmodesmata, or pathogen growth assays.

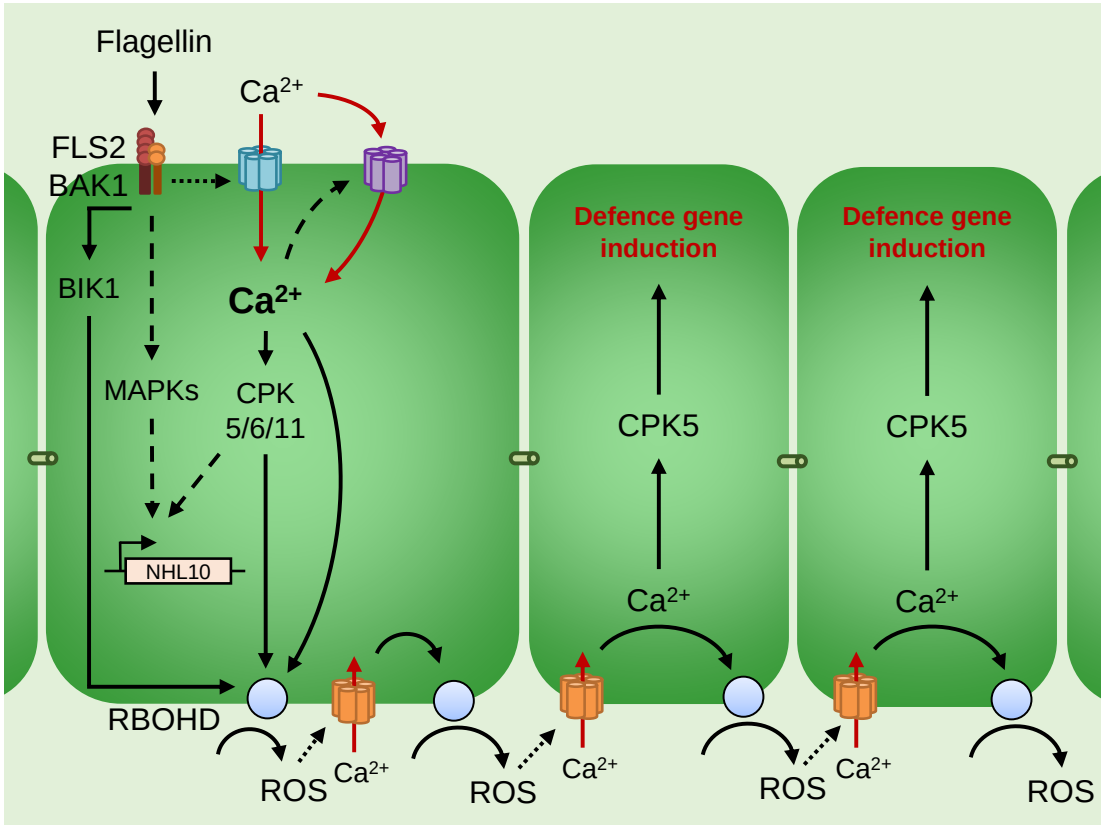

Figure 4.9 | Conceptual model of Ca^{2+} signalling in PTI.

The bacterial MAMP flagellin is perceived by the PRRs FLS2 and BAK1. This leads to BIK1 phosphorylation and activation, which in turn phosphorylates RBOHD in a Ca^{2+}-independent manner. The FLS2/BAK1 complex also hypothetically activates a plasma membrane-localised Ca^{2+} channel (in blue). Influx of Ca^{2+} to the cytosol is required for activation of RBOHD, through direct binding of Ca^{2+} to EF-hands domains in RBOHD, and by activating CPK5/6/11, which further phosphorylate RBOHD. This results in ROS production in the apoplast. Downstream of flagellin perception, activation of the MAPK and CPK pathways induces the expression of MAMP-responsive genes, including *NHL10*. It is possible that the increase in $[Ca^{2+}]_{cyt}$ can be further reinforced by activation of Ca^{2+}-dependent Ca^{2+} channels (purple), and/or via activation of ROS-dependent Ca^{2+}-channels (orange). A ROS-Ca^{2+} feed-forward loop can propagate the signal across cells and mediate distal induction of defence genes. Red arrows represent Ca^{2+} transport and black arrows represent direct (full) or indirect/hypothetical (dashed) activation mechanisms.

Chapter V

Nuclear calcium signals encoded by DMI1 and CNGC15 are required for root development

5.1. Introduction

In plant cells, nuclei are able to generate calcium (Ca^{2+}) signals independently of changes in its cytosolic concentration (Pauly *et al*., 2000, 2001). Using tobacco protoplasts expressing the bioluminescent Ca^{2+} sensor apoaequorin, these authors showed that the nucleus and the cytosol are differentially sensitive to the application of mastoparan, that the nucleus can mount an autonomous Ca^{2+} response (after eliciting cytosol lysis), and that the nucleus is not passively permeable to Ca^{2+} (Pauly *et al*., 2000). Artificially imposing hyper- and hypo-osmotic shocks to tobacco cell cultures expressing apoaequorin additionally showed that the Ca^{2+} responses are differentially modulated in either compartment (Pauly *et al*., 2001).

To this date, however, the only physiologically relevant and most extensively characterised example of nuclear Ca^{2+} signalling in plants is the case of the rhizobial and arbuscular mycorrhizal symbioses in legumes. Signalling molecules originating in the rhizobia or the fungi are perceived at the cell membrane and induce nuclear-associated Ca^{2+} oscillations that are required for transcriptional changes that establish the symbiosis (Oldroyd, 2013). In *Medicago truncatula*, three components are necessary for the generation of these Ca^{2+} signals: the potassium (K^+)-permeable channel DOES NOT MAKE INFECTIONS 1 (DMI1); the cyclic nucleotide-gated channels (CNGC) 15a, b, c; and the Ca^{2+}-dependent adenosine triphosphatase (Ca^{2+}-ATPase) MCA8 (Capoen *et al*., 2011; Charpentier *et al*., 2016). DMI1, CNGC15a/b/c, and MCA8 all localise to the nuclear membranes, suggesting that the nuclear envelope is the Ca^{2+} store (Capoen *et al*., 2011; Charpentier *et al*., 2016; Riely *et al*., 2007). DMI1 and the CNGC15 proteins interact in *M. truncatula*, and this may allow the simultaneous activation of both channels, predicted by mathematical modelling. In this

scenario, DMI1 functions not only as a counter-ion channel but also as a modulator of the Ca^{2+} signal (Charpentier *et al*., 2013, 2016).

Genes orthologous to *MtDMI1*, *MtCNGC15a/b/c*, and *MtMCA8* have been identified in non-symbiotic plant species, such as *Arabidopsis thaliana* (Capoen *et al*., 2011; Charpentier *et al*., 2016; Chen *et al*., 2009). Importantly, in Arabidopsis, a single *CNGC15* gene is found. Gene conservation suggests roles for nuclear Ca^{2+} signalling, mediated by these genes, that extend beyond symbiosis. However, no function has been assigned to these genes in non-symbiotic plant species until now, neither has nuclear Ca^{2+} signalling been associated with a key role in a specific developmental process.

The aim of the research presented in this chapter was to investigate the function of AtDMI1 and AtCNGC15 (henceforth referred to as DMI1 and CNGC15) in the non-symbiotic species *A. thaliana*. Using genetics, transcriptional analysis, cell biology, and Ca^{2+} imaging, I found that the nuclear Ca^{2+} signals encoded by DMI1 and CNGC15 are required for root development.

5.2. Results

5.2.1. *DMI1* and *CNGC15* are expressed in Arabidopsis roots

Transcriptomic data suggest that *DMI1* (*At5g49960*) and *CNGC15* (*At2g28260*) are expressed in Arabidopsis (see Appendix A and B for the expression profiles given by the Arabidopsis eFP Browser (Brady *et al*., 2007; Schmid *et al*., 2005; Winter *et al*., 2007). To validate these results, I used reverse transcription-quantitative polymerase chain reaction (RT-qPCR) to measure the expression of *DMI1* and *CNGC15* in different Arabidopsis organs. In all tissues tested, expression of both genes was detected, with *DMI1* being most highly expressed in rosette leaves and roots, and *CNGC15* in siliques and stems (Figure 5.1).

To characterise the expression pattern of *CNGC15*, I used plants expressing the *β-GLUCURONIDASE* (GUS) gene driven by a 1754 bp-long *CNGC15* native promoter (Myriam Charpentier, unpublished). A very strong GUS signal was detected in root tips as early as 1 day after germination (dag) (Figure 5.2 a). GUS activity was higher in the columella, and epidermal and cortex cell layers of the root meristem (Figure 5.2 c), and it was also detected in the hypocotyl-root junction (Figure 5.2 b, e), and the lateral root meristem (Figure 5.2 d).

Using transgenic plants expressing *DMI1-GFP* under its native promoter, it was shown that *DMI1* is expressed in meristematic cells, and localised at the nuclear envelope (Figure 5.3), similarly to the expression of *CNGC15*. In summary, both *DMI1* and *CNGC15* are expressed in the meristem of the Arabidopsis root.

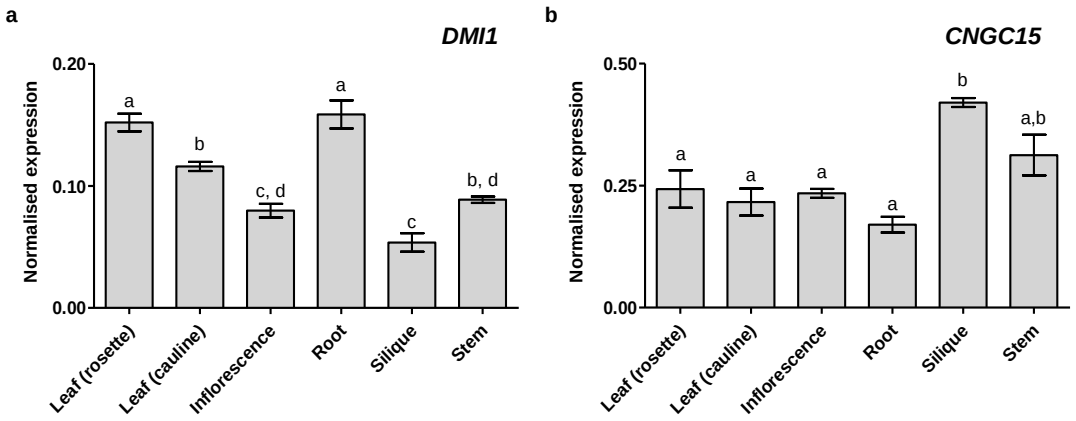

Figure 5.1 | *DMI1* and *CNGC15* are expressed in *A. thaliana*.

Quantitative expression analyses of the transcript level of *DMI1* (a) and *CNGC15* (b) by RT-qPCR in rosette leaves, cauline leaves, inflorescences, siliques, stems (5-week-old plants) and roots (2-week-old) (n = 4) of A. thaliana plants (Col-0). Expression was normalised to *UBOX* (*At5g15400*). Values are means ± s. e. m.. Different letters indicate statistical differences (one-way ANOVA with Bonferroni's multiple comparison post-test).

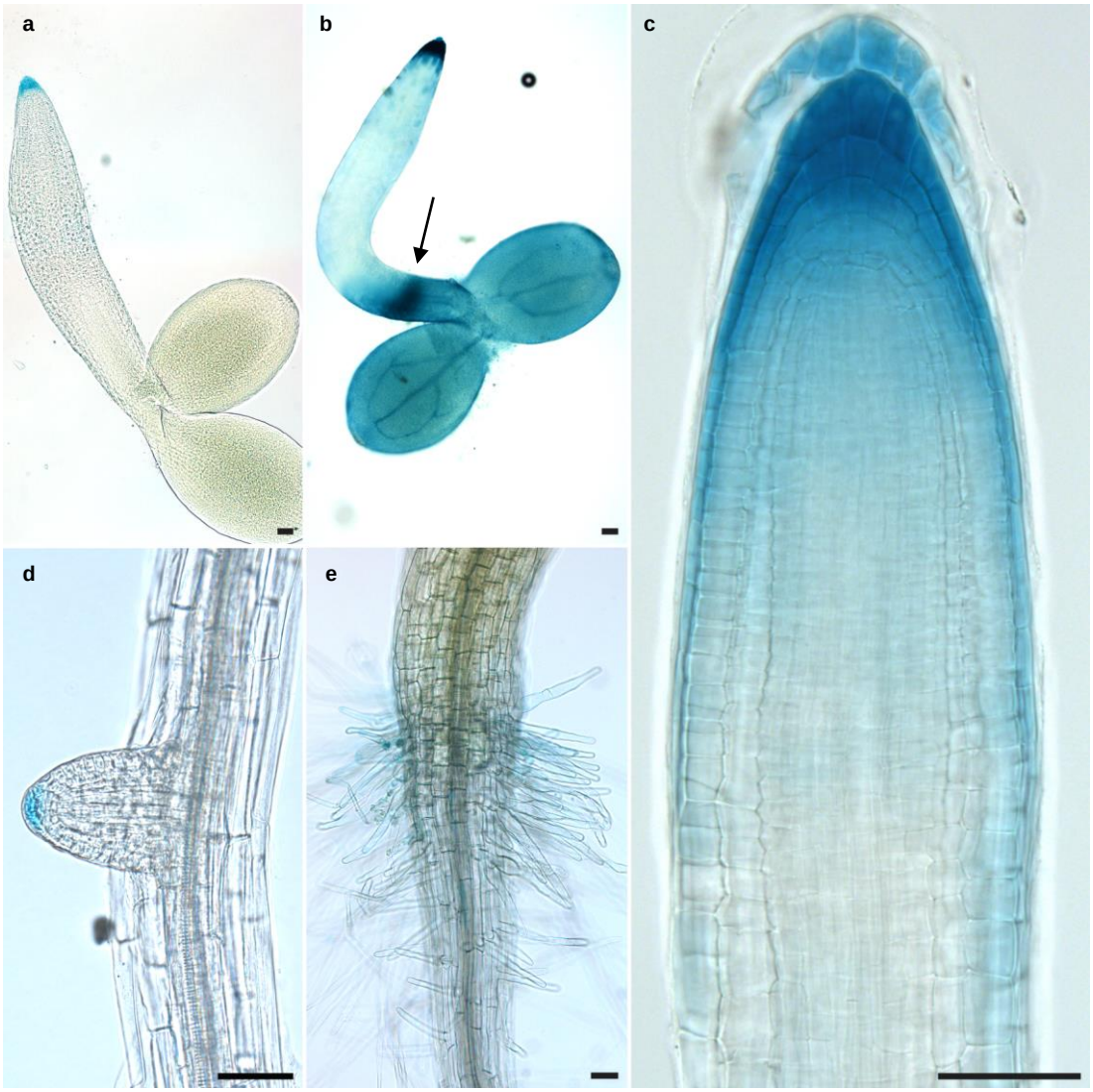

Figure 5.2 | *CNGC15* is expressed in the root meristem.

a-e, GUS staining in 1 day after germination (dag) *pAtCNGC15::GUS* Col-0 seedlings (a, b), 3 dag root meristem (c), 6 dag lateral root (d), 4 dag hypocotyl-root junction (e). The reaction was incubated for 30 min (a, c-e) or 24 h (b). The arrow in b points to the hypocotyl-root junction. Scale bars represent 50 µm.

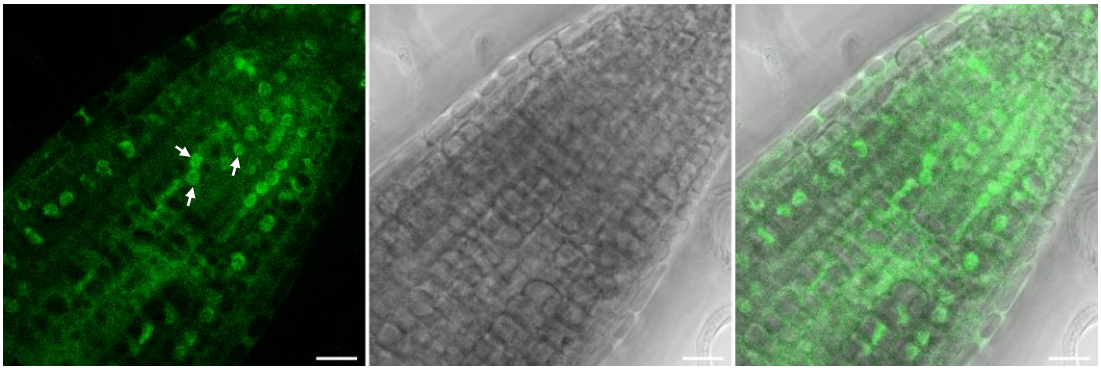

Figure 5.3 | DMI1 is expressed in the root meristem.

pAtDMI1::DMI1-GFP expression in the root meristem of 5 dag Col-0 plants (left: GFP channel; middle: bright field; right: composite image). White arrows indicate examples where GFP can be detected in nuclei. Scale bars represent 20 µm. This work was carried out by Myriam Charpentier (M. Charpentier, personal communication).

5.2.2. *dmi1* and *cngc15* mutants have defects in root development

To investigate the function of DMI1 and CNGC15 in Arabidopsis, two *dmi1* T-DNA insertion mutants, in a Col-0 background (named here *dmi1-1* and *dmi1-2*), and an ethyl methanesulfonate (EMS) *cngc15* mutant, in a Ler background (named *cngc15-1*) were retrieved from the Nottingham Arabidopsis Stock Centre (NASC, UK). The positions of the insertions in the *dmi1* mutants, and the position and polymorphism in *cngc15-1*, were confirmed by PCR and sequencing (Figure 5.4 a, b, c). *dmi1-1* has a T-DNA insertion in the sixth exon, whereas the insertion in *dmi1-2* sits 210 bp before the start codon. Expression of *DMI1* was downregulated in *dmi1-1* roots (approximately 25% of that observed in wild type), while in *dmi1-2* roots expression of *DMI1* was strongly upregulated (18 times higher than wild type) (Figure 5.4 d). To confirm that the full-length cDNA of *DMI1* was expressed in these samples, and to check for the occurrence of alternative splicing, primers flanking the entire predicted cDNA sequence were used in an RT-PCR reaction (Figure 5.4 b, middle). While no cDNA was detected in *dmi1-1*, in *dmi1-2* a single band, the same size of the one observed in wild type yet brighter, was observed, simultaneously confirming *DMI1* overexpression and the lack of alternative splicing. In *dmi1-1*, a truncated cDNA, featuring T-DNA-derived sequence, is nonetheless expressed (Figure 5.4 b, bottom). *dmi1-1* is thus a knock-down allele, expressing a truncated form of *DMI1*, and *dmi1-2* is a natural overexpression allele. Given their distinct expression profile, these alleles allow a comprehensive analysis of the role of DMI1 in Arabidopsis.

cngc15-1 harbours a G to A mutation on nucleotide +1570 (fifth exon), which results in a D408N non-synonymous mutation in the C-terminal domain of CNGC15 (Figure 5.4 c). Expression of *CNGC15* is not altered in *cngc15-1* roots (Figure 5.4 e).

Considering the central role that MtDMI1 and MtCNGC15a/b/c play in the rhizobial and mycorrhizal symbioses in the roots of *M. truncatula* (Charpentier *et al*., 2016), and that in Arabidopsis both *DMI1* and *CNGC15* are expressed in the root (Figures 5.1-5.3), root growth was monitored over time in *dmi1-1*, *dmi1-2*, and *cngc15-1*. Root length was measured and compared to wild-type (Col-0 or Ler) plants grown on the same plates as the mutant alleles, to account for differences caused by varying light conditions within the growth chamber. *dmi1-1* had significantly longer roots than Col-0 (Figure 5.5 a, g, h), as early as four dag, and most

obvious at 6, 7 and 12 dag. Conversely, *dmi1-2* had a short root phenotype, visible from six dag, one that worsened by 12 dag (Figure 5.5 b, g, h). Similarly to *dmi1-2*, *cngc15-1* also displayed a short root phenotype, strongly significant from the first time point at four dag, and sustained throughout the time course (Figure 5.5 c, g, h). *cngc15-1* plants were also shown to have reduced lateral root density at 12 dag (Figure 5.5 f), an effect that was not observed in the other mutants.

Normal root growth requires the maintenance and activity of the root meristem. Since *dmi1* and *cngc15* mutants show altered primary root length, I used confocal microscopy to characterise the meristematic and early elongation zones of the roots of these mutants at 6 and 12 dag (Figure 5.6). Meristem size was quantified by counting the number of cortical cells from the quiescent centre to the first rapidly elongated cell, and by measuring their lengths. Consistent with their short root phenotype, *dmi1-2* and *cngc15-1* had reduced meristem cell numbers (Figure 5.6 a, d, f), and meristem lengths (Figure 5.6 a, e, g), while in *dmi1-1* roots, no differences in meristem cell number or meristem length were observed (Figure 5.6 a, b, c). Interestingly, *cngc15-1* also displayed increased cell length (Figure 5.7 f, g), which was also observed in *dmi1-2*, albeit only in the meristem at 12 dag (Figure 5.7 d, e). In *dmi1-1*, no differences in meristem cell size were observed, but the first cells leaving the meristem were longer than wild type at six dag (Figure 5.7 b, c). Apart from altered cell number or cell size, no other differences in the anatomy of the primary root tip were detected in these mutants.

To further validate the EMS-induced polymorphism in *cngc15-1* as the cause of the root phenotype, *cngc15-1* complementation lines were generated and the root phenotype characterised (Figure 5.8). Expressing a *CNGC15-GFP* fusion under the *UBIQUITIN* promoter fully complemented the primary root length phenotype (Figure 5.8 a, b), meristem size, and cell size (Figure 5.8 c-f), confirming that *CNGC15* is required for normal root development in Arabidopsis.

Similarly, a *DMI1* overexpression line was generated in order to assess if the *dmi1-2* phenotype could be recapitulated. Expressing *DMI1* under the *UBIQUITIN* promoter (*UBI::DMI1*) led to *DMI1* overexpression in roots (Figure 5.9 a), shorter primary root length (Figure 5.9 b), and a smaller root meristem (Figure 5.9 c-e), similar to *dmi1-2* (Figure 5.4 e, Figure 5.5 b, g, and Figure 5.6 a, d-e). The difference in meristematic cell size on *dmi1-2* was

not seen in *UBI10::DMI1* (Figure 5.7 e, and Figure 5.9 f). The differences observed between the root phenotypes of this line and *dmi1-2* can possibly be due to *DMI1* being expressed in different cell types in each genotype.

In summary, *dmi1* and *cngc15* mutants have defects in primary root development, namely altered root length, as well as meristem and cell sizes. Mechanistically overexpressing *DMI1* mostly phenocopies *dmi1-2*, and the *cngc15-1* phenotype can be complemented with expression of the wild-type *CNGC15* sequence. The similarity between the *dmi1* and *cngc15* phenotypes, and because MtDMI1 and MtCNGC15a/b/c physically interact in *M. truncatula*, indicates that DMI1 and CNGC15 are part of the same signalling pathway that affects primary root development in Arabidopsis.

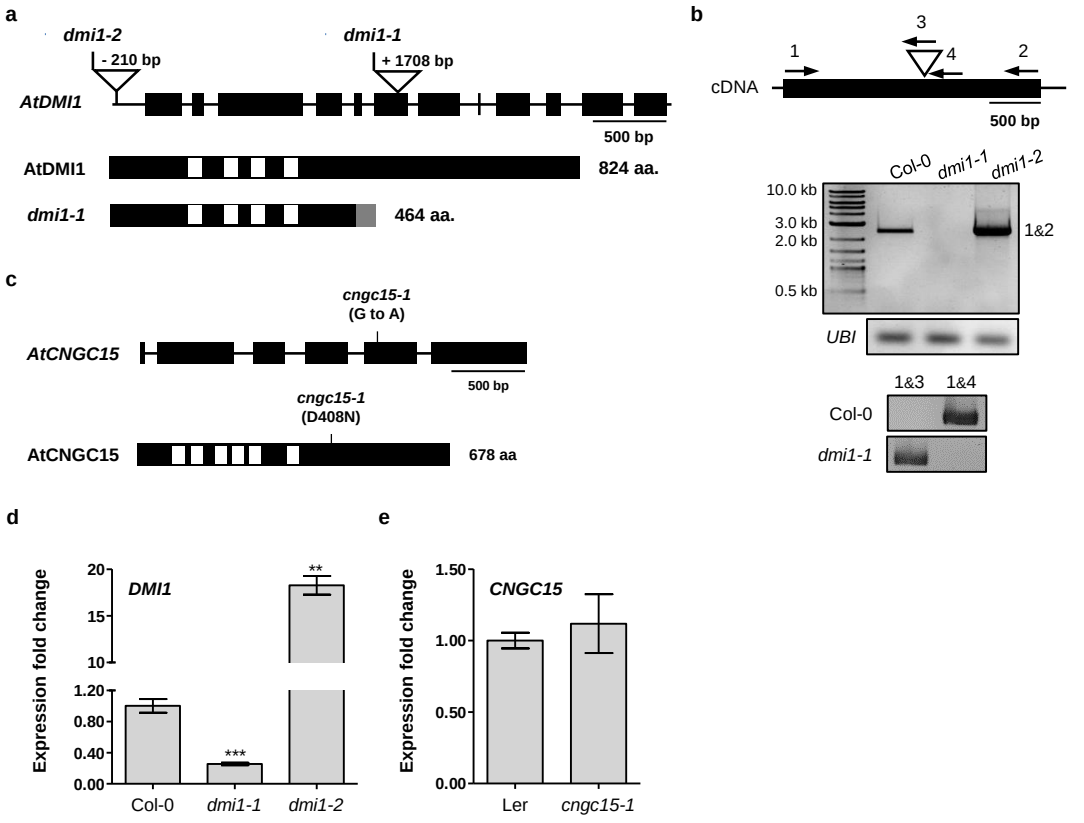

Figure 5.4 | Identification of *DMI1* and *CNGC15* mutants in *A. thaliana*.

a-c, Positions of the T-DNA insertions in *DMI1* (a, b) and the non-synonymous G to A point mutation in *CNGC15* (c), confirmed by PCR and sequencing. Exons are represented by black boxes and introns by black lines (top). The predicted structure of the wild-type amino acid sequences is represented, with transmembrane domains in white and the modified C-terminus derived from the T-DNA in grey (bottom). b, Expression analysis using RT-PCR in Col-0, *dmi1-1* and *dmi1-2*. The position of the primers on the cDNA is indicated by arrows (top) (key to primers: 1 – PG421; 2 – PG395; 3 – PG422; 4 – PG423). d, e, Quantitative expression analysis of the transcript level of *DMI1* (d) and *CNGC15* (e) by RT-qPCR in root samples (n = 3, pools of 40-60 plants). Expression was normalised to *UBOX* (*At5g15400*) and presented as fold change over control (Col-0 or Ler). Values are means ± s. e. m.. ** $p < 0.01$, *** $p < 0.001$ (two-tailed t-test with a prior F-test for homoscedasticity).

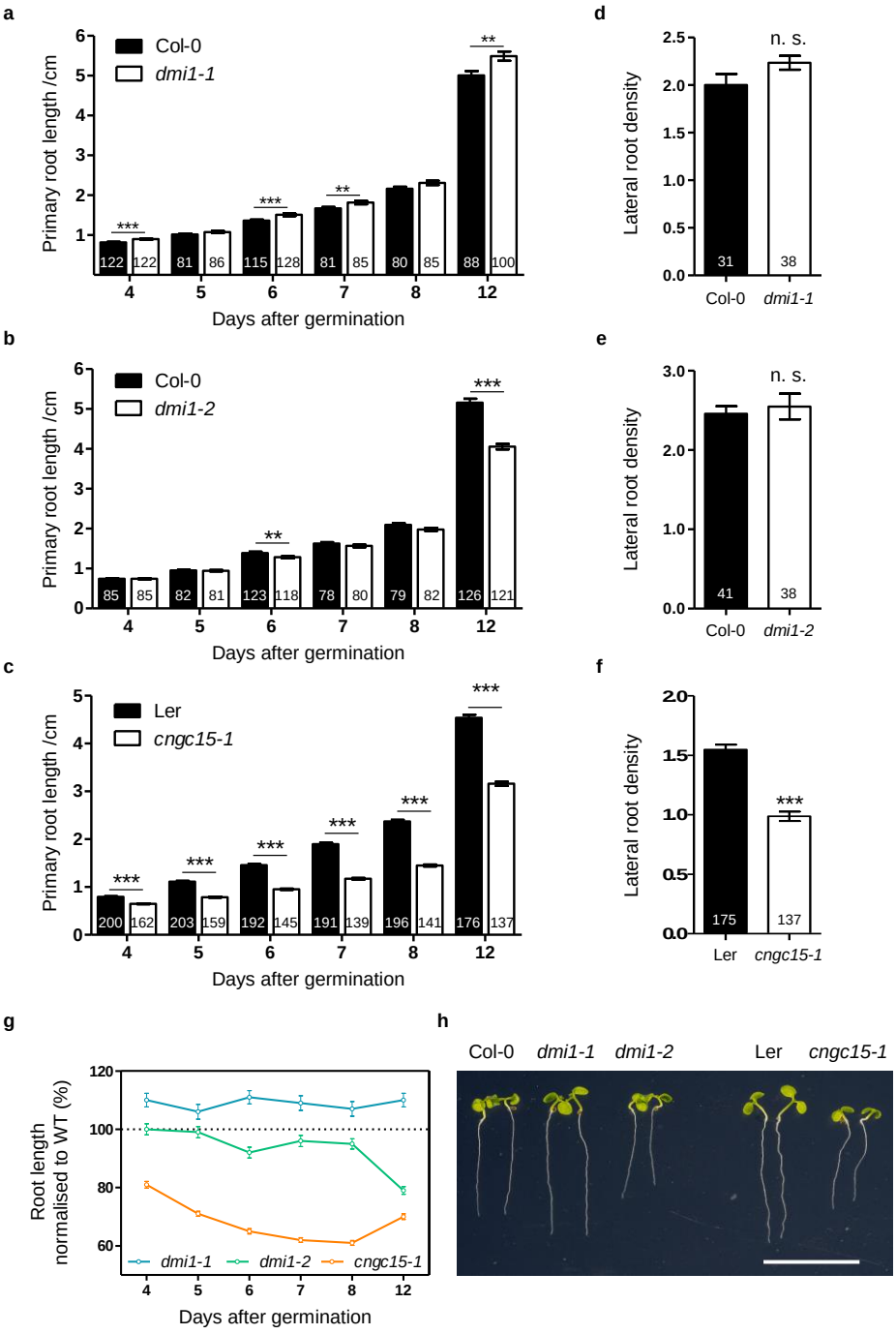

Figure 5.5 | Root phenotype of *dmi1* and *cngc15* mutants.

a, b, c, Primary root length quantification time course of wild type (Col-0 and Ler) and *dmi1-1* (a), *dmi1-2* (b), and *cngc15-1* (c). d, e, f, Lateral root density at 12 days after germination (dag) of wild type (Col-0 and Ler) and *dmi1-1* (d), *dmi1-2* (e), and *cngc15-1* (f). g, Primary root length normalised to the equivalent wild type. All values are means ± s. e. m.. Numbers in bars denote sample size (n). ** $p < 0.01$, *** $p < 0.001$ (two-tailed t-test with a prior F-test for homoscedasticity). h, Representative image of Col-0, *dmi1-1*, *dmi1-2*, Ler, and *cngc15-1* seedlings at six dag (scale bar represents 1 cm).

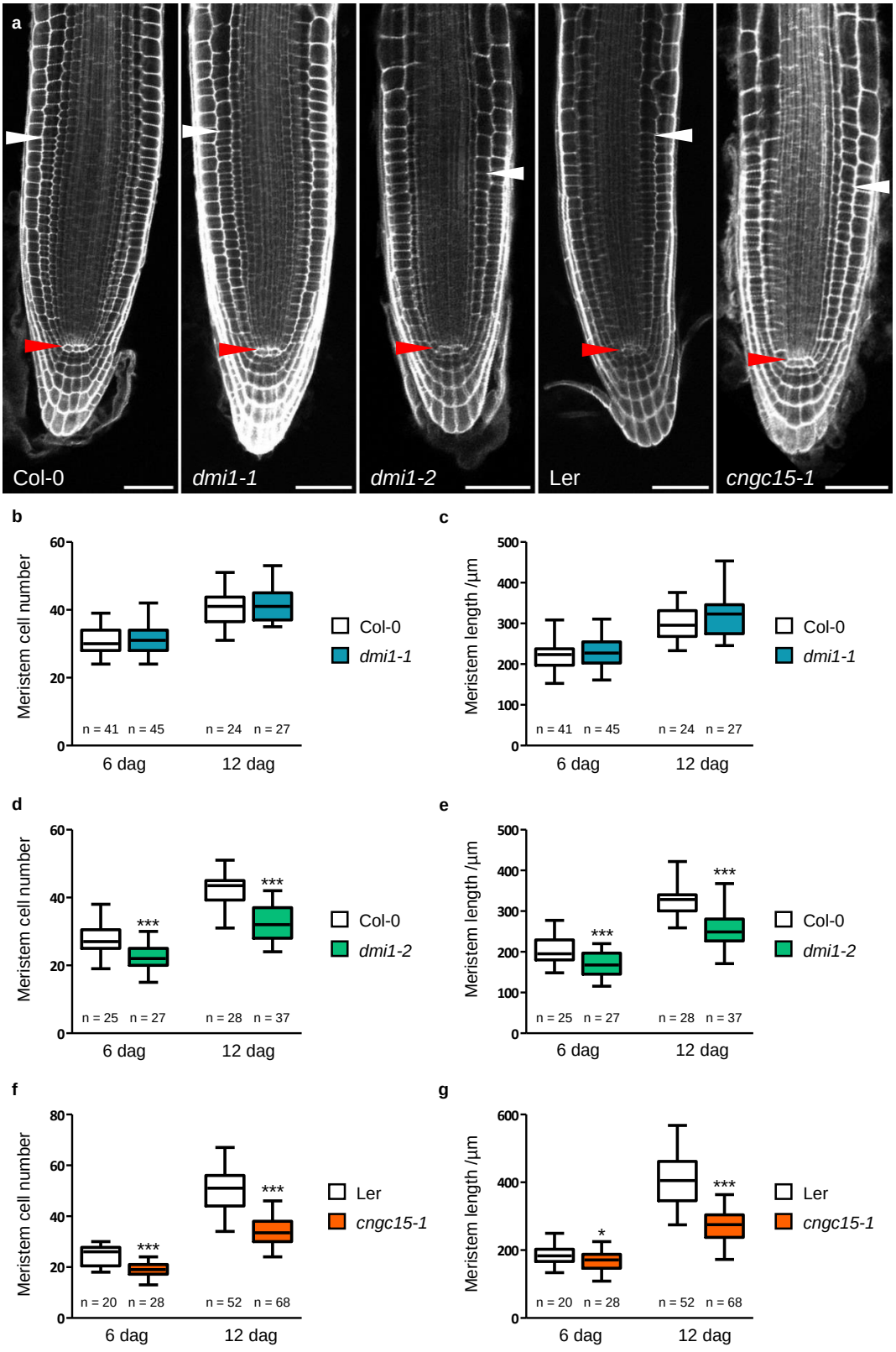

Figure 5.6 | Characterisation of the root meristem of *dmi1* and *cngc15-1* mutants, 6 and 12 days after germination (dag).

a, Longitudinal view of the root meristem of wild type (Col-0 and Ler) and *dmi1-1*, *dmi1-2*, and *cngc15-1*. White and red triangles mark the first elongated cortex cell and the quiescent centre, respectively. Scale bars represent 50 µm. b, d, f, Root meristem cell number of wild type (Col-0 and Ler) and *dmi1-1* (b), *dmi1-2* (f), and *cngc15-1* (f). c, e, g, Root meristem length of wild type (Col-0 and Ler) and *dmi1-1* (c), *dmi1-2* (e), and *cngc15-1* (g). Box and whisker plots show 25% and 75% percentiles, median, minimum and maximum. * $p < 0.05$, ** $p < 0.01$, *** $p < 0.001$ (two-tailed t-test with a prior F-test for homoscedasticity).

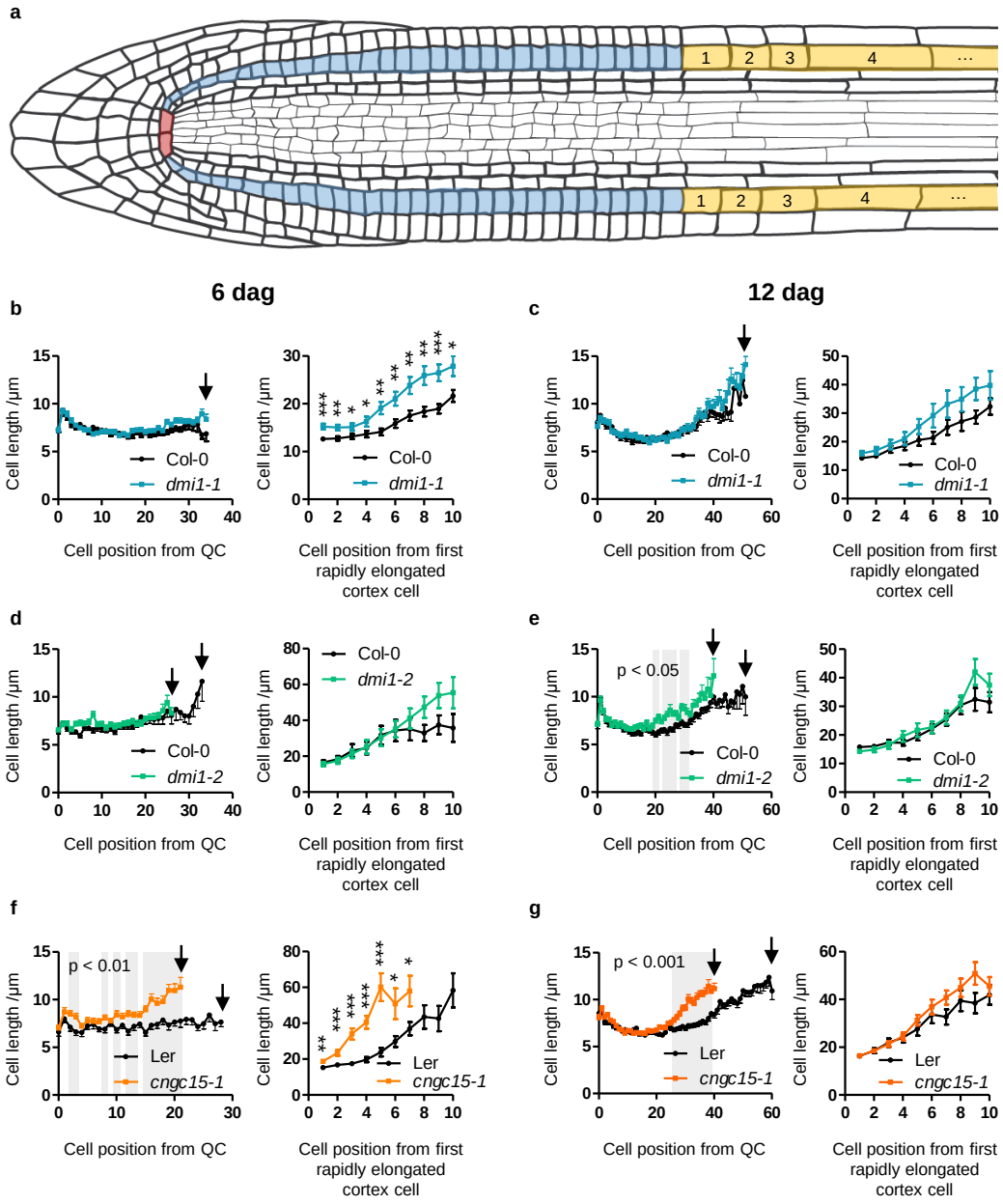

Figure 5.7 | Characterisation of cell size of meristematic and elongating root cells of *dmi1* and *cngc15* mutants, 6 and 12 days after germination (dag).

a, Schematic representation of an Arabidopsis primary root tip, with the cell files analysed highlighted (key - red: quiescent centre (QC); blue: meristematic cortex; yellow: elongating cortex). b-g, Cell length over cell position from the QC to the last meristematic cortex cell (left, in blue in a), and cell length over cell position from the first rapidly elongated cortex cell (right, in yellow in a) of wild type (Col-0 and Ler) and *dmi1-1* (b, c), *dmi1-2* (d, e), and *cngc15-1* (f, g), at six dag (b, d, f) and 12 dag (c, e, g). Black arrows mark the last meristematic cell and areas shaded in grey indicate significant differences between the genotypes (mean ± s. e. m.; * p<0.05, ** p<0.01, *** p<0.001 ($20 \leq n \leq 67$; two-tailed t-test with a prior F-test).

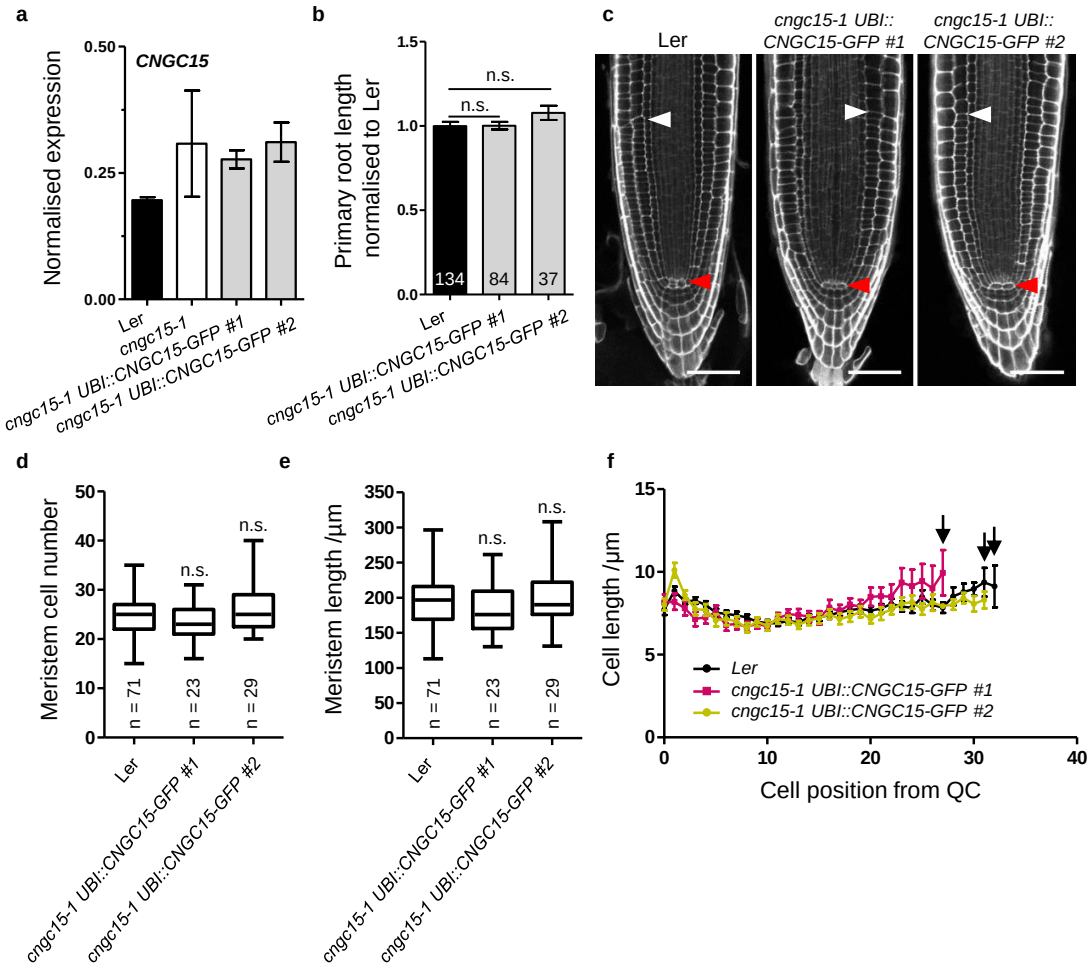

Figure 5.8 | Complementation of the *cngc15-1* phenotype.

a, b, Quantification of *CNGC15* transcript (n = 3 or 4, pools of 40-60 plants) (a) and primary root length at 12 days after germination (dag) (b) in root samples of Ler, *cngc15-1,* and two independent *cngc15-1* complementation lines (*cngc15-1 UBI::CNGC15-GFP* #1 and #2). Expression was normalised to *UBOX* (*At5g15400*). c, Longitudinal view of the root meristem of Ler and *cngc15-1* complementation lines (*cngc15-1 UBI::CNGC15-GFP* #1 and #2). White and red triangles mark the first elongated cortex cell and the quiescent centre (QC), respectively. Scale bars represent 50 µm. d, e, f, Root meristem cell number (d), root meristem length (e), and cell length over cell position from the QC to the last meristematic cell (black arrows) (f) of Ler and *cngc15-1* complementation lines (*cngc15-1 UBI::CNGC15-GFP* #1 and #2). Meristem cell number, length, and cell length profile were quantified at six dag. Box and whisker plots show 25% and 75% percentiles, median, minimum and maximum. Bar graphs show mean ± s. e. m.. Numbers in bars denote sample size (n). * $p < 0.05$, ** $p < 0.01$, *** $p < 0.001$ (two-tailed t-test with a prior F-test for homoscedasticity).

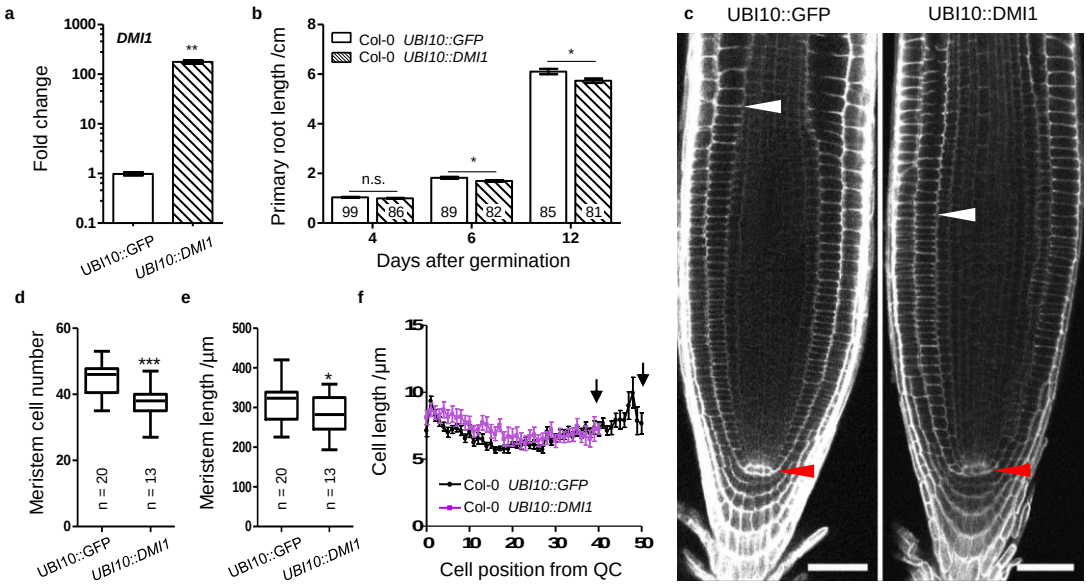

Figure 5.9 | Overexpression of *DMI1* recapitulates the *dmi1-2* phenotype.

a, b, Quantification of *DMI1* transcript (n = 3 or 4, pools of 40-60 plants) (a) and primary root length time course (b) in root samples of control (Col-0 *UBI10::GFP*) and a *DMI1* overexpression line (Col-0 *UBI10::DMI1*). Expression was normalised to *UBOX* (*At5g15400*). c, Longitudinal view of the root meristem of control (Col-0 *UBI10::GFP*) and the *DMI1* overexpression line (Col-0 *UBI10::DMI1*). White and red triangles mark the first elongated cortex cell and the quiescent centre (QC), respectively. Scale bars represent 50 µm. d, e, f, Root meristem cell number (d), root meristem length (e), and cell length over cell position from the QC to the last meristematic cell (black arrows) (f) of control (Col-0 *UBI10::GFP*) and *DMI1* overexpression line (Col-0 *UBI10::DMI1*). Meristem cell number, length, and cell length profile were quantified 12 days after germination. Box and whisker plots show 25% and 75% percentiles, median, minimum and maximum. Bar graphs show mean ± s. e. m.. Numbers in bars denote sample size (n). * $p < 0.05$, ** $p < 0.01$, *** $p < 0.001$ (two-tailed t-test with a prior F-test for homoscedasticity).

5.2.3. *dmi1* and *cngc15* mutants are affected in auxin signalling

The positioning of the transition zone in the root is defined by the balance between the endogenous levels of auxin and cytokinin (Ioio *et al*., 2008; Moubayidin *et al*., 2009; Mambro *et al*., 2017). To understand if the root phenotypes observed in the *dmi1* and *cngc15* mutants are caused by changes in endogenous levels of auxin in the root, homozygote *dmi1* and *cngc15* mutant lines expressing the auxin sensors DII-VENUS (Brunoud *et al*., 2012) and DR5-GFP (Friml *et al*., 2003) were generated (Myriam Charpentier, unpublished). While DR5-GFP fluorescence correlates with the auxin-induced activation of *DR5* expression, DII-VENUS more directly correlates to endogenous auxin levels, as the rationale of the reporter is the auxin-induced degradation of a fast maturing yellow fluorescent protein (VENUS) fused in-frame with the auxin-interaction domain (DII) of AUX/IAA proteins. These sensors are partly complementary and allow the detection of endogenous auxin distribution (Brunoud *et al*., 2012). DII-VENUS fluorescence intensity in the root tip was significantly reduced in *dmi1-1* roots and increased in *dmi1-2* and *cngc15-1* (Figure 5.10 a-e). Conversely, DR5-GFP fluorescence was significantly increased in *dmi1-1* roots, but reduced in *dmi1-2* and *cngc15-1* (Figure 5.10 f-j). These results provide strong evidence of increased levels of endogenous auxin in *dmi1-1*, and reduced amounts of endogenous auxin in *dmi1-2* and *cngc15-1*, specifically in the quiescent centre and the columella, in the root tip. Additionally, expression of *PIN3* and *PIN7*, but not *PIN1*, was altered in the roots of *dmi1-2* and *cngc15-1* plants (Figure 5.11), suggesting that the differences observed in the endogenous auxin levels in these mutants could be due to altered auxin transport, driven by changes in expression of a subset of *PIN* genes.

To investigate if auxin could rescue the *dmi1* and *cngc15-1* phenotypes, plants were grown in the presence of 100 nM auxin (IAA). The *dmi1-1* phenotype was rescued in all time points tested whereas, in *dmi1-2* roots, the differences in size observed were the same as in the absence of IAA, except at four dag (Figure 5.12 a, b). *cngc15-1* roots were insensitive to IAA treatment, as the differences in size between wild type and mutant were maintained (Figure 5.12 c). This was confirmed by confocal analysis of the root meristem of plants grown in the presence of 100 nM IAA at 12 dag (Figure 5.13 and Figure 5.14). No differences in meristem cell number or meristem size were seen in *dmi1-1* when compared to Col-0, at 12 dag, similarly to growth in the absence of IAA (Figure 5.13 a, b). The meristem cell number and meristem

size were reduced, compared to wild type, in both *dmi1-2* and *cngc15-1*, similarly to growth in the absence of IAA (Figure 5.13 c-f). Additionally, IAA produced no effect on the cell size of these mutants (Figure 5.14). While *cngc15-1* elongated cells are significantly longer than Ler grown in the presence of 100 nM IAA, this effect is due to an IAA-induced reduction of cell size in Ler, whereas there are no statistically significant differences between the size of *cngc15-1* cells grown in the presence or absence of IAA (Figure 5.14 e, f).

To evaluate if a cytokinin imbalance could also be responsible for the root phenotypes observed, the expression of genes known to be responsive to cytokinin, including Arabidopsis Response Regulator genes, genes involved in cytokinin biosynthesis, and a cytokinin receptor gene, was quantified in 12 dag root samples (Figure 5.15). No significant differences were seen in the expression of these genes in *dmi1-1*, *dmi1-2*, or *cngc15-1*.

Together, these results indicate that the root phenotypes observed are the result of altered auxin levels in the root tip, specifically in the columella and around the quiescent centre, possibly due to abnormal expression of *PIN3* and *PIN7*. Considering that the phenotypes of *dmi1-2* and *cngc15-1* are not rescued by supplementing the growth medium with IAA, DMI1 and CNGC15 are predicted to act downstream of IAA-induced signalling.

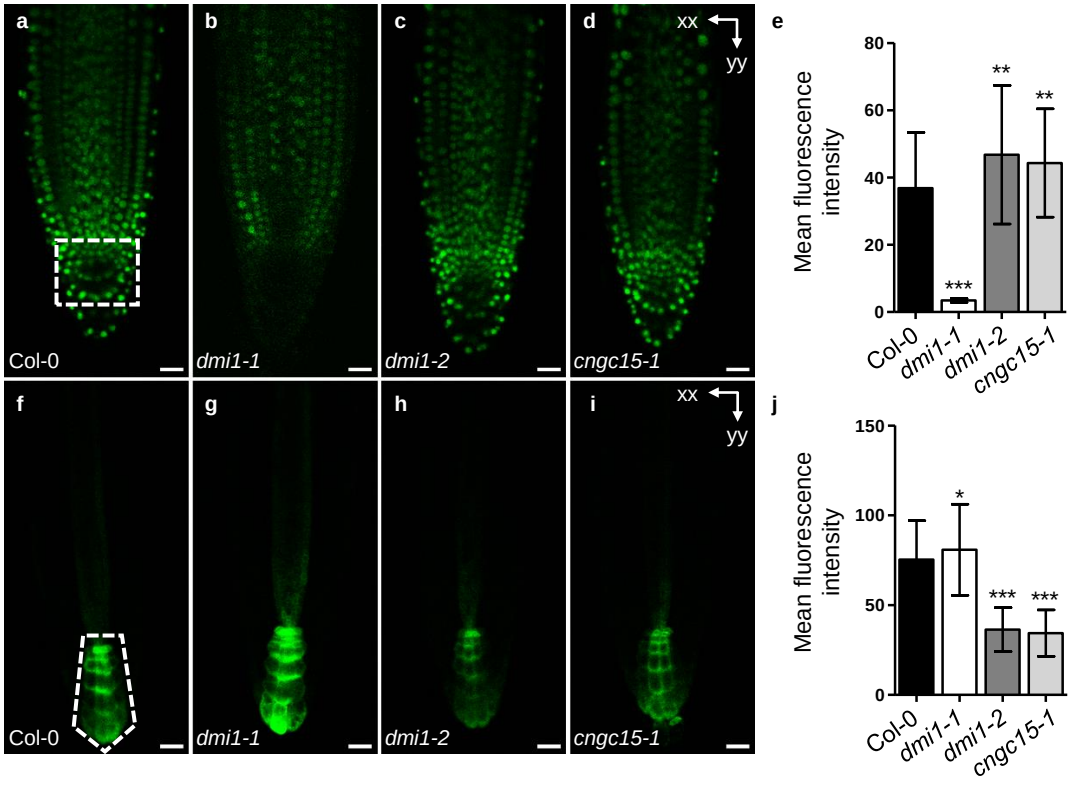

Figure 5.10 | *dmi1* and *cngc15* mutants have altered levels of endogenous auxin in the quiescent centre and columella.

Representative images of root tips of Col-0, *dmi1-1*, *dmi1-2*, and *cngc15-1* plants expressing *DII-VENUS* (a-d) or *DR5-GFP* (f-i) six days after germination. Dashed lines delimit area used for quantification. Scale bars represent 20 µm. e, j, Mean fluorescence intensity of the DII-VENUS (e) or DR5-GFP (j) signals in Col-0, *dmi1-1*, *dmi1-2*, and *cngc15-1*. Intensity was averaged across the xx axis for successive lines down the yy axis, within the delimited area (marked in a and f). The total area was the same for each plant. Values are means ± s. d.. ** $p < 0.01$, *** $p < 0.001$ (t-test with a prior F-test for homoscedasticity). This work was carried out by Myriam Charpentier (Myriam Charpentier, personal communication).

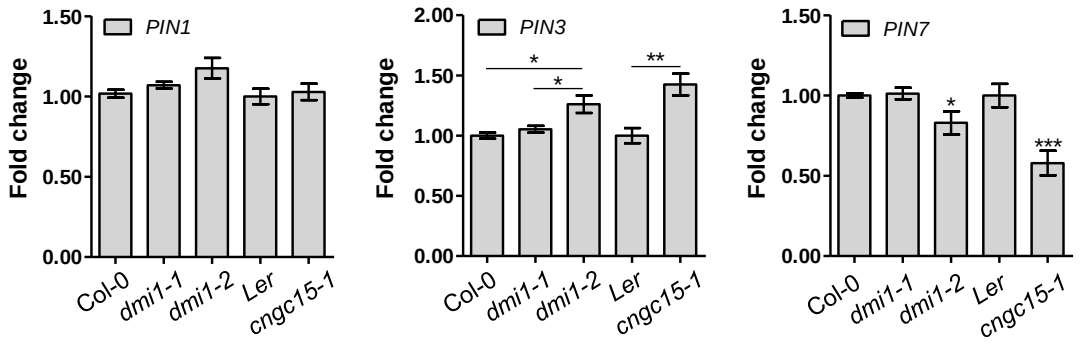

Figure 5.11 | *PIN3* and *PIN7* expression are changed in *dmi1* and *cngc15* mutants.

Quantitative expression analyses of the transcript level of *PIN1*, *PIN3*, and *PIN7* by qPCR in root samples of Col-0, *dmi1-1*, *dmi1-2*, Ler, and *cngc15-1* (n = 3 or 4, each sample was a pool of 40-60 plants) 12 days after germination. Expression was normalised to *UBOX* (*At5g15400*) and results are presented as fold change over wild type (Col-0 or Ler). Values are means ± s. e. m.. * $p < 0.05$, ** $p < 0.01$, *** $p < 0.001$ (two-tailed t-test with a prior F-test for homoscedasticity).

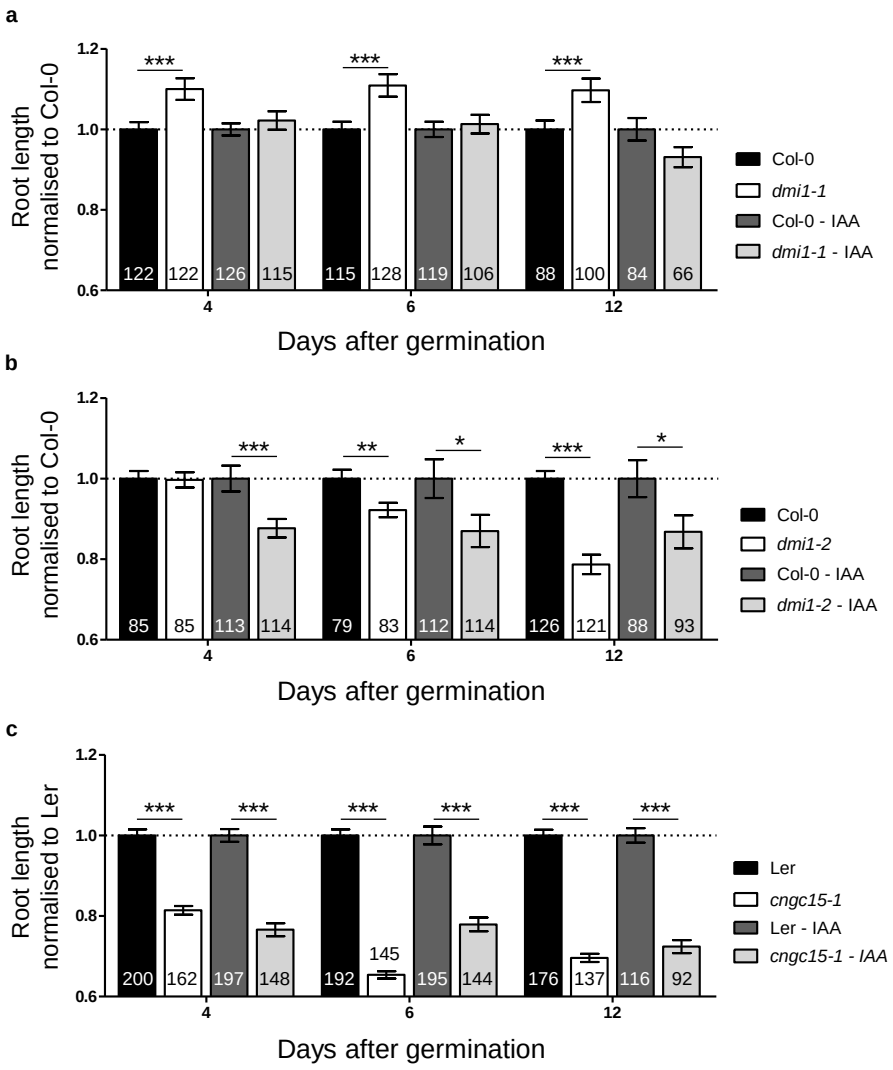

Figure 5.12 | Effect of exogenously applied auxin (IAA) on the root phenotype of *dmi1* and *cngc15* mutants.

a, b, c, Primary root length quantification time course of wild type (Col-0 and Ler) and *dmi1-1* (a), *dmi1-2* (b), and *cngc15-1* (c), grown in the absence or presence of 100 nM of indole-3-acetic acid (IAA). Values were normalised to wild type grown under the same conditions and represent means ± s. e. m.. Numbers in bars denote sample size (n). * $p < 0.05$, ** $p < 0.01$, *** $p < 0.001$ (two-tailed t-test with a prior F-test for homoscedasticity).

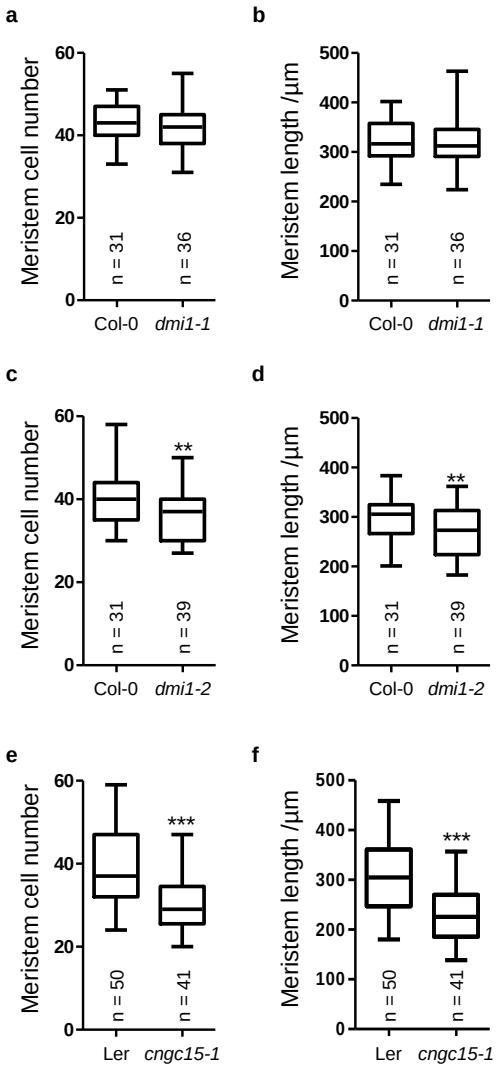

Figure 5.13 | Characterisation of the root meristem of *dmi1* and *cngc15* mutants, 12 days after germination in the presence of 100 nM IAA.

a, c, e, Root meristem cell number of wild type (Col-0 and Ler) and *dmi1-1* (a), *dmi1-2* (c) and *cngc15-1* (e). b, d, f, Root meristem length of wild type (Col-0 and Ler) and *dmi1-1* (b), *dmi1-2* (d), and *cngc15-1* (f). Box and whisker plots show 25% and 75% percentiles, median, minimum and maximum. ** $p < 0.01$, *** $p < 0.001$ (two-tailed t-test with a prior F-test for homoscedasticity).

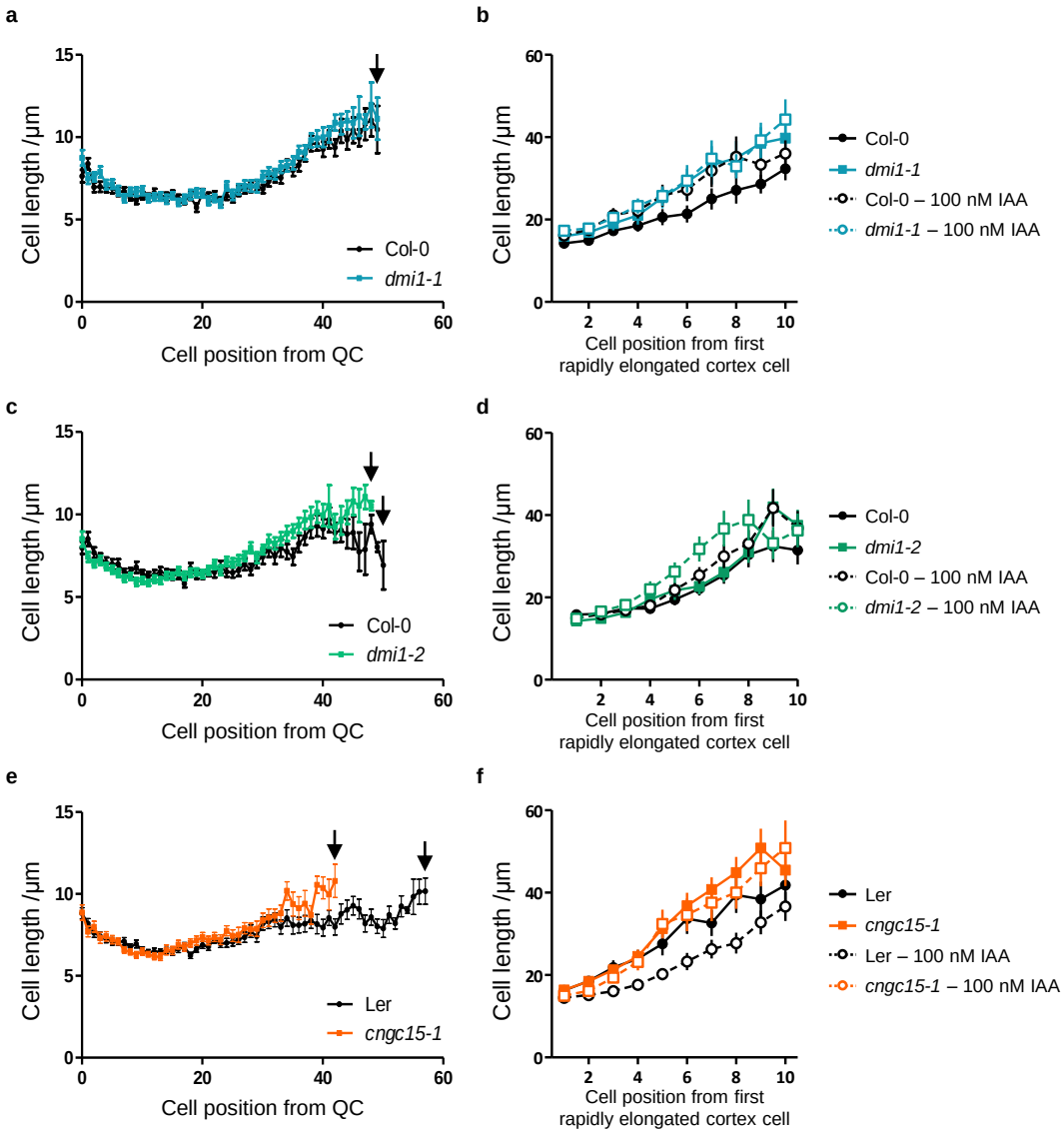

Figure 5.14 | Characterisation of cell size of meristematic and elongating root cells of *dmi1* and *cngc15* mutants, 12 days after germination in the presence of 100 nM IAA.

a, c, e, Cell length over cell position from the quiescent centre of meristematic cells of wild type (Col-0 and Ler) and *dmi1-1* (a), *dmi1-2* (c), and *cngc15-1* (e). Black arrows mark the last meristematic cell. b, d, f, Cell length over cell position from the first rapidly elongated cortex cell of wild type (Col-0 and Ler) and *dmi1-1* (b), *dmi1-2* (d), and *cngc15-1* (f). Values are means ± s. e. m..

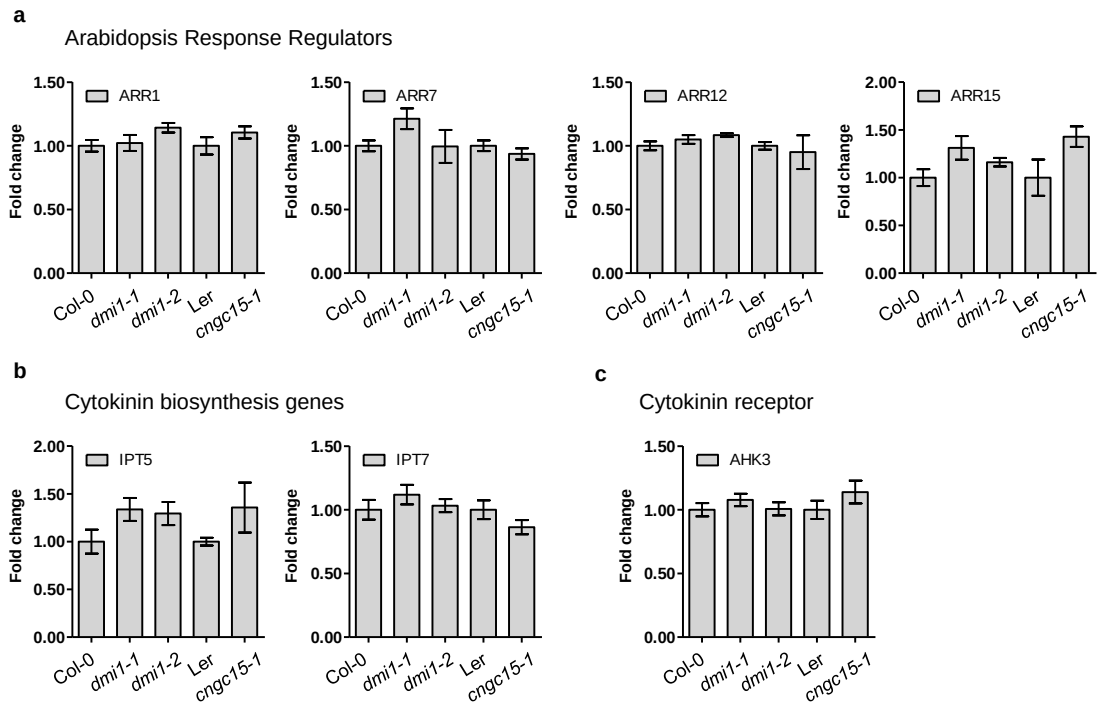

Figure 5.15 | Transcription of cytokinin marker genes is not affected in *dmi1* and *cngc15* mutants.

Quantitative expression analyses of the transcript level of Arabidopsis Response Regulator genes (a), cytokinin biosynthesis genes (b), and the cytokinin receptor *AHK3* (c), by qPCR in root samples of Col-0, *dmi1-1*, *dmi1-2*, Ler, and *cngc15-1* (n = 3 or 4, each sample was a pool of 40-60 plants), 12 days after germination. Expression was normalised to *UBOX* (*At5g15400*) and results are presented as fold change over wild type (Col-0 or Ler). Values are means ± s. e. m.. No statistical differences were found (two-tailed t-test with a prior F-test for homoscedasticity).

5.2.4. Nuclear Ca^{2+} signals occur during root growth in a *DMI1/CNGC15* dependent manner

To link the root phenotypes observed in *dmi1* and *cngc15* mutants to the predicted roles of DMI1 and CNGC15 as encoders of nuclear Ca^{2+} signals, I performed live Ca^{2+} imaging in five dag roots of wild-type and mutant plants expressing the dual-localised Ca^{2+} sensor G-GECO1.2-NES/R-GECO1.2-NLS (described in Chapter III). Seedlings were mounted in liquid medium, allowed to recover for at least 45 min, and imaged at 2 or 3-second intervals for a minimum of one hour, in the absence of any external stimulus. Nuclear- and cytosolic-localised Ca^{2+} signals were observed in the meristem and elongation zones of the root, across all genotypes. A spatial and temporal analysis of this response revealed that the signal occurs first in the nucleus, and subsequently extends to the cytosol (Figure 5.16). Nuclear signals occurred in the form of a single spike, with a mean duration of 39.5 s, in Col-0 (Table 5.1).

Table 5.1 | Mean duration of the nuclear Ca^{2+} signals observed in roots during growth.

Genotype	Mean duration/s	95% confidence interval	Number of traces (n)
Col-0	39.5	[36.5; 42.5]	81
dmi1-1	55.2	[49.9; 60.5]	68
dmi1-2	42.9	[39.6; 46.3]	57
cngc15-1	42.6	[38.1; 47.1]	58

Analysis of the spike shape using unbiased computational methods (Figure 5.17 a) allowed the calculation of the mean rise and fall times of the Ca^{2+} signal, defined as the time from the start of the pulse to the peak (rise), and the time from the peak to the end of the pulse (fall). Both rise and fall time were increased in *dmi1-1*, but did not change in *dmi1-2* or *cngc15-1* (Figure 5.17 b). Importantly, the frequency of the signals observed per plant was decreased in *dmi1-2* and *cngc15-1*, but not in *dmi1-1* (Figure 5.17 c). Additionally, the location of these signals in the roots of *dmi1-2* and *cngc15-1* also changed when compared to wild type. The proportion of traces in the meristem against the elongation zone was decreased in *cngc15-1* and *dmi1-2* when compared to *dmi1-1* (Figure 5.17 d).

These results indicate that DMI1 and CNGC15 have a role in generating nuclear Ca^{2+} signals during root growth. The absence of DMI1 led to changes in the Ca^{2+} kinetics, i.e. spike shape, but not in frequency or localisation. In contrast, overexpressing DMI1, or the point mutation in CNGC15, led to a reduced frequency of Ca^{2+} signals. This impairment was especially observed in the root meristem.

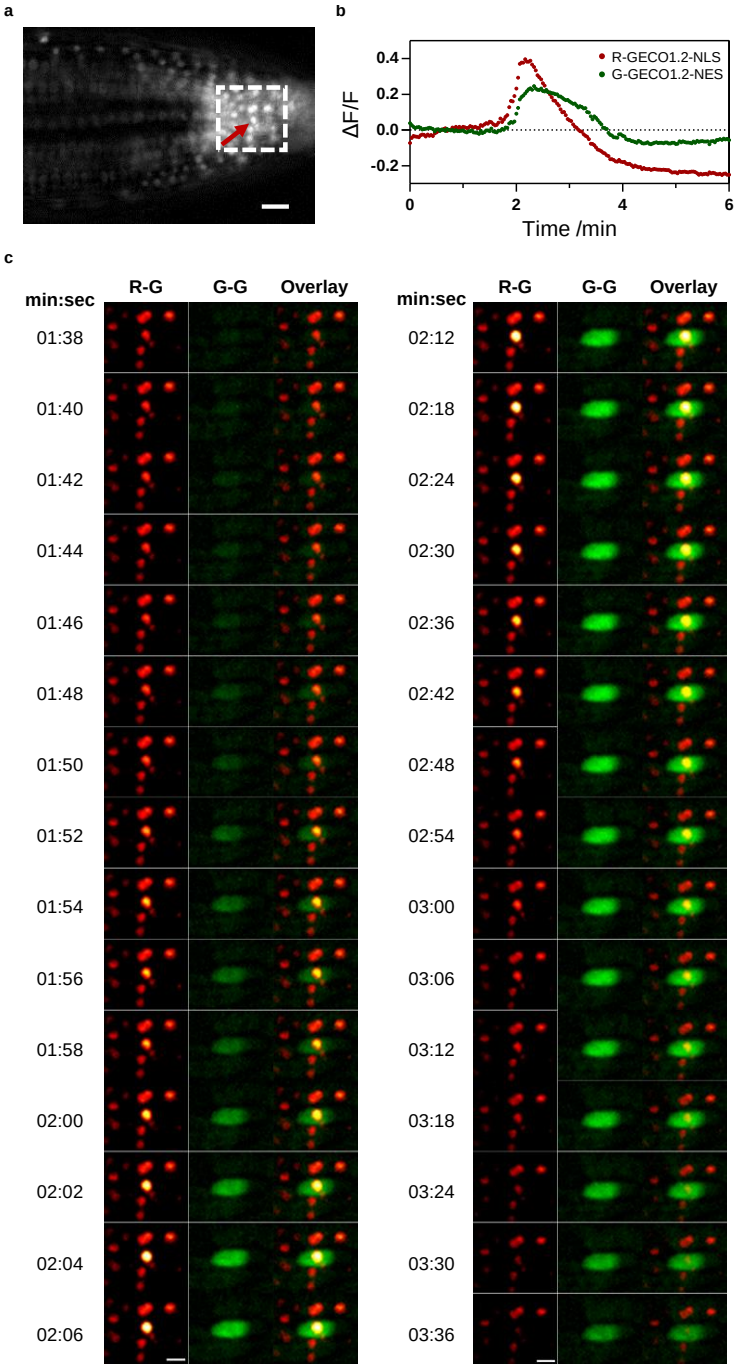

Figure 5.16 | Growth-induced Ca^{2+} signals originate in the nucleus.

a, b, Analysis of a representative growth-induced Ca^{2+} signal. Normalised fluorescence intensity over time (b), measured in the R-GECO1.2 (red) and G-GECO1.2 (green) channels, of the cell indicated by an arrow in a. Scale bar represents 20 µm. c, Sequence of images showing a representative growth-induced Ca^{2+} signal occurring first in the nucleus, and then expanding to the cytosol, of a cell in the root tip of a five dag seedling expressing the dual sensor G-GECO1.2-NES/R-GECO1.2-NLS. Frames are 2 seconds apart (left) and 6 seconds apart (right). Images are a digital magnification of the area within the dashed square in a. Scale bars represent 10 µm.

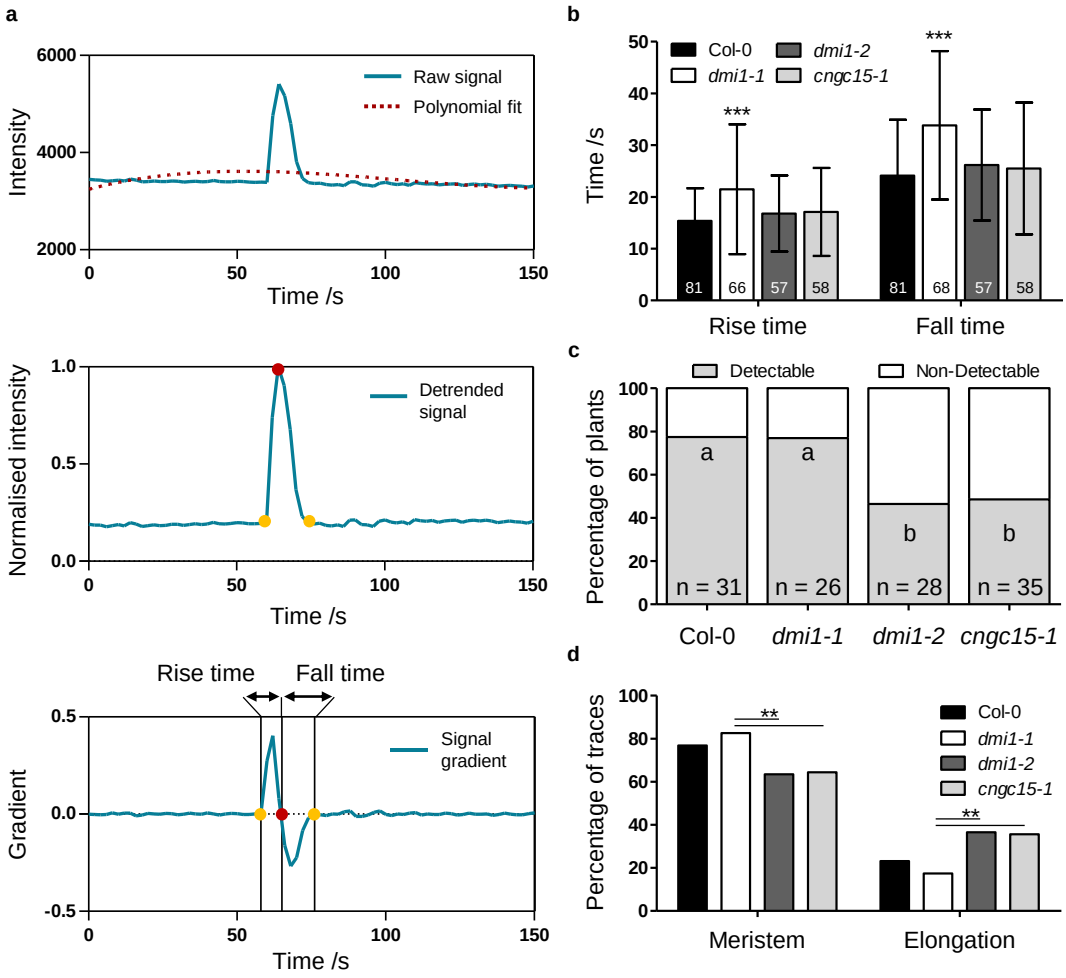

Figure 5.17 | DMI1 and CNGC15 are required for the generation of Ca^{2+} signals during root development.

a, Analysis of a representative trace. Raw signal (intensity over time) and polynomial fit used in the detrending (top). Normalised signal, obtained by removing the polynomial fit from the raw data, with points marking the beginning and end of the pulse (yellow circles), and the peak maximum (red circle) (middle). Signal gradient with beginning, end, and maximum of the pulse (as above), and indication of the rise and fall times (bottom) b, Rise and fall times. Values are means ± s.d.. *** $p < 0.001$ (two-tailed t-test with a prior F-test for homoscedasticity). c, Percentage of plants that displayed cell autonomous nuclear Ca^{2+} signals during root growth, at five dag, in Col-0, *dmi1-1*, *dmi1-2*, and *cngc15-1*. Numbers in bars represent the total of plants imaged (n) (X^2 test, different letters represent $p < 0.05$). d, Percentage of Ca^{2+} signals localised to the meristem and elongation zones in Col-0 (n = 69), *dmi1-1* (n = 69), *dmi1-2* (n = 52), and *cngc15-1* (n = 59) (** $p < 0.01$, X^2 test).

5.3. Discussion

Nuclear Ca^{2+} spiking is essential for the successful establishment of nitrogen-fixing rhizobial and arbuscular mycorrhizal symbioses. This is a process that involves intricate signalling pathways that orchestrate communication between vastly different organisms and lead to complex developmental changes in the plant. Nuclear Ca^{2+} spiking in response to nodulation (Nod) factors was first described over 20 years ago in alfalfa (Ehrhardt *et al*., 1996), but only recently were the Ca^{2+} channels required to encode this signal identified in the model legume species *M. truncatula* (Charpentier *et al*., 2016) and, importantly, no other examples of nuclear Ca^{2+} signalling in plants have been characterised. These nuclear Ca^{2+} signals are encoded by the MtCNGC15 proteins and the K^+-permeable channel MtDMI1 in response to Nod and mycorrhizal (Myc) factors, and are necessary for downstream symbiotic responses. Surprisingly, these genes are conserved across land plants, including non-symbiotic species, which suggests a role for nuclear Ca^{2+} signalling that likely extends beyond symbiosis but has thus far remained uncharacterised.

In this work, I have demonstrated for the first time that nuclear Ca^{2+} signals, mediated by DMI1 and CNGC15, occur in Arabidopsis root cells and are required for normal root development. Use of a dual-localised Ca^{2+} sensor allowed a detailed spatial and temporal analysis of this response, and revealed that the signal occurs first in the nucleus, and subsequently extends to the cytosol (Figure 5.16). These signals, which take the form of single spikes, were detected in meristematic and elongation cells, during growth, in the absence of any external stimuli. The kinetics of the Ca^{2+} signal was unchanged in *cngc15-1* (Figure 5.17 b). The D408N mutation in CNGC15 in the *cngc15-1* background is not localised in predicted transmembrane domains (Figure 5.4), and as such channel function might not be affected. However, channel regulation by currently unidentified interacting partners could be compromised, which includes possible phosphorylation of this amino acid (D408). In fact, aspartate phosphorylation has been described in eukaryotes as a signalling mechanism (Thomason and Kay, 2000). The proportion of plants showing nuclear Ca^{2+} signals was decreased in *cngc15-1* (Figure 5.17 c), which is consistent with the idea that channel activation by upstream signalling molecules is impaired. Conversely, the duration of the Ca^{2+} signal was increased in *dmi1-1* (Figure 5.17 b), which expresses a truncated form of DMI1 at low levels

(Figure 5.4 a, b, d). DMI1 has been predicted to be a modulator of the Ca^{2+} signal (Charpentier *et al*., 2013) and previous work has shown that the C-terminus of MtDMI1, missing in *dmi1-1*, is required for interaction with MtCNGC15a/b/c (Charpentier *et al*., 2016). Lack of a fully functional DMI1, in the presence of a wild-type CNGC15 that can adequately perceive activating stimuli, could explain why the Ca^{2+} signal was just as frequent in *dmi1-1* as in wild type, yet had different kinetics (Figure 5.17 b, c). In the *DMI1* overexpression allele, *dmi1-2*, the signal kinetics was not impaired, but the response was decreased, similarly to *cngc15-1* (Figure 5.17 b, c). In fact, *dmi1-2* mostly phenocopies *cngc15-1*. This indicates that, in Arabidopsis, DMI1 is important in inhibiting the activation of Ca^{2+} channel. The altered stoichiometry of the DMI1/CNGC15 complex, due to *DMI1* overexpression, could hinder or prevent activation of CNGC15 by other interacting partners, or could directly inhibit the Ca^{2+} machinery. To validate this interaction in Arabidopsis roots, I am generating SPLIT-YFP lines expressing Arabidopsis *DMI1* and *CNGC15*, as well as testing the effect of the truncated DMI1 expressed in *dmi1-1*, and the D408N point mutation in CNGC15 (Chapter II, Table 2.3).

The location of the Ca^{2+} signals within the root was also altered in these mutants, with fewer signals found in the meristem in *dmi1-2* and *cngc15-1*, but a higher proportion of signals found in the elongation zone (Figure 5.17 d). The reduction in the number of Ca^{2+} signals observed in the root tip roughly correlates to the reduction in auxin levels as measured by DR5-GFP and DII-VENUS (Figure 5.10). One can thus hypothesise that an auxin derived cue, or auxin itself, could be the elicitor of the nuclear Ca^{2+} signal. The fact that DMI1 and CNGC15 are predicted to act downstream of auxin-induced signalling, as their phenotypes are not recovered with auxin treatment (Figure 5.12, and 5.13), and considering that auxin is known to trigger Ca^{2+} signals in Arabidopsis roots, further supports this idea (Monshausen *et al*., 2011; Shih *et al*., 2015). It is also worth noting that *CNGC15* is highly expressed in tissues with high auxin content, namely the primary and lateral root tip, and the hypocotyl-root junction (Figure 5.2) (Junker *et al*., 2012).

In agreement with the observed altered auxin distribution (Figure 5.10), *dmi1* and *cngc15* mutants were shown to have clear defects in root development. *dmi1-2* and *cngc15-1* have reduced primary roots lengths (Figure 5.5 b, c, g, h), due to the reduced number of meristematic cells (Figure 5.6 a, d, f). A decrease in meristem size can be caused by reduced stem cell activity or by an increased ratio of elongation/differentiation to division in the

transition zone. It is unlikely that there were changes in stem cell activity in the quiescent centre, as that would alter the pattern of cell division (increased number of periclinal divisions in cortex-endodermis initials, for example), which would lead to abnormalities in root anatomy that were not seen in these mutants. On the other hand, *dmi1-2* and *cngc15-1* showed reduced levels of endogenous auxin in the meristem, which would lead to decreased rates of cell division (Blilou *et al*., 2005; Dello Ioio *et al*., 2007), and cause an increased elongation/differentiation to division ratio at the transition zone, resulting in a shorter meristem (Moubayidin *et al*., 2009). The lower auxin levels seen in the meristem of *dmi1-2* and *cngc15-1* also explain the effect on meristematic cell size observed in *cngc15-1* and, to a lesser extent, *dmi1-2*. Auxin depletion has been shown to trigger cells to enter the endoreduplication cycle (Ishida *et al*., 2010), during which DNA is replicated in the absence of cell division, leading to increased ploidy that usually correlates with increased cell size (Sugimoto-Shirasu and Roberts, 2003). If indeed that is the case remains to be evaluated. Finally, reduced auxin levels also explain the decreased lateral root density observed in *cngc15-1*, as auxin is required for lateral root formation (Benková *et al*., 2003) (reviewed by Fukaki and Tasaka, 2009 and Péret *et al*., 2009). I have shown that CNGC15 is strongly expressed in the lateral root meristem (Figure 5.2 f), so it is reasonable to anticipate that its function might be required for lateral root development.

Conversely, the primary root in *dmi1-1* plants was longer than wild type, but these had similarly sized meristems (Figures 5.5 a, g, h, and 5.6 a-c). A careful analysis of cell size revealed that the cells leaving the meristem at six dag in *dmi1-1* were significantly longer than wild type (at 12 dag this difference in cell length was lost) (Figure 5.7. b, c). No differences in meristematic cell size were observed. The transition zone is notoriously known for the interaction between auxin and cytokinin signalling (Moubayidin *et al*., 2009; Mambro *et al*., 2017). Both these hormones impact cell division and cell expansion in tissue-specific and dose-dependent ways. At this point, and without further data, it is unwise to predict what causes the cell size effect observed. A better estimate of the auxin and cytokinin levels in these cells would be informative.

Together, these results demonstrate that nuclear Ca^{2+} signals, mediated by DMI1 and CNGC15, are required to establish an adequate auxin maxima in the root tip, specifically in the columella and areas adjacent to the quiescent centre. This subsequently regulates meristem

size and root development. Steady-state levels of auxin are achieved through the coordinated effects of auxin synthesis, degradation, conjugation, and active and passive transport. In *dmi1-2* and *cngc15-1*, expression of *PIN3* and *PIN7* was altered, pointing to transport as the causative agent in the varying auxin levels. If transport is affected, it remains to be explained why *PIN3* is upregulated while *PIN7* is downregulated, or why the opposite change in expression is not observed in *dmi1-1*. Performing qPCR in whole roots does not provide the resolving power required to analyse a regulatory mechanism known to be cell type-specific. Ongoing work is aiming to evaluate if PIN polarity, as well as tissue-specific expression, is affected in these mutants, at the cellular resolution. One can hypothesise that higher expression of *PIN3* leads to an increased auxin efflux out of the columella and towards the shoot, which is not compensated by the decreased PIN7-driven auxin transport. Considering that differences in expression of PIN1, the main driver of auxin efflux rootwards, were not observed, and that *PIN7* expression may be reduced in the stele, less auxin would accumulate in the root tip and explain the phenotypes observed in *dmi1-2* and *cngc15-1*. If the PINs are downstream targets of the nuclear Ca^{2+} signals, it would be interesting to evaluate the effect on PINOID, a protein known to regulate PIN activity and polarity, and to be regulated in a Ca^{2+}-dependent way (Benjamins *et al*., 2003; Zhang *et al*., 2011).

In summary, this work demonstrates that nuclear Ca^{2+} signals, mediated through CNGC15 and DMI1, are required to establish a normal auxin maxima in the root tip, and thus regulate root meristem size. DMI1 plays a regulatory role in the process, mediating opening and closure of the Ca^{2+} channel (Figure 5.18). This nuclear Ca^{2+} machinery is likely downstream of auxin signalling, as growth on IAA does not rescue the root phenotypes observed on *dmi1-2* and *cngc15-1*. This work expands the roles played by nuclear Ca^{2+} signalling to a key developmental process, and further places these channels as possible integrators of multiple nuclear Ca^{2+} responses to diverse stimuli.

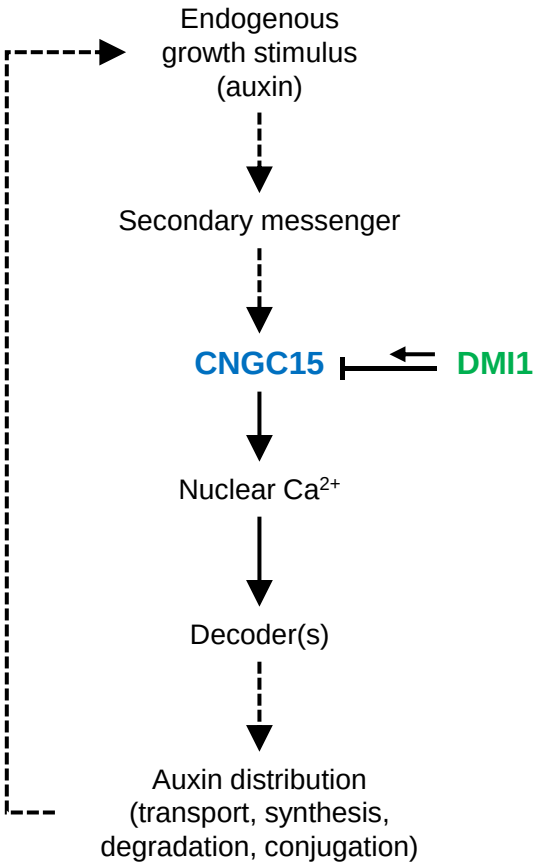

Figure 5.18 | Nuclear Ca^{2+} signals encoded by DMI1 and CNGC15 are required for root development.

An endogenous growth-derived stimulus induces nuclear Ca^{2+} signals through the DMI1/CNGC15 complex. The signal is interpreted by a currently unidentified decoder (Ca^{2+} sensing protein), which translates the information to downstream effectors. This signal is necessary to establish an adequate auxin distribution in the root tip, and consequently achieve normal root development. In this process, the K^+-permeable DMI1 channel plays a regulatory role in the opening and closure of the CNGC15 Ca^{2+} channel. It is possible that auxin itself is the elicitor of the Ca^{2+} signal, and is thereby regulating its own steady-state levels in the root tissue.

Chapter VI

General discussion

The field of plant calcium (Ca^{2+}) signalling has seen great advances over the last decade. This is in part due to emergent sequencing technologies, which made genomes of a variety of species readily available, allowing the identification of entire gene families involved in Ca^{2+} influx, efflux or decoding, but also, and importantly, due to a more widespread use of Ca^{2+} imaging as a phenotypic tool. The wealth of Ca^{2+} reporters currently available is discussed in Chapter III, where different sensors were used to report responses to various stimuli and a new reporter was tested.

The main objective of this thesis was to understand the regulation and impact of two distinct mechanisms of Ca^{2+} influx. In Chapter IV, the production of reactive oxygen species (ROS) upon application of the peptide flg22 was used to screen a collection of putative Ca^{2+} channel mutants. This screen identified the triple mutant *glr3.1glr3.3aglr3.6a* as required for a full ROS burst and induction of the defence gene *NHL10*. In Chapter V, I investigated the function of two genes, CNGC15 and DMI1, whose orthologues are required for nuclear Ca^{2+} spiking in the symbiotic response to nodulation (Nod) and mycorrhization (Myc) factors, in the non-symbiotic species *Arabidopsis thaliana*. CNGC15 and DMI1 were found to be required for the establishment of a normal auxin maximum in the root tip, and to mediate growth-associated nuclear Ca^{2+} signals in roots.

6.1. On the tools for *in vivo* calcium quantification

It is essential to accurately measure and quantify Ca^{2+} signals. This implies using the right Ca^{2+} reporter for each experiment, i.e., the one that has an affinity constant for Ca^{2+} that is best suited for the signal under analysis. It also means being aware of the strengths and limitations of each reporter, necessary to prevent potential imaging artefacts.

In this work and for the first time, Ca^{2+} signals were simultaneously quantified in the nucleus and the cytosol, using different reporters (R-GECO1.2 and G-GECO1.2) specifically

localised to the nucleus or excluded from it, in the same cell. With this tool it is now possible to accurately compare nuclear and cytosolic Ca^{2+} signals elicited by a stimulus, and quantify the response time and the signal kinetics in each cell compartment simultaneously in live Arabidopsis plants. Thus far, studies attempting to characterise nuclear versus cytosolic Ca^{2+} dynamics have used protoplasts, cell lines, or whole plants, but never were the two signals distinguished within the same plant (Pauly *et al*., 2000, 2001; Lecourieux *et al*., 2005; Walter *et al*., 2007; Mazars *et al*., 2009; Krebs and Schumacher, 2013). This reporter will help in the understanding of nuclear and cytosolic Ca^{2+} signalling mechanisms, by clarifying the spatial origin of a stimulus-induced signal, and untangling the possible interdependency of each cell compartment.

Importantly, possible developmental side effects caused by expression of Ca^{2+} reporters should be addressed. Waadt *et al*. (2017) analysed the growth of Col-0 lines expressing eight different Ca^{2+} reporters, and all had a level of reduction in rosette area. The severity of the phenotype also positively correlated with reporter expression level across independent lines expressing the same reporter. This could be the result of buffering of Ca^{2+}, which may perturb Ca^{2+} signalling, and/or interaction of the reporter's calmodulin (CaM) domain with endogenous signalling molecules. CaMeleon reporters have already been re-engineered to address this issue (Palmer *et al*., 2006). The interface between CaM and M13 was redesigned *in silico* by inserting steric bumps in the M13 peptide with complementary holes in CaM. These were then used in the cloning of a new group of CaMeleon reporters, which were less disturbed by endogenous CaM (Palmer *et al*., 2006). Another possibility is to further optimise troponin C-based Twitch Ca^{2+} reporters. Unlike CaM-based, which bind four Ca^{2+} ions, Twitch reporters bind one or two Ca^{2+} ions per reporter molecule, reducing the overall amount of Ca^{2+} that is buffered (Thestrup *et al*., 2014).

Moreover, it is crucial to have the appropriate experimental set-up. Ca^{2+} signals are elicited by a plethora of stimuli, notably touch and wounding. Ensuring an adequate resting period between sample manipulation and imaging is essential. Ideally, a progression towards protocols that do not require any handling of the plant material would be beneficial. This is the case of RootChip (Grossmann *et al*., 2011), a system in which plants grow directly in a microfluidic platform that allows live imaging and rapid modulation of the experimental conditions. Another example is the system described by Candeo *et al*. (2017), in which plants

grow on fluorinated ethylene propylene tubes filled with jellified medium, under positive gravitropism, and can be imaged when suitable, directly on the tube without physically handling the plant, while maintaining the gravity vector constant (Candeo *et al*., 2017).

The use of genetically-encoded Ca^{2+} sensors with a high dynamic range, fast association and dissociation kinetics, non-disturbing to endogenous signalling partners, in a range of spectrally non-overlapping colours and subcellularly targeted, under highly controlled growth and imaging conditions with minimal sample perturbation, will likely be central to characterise Ca^{2+} signalling pathways that present inherent and extensive biological complexity.

6.2. The Ca^{2+} signal in innate immunity

Ca^{2+} signalling is profusely intertwined with the signalling pathways that regulate plant defence. Similar to the symbiosis field, it has been known for a long time that activation of innate immunity is synonymous with triggering of Ca^{2+} signals and this has been informative in characterising the signalling pathway. Nonetheless and unlike symbiosis, the identity of the channels behind this process remains undiscovered.

As highlighted in Chapter IV, different channels have been hypothesised to contribute to the microbial-associated molecular pattern (MAMP)-induced Ca^{2+} signature. To validate the idea of a signal to which multiple channels contribute - first a channel that initiates the response followed by secondary channels that magnify it - it is necessary to image and quantify this signal. As discussed in Chapter III, the characterisation of the MAMP-induced Ca^{2+} signature with cellular resolution has been difficult, but with the development of novel Ca^{2+} reporters the situation might be changing. A thorough description of the wild-type Ca^{2+} response to MAMPs, such as flg22 or elf18, could be used to feed computer models that would aid in the quest for the predicted channels. This, along with the analysis of selected candidate mutants, such as the ones identified in Chapter IV, *glr3.1glr3.3aglr3.6a*, would inform whether these channels are in fact part of a signal amplification mechanism.

The question remains as to how the signal is generated in the first place, i.e., what links MAMP and damage-associated molecular pattern (DAMP) perception to channel activation. In innate immunity, different MAMPs or DAMPs are recognised by specific receptors on the

cell surface (FLS2, EFR, PEPR1, LYK5/CERK1, and LORE recognise flagellin, EF-Tu, AtPep1, chitin, and lipopolysaccharide, respectively), but activate the same downstream responses – ROS and Ca^{2+} bursts, mitogen-activated protein kinases, Ca^{2+}-dependent protein kinases, and defence genes. It is also known that this system is effectively integrated, as pathway confluence occurs already at the level of the plasma membrane. FLS2, EFR, and PEPR1 share the same co-receptor, BAK1, and all three associate with the cytoplasmic kinase PCRK1. Similarly, all three receptors along with LYK5/CERK1, associate with another cytoplasmic kinase, BIK1 (reviewed in Couto and Zipfel, 2016). If Ca^{2+} is part of a shared PTI output, and given that it occurs within a minute of MAMP/DAMP sensing (Ranf *et al*., 2008), it is conceivable that activation is effected by one of the shared kinases. If that is the case, the idea that each MAMP/DAMP induces specific Ca^{2+} signatures, as suggested by earlier work using aequorin (Ranf *et al*., 2011), should be revisited, as a common activation mechanism suggests the same signature. It has been shown that the aequorin signal integrates over a tissue the Ca^{2+} changes occurring across multiple cells (Thor and Peiter, 2014), and so it is conceivable that the cell signature could be the same, but the tissue-wide signature different, due to the varying expression patterns of the individual receptors. Nonetheless, if indeed there are different Ca^{2+} signatures for different MAMPs and DAMPs, the question then is if these encode different information, what that information is, and what are the different responses it instigates.

Finally, the nature of the systemic Ca^{2+} signal, and how it differs from local stimulation, remains to be investigated. TPC1, which is required in systemic Ca^{2+} signalling in response to salt stress and aphid feeding (Evans *et al*., 2016; Vincent *et al*., 2017), could be involved, especially if this would be part of a common signalling mechanism that is triggered by multiple stimuli. Although in *TPC1* mutant lines there were no differences in the Ca^{2+} or ROS bursts in response to flg22 or elf18 (Ranf *et al*., 2008), a careful analysis of a systemic response has not been reported. Here, again, Ca^{2+} reporters and proper imaging set-ups, that clearly distinguish local stimulation from distal induction, will be informative.

6.3. The role of CNGC15/DMI1 in root development

The work described in Chapter V demonstrates that nuclear Ca^{2+} signals, mediated by CNGC15 and DMI1, are required to establish a normal auxin maximum in the root tip, and thus regulate root meristem and total root length (Figure 5.18 and Figure 6.1). An endogenous growth-derived stimulus likely induces nuclear Ca^{2+} signals through the CNGC15/DMI1 complex. This information is decoded by a currently unidentified Ca^{2+} sensing protein and translated to downstream targets. This signal is necessary to establish an adequate auxin distribution in the root tip and normal root development. In this model, the K^+-permeable cation channel DMI1 regulates the opening and closure of the Ca^{2+} channel CNGC15. Auxin itself is possibly the elicitor of the nuclear Ca^{2+} spike, and thereby regulates its own steady-state levels in the root tissue. This work links for the first time nuclear Ca^{2+} and auxin signalling, and it is the first characterised example of nuclear Ca^{2+} signalling outside symbioses.

Previous work has shown that imposing different Ca^{2+} transients with voltage treatments induces specific transcriptional changes (Whalley *et al*., 2011; Whalley and Knight, 2013). Furthermore, artificially mimicking endogenous ABA-induced Ca^{2+} signals, through rapid medium changes between hyperpolarising and depolarising buffer, can induce the associated phenotypic response, i.e., stomatal closure, in an ABA-insensitive mutant (*gca2*), in which ABA-induced stomatal closure is abolished (Allen *et al.*, 2001). These studies support the "Ca^{2+} signature" hypothesis, which states that stimulus-specific information could be encoded in the amplitude, frequency, duration, and spatial location of the Ca^{2+} release. However, there are no other examples where imposing a Ca^{2+} transient results in a specific phenotypic output. Notably, this work demonstrates for the first time that a genetic manipulation of the Ca^{2+} signature, as opposed to abolishing the Ca^{2+} signal all together, can result in different phenotypes. In *dmi1-1*, in which expression of DMI1 is severely reduced, the duration of the Ca^{2+} spike is increased, which results in higher levels of endogenous auxin, longer cells in the elongation zone and a longer primary root (Figure 6.1). This supports the idea that information responsible for the control of a defined physiological response can be inherently encoded in the kinetics of nuclear Ca^{2+} signals, and that modulating these signals can serve to fine-tune the phenotypic result.

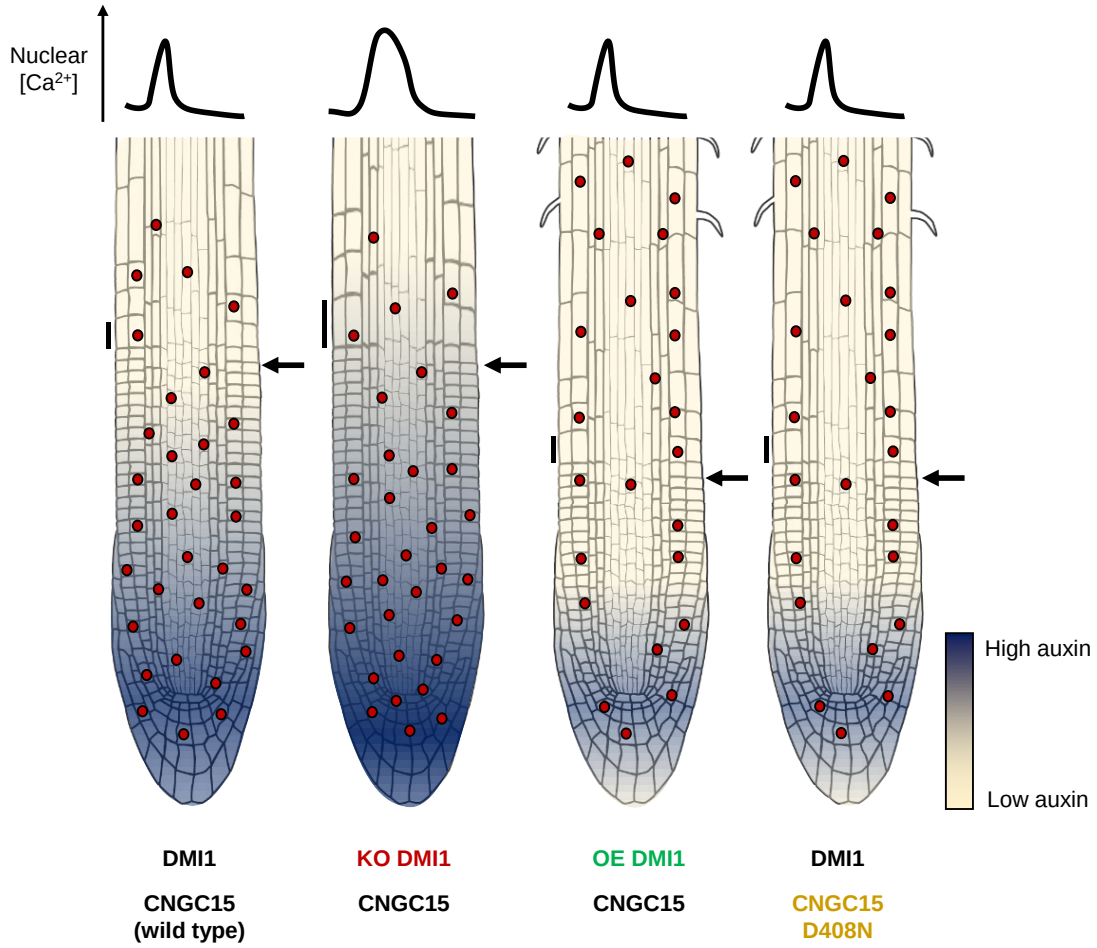

Figure 6.1 | Nuclear Ca^{2+} signalling regulates primary root development.

Summary of the effect of DMI1/CNGC15 mediated nuclear Ca^{2+} signals in root development. In wild-type plants, nuclear Ca^{2+} signals, in the form of single spikes (top), occur predominantly in the meristem, but also in the elongation zone (red circles). In the absence of *DMI1*, the Ca^{2+} signature changes (spikes become larger), and as a result the auxin maximum is increased in the quiescent centre, and the first rapidly elongating cells (vertical lines) and the primary root are longer. If *DMI1* is overexpressed, or in CNGC15 D408N mutant plants, the Ca^{2+} kinetics does not change, but the Ca^{2+} signals occur more often in the elongation zone. As a result, the auxin maximum in the quiescent centre is decreased, and the meristem and the primary root are shorter. Top, representation of the Ca^{2+} signal in each genetic background. Red circles represent nuclei where Ca^{2+} signals occur. Colour gradient represents endogenous auxin levels. Horizontal arrows mark the transition from meristematic to elongating cells.

Many questions are nevertheless left unanswered. Further work is required to determine what lies directly upstream and downstream of the generation of the nuclear Ca^{2+} signal. This work proposes that auxin is upstream and activates the channel, however it is not known how this is effected. Although the mechanism of activation is unknown, auxin can trigger CNGC14 in the plasma membrane (Shih *et al*., 2015). The authors exclude AUXIN-BINDING PROTEIN 1 (ABP1), which had been suggested to mediate auxin-induced ion signalling (Steffens *et al*., 2001; Yamagami *et al*., 2004), by quantifying the Ca^{2+} and pH responses in gravistimulated and auxin-treated *abp1* null alleles and observing no differences from wild type (Gao *et al*., 2015; Shih *et al*., 2015). Accumulation of endogenous cyclic guanosine 3′,5′-monophosphate (cGMP), a second messenger that is a possible activating ligand of CNGCs (Gao *et al*., 2014, 2016), is induced by auxin in mung bean (*Vigna radiate*), soybean (*Glycine max*), and Arabidopsis (Hu *et al*., 2005; Bai *et al*., 2012; Nan *et al*., 2014). This has been confirmed in Arabidopsis protoplasts expressing the cGMP reporter FlincG (Isner *et al*., 2012). The auxin-induced increase in endogenous cGMP is caused by increased activity of guanylate cyclase (GC), and cGMP promotes auxin-dependent developmental processes, such as primary root growth, likely through the effect of cGMP-dependent protein kinase (PKG) (Nan *et al*., 2014). This hypothesis is further supported by the work of Isner *et al*. (2012), which showed that several proteins quickly change their phosphorylation status upon cGMP treatment. This indicates a possible way through which auxin could activate CNGC15.

Drawing from the symbiotic model, the Ca^{2+} efflux mechanism responsible to restore nuclear [Ca^{2+}] to basal levels remains to be identified. The most likely candidates are the four ECAs identified in Arabidopsis, in particular ECA1 and ECA4, which are the closest orthologues to MtMCA8 (Capoen *et al*., 2011). While there are no published studies on ECA4, ECA1 has a demonstrated function as a Ca^{2+}-ATPase, and localises to the ER, albeit the authors cannot exclude localisation in other endomembranes (Liang *et al*., 1997; Liang and Sze, 1998). A T-DNA insertion mutant displays growth phenotypes (reduced fresh weight, chlorophyll contents, and root hair length) when grown in the presence of excess manganese (Mn^{2+}), indicating that ECA1 confers tolerance to this metal (Wu *et al*., 2002). ECA3, on the other hand, localises to the Golgi apparatus and *eca3* lines have impaired growth in the absence of Mn^{2+}, suggesting a role in Mn^{2+} nutrition (Mills *et al*., 2008). These mutants could be revisited and their root phenotypes analysed.

Downstream of nuclear Ca^{2+}, the decoder of the Ca^{2+} signal has not been identified. In arbuscular mycorrhizal and rhizobial symbioses, the Ca^{2+}/CaM-binding S/T kinase MtCCaMK is the decoder of nuclear Ca^{2+} spiking and is thought to act on multiple targets to elicit transcriptional changes that establish symbiotic transcriptional reprogramming. This protein would thus be the most obvious target. However, CCaMK is not conserved in Arabidopsis, as it is only present in arbuscular mycorrhizal host species (Delaux *et al*., 2014; Favre *et al*., 2014; Bravo *et al*., 2016). There are hundreds of possible candidates if one considers the CPKs, the different CBL/CIPK combinations, CaMs, and CaM-like proteins. However, given that the signal occurs in the nucleus, and similarly to MtCCaMK, this decoder is expected to be nuclear-targeted, a parameter that could be used in a bioinformatics analysis to decrease the number of possible candidates. Importantly, identifying the proteins downstream of the decoder would likely further explain the observable phenotype and elucidate if and how nuclear Ca^{2+} signalling is affecting auxin transport.

6.4. Other roles for nuclear Ca^{2+} signals

The fact that the DMI1/CNGC15 nuclear Ca^{2+} signalling machinery has been recruited to fulfil different functions in *M. truncatula* and Arabidopsis indicates that it could potentially be involved in other signalling pathways and developmental processes. This is already suggested by the fact that in *M. truncatula* MtCNGC15 proteins are necessary for fertilisation (Charpentier *et al*., 2016), a process that requires Ca^{2+} signals on both the female and male gametophytes (Hamamura *et al*., 2014; Iwano *et al*., 2012). If that is the case, it would be interesting to investigate if these two components, CNGC15 and DMI1, are always intrinsically linked, or if they can act independently. Knowing that DMI1 modulates the Ca^{2+} signal mediated by CNGC15, if these channels can act independently, one might expect a differently shaped Ca^{2+} signal.

Also, if DMI1/CNGC15 mediate signalling in different pathways, the question is at what point is specificity determined, i.e., at the level of channel activation or in the decoding. If the same signal can be induced and decoded in different ways, cell-specific and non-overlapping expression of the activators or the decoders would guarantee signal specificity. On

the other hand, if CNGC15/DMI1, or CNGC15 alone, can generate different Ca^{2+} signals, this would constitute yet another way to instil versatility in Ca^{2+} signalling pathways.

References

Abdel-Hamid, H., Chin, K., Moeder, W., Shahinas, D., Gupta, D., and Yoshioka, K. (2013). A Suppressor Screen of the Chimeric AtCNGC11/12 Reveals Residues Important for Intersubunit Interactions of Cyclic Nucleotide-Gated Ion Channels. Plant Physiol. *162*, 1681–1693.

Aida, M., Beis, D., Heidstra, R., Willemsen, V., Blilou, I., Galinha, C., Nussaume, L., Noh, Y.-S., Amasino, R., and Scheres, B. (2004). The PLETHORA Genes Mediate Patterning of the Arabidopsis Root Stem Cell Niche. Cell *119*, 109–120.

Akerboom, J., Rivera, J.D.V., Guilbe, M.M.R., Malavé, E.C.A., Hernandez, H.H., Tian, L., Hires, S.A., Marvin, J.S., Looger, L.L., and Schreiter, E.R. (2009). Crystal Structures of the GCaMP Calcium Sensor Reveal the Mechanism of Fluorescence Signal Change and Aid Rational Design. J. Biol. Chem. *284*, 6455–6464.

Ali, R., Zielinski, R.E., and Berkowitz, G.A. (2006). Expression of plant cyclic nucleotide-gated cation channels in yeast. J. Exp. Bot. *57*, 125–138.

Ali, R., Ma, W., Lemtiri-Chlieh, F., Tsaltas, D., Leng, Q., von Bodman, S., and Berkowitz, G.A. (2007). Death Don't Have No Mercy and Neither Does Calcium: Arabidopsis CYCLIC NUCLEOTIDE GATED CHANNEL2 and Innate Immunity. Plant Cell *19*, 1081–1095.

Allen, G.J., Chu, S.P., Schumacher, K., Shimazaki, C.T., Vafeados, D., Kemper, A., Hawke, S.D., Tallman, G., Tsien, R.Y., Harper, J.F., Chory, J., and Schroeder, J.I. (2000). Alteration of Stimulus-Specific Guard Cell Calcium Oscillations and Stomatal Closing in Arabidopsis det3 Mutant. Science *289*, 2338–2342.

Allen, G.J., Chu, S.P., Harrington, C.L., Schumacher, K., Hoffmann, T., Tang, Y.Y., Grill, E., and Schroeder, J.I. (2001). A defined range of guard cell calcium oscillation parameters encodes stomatal movements. Nature *411*, 1053–1057.

Alonso, M.T., Manjarrés, I.M., and García-Sancho, J. (2009). Modulation of calcium signalling by intracellular organelles seen with targeted aequorins. Acta Physiol. *195*, 37–49.

Ané, J.-M., Kiss, G.B., Riely, B.K., Penmetsa, R.V., Oldroyd, G.E.D., Ayax, C., Lévy, J., Debellé, F., Baek, J.-M., Kalo, P., Rosenberg, C., Roe, B.A., Long, S.R., Dénarié, J., and Cook, D.R. (2004). *Medicago truncatula* DMI1 Required for Bacterial and Fungal Symbioses in Legumes. Science *303*, 1364–1367.

Antosiewicz, D.M., Polisensky, D.H., and Braam, J. (1995). Cellular localization of the Ca^{2+} binding TCH3 protein of Arabidopsis. Plant J. *8*, 623–636.

Arazi, T., Kaplan, B., and Fromm, H. (2000). A high-affinity calmodulin-binding site in a tobacco plasma-membrane channel protein coincides with a characteristic element of cyclic nucleotide-binding domains. Plant Mol. Biol. *42*, 591–601.

Asai, T., Tena, G., Plotnikova, J., Willmann, M.R., Chiu, W.-L., Gomez-Gomez, L., Boller, T., Ausubel, F.M., and Sheen, J. (2002). MAP kinase signalling cascade in Arabidopsis innate immunity. Nature *415*, 977–983.

Bai, X., Todd, C.D., Desikan, R., Yang, Y., and Hu, X. (2012). N-3-oxo-decanoyl-L-homoserine-lactone activates auxin-induced adventitious root formation via hydrogen peroxide- and nitric oxide-dependent cyclic GMP signaling in mung bean. Plant Physiol. *158*, 725–736.

Balagué, C., Lin, B., Alcon, C., Flottes, G., Malmström, S., Köhler, C., Neuhaus, G., Pelletier, G., Gaymard, F., and Roby, D. (2003). HLM1, an Essential Signaling Component in the Hypersensitive Response, Is a Member of the Cyclic Nucleotide–Gated Channel Ion Channel Family. Plant Cell *15*, 365–379.

Bao, Y., Song, W.-M., Pan, J., Jiang, C.-M., Srivastava, R., Li, B., Zhu, L.-Y., Su, H.-Y., Gao, X.-S., Liu, H., Yu, X., Yang, L., Cheng, X.-H., and Zhang, H.-X. (2016a). Overexpression of the NDR1/HIN1-Like Gene NHL6 Modifies Seed Germination in Response to Abscisic Acid and Abiotic Stresses in Arabidopsis. PloS One *11*, e0148572.

Bao, Y., Song, W.-M., and Zhang, H.-X. (2016b). Role of Arabidopsis NHL family in ABA and stress response. Plant Signal. Behav. *11*, e1180493.

Baxter, I., Tchieu, J., Sussman, M.R., Boutry, M., Palmgren, M.G., Gribskov, M., Harper, J.F., and Axelsen, K.B. (2003). Genomic Comparison of P-Type ATPase Ion Pumps in Arabidopsis and Rice. Plant Physiol. *132*, 618–628.

Baxter, J., Moeder, W., Urquhart, W., Shahinas, D., Chin, K., Christendat, D., Kang, H.-G., Angelova, M., Kato, N., and Yoshioka, K. (2008). Identification of a functionally essential amino acid for Arabidopsis cyclic nucleotide gated ion channels using the chimeric AtCNGC11/12 gene. Plant J. *56*, 457–469.

Beck, M., Wyrsch, I., Strutt, J., Wimalasekera, R., Webb, A., Boller, T., and Robatzek, S. (2014). Expression patterns of FLAGELLIN SENSING 2 map to bacterial entry sites in plant shoots and roots. J. Exp. Bot. *65*, 6487–6498.

Benjamins, R., Quint, A., Weijers, D., Hooykaas, P., and Offringa, R. (2001). The PINOID protein kinase regulates organ development in Arabidopsis by enhancing polar auxin transport. Development *128*, 4057–4067.

Benjamins, R., Ampudia, C.S.G., Hooykaas, P.J.J., and Offringa, R. (2003). PINOID-Mediated Signaling Involves Calcium-Binding Proteins. Plant Physiol. *132*, 1623–1630.

Benková, E., Michniewicz, M., Sauer, M., Teichmann, T., Seifertová, D., Jürgens, G., and Friml, J. (2003). Local, Efflux-Dependent Auxin Gradients as a Common Module for Plant Organ Formation. Cell *115*, 591–602.

Berridge, M.J., Lipp, P., and Bootman, M.D. (2000). The versatility and universality of calcium signalling. Nat. Rev. Mol. Cell Biol. *1*, 11–21.

Berridge, M.J., Bootman, M.D., and Roderick, H.L. (2003). Calcium signalling: dynamics, homeostasis and remodelling. Nat. Rev. Mol. Cell Biol. *4*, 517–529.

Bethke, G., Pecher, P., Eschen-Lippold, L., Tsuda, K., Katagiri, F., Glazebrook, J., Scheel, D., and Lee, J. (2012). Activation of the Arabidopsis thaliana mitogen-activated protein kinase MPK11 by the flagellin-derived elicitor peptide, flg22. Mol. Plant-Microbe Interact. MPMI *25*, 471–480.

Bigeard, J., Colcombet, J., and Hirt, H. (2015). Signaling Mechanisms in Pattern-Triggered Immunity (PTI). Mol. Plant *8*, 521–539.

Bilgin, D.D., Zavala, J.A., Zhu, J., Clough, S.J., Ort, D.R., and DeLucia, E.H. (2010). Biotic stress globally downregulates photosynthesis genes. Plant Cell Environ. *33*, 1597–1613.

Blatt, M.R., Thiel, G., and Trentham, D.R. (1990). Reversible inactivation of K^+ channels of *Vicia* stomatal guard cells following the photolysis of caged inositol 1,4,5-trisphosphate. Nature *346*, 766–769.

Blilou, I., Xu, J., Wildwater, M., Willemsen, V., Paponov, I., Friml, J., Heidstra, R., Aida, M., Palme, K., and Scheres, B. (2005). The PIN auxin efflux facilitator network controls growth and patterning in Arabidopsis roots. Nature *433*, 39–44.

Blume, B., Nürnberger, T., Nass, N., and Scheel, D. (2000). Receptor-Mediated Increase in Cytoplasmic Free Calcium Required for Activation of Pathogen Defense in Parsley. Plant Cell *12*, 1425–1440.

Böhm, H., Albert, I., Fan, L., Reinhard, A., and Nürnberger, T. (2014). Immune receptor complexes at the plant cell surface. Curr. Opin. Plant Biol. *20*, 47–54.

Boller, T., and Felix, G. (2009). A Renaissance of Elicitors: Perception of Microbe-Associated Molecular Patterns and Danger Signals by Pattern-Recognition Receptors. Annu. Rev. Plant Biol. *60*, 379–406.

Borges, L.L., Santana, F.A., Castro, I.S.L., Arruda, K.M.A., Ramos, H.J. de O., Moreira, M.A., and Barros, E.G. de (2013). Differentially expressed proteins during an incompatible interaction between common bean and the fungus Pseudocercospora griseola. Mol. Breed. *32*, 933–942.

Bose, J., Pottosin, I., Shabala, S.S.S., Palmgren, M.G., and Shabala, S. (2011). Calcium Efflux Systems in Stress Signaling and Adaptation in Plants. Front. Plant Sci. *2*, 85.

Bouché, N., and Bouchez, D. (2001). Arabidopsis gene knockout: phenotypes wanted. Curr. Opin. Plant Biol. *4*, 111–117.

Boudsocq, M., Willmann, M.R., McCormack, M., Lee, H., Shan, L., He, P., Bush, J., Cheng, S.-H., and Sheen, J. (2010). Differential innate immune signalling via Ca^{2+} sensor protein kinases. Nature *464*, 418–422.

Brady, S.M., Orlando, D.A., Lee, J.-Y., Wang, J.Y., Koch, J., Dinneny, J.R., Mace, D., Ohler, U., and Benfey, P.N. (2007). A High-Resolution Root Spatiotemporal Map Reveals Dominant Expression Patterns. Science *318*, 801–806.

Bravo, A., York, T., Pumplin, N., Mueller, L.A., and Harrison, M.J. (2016). Genes conserved for arbuscular mycorrhizal symbiosis identified through phylogenomics. Nat. Plants *2*, 15208.

Brunoud, G., Wells, D.M., Oliva, M., Larrieu, A., Mirabet, V., Burrow, A.H., Beeckman, T., Kepinski, S., Traas, J., Bennett, M.J., and Vernoux, T. (2012). A novel sensor to map auxin response and distribution at high spatio-temporal resolution. Nature *482*, 103–106.

Campbell, A.K., Trewavas, A.J., and Knight, M.R. (1996). Calcium imaging shows differential sensitivity to cooling and communication in luminous transgenic plants. Cell Calcium *19*, 211–218.

Candeo, A., Doccula, F.G., Valentini, G., Bassi, A., and Costa, A. (2017). Light Sheet Fluorescence Microscopy Quantifies Calcium Oscillations in Root Hairs of Arabidopsis thaliana. Plant Cell Physiol. *58*, 1161–1172.

Capoen, W., Sun, J., Wysham, D., Otegui, M.S., Venkateshwaran, M., Hirsch, S., Miwa, H., Downie, J.A., Morris, R.J., Ane, J.-M., and Oldroyd, G.E.D. (2011). Nuclear membranes control symbiotic calcium signaling of legumes. Proc. Natl. Acad. Sci. U. S. A. *108*, 14348–14353.

Case, R.M., Eisner, D., Gurney, A., Jones, O., Muallem, S., and Verkhratsky, A. (2007). Evolution of calcium homeostasis: From birth of the first cell to an omnipresent signalling system. Cell Calcium *42*, 345–350.

Chabaud, M., Genre, A., Sieberer, B.J., Faccio, A., Fournier, J., Novero, M., Barker, D.G., and Bonfante, P. (2011). Arbuscular mycorrhizal hyphopodia and germinated spore exudates trigger Ca^{2+} spiking in the legume and nonlegume root epidermis. New Phytol. *189*, 347–355.

Charpentier, M., and Oldroyd, G.E.D. (2013). Nuclear Calcium Signaling in Plants. Plant Physiol. *163*, 496–503.

Charpentier, M., Bredemeier, R., Wanner, G., Takeda, N., Schleiff, E., and Parniske, M. (2008). *Lotus japonicus* CASTOR and POLLUX Are Ion Channels Essential for Perinuclear Calcium Spiking in Legume Root Endosymbiosis. Plant Cell *20*, 3467–3479.

Charpentier, M., Martins, T.V., Granqvist, E., Oldroyd, G.E.D., and Morris, R.J. (2013). The role of DMI1 in establishing Ca^{2+} oscillations in legume symbioses. Plant Signal. Behav. *8*, e22894.

Charpentier, M., Sun, J., Martins, T.V., Radhakrishnan, G.V., Findlay, K., Soumpourou, E., Thouin, J., Véry, A.-A., Sanders, D., Morris, R.J., and Oldroyd, G.E.D. (2016). Nuclear-localized cyclic nucleotide–gated channels mediate symbiotic calcium oscillations. Science *352*, 1102–1105.

Chen, C., Fan, C., Gao, M., and Zhu, H. (2009). Antiquity and Function of CASTOR and POLLUX, the Twin Ion Channel-Encoding Genes Key to the Evolution of Root Symbioses in Plants. Plant Physiol. *149*, 306–317.

Chin, K., DeFalco, T.A., Moeder, W., and Yoshioka, K. (2013). The Arabidopsis Cyclic Nucleotide-Gated Ion Channels AtCNGC2 and AtCNGC4 Work in the Same Signaling Pathway to Regulate Pathogen Defense and Floral Transition. Plant Physiol. *163*, 611–624.

Chinchilla, D., Zipfel, C., Robatzek, S., Kemmerling, B., Nürnberger, T., Jones, J.D.G., Felix, G., and Boller, T. (2007). A flagellin-induced complex of the receptor FLS2 and BAK1 initiates plant defence. Nature *448*, 497–500.

Choi, J., Tanaka, K., Cao, Y., Qi, Y., Qiu, J., Liang, Y., Lee, S.Y., and Stacey, G. (2014a). Identification of a Plant Receptor for Extracellular ATP. Science *343*, 290–294.

Choi, W.-G., Swanson, S.J., and Gilroy, S. (2012). High-resolution imaging of Ca^{2+}, redox status, ROS and pH using GFP biosensors. Plant J. *70*, 118–128.

Choi, W.-G., Toyota, M., Kim, S.-H., Hilleary, R., and Gilroy, S. (2014b). Salt stress-induced Ca^{2+} waves are associated with rapid, long-distance root-to-shoot signaling in plants. Proc. Natl. Acad. Sci. *111*, 6497–6502.

Clough, S.J., Fengler, K.A., Yu, I., Lippok, B., Smith, R.K., and Bent, A.F. (2000). The Arabidopsis dnd1 "defense, no death" gene encodes a mutated cyclic nucleotide-gated ion channel. Proc. Natl. Acad. Sci. *97*, 9323–9328.

Coll, N.S., Epple, P., and Dangl, J.L. (2011). Programmed cell death in the plant immune system. Cell Death Differ. *18*, 1247–1256.

Cosgrove, D.J., and Hedrich, R. (1991). Stretch-activated chloride, potassium, and calcium channels coexisting in plasma membranes of guard cells of Vicia faba L. Planta *186*, 143–153.

Couto, D., and Zipfel, C. (2016). Regulation of pattern recognition receptor signalling in plants. Nat. Rev. Immunol. *16*, 537–552.

Cui, H., Tsuda, K., and Parker, J.E. (2015). Effector-Triggered Immunity: From Pathogen Perception to Robust Defense. Annu. Rev. Plant Biol. *66*, 487–511.

Cutler, S., and McCourt, P. (2005). Dude, Where's My Phenotype? Dealing with Redundancy in Signaling Networks. Plant Physiol. *138*, 558–559.

Dangl, J.L., Horvath, D.M., and Staskawicz, B.J. (2013). Pivoting the Plant Immune System from Dissection to Deployment. Science *341*, 746–751.

Davenport, R. (2002). Glutamate Receptors in Plants. Ann. Bot. *90*, 549–557.

Davies, J.M. (2014). Annexin-Mediated Calcium Signalling in Plants. Plants *3*, 128–140.

DeFalco, T.A., Moeder, W., and Yoshioka, K. (2016a). Opening the Gates: Insights into Cyclic Nucleotide-Gated Channel-Mediated Signaling. Trends Plant Sci. *21*, 903–906.

DeFalco, T.A., Marshall, C.B., Munro, K., Kang, H.-G., Moeder, W., Ikura, M., Snedden, W.A., and Yoshioka, K. (2016b). Multiple Calmodulin-Binding Sites Positively and Negatively Regulate Arabidopsis CYCLIC NUCLEOTIDE-GATED CHANNEL 12. Plant Cell *28*, 1738–1751.

Delaux, P.-M., Varala, K., Edger, P.P., Coruzzi, G.M., Pires, J.C., and Ané, J.-M. (2014). Comparative phylogenomics uncovers the impact of symbiotic associations on host genome evolution. PLoS Genet. *10*, e1004487.

Dello Ioio, R., Linhares, F.S., Scacchi, E., Casamitjana-Martinez, E., Heidstra, R., Costantino, P., and Sabatini, S. (2007). Cytokinins Determine Arabidopsis Root-Meristem Size by Controlling Cell Differentiation. Curr. Biol. *17*, 678–682.

Demidchik, V., Shabala, S.N., Coutts, K.B., Tester, M.A., and Davies, J.M. (2003). Free oxygen radicals regulate plasma membrane Ca^{2+}- and K^{+}-permeable channels in plant root cells. J. Cell Sci. *116*, 81–88.

Dénarié, J., Debellé, F., and Promé, J.-C. (1996). Rhizobium Lipo-Chitooligosaccharide Nodulation Factors: Signaling Molecules Mediating Recognition and Morphogenesis. Annu. Rev. Biochem. *65*, 503–535.

Dengler, N.G. (2006). The shoot apical meristem and development of vascular architecture. Can. J. Bot. *84*, 1660–1671.

Dietrich, P., Anschütz, U., Kugler, A., and Becker, D. (2010). Physiology and biophysics of plant ligand-gated ion channels. Plant Biol. Stuttg. Ger. *12 Suppl 1*, 80–93.

Dodd, A.N., Jakobsen, M.K., Baker, A.J., Telzerow, A., Hou, S.-W., Laplaze, L., Barrot, L., Scott Poethig, R., Haseloff, J., and Webb, A.A.R. (2006). Time of day modulates low-temperature Ca^{2+} signals in Arabidopsis. Plant J. *48*, 962–973.

Dodd, A.N., Kudla, J., and Sanders, D. (2010). The Language of Calcium Signaling. Annu. Rev. Plant Biol. *61*, 593–620.

Dodds, P.N., and Rathjen, J.P. (2010). Plant immunity: towards an integrated view of plant–pathogen interactions. Nat. Rev. Genet. *11*, 539–548.

Drerup, M.M., Schlücking, K., Hashimoto, K., Manishankar, P., Steinhorst, L., Kuchitsu, K., and Kudla, J. (2013). The Calcineurin B-like calcium sensors CBL1 and CBL9 together with their interacting protein kinase CIPK26 regulate the Arabidopsis NADPH oxidase RBOHF. Mol. Plant *6*, 559–569.

Du, L., Ali, G.S., Simons, K.A., Hou, J., Yang, T., Reddy, A.S.N., and Poovaiah, B.W. (2009). Ca^{2+}/calmodulin regulates salicylic-acid-mediated plant immunity. Nature *457*, 1154–1158.

Dubiella, U., Seybold, H., Durian, G., Komander, E., Lassig, R., Witte, C.-P., Schulze, W.X., and Romeis, T. (2013). Calcium-dependent protein kinase/NADPH oxidase activation circuit is required for rapid defense signal propagation. Proc. Natl. Acad. Sci. *110*, 8744–8749.

Dutta, R., and Robinson, K.R. (2004). Identification and Characterization of Stretch-Activated Ion Channels in Pollen Protoplasts. Plant Physiol. *135*, 1398–1406.

Edel, K.H., and Kudla, J. (2015). Increasing complexity and versatility: how the calcium signaling toolkit was shaped during plant land colonization. Cell Calcium *57*, 231–246.

Edel, K.H., Marchadier, E., Brownlee, C., Kudla, J., and Hetherington, A.M. (2017). The Evolution of Calcium-Based Signalling in Plants. Curr. Biol. *27*, 667–679.

Ehlers, M.D., Fung, E.T., O'Brien, R.J., and Huganir, R.L. (1998). Splice Variant-Specific Interaction of the NMDA Receptor Subunit NR1 with Neuronal Intermediate Filaments. J. Neurosci. *18*, 720–730.

Ehrhardt, D.W., Wais, R., and Long, S.R. (1996). Calcium Spiking in Plant Root Hairs Responding to Rhizobium Nodulation Signals. Cell *85*, 673–681.

Engler, C., Kandzia, R., and Marillonnet, S. (2008). A One Pot, One Step, Precision Cloning Method with High Throughput Capability. PLoS ONE *3*, e3647.

Engler, C., Gruetzner, R., Kandzia, R., and Marillonnet, S. (2009). Golden Gate Shuffling: A One-Pot DNA Shuffling Method Based on Type IIs Restriction Enzymes. PLOS ONE *4*, e5553.

Espinoza, C., Liang, Y., and Stacey, G. (2017). Chitin receptor CERK1 links salt stress and chitin-triggered innate immunity in Arabidopsis. Plant J. *89*, 984–995.

Evans, M.J., Choi, W.-G., Gilroy, S., and Morris, R.J. (2016). A ROS-Assisted Calcium Wave Dependent on the AtRBOHD NADPH Oxidase and TPC1 Cation Channel Propagates the Systemic Response to Salt Stress. Plant Physiol. *171*, 1771–1784.

Farmer, E., Mousavi, S., and Lenglet, A. (2013). Leaf numbering for experiments on long distance signalling in Arabidopsis. Protoc. Exch.

Favre, P., Bapaume, L., Bossolini, E., Delorenzi, M., Falquet, L., and Reinhardt, D. (2014). A novel bioinformatics pipeline to discover genes related to arbuscular mycorrhizal symbiosis based on their evolutionary conservation pattern among higher plants. BMC Plant Biol. *14*, 333.

Finkler, A., Ashery-Padan, R., and Fromm, H. (2007). CAMTAs: Calmodulin-binding transcription activators from plants to human. FEBS Lett. *581*, 3893–3898.

Fischer, M., Schnell, N., Chattaway, J., Davies, P., Dixon, G., and Sanders, D. (1997). The Saccharomyces cerevisiae CCH1 gene is involved in calcium influx and mating. FEBS Lett. *419*, 259–262.

Forde, B.G., and Roberts, M.R. (2014). Glutamate receptor-like channels in plants: a role as amino acid sensors in plant defence? F1000Prime Rep. *6*.

Foskett, J.K., White, C., Cheung, K.-H., and Mak, D.-O.D. (2007). Inositol Trisphosphate Receptor Ca^{2+} Release Channels. Physiol. Rev. *87*, 593–658.

French, A.P., Wilson, M.H., Kenobi, K., Dietrich, D., Voß, U., Ubeda-Tomás, S., Pridmore, T.P., and Wells, D.M. (2012). Identifying biological landmarks using a novel cell measuring image analysis tool: Cell-o-Tape. Plant Methods *8*, 7.

Friml, J., Vieten, A., Sauer, M., Weijers, D., Schwarz, H., Hamann, T., Offringa, R., and Jürgens, G. (2003). Efflux-dependent auxin gradients establish the apical–basal axis of Arabidopsis. Nature *426*, 147–153.

Fukaki, H., and Tasaka, M. (2009). Hormone interactions during lateral root formation. Plant Mol. Biol. *69*, 437.

Galon, Y., Nave, R., Boyce, J.M., Nachmias, D., Knight, M.R., and Fromm, H. (2008). Calmodulin-binding transcription activator (CAMTA) 3 mediates biotic defense responses in Arabidopsis. FEBS Lett. *582*, 943–948.

Gao, M., Liu, J., Bi, D., Zhang, Z., Cheng, F., Chen, S., and Zhang, Y. (2008). MEKK1, MKK1/MKK2 and MPK4 function together in a mitogen-activated protein kinase cascade to regulate innate immunity in plants. Cell Res. *18*, 1190–1198.

Gao, Q.-F., Fei, C.-F., Dong, J.-Y., Gu, L.-L., and Wang, Y.-F. (2014). Arabidopsis CNGC18 Is a Ca^{2+}-Permeable Channel. Mol. Plant *7*, 739–743.

Gao, Q.-F., Gu, L.-L., Wang, H.-Q., Fei, C.-F., Fang, X., Hussain, J., Sun, S.-J., Dong, J.-Y., Liu, H., and Wang, Y.-F. (2016). Cyclic nucleotide-gated channel 18 is an essential Ca^{2+} channel in pollen tube tips for pollen tube guidance to ovules in Arabidopsis. Proc. Natl. Acad. Sci. 201524629.

Gao, Y., Zhang, Y., Zhang, D., Dai, X., Estelle, M., and Zhao, Y. (2015). Auxin binding protein 1 (ABP1) is not required for either auxin signaling or Arabidopsis development. Proc. Natl. Acad. Sci. *112*, 2275–2280.

Gelli, A., Higgins, V.J., and Blumwald, E. (1997). Activation of Plant Plasma Membrane Ca^{2+}-Permeable Channels by Race-Specific Fungal Elicitors. Plant Physiol. *113*, 269–279.

Genger, R.K., Jurkowski, G.I., McDowell, J.M., Lu, H., Jung, H.W., Greenberg, J.T., and Bent, A.F. (2008). Signaling Pathways That Regulate the Enhanced Disease Resistance of Arabidopsis "Defense, No Death" Mutants. Mol. Plant. Microbe Interact. *21*, 1285–1296.

Genre, A., Chabaud, M., Balzergue, C., Puech-Pagès, V., Novero, M., Rey, T., Fournier, J., Rochange, S., Bécard, G., Bonfante, P., and Barker, D.G. (2013). Short-chain chitin oligomers from arbuscular mycorrhizal fungi trigger nuclear Ca^{2+} spiking in *Medicago truncatula* roots and their production is enhanced by strigolactone. New Phytol. *198*, 190–202.

Gietz, R.D., and Woods, R.A. (2001). Genetic transformation of yeast. BioTechniques *30*, 816–820, 822–826, 828 passim.

Gilroy, S., Read, N.D., and Trewavas, A.J. (1990). Elevation of cytoplasmic calcium by caged calcium or caged inositol trisphosphate initiates stomatal closure. Nature *346*, 769–771.

Gobert, A., Park, G., Amtmann, A., Sanders, D., and Maathuis, F.J.M. (2006). Arabidopsis thaliana Cyclic Nucleotide Gated Channel 3 forms a non-selective ion transporter involved in germination and cation transport. J. Exp. Bot. *57*, 791–800.

Goedhart, J., van Weeren, L., Hink, M.A., Vischer, N.O.E., Jalink, K., and Gadella, T.W.J. (2010). Bright cyan fluorescent protein variants identified by fluorescence lifetime screening. Nat. Methods *7*, 137–139.

Göhre, V., Jones, A.M.E., Sklenář, J., Robatzek, S., and Weber, A.P.M. (2012). Molecular Crosstalk Between PAMP-Triggered Immunity and Photosynthesis. Mol. Plant. Microbe Interact. *25*, 1083–1092.

Gómez-Gómez, L., and Boller, T. (2000). FLS2: an LRR receptor-like kinase involved in the perception of the bacterial elicitor flagellin in Arabidopsis. Mol. Cell *5*, 1003–1011.

Gómez-Gómez, L., Felix, G., and Boller, T. (1999). A single locus determines sensitivity to bacterial flagellin in Arabidopsis thaliana. Plant J. *18*, 277–284.

Gong, M., Luit, A.H. van der, Knight, M.R., and Trewavas, A.J. (1998). Heat-Shock-Induced Changes in Intracellular Ca^{2+} Level in Tobacco Seedlings in Relation to Thermotolerance. Plant Physiol. *116*, 429–437.

Granqvist, E., Wysham, D., Hazledine, S., Kozlowski, W., Sun, J., Charpentier, M., Martins, T.V., Haleux, P., Tsaneva-Atanasova, K., Downie, J.A., Oldroyd, G.E.D., and Morris, R.J. (2012). Buffering Capacity Explains Signal Variation in Symbiotic Calcium Oscillations. Plant Physiol. *160*, 2300–2310.

Gravino, M., Savatin, D.V., Macone, A., and De Lorenzo, G. (2015). Ethylene production in Botrytis cinerea- and oligogalacturonide-induced immunity requires calcium-dependent protein kinases. Plant J. Cell Mol. Biol. *84*, 1073–1086.

Grieneisen, V.A., Xu, J., Marée, A.F.M., Hogeweg, P., and Scheres, B. (2007). Auxin transport is sufficient to generate a maximum and gradient guiding root growth. Nature *449*, 1008–1013.

Grossmann, G., Guo, W.-J., Ehrhardt, D.W., Frommer, W.B., Sit, R.V., Quake, S.R., and Meier, M. (2011). The RootChip: An Integrated Microfluidic Chip for Plant Science. Plant Cell *23*, 4234–4240.

Grynkiewicz, G., Poenie, M., and Tsien, R.Y. (1985). A new generation of Ca^{2+} indicators with greatly improved fluorescence properties. J. Biol. Chem. *260*, 3440–3450.

Hamamura, Y., Nishimaki, M., Takeuchi, H., Geitmann, A., Kurihara, D., and Higashiyama, T. (2014). Live imaging of calcium spikes during double fertilization in *Arabidopsis*. Nat. Commun. *5*, ncomms5722.

He, P., Shan, L., Lin, N.-C., Martin, G.B., Kemmerling, B., Nürnberger, T., and Sheen, J. (2006). Specific Bacterial Suppressors of MAMP Signaling Upstream of MAPKKK in Arabidopsis Innate Immunity. Cell *125*, 563–575.

Heese, A., Hann, D.R., Gimenez-Ibanez, S., Jones, A.M.E., He, K., Li, J., Schroeder, J.I., Peck, S.C., and Rathjen, J.P. (2007). The receptor-like kinase SERK3/BAK1 is a central regulator of innate immunity in plants. Proc. Natl. Acad. Sci. *104*, 12217–12222.

Hepler, P.K., Vidali, L., and Cheung, A.Y. (2001). Polarized cell growth in higher plants. Annu. Rev. Cell Dev. Biol. *17*, 159–187.

Himschoot, E., Beeckman, T., Friml, J., and Vanneste, S. Calcium is an organizer of cell polarity in plants. Biochim. Biophys. Acta BBA - Mol. Cell Res. *1853*, 2168–2172.

Hirschi, K.D. (2003). Insertional mutants: a foundation for assessing gene function. Trends Plant Sci. *8*, 205–207.

Horikawa, K., Yamada, Y., Matsuda, T., Kobayashi, K., Hashimoto, M., Matsu-ura, T., Miyawaki, A., Michikawa, T., Mikoshiba, K., and Nagai, T. (2010). Spontaneous network activity visualized by ultrasensitive Ca^{2+} indicators, yellow Cameleon-Nano. Nat. Methods *7*, 729–732.

Hu, X., Neill, S.J., Tang, Z., and Cai, W. (2005). Nitric Oxide Mediates Gravitropic Bending in Soybean Roots. Plant Physiol. *137*, 663–670.

Hua, B.-G., Mercier, R.W., Zielinski, R.E., and Berkowitz, G.A. (2003). Functional interaction of calmodulin with a plant cyclic nucleotide gated cation channel. Plant Physiol. Biochem. *41*, 945–954.

Huang, J.Z., and Huber, S.C. (2001). Phosphorylation of synthetic peptides by a CDPK and plant SNF1-related protein kinase. Influence of proline and basic amino acid residues at selected positions. Plant Cell Physiol. *42*, 1079–1087.

Huang, J.-Z., Hardin, S.C., and Huber, S.C. (2001). Identification of a Novel Phosphorylation Motif for CDPKs: Phosphorylation of Synthetic Peptides Lacking Basic Residues at P-3/P-4. Arch. Biochem. Biophys. *393*, 61–66.

Huh, S.M., Noh, E.K., Kim, H.G., Jeon, B.W., Bae, K., Hu, H.-C., Kwak, J.M., and Park, O.K. (2010). Arabidopsis Annexins AnnAt1 and AnnAt4 Interact with Each Other and Regulate Drought and Salt Stress Responses. Plant Cell Physiol. *51*, 1499–1514.

Iida, H., Nakamura, H., Ono, T., Okumura, M.S., and Anraku, Y. (1994). MID1, a novel Saccharomyces cerevisiae gene encoding a plasma membrane protein, is required for Ca^{2+} influx and mating. Mol. Cell. Biol. *14*, 8259–8271.

Ikura, M., Clore, G.M., Gronenborn, A.M., Zhu, G., Klee, C.B., and Bax, A. (1992). Solution structure of a calmodulin-target peptide complex by multidimensional NMR. Science *256*, 632–638.

Ioio, R.D., Nakamura, K., Moubayidin, L., Perilli, S., Taniguchi, M., Morita, M.T., Aoyama, T., Costantino, P., and Sabatini, S. (2008). A Genetic Framework for the Control of Cell Division and Differentiation in the Root Meristem. Science *322*, 1380–1384.

Ishida, T., Adachi, S., Yoshimura, M., Shimizu, K., Umeda, M., and Sugimoto, K. (2010). Auxin modulates the transition from the mitotic cycle to the endocycle in Arabidopsis. Development *137*, 63–71.

Isner, J.C., Nühse, T., and Maathuis, F.J.M. (2012). The cyclic nucleotide cGMP is involved in plant hormone signalling and alters phosphorylation of Arabidopsis thaliana root proteins. J. Exp. Bot. *63*, 3199–3205.

Iwano, M., Ngo, Q.A., Entani, T., Shiba, H., Nagai, T., Miyawaki, A., Isogai, A., Grossniklaus, U., and Takayama, S. (2012). Cytoplasmic Ca^{2+} changes dynamically during the interaction of the pollen tube with synergid cells. Development *139*, 4202–4209.

Jammes, F., Hu, H.-C., Villiers, F., Bouten, R., and Kwak, J.M. (2011). Calcium-permeable channels in plant cells. FEBS J. *278*, 4262–4276.

Jeworutzki, E., Roelfsema, M.R.G., Anschütz, U., Krol, E., Elzenga, J.T.M., Felix, G., Boller, T., Hedrich, R., and Becker, D. (2010). Early signaling through the Arabidopsis pattern recognition receptors FLS2 and EFR involves Ca^{2+}-associated opening of plasma membrane anion channels. Plant J. *62*, 367–378.

Jha, S.K., Sharma, M., and Pandey, G.K. (2016). Role of Cyclic Nucleotide Gated Channels in Stress Management in Plants. Curr. Genomics *17*, 315–329.

Johnson, C.H., Knight, M.R., Kondo, T., Masson, P., Sedbrook, J., Haley, A., and Trewavas, A. (1995). Circadian oscillations of cytosolic and chloroplastic free calcium in plants. Science *269*, 1863–1865.

Jones, J.D.G., and Dangl, J.L. (2006). The plant immune system. Nature *444*, 323–329.

Jung, C., Lyou, S.H., Yeu, S., Kim, M.A., Rhee, S., Kim, M., Lee, J.S., Choi, Y.D., and Cheong, J.-J. (2007). Microarray-based screening of jasmonate-responsive genes in Arabidopsis thaliana. Plant Cell Rep. *26*, 1053–1063.

Junker, A., Mönke, G., Rutten, T., Keilwagen, J., Seifert, M., Thi, T.M.N., Renou, J.-P., Balzergue, S., Viehöver, P., Hähnel, U., Ludwig-Müller, J., Altschmied, L., Conrad, U., Weisshaar, B., and Bäumlein, H. (2012). Elongation-related functions of LEAFY COTYLEDON1 during the development of Arabidopsis thaliana. Plant J. *71*, 427–442.

Jurkowski, G.I., Smith, R.K., Yu, I., Ham, J.H., Sharma, S.B., Klessig, D.F., Fengler, K.A., and Bent, A.F. (2004). Arabidopsis DND2, a Second Cyclic Nucleotide-Gated Ion Channel Gene for Which Mutation Causes the "Defense, No Death" Phenotype. Mol. Plant. Microbe Interact. *17*, 511–520.

Kadota, Y., Sklenar, J., Derbyshire, P., Stransfeld, L., Asai, S., Ntoukakis, V., Jones, J.D., Shirasu, K., Menke, F., Jones, A., and Zipfel, C. (2014). Direct Regulation of the NADPH Oxidase RBOHD by the PRR-Associated Kinase BIK1 during Plant Immunity. Mol. Cell *54*, 43–55.

Kanchiswamy, C.N., Malnoy, M., Occhipinti, A., and Maffei, M.E. (2014). Calcium Imaging Perspectives in Plants. Int. J. Mol. Sci. *15*, 3842–3859.

Kang, J., Tang, J., Donnelly, P., and Dengler, N. (2003). Primary vascular pattern and expression of ATHB-8 in shoots of Arabidopsis. New Phytol. *158*, 443–454.

Kang, S., Kim, H.B., Lee, H., Choi, J.Y., Heu, S., Oh, C.J., Kwon, S.I., and An, C.S. (2006). Overexpression in Arabidopsis of a Plasma Membrane-targeting Glutamate Receptor from Small Radish Increases Glutamate-mediated Ca^{2+} Influx and Delays Fungal Infection. Korean Soc. Mol. Cell. Biol. 418–427.

Kaplan, B., Sherman, T., and Fromm, H. (2007). Cyclic nucleotide-gated channels in plants. FEBS Lett. *581*, 2237–2246.

Keinath, N.F., Waadt, R., Brugman, R., Schroeder, J.I., Grossmann, G., Schumacher, K., and Krebs, M. (2015). Live Cell Imaging with R-GECO1 Sheds Light on flg22- and Chitin-Induced Transient $[Ca^{2+}]_{cyt}$ Patterns in Arabidopsis. Mol. Plant *8*, 1188–1200.

Keller, T., Damude, H.G., Werner, D., Doerner, P., Dixon, R.A., and Lamb, C. (1998). A Plant Homolog of the Neutrophil NADPH Oxidase gp91phox Subunit Gene Encodes a Plasma Membrane Protein with Ca^{2+} Binding Motifs. Plant Cell *10*, 255–266.

Kiegle, E., Moore, C.A., Haseloff, J., Tester, M.A., and Knight, M.R. (2000). Cell-type-specific calcium responses to drought, salt and cold in the Arabidopsis root. Plant J. *23*, 267–278.

Kiep, V., Vadassery, J., Lattke, J., Maaß, J.-P., Boland, W., Peiter, E., and Mithöfer, A. (2015). Systemic cytosolic Ca^{2+} elevation is activated upon wounding and herbivory in Arabidopsis. New Phytol. *207*, 996–1004.

Kim, Y.-Y., Choi, H., Segami, S., Cho, H.-T., Martinoia, E., Maeshima, M., and Lee, Y. (2009). AtHMA1 contributes to the detoxification of excess Zn(II) in Arabidopsis. Plant J. *58*, 737–753.

Knight, H., Trewavas, A.J., and Knight, M.R. (1996). Cold calcium signaling in Arabidopsis involves two cellular pools and a change in calcium signature after acclimation. Plant Cell *8*, 489–503.

Knight, H., Trewavas, A.J., and Knight, M.R. (1997). Calcium signalling in Arabidopsis thaliana responding to drought and salinity. Plant J. *12*, 1067–1078.

Knight, M.R., Campbell, A.K., Smith, S.M., and Trewavas, A.J. (1991). Transgenic plant aequorin reports the effects of touch and cold-shock and elicitors on cytoplasmic calcium. Nature *352*, 524–526.

Köhler, C., and Neuhaus, G. (2000). Characterisation of calmodulin binding to cyclic nucleotide-gated ion channels from Arabidopsis thaliana. FEBS Lett. *471*, 133–136.

Köhr, G., and Seeburg, P.H. (1996). Subtype-specific regulation of recombinant NMDA receptor-channels by protein tyrosine kinases of the src family. J. Physiol. *492*, 445–452.

Kong, D., Hu, H.-C., Okuma, E., Lee, Y., Lee, H.S., Munemasa, S., Cho, D., Ju, C., Pedoeim, L., Rodriguez, B., Wang, J., Im, W., Murata, Y., Pei, Z.-M., and Kwak, J.M. (2016). L-Met Activates Arabidopsis GLR

Ca^{2+} Channels Upstream of ROS Production and Regulates Stomatal Movement. Cell Rep. *17*, 2553–2561.

Krebs, M., and Schumacher, K. (2013). Live cell imaging of cytoplasmic and nuclear Ca^{2+} dynamics in Arabidopsis roots. Cold Spring Harb. Protoc. *2013*, 776–780.

Krebs, M., Held, K., Binder, A., Hashimoto, K., Den Herder, G., Parniske, M., Kudla, J., and Schumacher, K. (2012). FRET-based genetically encoded sensors allow high-resolution live cell imaging of Ca^{2+} dynamics. Plant J. *69*, 181–192.

Krol, E., Mentzel, T., Chinchilla, D., Boller, T., Felix, G., Kemmerling, B., Postel, S., Arents, M., Jeworutzki, E., Al-Rasheid, K.A.S., Becker, D., and Hedrich, R. (2010). Perception of the Arabidopsis Danger Signal Peptide 1 Involves the Pattern Recognition Receptor AtPEPR1 and Its Close Homologue AtPEPR2. J. Biol. Chem. *285*, 13471–13479.

Kurusu, T., Kuchitsu, K., Nakano, M., Nakayama, Y., and Iida, H. (2013). Plant mechanosensing and Ca^{2+} transport. Trends Plant Sci. *18*, 227–233.

Kwaaitaal, M., Huisman, R., Maintz, J., Reinstädler, A., and Panstruga, R. (2011). Ionotropic glutamate receptor (iGluR)-like channels mediate MAMP-induced calcium influx in *Arabidopsis thaliana*. Biochem. J. *440*, 355–365.

Lachaud, C., Da Silva, D., Cotelle, V., Thuleau, P., Xiong, T.C., Jauneau, A., Brière, C., Graziana, A., Bellec, Y., Faure, J.-D., Ranjeva, R., and Mazars, C. (2010). Nuclear calcium controls the apoptotic-like cell death induced by d-erythro-sphinganine in tobacco cells. Cell Calcium *47*, 92–100.

Lam, H.-M., Chiu, J., Hsieh, M.-H., Meisel, L., Oliveira, I.C., Shin, M., and Coruzzi, G. (1998). Glutamate-receptor genes in plants. Nature *396*, 125–126.

Laohavisit, A., Mortimer, J.C., Demidchik, V., Coxon, K.M., Stancombe, M.A., Macpherson, N., Brownlee, C., Hofmann, A., Webb, A.A.R., Miedema, H., Battey, N.H., and Davies, J.M. (2009). Zea mays Annexins Modulate Cytosolic Free Ca^{2+} and Generate a Ca^{2+}-Permeable Conductance. Plant Cell *21*, 479–493.

Laohavisit, A., Brown, A.T., Cicuta, P., and Davies, J.M. (2010). Annexins: Components of the Calcium and Reactive Oxygen Signaling Network. Plant Physiol. *152*, 1824–1829.

Laohavisit, A., Shang, Z., Rubio, L., Cuin, T.A., Véry, A.-A., Wang, A., Mortimer, J.C., Macpherson, N., Coxon, K.M., Battey, N.H., Brownlee, C., Park, O.K., Sentenac, H., Shabala, S., Webb, A.A.R., and Davies, J.M. (2012). Arabidopsis Annexin1 Mediates the Radical-Activated Plasma Membrane Ca^{2+}- and K^+-Permeable Conductance in Root Cells. Plant Cell *24*, 1522–1533.

Laohavisit, A., Richards, S.L., Shabala, L., Chen, C., Colaço, R.D.D.R., Swarbreck, S.M., Shaw, E., Dark, A., Shabala, S., Shang, Z., and Davies, J.M. (2013). Salinity-induced calcium signaling and root adaptation in Arabidopsis require the calcium regulatory protein annexin1. Plant Physiol. *163*, 253–262.

Lecourieux, D., Lamotte, O., Bourque, S., Wendehenne, D., Mazars, C., Ranjeva, R., and Pugin, A. (2005). Proteinaceous and oligosaccharidic elicitors induce different calcium signatures in the nucleus of tobacco cells. Cell Calcium *38*, 527–538.

Lee, J., Eschen-Lippold, L., Lassowskat, I., Böttcher, C., and Scheel, D. (2015). Cellular reprogramming through mitogen-activated protein kinases. Front. Plant Sci. *6*.

Lee, S., Lee, E.J., Yang, E.J., Lee, J.E., Park, A.R., Song, W.H., and Park, O.K. (2004). Proteomic Identification of Annexins, Calcium-Dependent Membrane Binding Proteins That Mediate Osmotic Stress and Abscisic Acid Signal Transduction in Arabidopsis. Plant Cell *16*, 1378–1391.

Leng, Q., Mercier, R.W., Yao, W., and Berkowitz, G.A. (1999). Cloning and First Functional Characterization of a Plant Cyclic Nucleotide-Gated Cation Channel. Plant Physiol. *121*, 753–761.

Li, F., Wang, J., Ma, C., Zhao, Y., Wang, Y., Hasi, A., and Qi, Z. (2013). Glutamate Receptor-Like Channel3.3 Is Involved in Mediating Glutathione-Triggered Cytosolic Calcium Transients, Transcriptional Changes, and Innate Immunity Responses in Arabidopsis. Plant Physiol. *162*, 1497–1509.

Li, L., Li, M., Yu, L., Zhou, Z., Liang, X., Liu, Z., Cai, G., Gao, L., Zhang, X., Wang, Y., Chen, S., and Zhou, J.-M. (2014). The FLS2-associated kinase BIK1 directly phosphorylates the NADPH oxidase RbohD to control plant immunity. Cell Host Microbe *15*, 329–338.

Liang, F., and Sze, H. (1998). A High-Affinity Ca^{2+} Pump, ECA1, from the Endoplasmic Reticulum Is Inhibited by Cyclopiazonic Acid but Not by Thapsigargin. Plant Physiol. *118*, 817–825.

Liang, F., Cunningham, K.W., Harper, J.F., and Sze, H. (1997). ECA1 complements yeast mutants defective in Ca^{2+} pumps and encodes an endoplasmic reticulum-type Ca^{2+}-ATPase in Arabidopsis thaliana. Proc. Natl. Acad. Sci. U. S. A. *94*, 8579–8584.

Lipka, U., Fuchs, R., Kuhns, C., Petutschnig, E., and Lipka, V. (2010). Live and let die – Arabidopsis nonhost resistance to powdery mildews. Eur. J. Cell Biol. *89*, 194–199.

Logan, D.C., and Knight, M.R. (2003). Mitochondrial and Cytosolic Calcium Dynamics Are Differentially Regulated in Plants. Plant Physiol. *133*, 21–24.

Lu, D., Wu, S., Gao, X., Zhang, Y., Shan, L., and He, P. (2010). A receptor-like cytoplasmic kinase, BIK1, associates with a flagellin receptor complex to initiate plant innate immunity. Proc. Natl. Acad. Sci. *107*, 496–501.

Luan, S. (2009). The CBL–CIPK network in plant calcium signaling. Trends Plant Sci. *14*, 37–42.

Luan, S., Kudla, J., Rodriguez-Concepcion, M., Yalovsky, S., and Gruissem, W. (2002). Calmodulins and Calcineurin B–like Proteins Calcium Sensors for Specific Signal Response Coupling in Plants. Plant Cell *14*, S389–S400.

Luit, A.H. van der, Olivari, C., Haley, A., Knight, M.R., and Trewavas, A.J. (1999). Distinct Calcium Signaling Pathways Regulate Calmodulin Gene Expression in Tobacco. Plant Physiol. *121*, 705–714.

Ma, Y., Walker, R.K., Zhao, Y., and Berkowitz, G.A. (2012). Linking ligand perception by PEPR pattern recognition receptors to cytosolic Ca^{2+} elevation and downstream immune signaling in plants. Proc. Natl. Acad. Sci. *109*, 19852–19857.

Macho, A.P., and Zipfel, C. (2014). Plant PRRs and the Activation of Innate Immune Signaling. Mol. Cell *54*, 263–272.

Maintz, J., Cavdar, M., Tamborski, J., Kwaaitaal, M., Huisman, R., Meesters, C., Kombrink, E., and Panstruga, R. (2014). Comparative Analysis of MAMP-induced Calcium Influx in Arabidopsis Seedlings and Protoplasts. Plant Cell Physiol. *55*, 1813–1825.

Mambro, R.D., Ruvo, M.D., Pacifici, E., Salvi, E., Sozzani, R., Benfey, P.N., Busch, W., Novak, O., Ljung, K., Paola, L.D., Marée, A.F.M., Costantino, P., Grieneisen, V.A., and Sabatini, S. (2017). Auxin minimum

triggers the developmental switch from cell division to cell differentiation in the Arabidopsis root. Proc. Natl. Acad. Sci. *114*, E7641–E7649.

Manohar, M., Shigaki, T., and Hirschi, K.D. (2011). Plant cation/H^+ exchangers (CAXs): biological functions and genetic manipulations. Plant Biol. *13*, 561–569.

Manzoor, H., Kelloniemi, J., Chiltz, A., Wendehenne, D., Pugin, A., Poinssot, B., and Garcia-Brugger, A. (2013). Involvement of the glutamate receptor AtGLR3.3 in plant defense signaling and resistance to Hyaloperonospora arabidopsidis. Plant J. Cell Mol. Biol. *76*, 466–480.

Marchadier, E., Oates, M.E., Fang, H., Donoghue, P.C.J., Hetherington, A.M., and Gough, J. (2016). Evolution of the Calcium-Based Intracellular Signaling System. Genome Biol. Evol. *8*, 2118–2132.

Mäser, P., Thomine, S., Schroeder, J.I., Ward, J.M., Hirschi, K., Sze, H., Talke, I.N., Amtmann, A., Maathuis, F.J.M., Sanders, D., Harper, J.F., Tchieu, J., Gribskov, M., Persans, M.W., Salt, D.E., Kim, S.A., and Guerinot, M.L. (2001). Phylogenetic Relationships within Cation Transporter Families of Arabidopsis. Plant Physiol. *126*, 1646–1667.

Mazars, C., Bourque, S., Mithöfer, A., Pugin, A., and Ranjeva, R. (2009). Calcium homeostasis in plant cell nuclei. New Phytol. *181*, 261–274.

McCormac, A.C., Elliott, M.C., and Chen, D.F. (1998). A simple method for the production of highly competent cells of Agrobacterium for transformation via electroporation. Mol. Biotechnol. *9*, 155–159.

Mcphalen, C., Strynadka, N., and James, M. (1991). Calcium-Binding Sites in Proteins - a Structural Perspective. Adv. Protein Chem. *42*, 77–144.

Meng, X., and Zhang, S. (2013). MAPK Cascades in Plant Disease Resistance Signaling. Annu. Rev. Phytopathol. *51*, 245–266.

Mészáros, T., Helfer, A., Hatzimasoura, E., Magyar, Z., Serazetdinova, L., Rios, G., Bardóczy, V., Teige, M., Koncz, C., Peck, S., and Bögre, L. (2006). The Arabidopsis MAP kinase kinase MKK1 participates in defence responses to the bacterial elicitor flagellin. Plant J. Cell Mol. Biol. *48*, 485–498.

Michard, E., Lima, P.T., Borges, F., Silva, A.C., Portes, M.T., Carvalho, J.E., Gilliham, M., Liu, L.-H., Obermeyer, G., and Feijó, J.A. (2011). Glutamate Receptor–Like Genes Form Ca^{2+} Channels in Pollen Tubes and Are Regulated by Pistil d-Serine. Science *332*, 434–437.

Miller, G., Schlauch, K., Tam, R., Cortes, D., Torres, M.A., Shulaev, V., Dangl, J.L., and Mittler, R. (2009). The Plant NADPH Oxidase RBOHD Mediates Rapid Systemic Signaling in Response to Diverse Stimuli. Sci. Signal. *2*, ra45-ra45.

Mills, R.F., Doherty, M.L., López-Marqués, R.L., Weimar, T., Dupree, P., Palmgren, M.G., Pittman, J.K., and Williams, L.E. (2008). ECA3, a Golgi-Localized P2A-Type ATPase, Plays a Crucial Role in Manganese Nutrition in Arabidopsis. Plant Physiol. *146*, 116–128.

Mittler, R., Vanderauwera, S., Suzuki, N., Miller, G., Tognetti, V.B., Vandepoele, K., Gollery, M., Shulaev, V., and Van Breusegem, F. (2011). ROS signaling: the new wave? Trends Plant Sci. *16*, 300–309.

Miwa, H., Sun, J., Oldroyd, G.E.D., and Allan Downie, J. (2006). Analysis of calcium spiking using a cameleon calcium sensor reveals that nodulation gene expression is regulated by calcium spike number and the developmental status of the cell. Plant J. *48*, 883–894.

Miyawaki, A., Llopis, J., Heim, R., McCaffery, J.M., Adams, J.A., Ikura, M., and Tsien, R.Y. (1997). Fluorescent indicators for Ca^{2+}based on green fluorescent proteins and calmodulin. Nature *388*, 882–887.

Moeder, W., Urquhart, W., Ung, H., and Yoshioka, K. (2011). The Role of Cyclic Nucleotide-Gated Ion Channels in Plant Immunity. Mol. Plant *4*, 442–452.

Monaghan, J., Matschi, S., Shorinola, O., Rovenich, H., Matei, A., Segonzac, C., Malinovsky, F.G., Rathjen, J.P., MacLean, D., Romeis, T., and Zipfel, C. (2014). The Calcium-Dependent Protein Kinase CPK28 Buffers Plant Immunity and Regulates BIK1 Turnover. Cell Host Microbe *16*, 605–615.

Monaghan, J., Matschi, S., Romeis, T., and Zipfel, C. (2015). The calcium-dependent protein kinase CPK28 negatively regulates the BIK1-mediated PAMP-induced calcium burst. Plant Signal. Behav. *10*, e1018497.

Monshausen, G.B., and Sievers, A. (2002). Basipetal propagation of gravity-induced surface pH changes along primary roots of Lepidium sativum L. Planta *215*, 980–988.

Monshausen, G.B., Messerli, M.A., and Gilroy, S. (2008). Imaging of the Yellow Cameleon 3.6 Indicator Reveals That Elevations in Cytosolic Ca^{2+} Follow Oscillating Increases in Growth in Root Hairs of Arabidopsis. Plant Physiol. *147*, 1690–1698.

Monshausen, G.B., Bibikova, T.N., Weisenseel, M.H., and Gilroy, S. (2009). Ca^{2+} Regulates Reactive Oxygen Species Production and pH during Mechanosensing in Arabidopsis Roots. Plant Cell *21*, 2341–2356.

Monshausen, G.B., Miller, N.D., Murphy, A.S., and Gilroy, S. (2011). Dynamics of auxin-dependent Ca^{2+} and pH signaling in root growth revealed by integrating high-resolution imaging with automated computer vision-based analysis. Plant J. *65*, 309–318.

Moreno, I., Norambuena, L., Maturana, D., Toro, M., Vergara, C., Orellana, A., Zurita-Silva, A., and Ordenes, V.R. (2008). AtHMA1 Is a Thapsigargin-sensitive Ca^{2+}/Heavy Metal Pump. J. Biol. Chem. *283*, 9633–9641.

Moubayidin, L., Di Mambro, R., and Sabatini, S. (2009). Cytokinin–auxin crosstalk. Trends Plant Sci. *14*, 557–562.

Moubayidin, L., Perilli, S., Dello Ioio, R., Di Mambro, R., Costantino, P., and Sabatini, S. (2010). The Rate of Cell Differentiation Controls the Arabidopsis Root Meristem Growth Phase. Curr. Biol. *20*, 1138–1143.

Mousavi, S.A.R., Chauvin, A., Pascaud, F., Kellenberger, S., and Farmer, E.E. (2013). GLUTAMATE RECEPTOR-LIKE genes mediate leaf-to-leaf wound signalling. Nature *500*, 422–426.

Mravec, J., Kubeš, M., Bielach, A., Gaykova, V., Petrášek, J., Skůpa, P., Chand, S., Benková, E., Zažímalová, E., and Friml, J. (2008). Interaction of PIN and PGP transport mechanisms in auxin distribution-dependent development. Development *135*, 3345–3354.

Mulkey, T.J., and Evans, M.L. (1981). Geotropism in Corn Roots: Evidence for Its Mediation by Differential Acid Efflux. Science *212*, 70–71.

Murata, Y., Mori, I.C., and Munemasa, S. (2015). Diverse stomatal signaling and the signal integration mechanism. Annu. Rev. Plant Biol. *66*, 369–392.

Nagai, T., Yamada, S., Tominaga, T., Ichikawa, M., and Miyawaki, A. (2004). Expanded dynamic range of fluorescent indicators for Ca^{2+} by circularly permuted yellow fluorescent proteins. Proc. Natl. Acad. Sci. U. S. A. *101*, 10554–10559.

Nan, W., Wang, X., Yang, L., Hu, Y., Wei, Y., Liang, X., Mao, L., and Bi, Y. (2014). Cyclic GMP is involved in auxin signalling during Arabidopsis root growth and development. J. Exp. Bot. *65*, 1571–1583.

Ngo, Q.A., Vogler, H., Lituiev, D.S., Nestorova, A., and Grossniklaus, U. (2014). A Calcium Dialog Mediated by the FERONIA Signal Transduction Pathway Controls Plant Sperm Delivery. Dev. Cell *29*, 491–500.

O'Connor, N., and Silver, R.B. (2013). Chapter 16 - Ratio Imaging: Practical Considerations for Measuring Intracellular Ca^{2+} and pH in Living Cells. In Methods in Cell Biology, G.S. and D.E. Wolf, ed. (Academic Press), pp. 387–406.

Ogasawara, Y., Kaya, H., Hiraoka, G., Yumoto, F., Kimura, S., Kadota, Y., Hishinuma, H., Senzaki, E., Yamagoe, S., Nagata, K., Nara, M., Suzuki, K., Tanokura, M., and Kuchitsu, K. (2008). Synergistic Activation of the Arabidopsis NADPH Oxidase AtrbohD by Ca^{2+} and Phosphorylation. J. Biol. Chem. *283*, 8885–8892.

Okumoto, S. (2012). Quantitative imaging using genetically encoded sensors for small molecules in plants. Plant J. *70*, 108–117.

Oldroyd, G.E.D. (2013). Speak, friend, and enter: signalling systems that promote beneficial symbiotic associations in plants. Nat. Rev. Microbiol. *11*, 252–263.

Oldroyd, G.E.D., and Downie, J.A. (2004). Calcium, kinases and nodulation signalling in legumes. Nat. Rev. Mol. Cell Biol. *5*, 566–576.

Oldroyd, G.E.D., and Downie, J.A. (2008). Coordinating nodule morphogenesis with rhizobial infection in legumes. Annu. Rev. Plant Biol. *59*, 519–546.

Ortiz-Ramírez, C., Michard, E., Simon, A.A., Damineli, D.S.C., Hernández-Coronado, M., Becker, J.D., and Feijó, J.A. (2017). Glutamate receptor-like channels are essential for chemotaxis and reproduction in mosses. Nature *549*, 91–95.

Paidhungat, M., and Garrett, S. (1997). A homolog of mammalian, voltage-gated calcium channels mediates yeast pheromone-stimulated Ca^{2+} uptake and exacerbates the cdc1(Ts) growth defect. Mol. Cell. Biol. *17*, 6339–6347.

Palmer, A.E., Giacomello, M., Kortemme, T., Hires, S.A., Lev-Ram, V., Baker, D., and Tsien, R.Y. (2006). Ca^{2+} Indicators Based on Computationally Redesigned Calmodulin-Peptide Pairs. Chem. Biol. *13*, 521–530.

Pauly, N., Knight, M.R., Thuleau, P., van der Luit, A.H., Moreau, M., Trewavas, A.J., Ranjeva, R., and Mazars, C. (2000). Control of free calcium in plant cell nuclei. Nature *405*, 754–755.

Pauly, N., Knight, M.R., Thuleau, P., Graziana, A., Muto, S., Ranjeva, R., and Mazars, C. (2001). The nucleus together with the cytosol generates patterns of specific cellular calcium signatures in tobacco suspension culture cells. Cell Calcium *30*, 413–421.

Pei, Z.-M., Murata, Y., Benning, G., Thomine, S., Klüsener, B., Allen, G.J., Grill, E., and Schroeder, J.I. (2000). Calcium channels activated by hydrogen peroxide mediate abscisic acid signalling in guard cells. Nature *406*, 731–734.

Peiter, E., Maathuis, F.J.M., Mills, L.N., Knight, H., Pelloux, J., Hetherington, A.M., and Sanders, D. (2005). The vacuolar Ca^{2+}-activated channel TPC1 regulates germination and stomatal movement. Nature *434*, 404–408.

Peiter, E., Sun, J., Heckmann, A.B., Venkateshwaran, M., Riely, B.K., Otegui, M.S., Edwards, A., Freshour, G., Hahn, M.G., Cook, D.R., Sanders, D., Oldroyd, G.E.D., Downie, J.A., and Ané, J.-M. (2007). The *Medicago truncatula* DMI1 Protein Modulates Cytosolic Calcium Signaling. Plant Physiol. *145*, 192–203.

Péret, B., De Rybel, B., Casimiro, I., Benková, E., Swarup, R., Laplaze, L., Beeckman, T., and Bennett, M.J. (2009). Arabidopsis lateral root development: an emerging story. Trends Plant Sci. *14*, 399–408.

Pérez Koldenkova, V., and Nagai, T. (2013). Genetically encoded Ca2 + indicators: Properties and evaluation. Biochim. Biophys. Acta BBA - Mol. Cell Res. *1833*, 1787–1797.

Petrášek, J., Mravec, J., Bouchard, R., Blakeslee, J.J., Abas, M., Seifertová, D., Wiśniewska, J., Tadele, Z., Kubeš, M., Čovanová, M., Dhonukshe, P., Skůpa, P., Benková, E., Perry, L., Křeček, P., Lee, O.R., Fink, G.R., Geisler, M., Murphy, A.S., Luschnig, C., Zažímalová, E., and Friml, J. (2006). PIN Proteins Perform a Rate-Limiting Function in Cellular Auxin Efflux. Science *312*, 914–918.

Pfaffl, M.W. (2001). A new mathematical model for relative quantification in real-time RT-PCR. Nucleic Acids Res. *29*, e45.

Pittman, J.K., and Hirschi, K.D. (2016). CAX-ing a wide net: Cation/H^+ transporters in metal remediation and abiotic stress signalling. Plant Biol. Stuttg. Ger. *18*, 741–749.

Plieth, C. (2001). Plant calcium signaling and monitoring: pros and cons and recent experimental approaches. Protoplasma *218*, 1–23.

Poovaiah, B.W., Du, L., Wang, H., and Yang, T. (2013). Recent Advances in Calcium/Calmodulin-Mediated Signaling with an Emphasis on Plant-Microbe Interactions. Plant Physiol. *163*, 531–542.

Porumb, T., Yau, P., Harvey, T.S., and Ikura, M. (1994). A calmodulin-target peptide hybrid molecule with unique calcium-binding properties. Protein Eng. *7*, 109–115.

Price, M.B., Jelesko, J., and Okumoto, S. (2012). Glutamate receptor homologs in plants: functions and evolutionary origins. Plant Traffic Transp. *3*, 235.

Price, M.B., Kong, D., and Okumoto, S. (2013). Inter-subunit interactions between Glutamate-Like Receptors in Arabidopsis. Plant Signal. Behav. *8*, e27034.

Qi, Z., Stephens, N.R., and Spalding, E.P. (2006). Calcium Entry Mediated by GLR3.3, an Arabidopsis Glutamate Receptor with a Broad Agonist Profile. Plant Physiol. *142*, 963–971.

Ranf, S., Wünnenberg, P., Lee, J., Becker, D., Dunkel, M., Hedrich, R., Scheel, D., and Dietrich, P. (2008). Loss of the vacuolar cation channel, AtTPC1, does not impair Ca^{2+} signals induced by abiotic and biotic stresses. Plant J. Cell Mol. Biol. *53*, 287–299.

Ranf, S., Eschen-Lippold, L., Pecher, P., Lee, J., and Scheel, D. (2011). Interplay between calcium signalling and early signalling elements during defence responses to microbe- or damage-associated molecular patterns. Plant J. *68*, 100–113.

Ranf, S., Grimmer, J., Pöschl, Y., Pecher, P., Chinchilla, D., Scheel, D., and Lee, J. (2012). Defense-Related Calcium Signaling Mutants Uncovered via a Quantitative High-Throughput Screen in Arabidopsis thaliana. Mol. Plant *5*, 115–130.

Ranf, S., Eschen-Lippold, L., Fröhlich, K., Westphal, L., Scheel, D., and Lee, J. (2014). Microbe-associated molecular pattern-induced calcium signaling requires the receptor-like cytoplasmic kinases, PBL1 and BIK1. BMC Plant Biol. *14*, 374.

Ranf, S., Gisch, N., Schäffer, M., Illig, T., Westphal, L., Knirel, Y.A., Sánchez-Carballo, P.M., Zähringer, U., Hückelhoven, R., Lee, J., and Scheel, D. (2015). A lectin S-domain receptor kinase mediates lipopolysaccharide sensing in Arabidopsis thaliana. Nat. Immunol. *16*, 426–433.

Ranty, B., Aldon, D., Cotelle, V., Galaud, J.-P., Thuleau, P., and Mazars, C. (2016). Calcium Sensors as Key Hubs in Plant Responses to Biotic and Abiotic Stresses. Front. Plant Sci. *7*.

Richards, S.L., Laohavisit, A., Mortimer, J.C., Shabala, L., Swarbreck, S.M., Shabala, S., and Davies, J.M. (2014). Annexin 1 regulates the H2O2-induced calcium signature in Arabidopsis thaliana roots. Plant J. *77*, 136–145.

Riely, B.K., Lougnon, G., Ané, J.-M., and Cook, D.R. (2007). The symbiotic ion channel homolog DMI1 is localized in the nuclear membrane of *Medicago truncatula* roots. Plant J. *49*, 208–216.

Roelfsema, M.R.G., and Hedrich, R. (2010). Making sense out of Ca^{2+} signals: their role in regulating stomatal movements. Plant Cell Environ. *33*, 305–321.

Roy, S.J., Gilliham, M., Berger, B., Essah, P.A., Cheffings, C., Miller, A.J., Davenport, R.J., Liu, L.-H., Skynner, M.J., Davies, J.M., Richardson, P., Leigh, R.A., and Tester, M. (2008). Investigating glutamate receptor-like gene co-expression in Arabidopsis thaliana. Plant Cell Environ. *31*, 861–871.

Sabatini, S., Beis, D., Wolkenfelt, H., Murfett, J., Guilfoyle, T., Malamy, J., Benfey, P., Leyser, O., Bechtold, N., Weisbeek, P., and Scheres, B. (1999). An Auxin-Dependent Distal Organizer of Pattern and Polarity in the Arabidopsis Root. Cell *99*, 463–472.

Salvador-Recatalà, V., Tjallingii, W.F., and Farmer, E.E. (2014). Real-time, in vivo intracellular recordings of caterpillar-induced depolarization waves in sieve elements using aphid electrodes. New Phytol. *203*, 674–684.

Sanders, D., Brownlee, C., and Harper, J.F. (1999). Communicating with Calcium. Plant Cell *11*, 691–706.

Sato, E.M., Hijazi, H., Bennett, M.J., Vissenberg, K., and Swarup, R. (2015). New insights into root gravitropic signalling. J. Exp. Bot. *66*, 2155–2165.

Schmid, M., Davison, T.S., Henz, S.R., Pape, U.J., Demar, M., Vingron, M., Schölkopf, B., Weigel, D., and Lohmann, J.U. (2005). A gene expression map of Arabidopsis thaliana development. Nat. Genet. *37*, 501–506.

Schulz, P., Herde, M., and Romeis, T. (2013). Calcium-Dependent Protein Kinases: Hubs in Plant Stress Signaling and Development. Plant Physiol. *163*, 523–530.

Sebastià, C.H., Hardin, S.C., Clouse, S.D., Kieber, J.J., and Huber, S.C. (2004). Identification of a new motif for CDPK phosphorylation in vitro that suggests ACC synthase may be a CDPK substrate. Arch. Biochem. Biophys. *428*, 81–91.

Seybold, H., Trempel, F., Ranf, S., Scheel, D., Romeis, T., and Lee, J. (2014). Ca^{2+} signalling in plant immune response: from pattern recognition receptors to Ca^{2+} decoding mechanisms. New Phytol. *204*, 782–790.

Shan, L., He, P., Li, J., Heese, A., Peck, S.C., Nürnberger, T., Martin, G.B., and Sheen, J. (2008). Bacterial Effectors Target the Common Signaling Partner BAK1 to Disrupt Multiple MAMP Receptor-Signaling Complexes and Impede Plant Immunity. Cell Host Microbe *4*, 17–27.

Shih, H.-W., DePew, C.L., Miller, N.D., and Monshausen, G.B. (2015). The Cyclic Nucleotide-Gated Channel CNGC14 Regulates Root Gravitropism in Arabidopsis thaliana. Curr. Biol. *25*, 3119–3125.

Shimizu, T., Nakano, T., Takamizawa, D., Desaki, Y., Ishii-Minami, N., Nishizawa, Y., Minami, E., Okada, K., Yamane, H., Kaku, H., and Shibuya, N. (2010). Two LysM receptor molecules, CEBiP and OsCERK1, cooperatively regulate chitin elicitor signaling in rice. Plant J. Cell Mol. Biol. *64*, 204–214.

Shimomura, O., and Johnson, F.H. (1970). Calcium Binding, Quantum Yield, and Emitting Molecule in Aequorin Bioluminescence. Nature *227*, 1356–1357.

Shimomura, O., Johnson, F.H., and Morise, H. (1974). Mechanism of the luminescent intramolecular reaction of aequorin. Biochemistry (Mosc.) *13*, 3278–3286.

Sieberer, B.J., Chabaud, M., Timmers, A.C., Monin, A., Fournier, J., and Barker, D.G. (2009). A Nuclear-Targeted Cameleon Demonstrates Intranuclear Ca^{2+} Spiking in *Medicago truncatula* Root Hairs in Response to Rhizobial Nodulation Factors. Plant Physiol. *151*, 1197–1206.

Sieberer, B.J., Chabaud, M., Fournier, J., Timmers, A.C.J., and Barker, D.G. (2012). A switch in Ca^{2+} spiking signature is concomitant with endosymbiotic microbe entry into cortical root cells of *Medicago truncatula*. Plant J. *69*, 822–830.

Singh, S.K., Chien, C.-T., and Chang, I.-F. (2016). The Arabidopsis glutamate receptor-like gene GLR3.6 controls root development by repressing the Kip-related protein gene KRP4. J. Exp. Bot. erv576.

Spalding, E.P. (2000). Ion channels and the transduction of light signals. Plant Cell Environ. *23*, 665–674.

Spalding, E.P., and Harper, J.F. (2011). The ins and outs of cellular Ca^{2+} transport. Curr. Opin. Plant Biol. *14*, 715–720.

Steffens, B., Feckler, C., Palme, K., Christian, M., Böttger, M., and Lüthen, H. (2001). The auxin signal for protoplast swelling is perceived by extracellular ABP1. Plant J. *27*, 591–599.

Stephens, N.R., Qi, Z., and Spalding, E.P. (2008). Glutamate Receptor Subtypes Evidenced by Differences in Desensitization and Dependence on the GLR3.3 and GLR3.4 Genes. Plant Physiol. *146*, 529–538.

Suarez-Rodriguez, M.C., Adams-Phillips, L., Liu, Y., Wang, H., Su, S.-H., Jester, P.J., Zhang, S., Bent, A.F., and Krysan, P.J. (2007). MEKK1 Is Required for flg22-Induced MPK4 Activation in Arabidopsis Plants. Plant Physiol. *143*, 661–669.

Sugano, S., Jiang, C.-J., Miyazawa, S.-I., Masumoto, C., Yazawa, K., Hayashi, N., Shimono, M., Nakayama, A., Miyao, M., and Takatsuji, H. (2010). Role of OsNPR1 in rice defense program as revealed by genome-wide expression analysis. Plant Mol. Biol. *74*, 549–562.

Sugimoto-Shirasu, K., and Roberts, K. (2003). “Big it up”: endoreduplication and cell-size control in plants. Curr. Opin. Plant Biol. *6*, 544–553.

Sun, J., Miller, J.B., Granqvist, E., Wiley-Kalil, A., Gobbato, E., Maillet, F., Cottaz, S., Samain, E., Venkateshwaran, M., Fort, S., Morris, R.J., Ané, J.-M., Dénarié, J., and Oldroyd, G.E.D. (2015). Activation of Symbiosis Signaling by Arbuscular Mycorrhizal Fungi in Legumes and Rice. Plant Cell *27*, 823–838.

Sun, Y., Li, L., Macho, A.P., Han, Z., Hu, Z., Zipfel, C., Zhou, J.-M., and Chai, J. (2013). Structural Basis for flg22-Induced Activation of the Arabidopsis FLS2-BAK1 Immune Complex. Science *342*, 624–628.

Sze, H., Liang, F., Hwang, I., Curran, A.C., and Harper, and J.F. (2000). Diversity and regulation of plant Ca^{2+} pumps: insights from expression in yeast. Annu. Rev. Plant Physiol. Plant Mol. Biol. *51*, 433–462.

Tanaka, K., Swanson, S.J., Gilroy, S., and Stacey, G. (2010). Extracellular Nucleotides Elicit Cytosolic Free Calcium Oscillations in Arabidopsis. Plant Physiol. *154*, 705–719.

Tanaka, K., Choi, J., and Stacey, G. (2013). Aequorin Luminescence-Based Functional Calcium Assay for Heterotrimeric G-Proteins in Arabidopsis. In G Protein-Coupled Receptor Signaling in Plants, M.P. Running, ed. (Humana Press), pp. 45–54.

Tang, R.-H., Han, S., Zheng, H., Cook, C.W., Choi, C.S., Woerner, T.E., Jackson, R.B., and Pei, Z.-M. (2007). Coupling Diurnal Cytosolic Ca^{2+} Oscillations to the CAS-IP3 Pathway in Arabidopsis. Science *315*, 1423–1426.

Tapken, D., Anschütz, U., Liu, L.-H., Huelsken, T., Seebohm, G., Becker, D., and Hollmann, M. (2013). A Plant Homolog of Animal Glutamate Receptors Is an Ion Channel Gated by Multiple Hydrophobic Amino Acids. Sci. Signal. *6*, ra47-ra47.

Teardo, E., Formentin, E., Segalla, A., Giacometti, G.M., Marin, O., Zanetti, M., Lo Schiavo, F., Zoratti, M., and Szabò, I. (2011). Dual localization of plant glutamate receptor AtGLR3.4 to plastids and plasmamembrane. Biochim. Biophys. Acta BBA - Bioenerg. *1807*, 359–367.

Teardo, E., Carraretto, L., Bortoli, S.D., Costa, A., Behera, S., Wagner, R., Schiavo, F.L., Formentin, E., and Szabo, I. (2015). Alternative Splicing-Mediated Targeting of the Arabidopsis GLUTAMATE RECEPTOR3.5 to Mitochondria Affects Organelle Morphology. Plant Physiol. *167*, 216–227.

Thestrup, T., Litzlbauer, J., Bartholomäus, I., Mues, M., Russo, L., Dana, H., Kovalchuk, Y., Liang, Y., Kalamakis, G., Laukat, Y., Becker, S., Witte, G., Geiger, A., Allen, T., Rome, L.C., Chen, T.-W., Kim, D.S., Garaschuk, O., Griesinger, C., and Griesbeck, O. (2014). Optimized ratiometric calcium sensors for functional in vivo imaging of neurons and T $lympho_{cyt}$es. Nat. Methods *11*, 175–182.

Thomason, P., and Kay, R. (2000). Eukaryotic signal transduction via histidine-aspartate phosphorelay. J. Cell Sci. *113*, 3141–3150.

Thor, K., and Peiter, E. (2014). Cytosolic calcium signals elicited by the pathogen-associated molecular pattern flg22 in stomatal guard cells are of an oscillatory nature. New Phytol. *204*, 873–881.

Tian, L., Hires, S.A., Mao, T., Huber, D., Chiappe, M.E., Chalasani, S.H., Petreanu, L., Akerboom, J., McKinney, S.A., Schreiter, E.R., Bargmann, C.I., Jayaraman, V., Svoboda, K., and Looger, L.L. (2009). Imaging neural activity in worms, flies and mice with improved GCaMP calcium indicators. Nat. Methods *6*, 875–881.

Torre, F. de la, Gutiérrez-Beltrán, E., Pareja-Jaime, Y., Chakravarthy, S., Martin, G.B., and Pozo, O. del (2013). The Tomato Calcium Sensor Cbl10 and Its Interacting Protein Kinase Cipk6 Define a Signaling Pathway in Plant Immunity. Plant Cell *25*, 2748–2764.

Torres, M.A., and Dangl, J.L. (2005). Functions of the respiratory burst oxidase in biotic interactions, abiotic stress and development. Curr. Opin. Plant Biol. *8*, 397–403.

Traynelis, S.F., Wollmuth, L.P., McBain, C.J., Menniti, F.S., Vance, K.M., Ogden, K.K., Hansen, K.B., Yuan, H., Myers, S.J., and Dingledine, R. (2010). Glutamate Receptor Ion Channels: Structure, Regulation, and Function. Pharmacol. Rev. *62*, 405–496.

Truman, W., Sreekanta, S., Lu, Y., Bethke, G., Tsuda, K., Katagiri, F., and Glazebrook, J. (2013). The CALMODULIN-BINDING PROTEIN60 Family Includes Both Negative and Positive Regulators of Plant Immunity. Plant Physiol. *163*, 1741–1751.

Ungerer, N., Mücke, N., Broecker, J., Keller, S., Frings, S., and Möhrlen, F. (2011). Distinct Binding Properties Distinguish LQ-Type Calmodulin-Binding Domains in Cyclic Nucleotide-Gated Channels. Biochemistry (Mosc.) *50*, 3221–3228.

Urquhart, W., Gunawardena, A.H.L.A.N., Moeder, W., Ali, R., Berkowitz, G.A., and Yoshioka, K. (2007). The chimeric cyclic nucleotide-gated ion channel ATCNGC11/12 constitutively induces programmed cell death in a Ca^{2+} dependent manner. Plant Mol. Biol. *65*, 747–761.

Urquhart, W., Chin, K., Ung, H., Moeder, W., and Yoshioka, K. (2011). The cyclic nucleotide-gated channels AtCNGC11 and 12 are involved in multiple Ca^{2+}-dependent physiological responses and act in a synergistic manner. J. Exp. Bot. *62*, 3671–3682.

Valmonte, G.R., Arthur, K., Higgins, C.M., and MacDiarmid, R. (2013). Calcium-dependent protein kinases in plants: Evolution, expression, and function. Plant Cell Physiol. *55*, 551–569.

Vanneste, S., and Friml, J. (2013). Calcium: The Missing Link in Auxin Action. Plants *2*, 650–675.

Vatsa, P., Chiltz, A., Bourque, S., Wendehenne, D., Garcia-Brugger, A., and Pugin, A. (2011). Involvement of putative glutamate receptors in plant defence signaling and NO production. Biochimie *93*, 2095–2101.

Verret, F., Wheeler, G., Taylor, A.R., Farnham, G., and Brownlee, C. (2010). Calcium channels in photosynthetic eukaryotes: implications for evolution of calcium-based signalling. New Phytol. *187*, 23–43.

Vincent, T.R., Avramova, M., Canham, J., Higgins, P., Bilkey, N., Mugford, S.T., Pitino, M., Toyota, M., Gilroy, S., Miller, A.J., Hogenhout, S.A., and Sanders, D. (2017). Interplay of Plasma Membrane and Vacuolar Ion Channels, Together with BAK1, Elicits Rapid Cytosolic Calcium Elevations in Arabidopsis during Aphid Feeding. Plant Cell *29*, 1460–1479.

Vincill, E.D., Bieck, A.M., and Spalding, E.P. (2012). Ca^{2+} Conduction by an Amino Acid-Gated Ion Channel Related to Glutamate Receptors. Plant Physiol. *159*, 40–46.

Vincill, E.D., Clarin, A.E., Molenda, J.N., and Spalding, E.P. (2013). Interacting Glutamate Receptor-Like Proteins in Phloem Regulate Lateral Root Initiation in Arabidopsis. Plant Cell *25*, 1304–1313.

Vissel, B., Krupp, J.J., Heinemann, S.F., and Westbrook, G.L. (2001). A use-dependent tyrosine dephosphorylation of NMDA receptors is independent of ion flux. Nat. Neurosci. *4*, 587–596.

Waadt, R., Krebs, M., Kudla, J., and Schumacher, K. (2017). Multiparameter imaging of calcium and abscisic acid and high-resolution quantitative calcium measurements using R-GECO1-mTurquoise in Arabidopsis. New Phytol. *216*, 303–320.

Wais, R.J., Galera, C., Oldroyd, G., Catoira, R., Penmetsa, R.V., Cook, D., Gough, C., Dénarié, J., and Long, S.R. (2000). Genetic analysis of calcium spiking responses in nodulation mutants of *Medicago truncatula*. Proc. Natl. Acad. Sci. *97*, 13407–13412.

Walter, A., Mazars, C., Maitrejean, M., Hopke, J., Ranjeva, R., Boland, W., and Mithöfer, A. (2007). Structural Requirements of Jasmonates and Synthetic Analogues as Inducers of Ca^{2+} Signals in the Nucleus and the Cytosol of Plant Cells. Angew. Chem. Int. Ed. *46*, 4783–4785.

Wang, L., Tsuda, K., Truman, W., Sato, M., Nguyen, L.V., Katagiri, F., and Glazebrook, J. (2011). CBP60g and SARD1 play partially redundant critical roles in salicylic acid signaling. Plant J. *67*, 1029–1041.

Wang, Q., Shui, B., Kotlikoff, M.I., and Sondermann, H. (2008). Structural basis for Calcium Sensing by GCaMP2. Struct. Lond. Engl. 1993 *16*, 1817–1827.

Wang, X., Ma, X., Wang, H., Li, B., Clark, G., Guo, Y., Roux, S., Sun, D., and Tang, W. (2015). Proteomic study of microsomal proteins reveals a key role for Arabidopsis annexin 1 in mediating heat stress-induced increase in intracellular calcium levels. Mol. Cell. Proteomics *14*, 686–694.

Wang, Y., Kang, Y., Ma, C., Miao, R., Wu, C., Long, Y., Ge, T., Wu, Z., Hou, X., Zhang, J., and Qi, Z. (2016). CNGC2 is a Ca^{2+} Influx Channel that Prevents Accumulation of Apoplastic Ca^{2+} in the Leaf. Plant Physiol. *173*, 1342–1354.

Wang, Y.-F., Munemasa, S., Nishimura, N., Ren, H.-M., Robert, N., Han, M., Puzõrjova, I., Kollist, H., Lee, S., Mori, I., and Schroeder, J.I. (2013). Identification of Cyclic GMP-Activated Nonselective Ca^{2+}-Permeable Cation Channels and Associated CNGC5 and CNGC6 Genes in Arabidopsis Guard Cells. Plant Physiol. *163*, 578–590.

Webb, A.A.R., Mcainsh, M.R., Taylor, J.E., and Hetherington, A.M. (1996). Calcium Ions as Intracellular Second Messengers in Higher Plants. In Advances in Botanical Research, J.A. Callow, ed. (Academic Press), pp. 45–96.

Weber, E., Engler, C., Gruetzner, R., Werner, S., and Marillonnet, S. (2011). A Modular Cloning System for Standardized Assembly of Multigene Constructs. PLoS ONE *6*, e16765.

Weiland, M., Mancuso, S., and Baluska, F. (2016). Signalling via glutamate and GLRs in Arabidopsis thaliana. Funct. Plant Biol. *43*, 1–25.

Weinl, S., Held, K., Schlücking, K., Steinhorst, L., Kuhlgert, S., Hippler, M., and Kudla, J. (2008). A plastid protein crucial for Ca^{2+}-regulated stomatal responses. New Phytol. *179*, 675–686.

Weller, B., Zourelidou, M., Frank, L., Barbosa, I.C.R., Fastner, A., Richter, S., Jürgens, G., Hammes, U.Z., and Schwechheimer, C. (2017). Dynamic PIN-FORMED auxin efflux carrier phosphorylation at the plasma membrane controls auxin efflux-dependent growth. Proc. Natl. Acad. Sci. *114*, E887–E896.

Whalley, H.J., and Knight, M.R. (2013). Calcium signatures are decoded by plants to give specific gene responses. New Phytol. *197*, 690–693.

Whalley, H.J., Sargeant, A.W., Steele, J.F.C., Lacoere, T., Lamb, R., Saunders, N.J., Knight, H., and Knight, M.R. (2011). Transcriptomic Analysis Reveals Calcium Regulation of Specific Promoter Motifs in Arabidopsis. Plant Cell *23*, 4079–4095.

Wheeler, G.L., and Brownlee, C. (2008). Ca^{2+} signalling in plants and green algae – changing channels. Trends Plant Sci. *13*, 506–514.

Wilkins, K.A., Matthus, E., Swarbreck, S.M., and Davies, J.M. (2016). Calcium-Mediated Abiotic Stress Signaling in Roots. Front. Plant Sci. *7*.

Winter, D., Vinegar, B., Nahal, H., Ammar, R., Wilson, G.V., and Provart, N.J. (2007). An "Electronic Fluorescent Pictograph" Browser for Exploring and Analyzing Large-Scale Biological Data Sets. PLoS ONE *2*.

Wiśniewska, J., Xu, J., Seifertová, D., Brewer, P.B., Růžička, K., Blilou, I., Rouquié, D., Benková, E., Scheres, B., and Friml, J. (2006). Polar PIN Localization Directs Auxin Flow in Plants. Science *312*, 883–883.

Wu, J., Liu, L., Matsuda, T., Zhao, Y., Rebane, A., Drobizhev, M., Chang, Y.-F., Araki, S., Arai, Y., March, K., Hughes, T.E., Sagou, K., Miyata, T., Nagai, T., Li, W., and Campbell, R.E. (2013). Improved Orange and Red Ca^{2+} Indicators and Photophysical Considerations for Optogenetic Applications. ACS Chem. Neurosci. *4*, 963–972.

Wu, Z., Liang, F., Hong, B., Young, J.C., Sussman, M.R., Harper, J.F., and Sze, H. (2002). An Endoplasmic Reticulum-Bound Ca^{2+}/Mn^{2+} Pump, ECA1, Supports Plant Growth and Confers Tolerance to Mn^{2+} Stress. Plant Physiol. *130*, 128–137.

Wudick, M.M., and Feijó, J.A. (2014). At the Intersection: Merging Ca^{2+} and ROS Signaling Pathways in Pollen. Mol. Plant *7*, 1595–1597.

Yamagami, M., Haga, K., Napier, R.M., and Iino, M. (2004). Two Distinct Signaling Pathways Participate in Auxin-Induced Swelling of Pea Epidermal Protoplasts. Plant Physiol. *134*, 735–747.

Yoshioka, K., Kachroo, P., Tsui, F., Sharma, S.B., Shah, J., and Klessig, D.F. (2001). Environmentally sensitive, SA-dependent defense responses in the cpr22 mutant of Arabidopsis. Plant J. Cell Mol. Biol. *26*, 447–459.

Yoshioka, K., Moeder, W., Kang, H.-G., Kachroo, P., Masmoudi, K., Berkowitz, G., and Klessig, D.F. (2006). The Chimeric Arabidopsis CYCLIC NUCLEOTIDE-GATED ION CHANNEL11/12 Activates Multiple Pathogen Resistance Responses. Plant Cell *18*, 747–763.

Yu, I., Fengler, K.A., Clough, S.J., and Bent, A.F. (2000). Identification of Arabidopsis Mutants Exhibiting an Altered Hypersensitive Response in Gene-for-Gene Disease Resistance. Mol. Plant. Microbe Interact. *13*, 277–286.

Yu, I.C., Parker, J., and Bent, A.F. (1998). Gene-for-gene disease resistance without the hypersensitive response in Arabidopsis dnd1 mutant. Proc. Natl. Acad. Sci. *95*, 7819–7824.

Yuan, F., Yang, H., Xue, Y., Kong, D., Ye, R., Li, C., Zhang, J., Theprungsirikul, L., Shrift, T., Krichilsky, B., Johnson, D.M., Swift, G.B., He, Y., Siedow, J.N., and Pei, Z.-M. (2014). OSCA1 mediates osmotic-stress-evoked Ca^{2+} increases vital for osmosensing in Arabidopsis. Nature *514*, 367–371.

Yuan, P., Jauregui, E., Du, L., Tanaka, K., and Poovaiah, B. (2017). Calcium signatures and signaling events orchestrate plant–microbe interactions. Curr. Opin. Plant Biol. *38*, 173–183.

Zelman, A.K., Dawe, A., Gehring, C., and Berkowitz, G.A. (2012). Evolutionary and Structural Perspectives of Plant Cyclic Nucleotide-Gated Cation Channels. Front. Plant Sci. *3*.

Zhang, J., Li, W., Xiang, T., Liu, Z., Laluk, K., Ding, X., Zou, Y., Gao, M., Zhang, X., Chen, S., Mengiste, T., Zhang, Y., and Zhou, J.-M. (2010a). Receptor-like Cytoplasmic Kinases Integrate Signaling from Multiple Plant Immune Receptors and Are Targeted by a *Pseudomonas syringae* Effector. Cell Host Microbe *7*, 290–301.

Zhang, J., Vanneste, S., Brewer, P.B., Michniewicz, M., Grones, P., Kleine-Vehn, J., Löfke, C., Teichmann, T., Bielach, A., Cannoot, B., Hoyerová, K., Chen, X., Xue, H.-W., Benková, E., Zažímalová, E., and Friml, J. (2011). Inositol Trisphosphate-Induced Ca^{2+} Signaling Modulates Auxin Transport and PIN Polarity. Dev. Cell *20*, 855–866.

Zhang, L., Du, L., and Poovaiah, B.W. (2014). Calcium signaling and biotic defense responses in plants. Plant Signal. Behav. *9*, e973818.

Zhang, Y., Xu, S., Ding, P., Wang, D., Cheng, Y.T., He, J., Gao, M., Xu, F., Li, Y., Zhu, Z., Li, X., and Zhang, Y. (2010b). Control of salicylic acid synthesis and systemic acquired resistance by two members of a plant-specific family of transcription factors. Proc. Natl. Acad. Sci. *107*, 18220–18225.

Zhang, Y., Wang, Y., Taylor, J.L., Jiang, Z., Zhang, S., Mei, F., Wu, Y., Wu, P., and Ni, J. (2015). Aequorin-based luminescence imaging reveals differential calcium signalling responses to salt and reactive oxygen species in rice roots. J. Exp. Bot. *66*, 2535–2545.

Zhao, Y., Araki, S., Wu, J., Teramoto, T., Chang, Y.-F., Nakano, M., Abdelfattah, A.S., Fujiwara, M., Ishihara, T., Nagai, T., and Campbell, R.E. (2011). An Expanded Palette of Genetically Encoded Ca^{2+} Indicators. Science *333*, 1888–1891.

Zhou, L., Lan, W., Jiang, Y., Fang, W., and Luan, S. (2014). A calcium-dependent protein kinase interacts with and activates a calcium channel to regulate pollen tube growth. Mol. Plant *7*, 369–376.

Zhu, J., Wu, X., Yuan, S., Qian, D., Nan, Q., An, L., and Xiang, Y. (2014). Annexin5 Plays a Vital Role in Arabidopsis Pollen Development via Ca^{2+}-Dependent Membrane Trafficking. PLoS ONE *9*, e102407.

Zhu, X., Dunand, C., Snedden, W., and Galaud, J.-P. (2015). CaM and CML emergence in the green lineage. Trends Plant Sci. *20*, 483–489.

Zieschang, H.E., Köhler, K., and Sievers, A. (1993). Changing proton concentrations at the surfaces of gravistimulated Phleum roots. Planta *190*, 546–554.

Zimmermann, S., Nürnberger, T., Frachisse, J.-M., Wirtz, W., Guern, J., Hedrich, R., and Scheel, D. (1997). Receptor-mediated activation of a plant Ca^{2+}-permeable ion channel involved in pathogen defense. Proc. Natl. Acad. Sci. *94*, 2751–2755.

Zipfel, C. (2014). Plant pattern-recognition receptors. Trends Immunol. *35*, 345–351.

Zipfel, C., Robatzek, S., Navarro, L., Oakeley, E.J., Jones, J.D.G., Felix, G., and Boller, T. (2004). Bacterial disease resistance in Arabidopsis through flagellin perception. Nature *428*, 764–767.

Zipfel, C., Kunze, G., Chinchilla, D., Caniard, A., Jones, J.D.G., Boller, T., and Felix, G. (2006). Perception of the Bacterial PAMP EF-Tu by the Receptor EFR Restricts Agrobacterium-Mediated Transformation. Cell *125*, 749–760.

Zourelidou, M., Absmanner, B., Weller, B., Barbosa, I.C., Willige, B.C., Fastner, A., Streit, V., Port, S.A., Colcombet, J., Bentem, S. de la F. van, Hirt, H., Kuster, B., Schulze, W.X., Hammes, U.Z., and Schwechheimer, C. (2014). Auxin efflux by PIN-FORMED proteins is activated by two different protein kinases, D6 PROTEIN KINASE and PINOID. eLife *3*, e02860.

Acronyms and abbreviations

AMF	Arbuscular mycorrhizal fungi
ABA	Abscisic acid
ACS2	1-*AMINOCYCLOPROPANE-1-CARBOXYLATE SYNTHASE*
AHK3	HISTIDINE KINASE 3
ANN	ANNEXIN
ANOVA	Analysis of variance
ARR	Arabidopsis Response Regulator
ATP	Adenosine triphosphate
Ca^{2+}	Calcium ion
CaM	Calmodulin (Ca^{2+}-modulated protein)
CAX	Ca^{2+}-exchanger
CBL	Calcineurin B-like
CDPK	Ca^{2+}-dependent protein kinase
CER	Controlled environment room
CFP	Cyan fluorescent protein
cGMP	Cyclic guanosine 3', 5'-monophosphate
CIPK	CBL-interacting protein kinase
CNGC	Cyclic nucleotide-gated channel
CPK	Ca^{2+}-dependent protein kinase (in Arabidopsis)
CO8	Chitooctaose
DAMP	Damage-associated molecular pattern
DMSO	Dimethyl sulfoxide
DNA	Deoxyribonucleic acid
E	Amplification efficiency
ECFP	Enhanced cyan fluorescent protein
EDS1	*ENHANCED DISEASE SUSCEPTIBILITY 1*
EFR	EF-Tu RECEPTOR
EGTA	Ethylene glycol-bis(β-aminoethyl ether)-N,N,N',N'-tetraacetic acid
EMS	Ethyl methanesulfonate
ER	Endoplasmic reticulum
ETI	Effector-triggered immunity
FLS2	FLAGELLIN SENSING 2
FRET	Förster resonance energy transfer
GC	Guanylate cyclase

GCA2	GROWTH CONTROL EXERTED BY ABA 2
GECO	Genetically-encoded fluorescent indicator for optical imaging
GFP	Green fluorescent protein
GLR	Glutamate receptor-like
GUS	Beta-glucuronidase
HEK	Human embryonic kidney
HPTII	*HYGROMYCIN PHOSPHOTRANSFERASE II*
HR	Hypersensitive response
IAA	Indole-3-acetic acid
InsP3	Inositol (1, 4, 5)-trisphosphate
IPT	Isopentenyltransferase
IP3	Inositol (1, 4, 5)-trisphosphate receptor
K^+	Potassium ion
K_d	Dissociation constant
KRP4	KIP-RELATED PROTEIN 4
LB	Lysogeny broth
LORE	Lipooligosaccharide-specific reduced elicitation
LP	Left border primer
LRR	Leucine-rich repeat
MAMP	Microbial-associated molecular patterns
MAPK	Mitogen-activated protein kinases
MS	Murashige and Skoog
MSL	Mechanosensitive channel of small conductance-like
M13	Myosin light-chain kinase peptide
NAA	1-Naphthaleneacetic acid
NADPH	Nicotinamide adenine dinucleotide phosphate
NES	Nuclear exclusion signal
NHL10	*NDR1/HIN1-LIKE 10/YLS9*
NLR	Nucleotide-binding domain leucine-rich repeat
NLS	Nuclear localisation signal
NOS	Nopaline synthase
OSCA	Hyperosmolality-gated Ca^{2+}-permeable channel
PAMP	Pathogen-associated molecular patterns
PBP1	PID-BINDING PROTEIN 1
PCR	Polymerase chain reaction
PEPR	AtPEP1 Receptor
PID	PINOID
PIN	PIN-FORMED

PKG	cGMP-dependent protein kinase
PRR	Pattern recognition receptors
PTI	Pattern-triggered immunity
QC	Quiescent centre
RBOHD	RESPIRATORY BURST OXIDASE HOMOLOGUE
RLU	Relative light units
RNA	Ribonucleic acid
ROI	Regions of interest
ROS	Reactive oxygen species
RP	Right border primer
S. e. m.	Standard error of mean
S. d.	Standard deviation
SA	Salicylic acid
SD	Synthetic Defined
SERCA	Sarco/endoplasmic reticulum Ca^{2+}-ATPase
T_a	Annealing temperature
TAE	Tris base, acetic acid and EDTA
TAIR	The Arabidopsis Information Resource
TCH3	TOUCH 3
T35S	35S terminator
UBI10	UBIQUITIN 10
YC	Yellow cameleons
YFP	Yellow fluorescent protein

Appendix A – Expression map of *AtCNGC15*

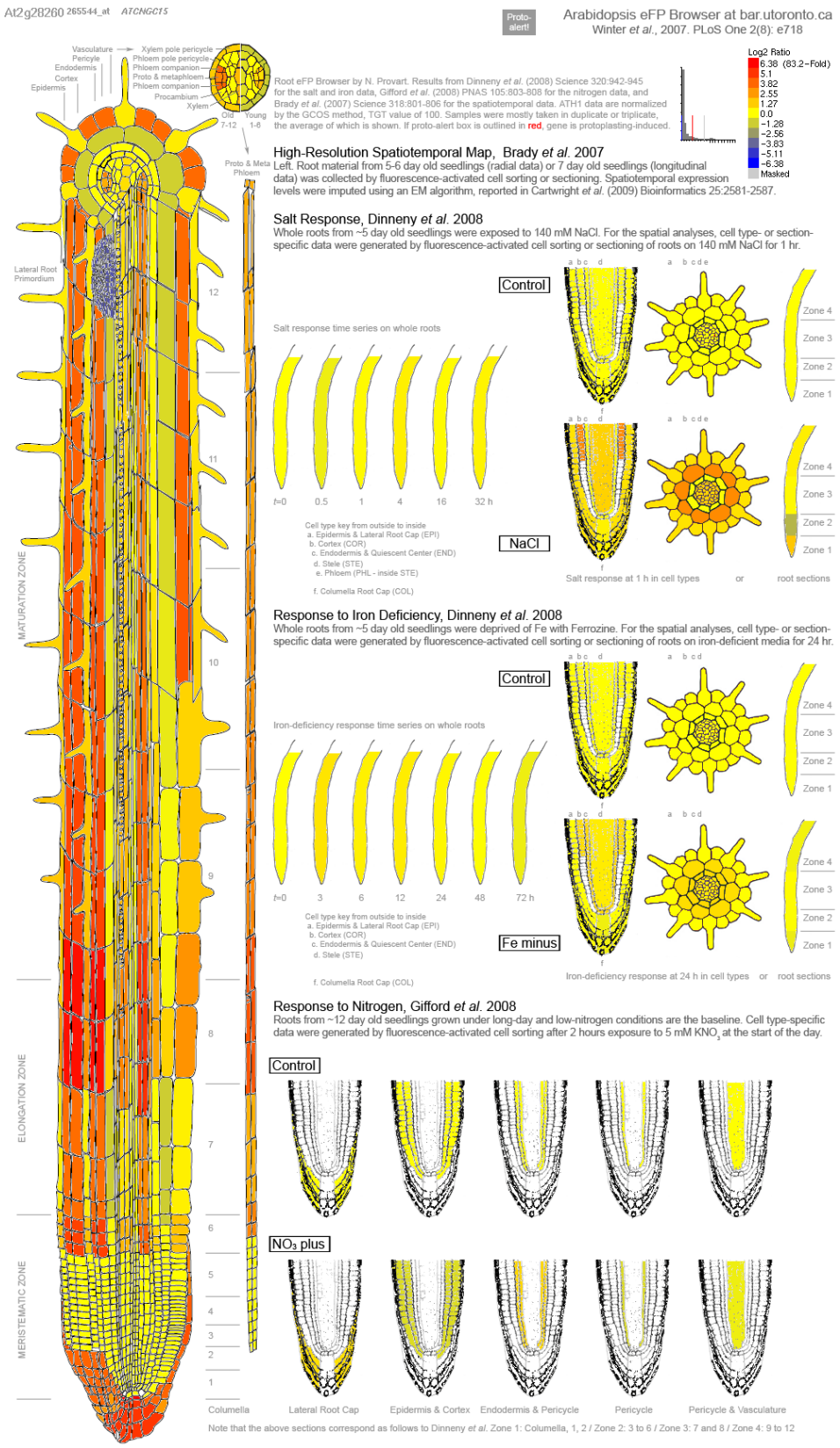

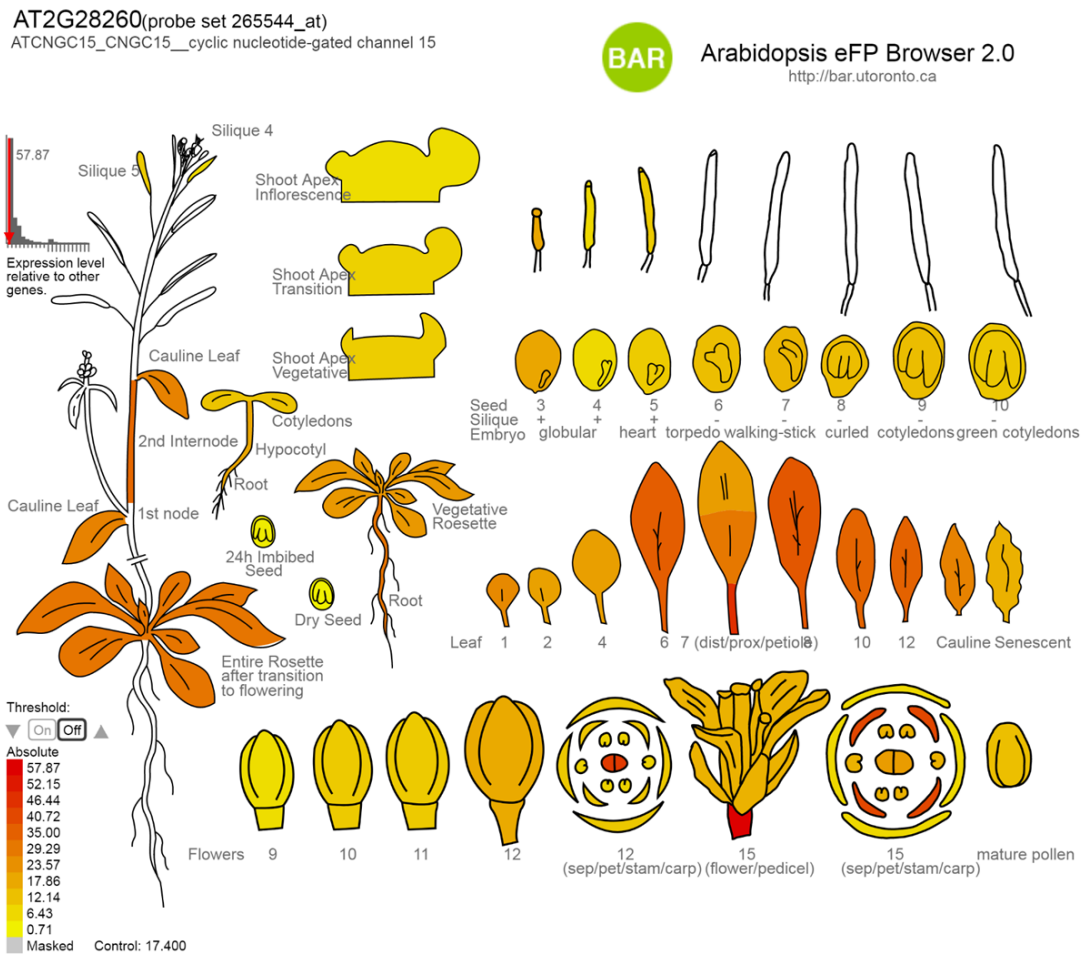
AT2G28260(probe set 265544_at)
ATCNGC15_CNGC15__cyclic nucleotide-gated channel 15
BAR
Arabidopsis eFP Browser 2.0
http://bar.utoronto.ca
57.87
Expression level relative to other genes.
Silique 4
Silique 5
Shoot Apex Inflorescence
Shoot Apex Transition
Shoot Apex Vegetative
Cauline Leaf
Cotyledons
2nd Internode
Hypocotyl
Root
Cauline Leaf
1st node
24h Imbibed Seed
Dry Seed
Vegetative Rosette
Root
Entire Rosette after transition to flowering
Seed
Silique Embryo
3 + globular
4 + heart
5 + torpedo
6 - walking-stick
7 - curled
8 - cotyledons
9 - green cotyledons
10 -
Leaf 1 2 4 6 7 (dist/prox/petiole) 8 10 12 Cauline Senescent
Flowers 9 10 11 12
12 (sep/pet/stam/carp)
15 (flower/pedicel)
15 (sep/pet/stam/carp)
mature pollen
Threshold:
On Off
Absolute
57.87
52.15
46.44
40.72
35.00
29.29
23.57
17.86
12.14
6.43
0.71
Masked
Control: 17.400

Appendix B – Expression map of *AtDMI1*

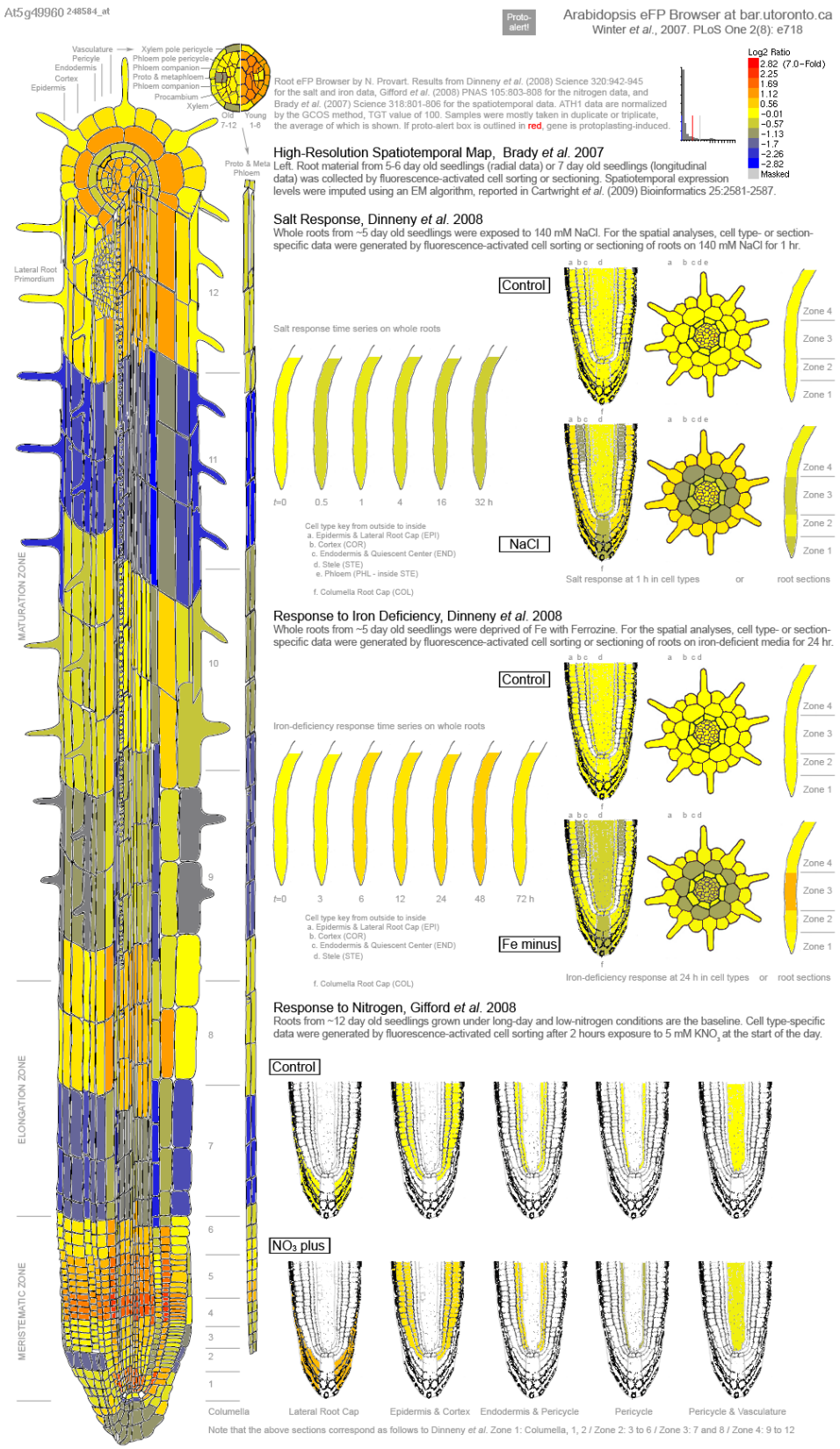

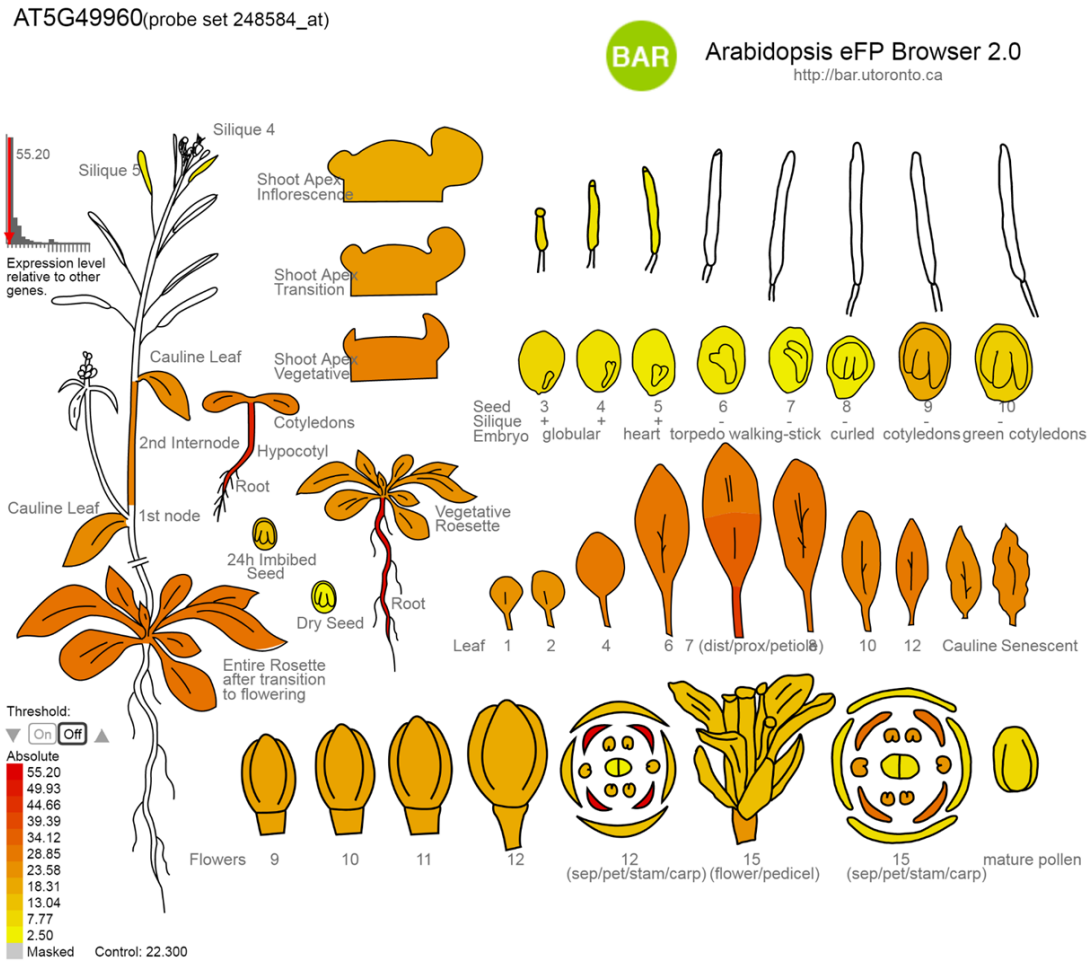
AT5G49960(probe set 248584_at)
BAR
Arabidopsis eFP Browser 2.0
http://bar.utoronto.ca
55.20
Expression level relative to other genes.
Silique 4
Silique 5
Shoot Apex Inflorescence
Shoot Apex Transition
Shoot Apex Vegetative
Cauline Leaf
Cotyledons
2nd Internode
Hypocotyl
Root
Cauline Leaf
1st node
24h Imbibed Seed
Dry Seed
Vegetative Roesette
Root
Entire Rosette after transition to flowering
Seed
Silique Embryo
3 + globular
4 + heart
5 + torpedo
6 - walking-stick
7 - curled
8 - cotyledons
9 - green cotyledons
10 - cotyledons
Leaf 1 2 4 6 7 (dist/prox/petiole) 8 10 12 Cauline Senescent
Flowers 9 10 11 12
12 (sep/pet/stam/carp)
15 (flower/pedicel)
15 (sep/pet/stam/carp)
mature pollen
Threshold:
On Off
Absolute
55.20
49.93
44.66
39.39
34.12
28.85
23.58
18.31
13.04
7.77
2.50
Masked
Control: 22.300